POSIVA

POSIVA 2007-03

Olkiluoto Site Description 2006

Johan Andersson
Henry Ahokas
John A. Hudson
Lasse Koskinen, Ari Luukkonen, Jari Löfman
Vesa Keto, Petteri Pitkänen
Jussi Mattila, Ari T.K. Ikonen, Mia Ylä-Mella

March 2007

POSIVA OY
FIN-27160 OLKILUOTO, FINLAND
Phone (02) 8372 31 (nat.), (+358-2-) 8372 31 (int.)
Fax (02) 8372 3709 (nat.), (+358-2-) 8372 3709 (int.)

POSIVA 2007-03

Olkiluoto Site Description 2006

Johan Andersson
JA Streamflow AB

Henry Ahokas
Pöyry Environment Oy

John A. Hudson
Rock Engineering Consultants

Lasse Koskinen, Ari Luukkonen, Jari Löfman, Vesa Keto, Petteri Pitkänen
VTT

Jussi Mattila, Ari T.K. Ikonen, Mia Ylä-Mella
Posiva Oy

March 2007

Base maps: © National Land Survey, permission 41/MYY/07

POSIVA OY
FI-27160 OLKILUOTO, FINLAND
Phone (02) 8372 31 (nat.), (+358-2-) 8372 31 (int.)
Fax (02) 8372 3709 (nat.), (+358-2-) 8372 3709 (int.)

ISBN 978-951-652-151-3
ISSN 1239-3096

Posiva-raportti – Posiva Report

Posiva Oy
FI-27160 OLKILUOTO, FINLAND
Puh. 02-8372 (31) – Int. Tel. +358 2 8372 (31)

Raportin tunnus – Report code
POSIVA 2007-03

Julkaisuaika – Date
March 2007

Tekijä(t) – Author(s)

Johan Andersson, JA Streamflow AB
Henry Ahokas, Pöyry Environment Oy
John A. Hudson, Rock Engineering Consultants
Lasse Koskinen, Ari Luukkonen, Jari Löfman, Vesa Keto, Petteri Pitkänen; VTT
Jussi Mattila , Ari T.K. Ikonen, Mia Ylä-Mella; Posiva Oy

Toimeksiantaja(t) – Commissioned by

Posiva Oy

Nimeke – Title

OLKILUOTO SITE DESCRIPTION 2006

Tiivistelmä – Abstract

This second version of the Olkiluoto Site Report, produced by the OMTF (Olkiluoto Modelling Task Force), updates the Olkiluoto Site Report 2004 (Posiva 2005) with the data and knowledge obtained up to December 2005.

The main product of the modelling has been to develop a descriptive model of the site (the Site Descriptive Model), i.e. a model describing the geometry, properties of the bedrock and the water and the associated interacting processes and mechanisms. For practical reasons, the Site Descriptive Model is divided into five parts: surface system, geology, rock mechanics, hydrogeology and hydrogeochemistry, which are presented in individual chapters. Four separated models are presented: the geological, rock mechanics, hydrogeological and hydrogeochemical models. The consistency between the hydrogeological and hydrogeochemical models is assessed in a joint chapter.

Chapter 1 presents an outline of the report, explains the background to its development and sets out its objectives and scope. It is also introduces and explains the integrated modelling methodology, the nomenclature used in the descriptions of the models and the prediction/outcome studies. Chapter 2 provides a brief overview of the data used for producing the Site Description. Chapters 3 to 8 present the descriptive modelling, which involves interpreting data, interpolating or extrapolating between measurement points and calibrating the model against data, based on the various assumptions made about each conceptual model. Chapter 9 presents the results of the prediction/outcome studies performed during 2005 and Chapter 10 the overall consistency and confidence assessment. Overall conclusions are provided in Chapter 11.

The main advances since Site Report 2004 are:

- A new geological model is presented in Chapter 4, representing a significant change from Bedrock Model 2003/1 (Vaittinen et al. 2003). There has been extensive use of geological data, whereas hydrogeological data have deliberately not been used and more subjective criteria are used for identifying faults.
- Regarding the rock mechanics description, presented in Chapter 5, additional data have been assessed and the overall level of rock mechanics understanding has increased compared with previous model versions.
- A new hydrogeological model has been developed, which is presented in Chapter 6, which places more emphasis on the hydraulic data. Pressure anomalies are now stronger drivers for including hydraulic zones in the model and the number of explicit uncertain cases is greater.
- The hydrogeochemical description, presented in Chapter 7, is consistent with the previous model and there is an increased level of internal consistency in the hydrogeochemical understanding. Information on gases and understanding of their origin has increased significantly.

Based on these descriptions, the report also makes a second set of predictions in Chapter 9 concerning the expected geology and rock mechanics properties to be found during the excavation of the ONKALO and also predicts the hydrogeological and hydrogeochemical impacts of these excavations. Two types of predictions are made: type A predictions, that use only the latest version of the overall Site Model; and type B predictions, that also use all the data from the tunnel, which are derived from activities, such as tunnel mapping and Pilot holes.

The Site Descriptive Modelling involves uncertainties and it is necessary to assess the confidence in such modelling. This has been assessed through special protocols in a technical auditing exercise, which is presented in Chapter 10. These protocols investigate whether all data have been considered and understood; where the uncertainties lie and what the potential is for alternative interpretations; whether there is sufficient consistency between disciplines and consistency with the past evolution of the site; as well as comparisons with previous model versions.

Chapter 11 concludes that, overall, the uncertainty and confidence assessment demonstrates an evolving confidence in the Site Description. It is also concluded that the main remaining challenge of the site characterisation work is to properly assess the confidence in the Site Description outside the well-characterised ONKALO volume, and actions have been identified in order to handle this. The remaining uncertainty issues are presented in Chapter 11 and are associated with the detailed scale characterisation of the rock – plans and actions for their resolution have also been identified.

Avainsanat - Keywords

Description of the Olkiluoto site, integration, prediction/outcome studies, conceptual model, model uncertainty

ISBN	ISSN
ISBN 978-951-652-151-3	ISSN 1239-3096
Sivumäärä – Number of pages	Kieli – Language
536	English

Posiva-raportti – Posiva Report

Posiva Oy
FI-27160 OLKILUOTO, FINLAND
Puh. 02-8372 (31) – Int. Tel. +358 2 8372 (31)

Raportin tunnus – Report code
POSIVA 2007-03

Julkaisuaika – Date
Maaliskuu 2007

Tekijä(t) – Author(s)
Johan Andersson, JA Streamflow AB
Henry Ahokas, Pöyry Environment Oy
John A. Hudson, Rock Engineering Consultants
Lasse Koskinen, Ari Luukkonen, Jari Löfman, Vesa Keto, Petteri Pitkänen; VTT
Jussi Mattila , Ari T.K. Ikonen, Mia Ylä-Mella; Posiva Oy

Toimeksiantaja(t) – Commissioned by
Posiva Oy

Nimeke – Title

OLKILUODON LOPPUSIJOITUSPAIKAN KUVAUS 2006

Tiivistelmä – Abstract

Olkiluodon loppusijoituspaikan toinen kuvaus, Olkiluoto Site Description 2006, on vuoden 2004 kuvauksen päivitys. Se perustuu tutkimustietoon, joka oli käytettävissä vuoden 2006 lopussa.

Mallinnuksen päätavoitteena oli kuvata loppusijoituspaikan geometria, kallioperän ja pohjaveden ominaisuudet sekä eri tutkimusaloihin liittyvien vuorovaikutussuhteiden prosessit ja mekanismit. Loppusijoituspaikan kuvaus on jaettu viiteen osaan: biosfääri, geologia, kalliomekaniikka, hydrogeologia ja hydrogeokemia. Kukin osa-alue esitetään omassa luvussaan. Hydrogeologisten ja hydrogeokemiallisten mallien integrointia on käsitelty erillisessä luvussa.

Raportin ensimmäisessä luvussa kuvataan raportin sisältö, tausta ja määritellään mallinnustyön laajuus sekä päätavoitteet. Ensimmäisessä luvussa esitetään myös pääpiirteittäin integrointiin liittyvä mallinnusmetodologia, mallikuvauksissa käytetty nimistö sekä ennuste/toteuma-mallinnus. Toisessa luvussa on lyhyt kuvaus mallinnuksessa käytetystä tutkimustiedosta. Itse mallinnustulokset löytyvät luvuista 3-8, jotka sisältävät tutkimustiedon tulkintaa, mittauspisteiden välistä inter- ja ekstrapolointia sekä mallien kalibrointia olemassa olevalla tutkimus- ja mittaustiedolla. Luvussa yhdeksän on vuonna 2005 tehtyjen ennuste/toteuma mallinnusten tulokset ja luvussa kymmenen arvioidaan eri mallien välistä yhtenevyyttä ja luotettavuutta. Luku yksitoista sisältää raportin johtopäätökset.

Huomattavimmat muutokset vuoden 2004 loppusijoituspaikan kuvaukseen verrattuna ovat:

- Uusi geologinen malli (Luku 4) on huomattava muutos vuoden 2003 kalliomalliin verrattuna (Bedrock Model 2003/1). Uusi geologinen malli perustuu aiemmasta kalliomallista poiketen puhtaasti geologiseen tutkimustietoon.
- Kalliomekaniikan kuvaus (Luku 5) sisältää lisää tutkimustiedon tulkintaa ja käsitys Olkiluodon kallioperän mekaanisista ominaisuuksista on lisääntynyt edelliseen malliversioon verrattuna
- Uusi hydrogeologinen malli on julkaistu (Luku 6). Mallissa korostuu hydrogeologisen datan käyttö mm. paineanimalioita käytetään voimakkaammin hydrogeologisten rakenteiden tulkinnassa ja muodostamisessa
- Hydrogeokemiallinen kuvaus (Luku 7) on yhtenevä aiempien kuvausten kanssa ja on näin ollen lisännyt luottamusta siihen, että Olkiluodon hydrogeokemialliset olosuhteet tunnetaan jo melko hyvin. Käsitys pohjaveteen liuenneiden kaasujen alkuperästä on lisääntynyt huomattavasti aiempiin tulkintoihin verrattuna.

Uusiin malliversioihin perustuvat ennusteet on esitetty luvussa 9. Ne sisältävät odotettavissa olevat kallioperän geologiset ja kalliomekaaniset ominaisuudet tunnelin edetessä sekä ennusteen rakentamisen aiheuttamista hydrogeologisista ja hydrogeokemiallisista muutoksista. Ennusteita tehdään kahden tyyppisiä: A-ennusteet perustuvat ainoastaan viimeisimpään Olkiluodon loppusijoituspaikan kuvaukseen ja B-ennusteet käyttävät olemassa olevan mallin lisäksi hyödykseen kaikkea käytettävissä oleva tutkimustietoa (esim. tunnelin kartoitustietoja ja pilottireikäkairauksesta ja -tutkimuksista saatavia tietoja).

Olkiluodon loppusijoituspaikan kuvaus (Olkiluoto Site Description 2006) sisältää edelleen epävarmuuksia ja tämäntyyppisen mallinnustyön luotettavuutta on aina arvioitava. Nyt julkaistavan loppusijoituspaikan kuvauksen luotettavuuden arviointi on esitetty luvussa kymmenen. Luotettavuuden arvioinnissa on pohdittu mm. ymmärretäänkö kaikki käytettävissä oleva tutkimustieto ja onko kaikkea mahdollista tietoa käytetty, missä pahimmat epävarmuudet ovat ja löytyykö tiedolle vaihtoehtoisia tulkintatapoja. Lisäksi tutkitaan mallien välisiä yhteneväisyyksiä ja eroavaisuuksia sekä tähän mennessä saavutetun yhteneväisyyden riittävyyttä, tutkitaan mallien yhteneväisyyttä loppusijoituspaikan kehityskulkuun verrattuna ja verrataan uusia malleja aikaisempiin malliversioihin.

Yhteenvetona (Luku 11) voidaan todeta, että yleisesti ottaen luottamus käsitykseen loppusijoituspaikan ominaisuuksista on kehittynyt tehtyjen tutkimusten ja mallinnustyön lopputuloksena. Johtopäätöksissä todetaan, että kuvauksen laajentaminen keskeisen tutkimusalueen, ONKALO-alueen, ulkopuolelle on keskeisin haaste lähitulevaisuudessa ja siihen liittyy myöskin olemassa olevien mallien suurimmat epävarmuudet; ko. alueilta tutkimustietoa on suhteellisen vähän käytettävissä. Kuten edellä on todettu, tähänkin kuvaukseen loppusijoituspaikan ominaisuuksista liittyy edelleen selvittämättömiä/epävarmoja asioita. Keskeisimmät keskeneräiset asiat ja niiden ratkaisemiseksi laaditut suunnitelmat on koottu lukuun yksitoista. Monien vielä epävarmojen asioiden selvittäminen vaatii loppusijoituskallion ominaisuuksien yhä yksityiskohtaisempaa karakterisointia.

Avainsanat - Keywords
Olkiluodon loppusijoituspaikan kuvaus, konseptuaalinen malli, ennuste/toteuma, mallinnukset, mallin epävarmuus

ISBN
ISBN 978-951-652-151-3

ISSN
ISSN 1239-3096

Sivumäärä – Number of pages
536

Kieli – Language
Englanti

TABLE OF CONTENTS

ABSTRACT
TIIVISTELMÄ

PREFACE 5
ACRONYMS 7

1 INTRODUCTION 9
1.1 Background 9
1.1.1 Objectives and scope 11
1.2 Integrated modelling methodology 11
1.3 This report 14

2 APPLIED INVESTIGATION DATA 15
2.1 Overview 15
2.2 Surface-based investigations 15
2.2.1 Geological data 15
2.2.2 Geophysical data 20
2.2.3 Hydrogeological data 23
2.2.4 Hydrogeochemical and microbiological data 26
2.2.5 Rock Mechanics Data 28
2.3 ONKALO-based investigations 33
2.3.1 Geological mapping 33
2.3.2 Pilot holes 34
2.3.3 Rock mechanics data 35
2.3.4 Hydraulic data 37

3 SURFACE CONDITIONS 41
3.1 Climate and meteorology 41
3.1.1 Weather statistics 41
3.1.2 Snow cover and ground frost 42
3.1.3 Deposition 42
3.2 Ecosystems and land-use 43
3.2.1 Land-use in Olkiluoto 43
3.2.2 Terrestrial ecosystems 44
3.2.3 Baltic ecosystems 45
3.3 Overburden 46
3.3.1 Terrestrial overburden 46
3.3.2 Hydrogeochemistry of overburden groundwater 47
3.3.3 Sea bottom sediments 49
3.4 Interaction with other disciplines 50

4 BEDROCK GEOLOGY 53
4.1 Objectives of and approaches to the geological modelling 53
4.1.1 Purpose and uses of the Geological Site Model 53
4.1.2 Conceptual model 54
4.1.3 Modelling methods 58
4.2 Data Evaluation 65
4.2.1 Surface geological data 65
4.2.2 Drill core investigations 65
4.2.3 ONKALO underground rock characterisation facility 67
4.2.4 Geophysical data 67
4.3 The Geological Site Model 69

4.3.1 Lithology ... 69
4.3.2 Alteration ... 75
4.3.3 Ductile deformation ... 79
4.3.4 Brittle deformation ... 81
4.3.5 Fracturing (DFN-model and fracture characterisation) ... 85
4.4 Interaction with other disciplines ... 86
4.5 Uncertainties ... 87

5 ROCK MECHANICS ... 93
5.1 Objectives of and approaches to the rock mechanics modelling ... 93
5.1.1 Purpose and uses of the rock mechanics model ... 93
5.1.2 The rock mechanics conceptual model ... 94
5.1.3 Modelling methods ... 96
5.1.4 Rock mechanics model components and parameters ... 96
5.2 Evaluation of information ... 101
5.3 Interaction with other disciplines ... 102
5.4 Rock Mechanics Modelling ... 102
5.4.1 In situ stress ... 102
5.4.2 Intact rock properties ... 118
5.4.3 Physical properties ... 134
5.4.4 Thermal properties ... 134
5.4.5 Drilling properties ... 136
5.4.6 Mechanical properties of brittle deformation zones ... 136
5.4.7 Gemetrical and mechanical properties of fractures ... 137
5.4.8 Mechanical properties of the rock mass ... 147
5.4.9 Bedrock stability measurements ... 147
5.5 Evaluation of uncertainties ... 148
5.5.1 Evaluation of uncertainties relating to in situ stress ... 148
5.5.2 Uncertainties in the intact rock properties ... 150
5.5.3 Uncertainties in physical properties ... 151
5.5.4 Uncertainties relating to thermal properties ... 151
5.5.5 Uncertainties related to fracture properties ... 151
5.5.6 Uncertainties related to brittle deformation zone properties ... 151
5.5.7 Uncertainties related to rock mass properties ... 152
5.5.8 Evaluation of uncertainties to microseismic measurements ... 152

6 HYDROGEOLOGY ... 155
6.1 Objectives of hydrogeological modelling ... 155
6.1.1 Hydrogeological modelling in this report ... 156
6.1.2 This chapter ... 158
6.2 Hydrogeological data and information ... 158
6.2.1 Measured transmissivities of rock fractures ... 159
6.2.2 Water table and land uplift ... 168
6.2.3 Groundwater pressure/freshwater head ... 170
6.2.4 Groundwater and sea water salinity ... 170
6.2.5 The Posiva Flow Log flow rates ... 171
6.2.6 Posiva Cross Flow measurements ... 172
6.2.7 Inflow of groundwater in the ONKALO ... 172
6.3 Groundwater flow model on the site scale ... 173
6.3.1 Model components and parameters ... 173
6.3.2 Boundary conditions and initial state ... 176
6.3.3 Structural model for hydrogeological zones ... 181
6.3.4 Hydrogeological properties - porous medium description ... 209
6.4 DFN modelling ... 219

6.4.1 Background ... 219
6.4.2 DFN models ... 220
6.4.3 Results ... 220
6.4.4 Hydrogeological DFN modelling plans for the future ... 222
6.5 Consistency with other disciplines ... 222

7 HYDROGEOCHEMISTRY ... 225
7.1 Objectives and purposes of the hydrogeochemical modelling ... 225
7.2 Hydrogeochemical approaches and information ... 226
7.2.1 Palaeohydrogeological setting ... 226
7.2.2 Modelling methods ... 230
7.2.3 Water samples and databases ... 231
7.3 Interpretation of hydrogeochemical information ... 234
7.3.1 Baseline conditions and complementary information since Olkiluoto Site Description 2004 ... 234
7.3.2 Evaluation of recent data ... 261
7.3.3 Temporal changes in monitoring data ... 266
7.4 Interaction with other disciplines ... 268
7.5 Hydrogeochemical modelling ... 270
7.5.1 Interpretation of pH and redox measurements ... 270
7.5.2 Results of mass-balance modelling ... 278
7.6 Evaluation of uncertainties and sensitivities ... 288
7.7 Discussion ... 289

8 HYDROGEOLOGY – MODELLING OF FLOW AND SALINITY EVOLUTION. 291
8.1 Modelling approach ... 291
8.2 Calibration ... 291
8.2.1 Measured inflow into the ONKALO ... 292
8.2.2 Measured pressure in drillholes ... 292
8.2.3 Measured salinity in drillholes ... 293
8.3 Results ... 299
8.3.1 Flow pattern ... 299
8.3.2 Evolution of salinity field ... 309
8.4 Evaluation of sensitivities ... 316
8.4.1 Hydraulic conductivity and transmissivity ... 316
8.4.2 Initial and boundary conditions ... 317
8.4.3 Porosity ... 318
8.4.4 Dispersion ... 319
8.4.5 Conceptual geometry of hydrogeological zones ... 319
8.5 APPENDIX to Chapter 8 ... 324

9 PREDICTIONS OF PROPERTIES IN THE ONKALO AND THE IMPACT OF CONSTRUCTION ... 335
9.1 General ... 335
9.2 Geological conditions ... 336
9.2.1 Introduction ... 336
9.2.2 Comparisons – why are they lagging behind? ... 338
9.2.3 Lithology ... 338
9.2.4 Ductile deformation ... 340
9.2.5 Brittle deformation - Fracturing ... 342
9.2.6 Brittle deformation - Zone intersections ... 347
9.2.7 Alteration ... 350
9.2.8 Conclusions ... 352
9.3 Rock Mechanics ... 355

9.3.1 Motivation and value of rock mechanics prediction-outcome studies ... 355
9.3.2 Predictions and outcomes of rock mechanics properties ... 355
9.3.3 Obtaining the information concerning the outcomes ... 359
9.3.4 Comparison between prediction and outcome, averaging and bias ... 361
9.3.5 Future work and final goal ... 369
9.4 Hydrogeologic Impacts ... 372
9.4.1 Modelling Approaches and Assumptions ... 373
9.4.2 Drawdown, inflow and head responses ... 375
9.4.3 Evolution of groundwater salinity ... 402
9.5 Fracture mineral buffers – predictive approach ... 416
9.5.1 Water compositions and fracture minerals ... 417
9.5.2 Kinetic mineral dissolution and precipitation ... 418
9.5.3 Fracture properties for reactive transport calculations ... 418
9.5.4 Results of kinetic calculations ... 422
9.5.5 High pH water flow with velocity 2 millimetres/h ... 426
9.5.6 Concluding remarks ... 431
Appendix to Chapter 9 ... 433

10 OVERALL CONSISTENCY AND CONFIDENCE ASSESSMENT ... 441
10.1 Main issues concerning the 2006 Site Model ... 441
10.1.1 Geology/hydrogeology issues ... 441
10.1.2 Rock Mechanics / Geology and hydrogeology issues ... 444
10.1.3 Hydrogeochemistry and hydrogeology issues ... 447
10.1.4 Transport properties ... 451
10.2 Uncertainty audit ... 452
10.2.1 Use of data, accuracy and bias ... 452
10.2.2 Potential for alternative interpretations ... 454
10.2.3 Consistency between disciplines ... 455
10.2.4 Advances since Site Model 2004 ... 456
10.3 Overall judgement ... 457

11 OVERALL EVALUATION AND INPUT TO FURTHER CHARACTERISATION 483
11.1 Overall achievements ... 483
11.2 Site synopsis ... 484
11.2.1 Geological description ... 484
11.2.2 Rock mechanics properties ... 487
11.2.3 Thermal properties ... 488
11.2.4 Rock stress ... 489
11.2.5 Hydrogeological properties ... 491
11.2.6 Hydrogeochemistry and its past evolution ... 495
11.2.7 Groundwater flow and evolution of groundwater composition ... 499
11.2.8 Prediction/Outcome studies ... 503
11.3 Issues to be considered for further site characterisation and modelling ... 506

REFERENCES ... 509

PREFACE

This Olkiluoto Site Report 2006 has been produced by the OMTF (Olkiluoto Modelling Task Force), which covers the areas of geology, rock mechanics, hydrogeology and hydrogeochemistry. The outline and general content of the report has been developed by the OMTF Core Group and discussed at its meetings. The main authors are listed on the front page. In addition, several other persons have provided important input:

- Geology: Seppo Paulamäki (Geological Survey of Finland), Markku Paananen (Geological Survey of Finland), Seppo Gehör (Kivitieto Oy), Aulis Kärki (Kivitieto Oy), Kai Front (VTT), Ismo Aaltonen, Turo Ahokas (Posiva Oy), Kimmo Kemppainen (Posiva Oy) and Liisa Wikström (Posiva Oy)

- Rock Mechanics: Erik Johansson (Saanio & Riekkola Oy), Matti Hakala (KMS Hakala Oy), Jonny Sjöberg (Vattenfall AB), Pauli Syrjänen (Gridpoint Oy) and Sanna Riikonen (Posiva Oy).

- Hydrogeology: Antti Poteri (VTT) and Pirjo Hellä (Pöyry Oy).

- Geochemistry: Sami Partamies (VTT) and Eveliina Tammisto (Pöyry Oy).

Furthermore, Tim McEwen, (McEwen Consulting, UK), has spent a major effort in editing the report, trying to sort out the English and identifying and correcting logical mistakes. Also the contributions of the Safety Assessment group representative in the OMTF, Pirjo Hellä (Pöyry Oy) are greatfully acknowledged.

Johan Andersson (Chairman of the OMTF)

ACRONYMS

BDZ	Brittle deformation zone
BFI	Brittle fault zone intersection
BFZ	Brittle fault zone
BJI	Brittle joint intersection
BJZ	Brittle joint zone
BP	Before (the) present
BR-WCF	Water conducting fractures in the background rock
DFN	Discrete fracture network
DIC	Dissolved inorganic carbon
DIFF	Difference flow meter
DP	Dual porosity
DSI	Low-grade ductile shear zone intersection
EBS	Engineered barrier system
EDZ	Excavation damage zone
GSM	Geological Site Model
HGI	High-grade ductile shear intersection
HTU	Hydraulic testing unit
HZ	Hydrogeological Zone
LZF	Local fracture zone
LFZ-WCF	Water conducting fractures
masl	metres above sea level
mbsl	metres below sea level
MFZ	Major fracture zone
NPP	Nuclear power plant
OMTF	Olkiluoto Modelling Task Force
PFL	Posiva flow log
P/O	Prediction/Outcome
SDM	Site Descriptive Model
SFR	Sparsely fractured rock
SMI	Semi-brittle fault zone intersection
TDS	Total dissolved solids
TGG	Tonalitic-granodioritic-granitic gneiss
VLJ	The low level waste repository at Olkiluoto
VSP	Vertical seismic profiling
WCA	Well characterised area
WVSP	Walkaway vertical seismic profiling

1 INTRODUCTION

This current Olkiluoto Site Report: Version 2006 is a description of the Olkiluoto Site, in which knowledge from various scientific disciplines has been integrated to produce a coherent picture, and is based on the data available around the end of 2005, i.e. when the excavation of the ONKALO facility had reached a tunnel length of approximately 1 km, 100 m below the surface. However, results of monitoring data obtained later are sometimes commented on – if appropriate. Posiva's Safety Case will be organised in a portfolio of approximately ten main reports, which will be periodically updated. The Site Report describing the present state and past evolution of the Olkiluoto site, as well as the disturbance caused by the construction of ONKALO and the first stage of the repository, forms the geoscientific basis of the Safety Case. The current Site Report is the second version of such a report and supplements the site syntheses that have already been published.

1.1 Background

Posiva is the nuclear waste management organisation in Finland and is responsible for research into the final disposal of spent nuclear fuel and for the construction, operation and eventual backfilling and closure of the final disposal facility. In 2001 the Parliament ratified the Government's favourable Decision in Principle (DiP) on Posiva's application to locate the repository at Olkiluoto, where spent fuel from the Finnish nuclear power reactors is planned to be disposed of in a KBS-3 type repository to be constructed at a depth of between 400 and 600 m in the crystalline bedrock.

Pursuant to the guidelines given by the Ministry of Trade and Industry (KTM) Posiva aims at submission of the application of the construction license for the disposal facility by the end of the year 2012. Current plans and activities to attain this goal are described in Posiva's Programme for Research, Development and Technical Design for 2007–2009 (TKS-2006, Posiva 2006). Regarding the rock, an important part of this plan is the continued construction of the underground rock characterisation facility, ONKALO, which started in autumn 2004, as well as further surface based characterisation of the Olkiluoto island.

Olkiluoto is a large island (~ 10 km^2) on the Baltic Sea coast and separated from the mainland by a narrow strait,. The Olkiluoto nuclear power plant, with two reactors in operation and a third one under construction, and the VLJ repository for low and intermediate waste are located in the western part of the island. The repository for spent fuel will be constructed in the central part of the island (Figure 1-1). The suitability of Olkiluoto as a location for a spent fuel repository has been investigated over a period of fifteen years by means of ground- and air-based methods and from shallow and deep (300 – 1000 m) boreholes.

The investigations to be carried out in the ONKALO aim at further characterisation of the bedrock properties and groundwater characteristics and to help support decisions for selecting the most suitable locations for the first deposition tunnels and disposal holes for spent fuel canisters (Posiva 2003b). Tests and demonstrations of repository technologies will also be carried out in the ONKALO. When completed, the

underground parts of the ONKALO will consist of a system of exploratory tunnels accessed by an inclined tunnel, or ramp, and either one or two shaft(s). The main characterisation level will be located at a depth of about 400 m and the lower characterisation level at a depth of about 500 m. Demonstrations and tests of repository technologies will be mainly carried out at the main characterisation level, but characterisation of the rock mass is already taking place using pilot holes drilled along parts of the tunnel axis, prior to its excavation, by tunnel mapping and by monitoring the impact of construction, as outlined in the Underground Characterisation and Research Programme (UCRP), (Posiva, 2003b) and the Programme for Research, Development and Technical Design for 2004 – 2006 (TKS-2003), (Posiva, 2003e). Surface based-investigations, including the drilling of additional deep boreholes and the excavation of further investigation trenches, are also taking place.

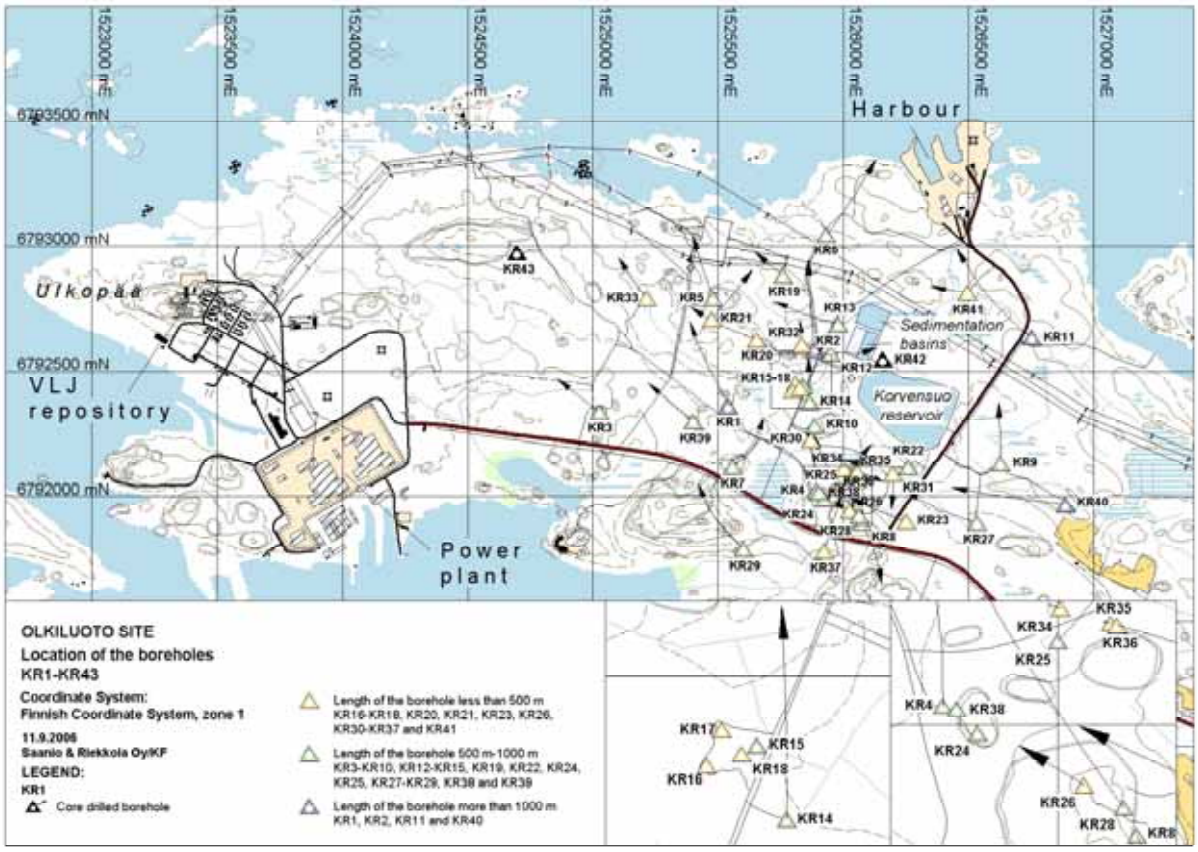

Figure 1-1. *Deep boreholes at Olkiluoto. The size of the grid squares is 500 x 500 m.*

The ONKALO, as well as other characterisation activities at Olkiluoto, produces a substantial amount of data. These data need to be incorporated into models of the site to be used as input, both for the further construction of the ONKALO and for use in subsequent safety analyses and licence applications.

The Olkiluoto Modelling Task Force (OMTF) has been established for planning and integrating the results of the investigations and for undertaking the modelling work of the various disciplines. The main duty of the OMTF is to develop site descriptive

models of the Olkiluoto site, as well as predicting and evaluating the disturbance created by the construction of the ONKALO ramp and the characterisation tunnels. The resulting (geo)syntheses are reported in a series of Site Reports, which will form part of the Safety Case portfolio, as outlined in Vieno & Ikonen (2005). The Olkiluoto Site Description 2004 (Posiva 2005) is the first such synthesis. However, investigations have been taking place at Olkiluoto for many years and several site syntheses were compiled before construction of the ONKALO commenced, including Anttila et al. (1999) and the Baseline report (Posiva 2003a).

1.1.1 Objectives and scope

The objective of this second version of the Olkiluoto Site Report is to update the Olkiluoto Site Report 2004 with the data and knowledge obtained up to December 2005. More specifically, this Site Report will:

- describe the present state and past evolution of the Olkiluoto site,
- by making use of repeated Prediction/Outcome studies, assess how the increased knowledge and experience gained from the construction of the ONKALO has enhanced the level of site understanding and the predictive capability of the modelling teams, and
- assess the disturbances caused by the construction of ONKALO.

1.2 Integrated modelling methodology

The OMTF consists of modelling teams covering the subjects of Geology, Rock Mechanics, Hydrogeology and Hydrogeochemistry. A Task Force Core Group, consisting of representatives from the modelling teams, plus the Task Force Leader, has been established. The Task Force Core Group meets regularly and frequently, plans the modelling work, assesses progress and discusses all major findings, in order to ensure that the information and hypotheses generated in one discipline are disseminated and are compatible with those in the other disciplines; in addition, its task is to identify integration needs and consider other critical issues. Cross-discipline interactions are ensured by regular and comprehensive information sharing discussions and are one of the main themes of the OMTF meetings, and the production of a jointly-prepared Site Report further enhances integration.

An integrated modelling methodology has been developed. It is based on:

- A common format for developing the modelling components that will make up an overall Site Descriptive Model;
- Cross-discipline Workshops to ensure a common basis for modelling;
- Prediction/outcome studies that conform to a common methodology and
- Carrying out an overall confidence assessment

Site Descriptive Model

The main product of the modelling is a descriptive model of the site, i.e. a model describing the geometry, properties of the bedrock and the water, and the interacting processes and mechanisms that are relevant for understanding the evolution of the site to the present day and the potential for future radionuclide migration. This Site Descriptive Model (SDM) is, therefore, distinct from the measured data themselves. Modelling involves interpreting data, extrapolating or interpolating between measurement points and calibrating the numerical models used to simulate the system against data, based on the various assumptions inherent in the conceptual model(s) being employed. The SDM is divided into the following disciplines: surface system, geology, rock mechanics, hydrogeology and hydrogeochemistry. These disciplines are presented in individual chapters in this Site Report.

Integration of understanding across scientific disciplines is enhanced by requiring the presentation of information from each discipline to follow a pre-set outline, including

- Presentation of the conceptual model,
- Evaluation of information (in terms of its sufficiency, quality, whether it is representative etc.),
- Assessment of interaction with other disciplines,
- Presentation of the descriptive modelling and
- Evaluation of uncertainties.

The process of undertaking prediction/outcome studies and the need to complete an overall confidence assessment, also enhance integration.

Although the SDM should be an integrated description, encompassing all different disciplines, it is a necessary and practical requirement to divide such a model into different discipline-specific models. The following nomenclature is used in this regard:

Geological model: For convenience of description and handling, the geological model has been subdivided into a series of subsidiary descriptions covering lithology, alteration, ductile deformation, brittle deformation and fracturing. This subdivision is for the convenience of handling different types of data and should not be regarded as of fundamental significance. For example, the deformation zone model and fracture system model (DFN-model) both represent the effects of brittle deformation at the site, describing deterministic large-scale features and stochastic small-scale features, respectively. However, this is clearly an artificial subdivision, geologically, since these features are closely related with regard to their mode of formation. Similarly, the lithological model may have considerable significance for the distribution of fracturing in space. The geological model does not contain any kind of description of the hydrogeological features.

Rock mechanics model: The rock mechanics model consists of the geometrical, mechanical and thermal descriptions of the rock mass. The geometrical description will

be based on the bedrock geological model, as described above. The mechanical description includes the in situ stress state and the deformation and strength properties of the intact rock, the fractures, the rock mass between deformation zones and the deformation zones themselves. The thermal description is based on the thermal properties of the intact rock. The rock mechanics model will also include a description of the effects of excavation. There is also a need to consider the interaction of the rock mechanics model with the hydrogeological model.

Hydrogeological model: This model consists of the hydrostructure model and the flow model. (This type of model is referred to as the descriptive hydrogeological model by SKB, e.g. see SKB 2001b and Rhén et al. 2003). The hydrostructure model is the geometrical distribution of the permeable features of the rock. It is clearly closely related to the geometrical structure of the geological bedrock model, but is not identical, and one of the modelling tasks is to describe its relationship with the geological model. The geometrical structures, including the deformation zones of the geological model, are not necessarily identical to the geometrical structure of the hydrogeological model. There is a need to introduce "hydrogeological zones" or to combine geological features into less complex hydraulic ones; nevertheless, the geometries of the two models should naturally be closely related. The groundwater simulation model with its boundary conditions and assigned hydraulic properties is called the flow model.

The ***hydrogeochemical model*** consists of a description of the groundwater composition and an assessment of the processes controlling the evolution of the groundwater composition in time and space.

Prediction/outcome studies

The adequacy of the site model is tested by making different kinds of predictions, A, B and C as the tunnel work progresses:

> Type A predictions only use the latest version of the overall Site Model.
>
> Type B predictions also use data that were not available at the time of producing the Site Model, such as results from recently completed tunnel mapping and pilot holes.
>
> Type C predictions occur after excavation and involve establishing whether the modelling methods applied could indeed have predicted the known outcome by judicious adjustment of input parameters.

Predictions concern both what will be encountered during construction of the ONKALO, such as the lithology of the rock mass and the rock mechanics properties, and the disturbance caused by the construction, such as drawdown and upconing. Clearly, strong deviations between the A, B and C predictions are reasons to update the overall Site Model, however, it may not be feasible to formulate strict criteria for determining the level of 'success' or 'failure' for all parameters. Instead a set of principles for the prediction/outcome studies have been established. It is important to understand that the objective of the studies is not to strive for exact matches or for fully-calibrated models, but to develop a prediction methodology that is sufficient with regard

to the needs of the Design work and the Safety Case. A summary of the prediction/outcome work performed, is presented in Chapter 9

Overall Confidence Assessment

The Site Descriptive Modelling is naturally associated with uncertainties and it is necessary to assess the level of confidence in the modelling. Chapter 10 assesses the overall consistency and confidence in Site Model 2006. It focuses on discussing the main issues of importance that are judged to still require further attention. A more formal audit of aspects of uncertainty, handling of data, need for alternatives, interdisciplinary consistency and changes since Site Model 2004 is also presented.

1.3 This report

The essential elements of this report have been set out in the previous section. Chapter 2 provides a brief overview of the data used for producing the Site Description. Chapters 3 to 8 present the descriptive modelling, which involves interpreting data, interpolating or extrapolating between measurement points and calibrating the model against data, based on the various assumptions made about each conceptual model. For practical reasons, the SDM is divided into the various disciplines: surface system, geology, rock mechanics, hydrogeology and hydrogeochemistry, which are presented in separate chapters. Chapter 9 presents the results of the prediction/outcome studies performed during 2005 and Chapter 10 the overall consistency and confidence assessment. Overall conclusions together with a site synthesis are provided in Chapter 11.

2 APPLIED INVESTIGATION DATA

This chapter provides a brief overview of the data collected since Site Report 2004 (Posiva 2005). The aim of this chapter is to provide traceable references to the sources of the new data collected, not present the data themselves.

2.1 Overview

Site investigations at Olkiluoto have continued very intensively at the surface since Site Report 2004 (Posiva 2005), being concentrated mainly in the ONKALO area. The investigation site to date contains 40 deep drillholes, whose main aim has been to obtain data for planning the ONKALO and also for the development of site understanding. Since the construction of the ONKALO started in autumn 2004 underground investigations have also taken place taking advantage of the shaft and drift excavation works. Geological mapping of the ONKALO tunnel has been from the start the most visible investigation method in the ONKALO. Flow measurements in probe holes also started from the beginning of construction activities, followed by pilot hole drilling and associated investigations. So far five pilot holes have been drilled and investigated and these have provided valuable information for construction purposes; pilot holes also have an important role to play in the prediction outcome studies.

Prior to the start of construction, baseline conditions were established (Posiva 2003) and in 2004 monitoring of the changes caused by construction of the ONKALO also started. The monitoring programme related to this construction (Posiva 2003) includes rock mechanical, hydrogeological and hydrogeochemical monitoring and, in addition, monitoring of the biosphere is also taking place.

2.2 Surface-based investigations

2.2.1 Geological data

Additional geological outcrop mapping was performed in the eastern part of Olkiluoto Island, the purpose of which was to collect structural geological and lithological data from new outcrops for use in the new geological model and to crosscheck the results of old outcrop mapping for consistency.

Since Site Report 2004 four additional investigation trenches have been excavated and mapped (Figure 2-1). Investigation trench OL-TK8 (Engström 2005) was excavated in the northern part of the island. In addition, in 2005, three more trenches were excavated – OL-TK9, OL-TK10 and OL-TK12. OL-TK9 was excavated in the western part of the investigation area, next to trench OL-TK3. The purpose of this new trench was to clarify the nature of the fracture zone observed during the mapping of OL-TK3 and also to obtain information concerning the seismic anomalies observed in the area. OL-TK10 was excavated in the eastern part of the island, close to the Korvensuo reservoir, for characterising the fracturing and lithology of the area. The trench is also located on the assumed location of a major fold hinge, which is seen for example in the magnetic map of Olkiluoto. OL-TK12 was excavated in the central part of the investigation area,

between trenches OL-TK4 and OL-TK2, and on the location of a strong magnetic anomaly observed in the new method-specific lineament map of Olkiluoto. The results of the mapping of OL-TK9, OL-TK10 and OL-TK12 have not been published yet and are not used in Geological model v.0.

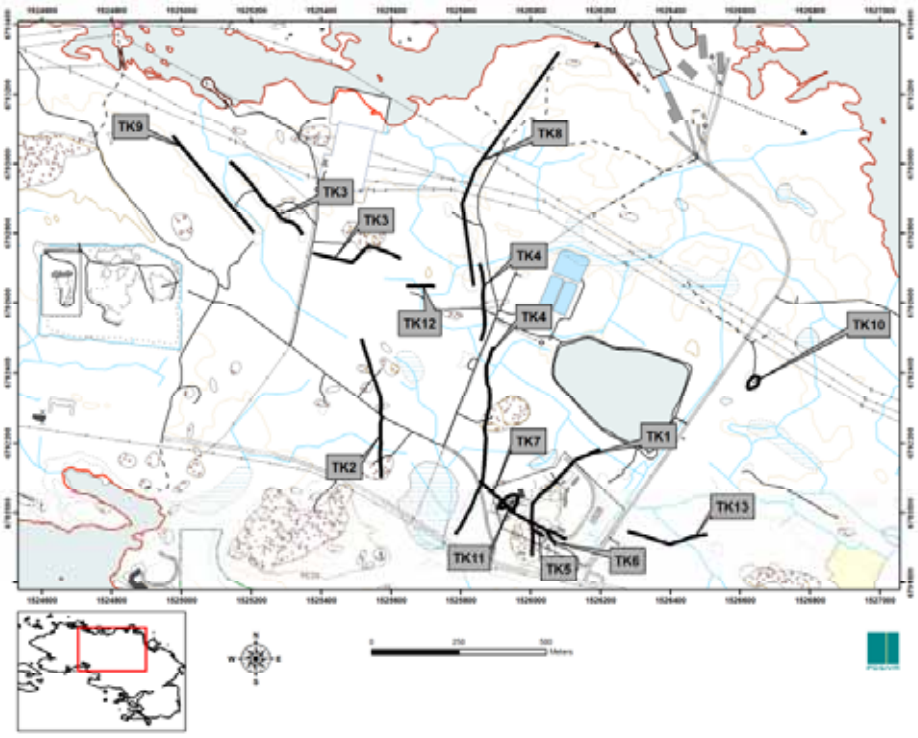

Figure 2-1. *Investigation trenches OL-TK8, OL-TK9, OL-TK10 and OL-TK12.*

There are currently 43 deep drillholes within the Olkiluoto investigation area (Figure 2-2). All drillholes except OL-KR10, OL-KR24, OL-KR38 are inclined and with depths in the range 98-1050 m. Drillholes OL-KR1-OL-KR12 have been drilled using a double core barrel, with the remainder having been drilled using a triple tube barrel, which enables better retrieval of intact core samples for mineralogical and other core studies. Since the drilling of drillhole OL-KR15, short (maximum length 40 m) B-holes have been drilled in the vicinity of the deep holes, so that drill core from the upper part of the bedrock can also be investigated in detail. The results of petrographic and mineralogical studies of the core samples from drillholes OL-KR1-OL-KR23 will be reported by Kärki & Paulamäki (2006). All drillhole data from OL-KR1 to OL-KR33 have been used in geological model v. 0 (Paulamäki et al. 2006**,** see Chapter 4).

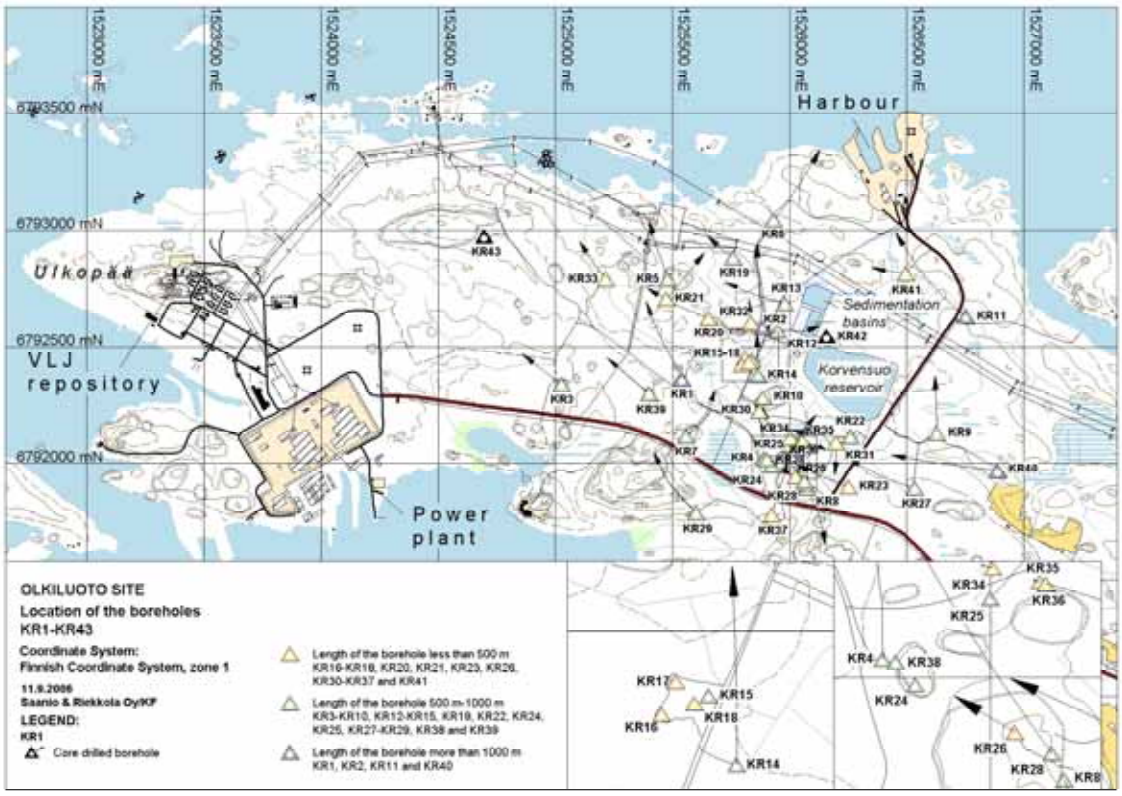

Figure 2-2. *Locations of investigation drillholes OL-KR1-OL-KR43.*

Table 2-1. *List of geological investigations carried out at Olkiluoto. References to reports containing data collected since Site Description 2004 are shown in bold.*

Investigations	References
Surface investigations	
Geology and hydrogeology on the Ulkopää site	Äikäs (1986)
Petrographic and mineralogical study at the Ulkopää site	Lindberg (1986)
Bedrock and fracture mapping	Paulamäki (1989)
Mapping of ductile structures	Paulamäki & Koistinen (1991)
Fracture mapping above the VLJ repository	Sacklén (1994)
Geological mapping of two sludge basins	Äikäs (1995)
Geological mapping of investigation trench TK1[1,2]	Paulamäki (1995)
Geological mapping of investigation trench TK2[1,2]	Paulamäki (1996)
Geological mapping of investigation trench TK3[1,2]	Lindberg & Paulamäki (2003)
Geological mapping of investigation trench TK4[1,2]	Paulamäki (2004a)
Geological mapping of investigation trenches TK5-TK6[1,2]	Paulamäki & Aaltonen (2004)
Geological mapping of investigation trench TK7[1,2]	Paulamäki (2004b)
Dating of the diabase dyke from investigation trench TK3[1,2]	Mänttäri et al. (2004)
Geological mapping of investigation trench TK11, the storage hall area	Mattila et al. (2006)
Geological mapping of the Olkiluoto 3 construction site[1,2]	**Talikka (2005) (WR 2005-32)**
Geological mapping of the ONKALO open cut[1,2]	**Talikka (2005) (WR 2005-33)**

Geological mapping of the investigation trench OL-TK8 at the Olkiluoto study site[1,2]	**Engström (2005) (WR 2005-44)**
Geological mapping of the investigation trench OL-TK9 at the Olkiluoto study site	**Nordbäck & Talikka (2006) (WR 2006-51)**
Subsurface mapping	
Engineering geological mapping of the access tunnel of the VLJ repository	Ikävalko & Niskanen (1989)
Geological mapping of the VLJ repository	Ikävalko & Äikäs (1991)
Fracture mapping of the research tunnel in the VLJ repository	Äikäs & Sacklén (1993)
Core drilling	
Shallow drillings by IVO	Imatran Voima Oy (1974), Jokinen (1990)
Drilling of deep borehole OL-KR1[1,2]	Suomen Malmi (1989a)
Shallow boreholes, PP1-PP36[1,2]	Suomen Malmi (1989b)
Drilling of deep borehole OL-KR2[1,2]	Suomen Malmi (1989c), Rautio (1995c)
Drilling of deep borehole OL-KR3[1,2]	Suomen Malmi (1989d)
Drilling of deep borehole OL-KR4[1,2]	Suomen Malmi (1990a), Rautio (1995b)
Drilling of deep borehole OL-KR5[1,2]	Suomen Malmi (1990b)
Drilling of deep borehole OL-KR6[1,2]	Rautio & With (1990), Rautio (2000b)
Drilling of deep borehole OL-KR7[1,2]	Jokinen (1994), Rautio (2000a)
Drilling of deep borehole OL-KR8[1,2]	Rautio (1995a), Niinimäki (2002g)
Drilling of deep borehole OL-KR9[1,2]	Rautio (1996b)
Drilling of deep borehole OL-KR10[1,2]	Rautio (1996a)
Drilling of deep borehole OL-KR11[1,2]	Rautio (1999)
Drilling of deep borehole OL-KR12[1,2]	Niinimäki (2000)
Drilling of deep borehole OL-KR13[1,2]	Niinimäki (2001a)
Drilling of deep borehole OL-KR14[1,2]	Niinimäki (2001b)
Drilling of deep borehole OL-KR15[1,2]	Niinimäki (2002a)
Drilling of deep borehole OL-KR16[1,2]	Niinimäki (2002b)
Drilling of deep borehole OL-KR17[1,2]	Niinimäki (2002c)
Drilling of deep borehole OL-KR18[1,2]	Niinimäki (2002d)
Drilling of deep borehole OL-KR19[1,2]	Niinimäki (2002e)
Drilling of deep borehole OL-KR20[1,2]	Niinimäki (2002f)
Drilling of deep borehole OL-KR21[1,2]	Niinimäki (2002h)
Drilling of deep borehole OL-KR22[1,2]	Niinimäki (2002i), Niinimäki (2004b)
Drilling of deep borehole OL-KR23[1,2]	Niinimäki (2002j)
Drilling of deep borehole OL-KR24[1,2]	Niinimäki (2003a)
Drilling of deep borehole OL-KR25[1,2]	Niinimäki (2003b)
Drilling of deep borehole OL-KR26[1,2]	Niinimäki (2003c)
Drilling of deep borehole OL-KR27[1,2]	Niinimäki (2003d)
Drilling of deep borehole OL-KR28[1,2]	Niinimäki (2003e)
Drilling of shallow core drilling holes, percussion drillings, video recordings of borehole and installing groundwater monitoring pipes at Olkiluoto in winter and spring of 2004	**Rautio & Niinimäki (2004) (WR 2004-37)**
Drilling of deep borehole OL-KR29[1,2]	**Rautio (2004a) (WR 2004-50)**
Drilling of deep borehole OL-KR30[1,2]	**Rautio (2004b) (WR 2004-55)**
Drilling of deep borehole OL-KR31[1,2]	**Rautio (2004c) (WR 2004-61)**
Drilling of deep borehole OL-KR32[1,2]	**Rautio (2005a) (WR 2005-01)**
Drilling of deep borehole OL-KR33[1,2]	**Rautio (2005b) (WR 2005-02)**
Drilling of deep borehole OL-KR34	**Rautio (2005c) (WR 2005-36)**
Drilling of deep borehole OL-KR35	**Rautio (2005d) (WR 2005-37)**

Drilling of deep borehole OL-KR36	**Niinimäki (2005a) (WR 2005-38)**
Drilling of deep borehole OL-KR37	**Niinimäki (2005b) (WR 2005-62)**
Drilling of deep borehole OL-KR38	**Rautio (2005e) (WR 2005-58)**
Drilling of deep borehole OL-KR39	**Niinimäki (2005c) (WR 2005-68)**
Core drilling of deep borehole OL-KR40	**Pussinen & Niinimäki (2006) (WR 2006-49)**
Core drilling of deep borehole OL-KR41	**Pussinen & Niinimäki (2006) (WR 2006-84)**
Core drilling of deep borehole OL-KR42	**Pussinen & Niinimäki (2006) (WR 2006-97)**
Core drilling of deep borehole OL-KR43	**Niinimäki (2006) (WR2006-115)**
Borehole investigations	
Petrography, lithogeochemistry and petrophysics, borehole KR1-KR5 [1,2]	Lindberg & Paananen (1991a)
Petrography, lithogeochemistry and petrophysics, borehole KR6[1,2]	Lindberg & Paananen (1992)
Dating of fracture minerals, borehole KR1	Blomqvist et al. (1992)
Petrology and low temperature fracture minerals, boreholes KR2-KR8 and KR10[1,2]	Gehör et al. (1996)
Petrology and low temperature fracture minerals, borehole KR9[1,2]	Gehör et al. (1997)
Isotopic and fluid inclusion study of fracture calcite, borehole KR1[1,2]	Blyth et al. (1998)
Petrology and low temperature fracture minerals, borehole KR11[1,2]	Gehör et al. (2000)
C, O and Sr isotopic characteristics of fracture calcites	Karhu (2000)
Petrology and low temperature fracture minerals, boreholes KR6-KR7 and KR12[1,2]	Gehör et al. (2001)
Foliation: Geological background, rock mechanics significance and preliminary investigations at Olkiluoto[1,2]	**Milnes et al. (2006) (WR 2006-03)**
U-Pb ages for tonalitic gneiss, pegmatitic granite and diabase dyke, Olkiluoto study site Eurajoki, SW Finland	**Mänttäri et al. (2006) (WR 2006-12)**
Statistical model of fractures based on data from OL-TK7, OL-TK11, OL-KR24, OL-PH1 and ONKALO PL 0-140 m[1,2]	**Tuominen et al. (2006) (WR2006-22)**
Summary reports	
Geology and hydrology of the Ulkopää Cape at Olkiluoto	Ahokas & Äikäs (1991)
Geology of the Olkiluoto area	Anttila et al. (1992)
Geological and geophysical investigations at the Olkiluoto site	Anttila & Heikkinen (1996)
Olkiluoto site report	Anttila et al. (1999)
Bedrock of southern Satakunta[1,2]	Paulamäki et al. (2002)
Baseline conditions at Olkiluoto	Posiva (2003)
Petrology of Olkiluoto[1,2]	**Kärki & Paulamäki (2006)**
Revision of the lineament interpretations of the Olkiluoto area in the light of acoustic-seismic data from adjacent marine areas	**Kuivamäki (2005) (WR 2005-16)**
Lineament interpretation of the Olkiluoto area[1,2]	**Korhonen et al. (2005) (WR 2005-34)**
Geological model of ONKALO area[1,2]	**Paananen et al. (WR 2006-13)**

[1]Used in Geological model of ONKALO area v. 0
[2]Used in Geological Site Model v. 0

2.2.2 Geophysical data

Geophysical surveys have continued in the Olkiluoto area according to the plan established in TKS-2003. All new drillholes have been surveyed by standard geophysical logging methods (magnetic susceptibility, resistivity, density, natural gamma-gamma radiation, seismic P-wave velocity, calliper and fluid logging) and drillhole imaging tool (Lahti 2004, Lahti & Heikkinen 2005, Majapuro 2005, Majapuro 2005, Majapuro 2006).

Results from geophysical 3D imaging of rock properties (VSP, magnetic, electromagnetic (Slingram, Gefinex 400S) and mise-à-la-masse (charged potential)) have been used to help both the lithological and structural modelling in both the ONKALO and Site areas. Geophysical interpretations were used in particular to investigate the continuity and orientation of several structures.

New mise-à-la-masse (charged potential) surveys were also carried out during 2005 (Lehtonen 2006) and in the beginning of 2006 (Lehtonen 2006) to produce more information concerning previously identified structures. The conductive zones followed by mise-à-la-masse surveying seem to be correlated with modelled hydrogeological features. These surveys also made it possible to establish the likely locations of outcrops of some of the major fracture zones.

A small mise-à-la-masse test survey was carried out in the ONKALO at the beginning of 2006 to determine the potential for using this method to examine the continuation of so-called long fractures (single fractures) in the tunnel, from the tunnel to the ground surface and to the drillholes near the tunnel. The results are still being evaluated, but preliminary results suggest that this method seems to work well at this scale and its use will be reported in 2006.

In drillholes OL-KR1, OL-KR4 and OL-KR27 gamma spectrometer surveys were carried out during 2005 to see whether this method could be used to define the alteration properties of the rock. The measurements are presented in two separate working reports by Julkunen & Kallio (2005), but the results are still being evaluated.

Electromagnetic soundings (Gefinex 400S) have been carried out annually since 2004 at fixed stations in the ONKALO area for monitoring possible changes in the conductivity of the bedrock (i.e. due to potential changes in the level of saline groundwater). No changes have been detected to date (Lehtimäki & Jokinen 2004 and 2005).

A refraction seismic survey was started in 2005 in the eastern extension area to help select a suitable location for a new trench (TK13). This survey was completed at the beginning of summer 2006 and the results were made available for use in autumn 2006.

Seismic VSP and single-hole surveys were carried out in 2005 to obtain more information on the area of the ONKALO access tunnel. A report of this work is in preparation (Enescu et al 2006).

Some geophysical anomalies and zones detected by geophysics exist which are not included in the new geological model (either because no geological features were

detected or because no geological information was available), or in fact in any other model. However, integrated modelling work was started in spring 2006 in order to create an "electric model" of the Olkiluoto area. All electric and electromagnetic data and models (electric soundings, slingram, mise-à-la-masse, Gefinex 400S, drillhole resistivity) will be reflected in this model and reported by the geophysical modelling team before the end of 2006.

Table 2 *List of geophysical investigations carried out at Olkiluoto. References to reports containing data collected since Site Description 2004 are shown in bold.*

Geophysical data	References
Ground surveys	Taanila 1975 Taanila & Hytti 1978 Laurila 1989 (WR 89-35)[1,2] Paananen et al. 1991 (WR 91-28)[1,2] Jokinen & Jokinen 1994 (PATU WR 94-44)[1,2] Elo 2001 (WR 2001-05) Leino 2001 (WR 2001-27) Ihalainen & Lahti 2002 (WR 2002-24)[1,2] Lahti 2002 (WR 2002-51)[1,2] Sutinen 2002 (WR 2002-52)[1,2] Ihalainen 2003 (WR 2003-12)[1,2] Lahti & Tammenmaa (WR 2003-23)[1,2] Ahokas 2003 (WR 2003-24)[1,2] Lehtimäki 2003 (WR 2003-62)[1,2] Lehtimäki 2003 (WR 2003-63)[1,2] Sutinen 2003 (WR 2003-75)[1,2] Cosma et al. 2003 (POSIVA-2003-01)[1,2] **Heikkinen et al. 2004 (WR 2004-16)**[1,2] **Lahti 2004 (WR 2004-29)**[1,2] **Lehtimäki & Jokinen 2004 (WR 2004-38)**[1,2] **Ihalainen 2005 (WR 2005-15)**[1,2] **Lehtimäki & Jokinen 2005 (WR 2005-43)**[1,2]
Drillhole geophysics	Okko et al. 1990 (WR 90-08) Okko et al. 1990 (WR 90-47) Carlsten 1996 (WR 96-03e) Okko et al. 1996 (PATU WR 96-08) Laurila & Tammenmaa 1996 (WR 96-14)[1,2] Lowit et al. 1996 (WR 96-33e)[1,2] Julkunen et al. 1996 (WR 96-41)[1,2] Carlsten 1996 (WR 96-54e)[1,2] Stråhle 1996 (WR 96-59e)[1,2] Siddans & Wild 1996 (WR 96-66e)[1,2] Front et al. 1997 (WR 97-17)[1,2] Ikävalko 1998 (WR 98-04) Heikkonen et al. 1999 (WR 99-61) Julkunen et al. 2000 (WR 2000-02)[1,2] Julkunen et al. 2000 (WR 2000-37)[1,2] Okko et al. 2000 (WR 2000-39)[1,2]

	Front et al. 2001 (WR 2001-02)[1,2] Front et al. 2001 (WR 2001-03)[1,2] Lahti et al. 2001 (WR 2001-30)[1,2] Saksa et al. 2001 (WR 2001-35) Wild et al. 2002 (WR 2002-02)[1,2] Wild et al. 2002 (WR 2002-11)[1,2] Julkunen et al. 2002 (WR 2002-32)[1,2] Lahti et al. 2003 (WR 2003-05)[1,2] Julkunen et al. 2003 (WR 2003-10)[1,2] Julkunen et al. 2003 (WR 2003-50)[1,2] Julkunen et al. 2004 (WR 2004-11)[1,2] Julkunen et al. 2004 (WR 2004-17)[1,2] Julkunen et al. 2004 (WR 2004-18)[1,2] Lahti 2004 (WR 2004-27)[1,2] Lahti 2004 (WR 2004-28)[1,2] Lahti & Heikkinen 2004 (WR 2004-43)[1,2] Heikkinen et al. 2004 (WR 2004-60) Enescu et al. 2004 (WR 2004-62 Vol.1 and 2)[1,2] **Lahti & Heikkinen 2005 (WR 2005-04)**[1,2] **Lahti 2005 (WR 2005-06)**[1,2] **Lahti & Heikkinen 2005 (WR 2005-17)**[1,2] **Majapuro 2005 (WR 2005-50)**[1,2] **Palmén et al. 2005 (WR 2005-60)** **Julkunen & Kallio 2005 (WR 2005-69)** **Majapuro 2005 (WR 2005-73)**[1,2] **Julkunen & Kallio 2005 (WR 2005-74)** **Majapuro 2006 (WR 2006-07)**
VSP (+HSP, etc.)	Cosma et al. 1996 (WR 96-11e)[1,2] Cosma et al. 1996 (WR 96-60e)[1,2] Rantataro 2001 (WR 2001-11) Kuivamäki 2002 (WR 2002-xx) Rantataro 2002 (WR 2002-38) Enescu et al. 2003 (WR 2003-13)[1,2] Enescu et al. 2004 (WR 2004-62 Vol.1)[1,2] Heikkinen et al. 2004 (WR 2004-62 Vol.2)[1,2] **Enescu et al. 2006 (to be published)**
Mise-a-la-masse	Paananen 1996 (WR 96-13)[1,2] Lahti & Laurila 2003 (WR 2003-25)[1,2] Lehtonen & Heikkinen 2004 (WR 2004-51)[1,2] **Lehtonen 2006 (WR 2006-08)**[1,2] **Lehtonen 2006 (in print)**[1,2]
Summary geophysics	Heikkinen et al. 1992 (YJT-92-34) Hinkkanen et al. 1996 (WR PATU-96-84) Anttila & Heikkinen 1996 (WR PATU-96-89)
Thermal studies	Kukkonen & Lindberg 1995 (YJT-95-08) Kukkonen & Lindberg 1998 (WR 98-09e) Kukkonen et al. 2000 (WR 2000-25) Kukkonen 2000 (WR 2000-40) Kukkonen et al. 2001 (WR 2001-23) Ilkka Suppala et al. 2004 (WR 2004-20)

Other	Heikkinen et al 1996 (WR PATU-96-09) Ikonen 1996 (WR 96-45e) Öhberg 1996 (WR 96-94) Anttila et al. 1999 (POSIVA-99-10) Ruotsalainen et al. 2000 (WR 2000-26) Paananen 2004 (WR 2004-01) Nummela 2004 (WR 2004-22)

1 Used in Geological model of ONKALO area v. 0
2 Used in Geological Site Model v. 0

2.2.3 Hydrogeological data

Determination of the surface runoff of the local catchments area has continued at four measuring weirs. The results up to 2005 are presented in Ahokas et al. (2005).

Measurement of hydraulic conductivities has taken place using the HTU (Hydraulic Testing Unit) and the DIFF (Difference flow meter). Since the Site 2004 Report DIFF measurements have been carried out systematically in all new drillholes (OL-KR29-OL-KR40). Fracture or section-specific flow into or out of the drillhole is measured with and without pumping in order to measure the transmissivity and fresh water head of hydraulically conductive fractures. Additionally, the EC of borehole water and groundwater from specific fractures can be measured, as well as the temperature of the water and the single point resistance of the borehole wall. The latest results have been reported in Pöllänen & Rouhiainen (2005a and 2005b), Pöllänen et al. 2005 and Pöllänen 2006. At the same time monitoring of flow conditions and in situ borehole and fracture-specific EC has taken place in selected drillholes (OL-KR2, OL-KR7, OL-KR8, OL-KR10, OL-KR14, OL-KR22, OL-KR22B, OL-KR27 and OL-KR28) (Pöllänen et. al 2006, Ahokas et al. 2005). Measurements with the HTU tool have been carried out in selected drillholes mainly at repository depths (i.e. below –300 m) in order to measure transmissivities, which are lower than the measuring limit of the DIFF-tool ($T < 10^{-9} m^2/s$). HTU results from drillholes OL-KR14, OL-KR15, OL-KR2 OL-KR16-OL-KR18 and OL-KR4 have been reported by Hämäläinen (2006a, 2006b, 2006c and 2006d and 2006e). The HTU tool is also used in monitoring the long period changes in water conductivity in selected borehole sections in drillholes OL-KR4, OL-KR8, OL-KR28 and OL-KR31. The results are published in Hämäläinen (2006).

Slug tests have been used to determine hydraulic conductivities in shallow drillholes and groundwater observation tubes since 2003. Every summer about 10-20 measurement points have been selected for the measurements. The results from summer 2004 have been reported by Tammisto and Hellä (2005) and those for 2005 will be published in 2007.

Long term monitoring of the groundwater table has continued regularly since Site Report 2004. The monitoring network now contains 59 shallow holes. Ahokas et al. (2005) have reported the latest results. The measurement of hydraulic heads at depth is carried out with multi-packer systems. The automatic measuring system is described in detail in the Baseline report (Posiva 2003). The following drillholes are so far equipped

with multi-packer system: OL-KR1, OL-KR3, OL-KR5, OL-KR9, OL-KR11, OL-KR12, OL-KR15-OL-KR18, OL-KR20, OL-KR23, OL-KR25 and OL-KR29, and the results from these drillholes are presented in Ahokas et al. (2005). An evaluation of the representativity of head measurements, made using different methods, is still in preparation (Ahokas et al. 2006, to be published).

It was intended to include the results from cross drillhole flow measurements, using the new TRANS-tool, but these tests have been delayed due to technical problems, and the results are not available for modelling purposes.

Table 3 *List of hydrogeological investigations carried out at Olkiluoto. References to reports containing data collected since Site Description 2004 are shown in bold.*

Investigation or analysis	Area or drillhole	Reference
Hydrological monitoring	VLJ-repository site	Öhberg & Ahokas 1991; Nykyri et al. 1994, 1995a, b; Öhberg 1996, 1997; Hakala & Öhberg 1998; Sievänen & Öhberg 1999, 2000; Hagros & Öhberg 2001, 2002, 2003, 2004
	Results of monitoring at Olkiluoto in 2004: Hydrology	**Ahokas et al. 2005 (WR 2005-28)**[1, 2]
	Monitoring measurements with HTU during year 2005, boreholes OL-KR4, KR8, KR28 and KR31	**Hämäläinen 2006 (WR 2006-23)**[1, 2]
	Monitoring measurements by difference flow logging method during the year 2005, boreholes KR2, KR4, KR10, KR14, KR22, KR22B, KR27 and KR28	**Pöllänen et al. (WR 2006-39)**[1,2] **to be published**
	Results of monitoring at Olkiluoto in 2005: Hydrology	**Tammisto et al. (WR2006-54)**[1,2]
Groundwater table and hydrogeological conditions at Ulkopää cape 1985-1987	VLJ-REPOSITORY SITE	Ahokas, 1988
Summary of results of measurements of hydraulic conductivity and differences between different methods in drillholes KR1 - KR10 at	KR1-KR10	Ahokas, H. 2001[1,2]

Olkiluoto. [1, 2]		
Hydrogeological Studies – Summary Report	Olkiluoto island	Ahokas, et al. 1997
Surface run-off	Measuring weirs MP1-MP4	Ahokas et al 2005 (WR 2005-28)
Infiltration of rain water into overburden	20 lysimeters	Haapanen 2005 (WR 2005-31) Haapanen 2006 (WR 2006-68)
Long-term monitoring of precipitation, sea level, water-table and hydraulic head in open and packed-off drillholes	In total 40 observation holes In total 28 observation holes In total 33 observation holes In total 92 observation holes	Ahokas & Herva 1993[1,2], Hänninen 1996[1,2], Lehtimäki 2001[1,2], Voipio et al. 2003[1,2]
Measurement of hydraulic conductivity by HTU-tool	OL-KR1-OL-KR5 OL-KR2, OL-KR4, OL-KR8, OL-KR10, OL-KR1 EP8 OL-KR1, OL-KR7, OL-KR10 OL-KR12 OL-KR13 **OL-KR14** **OL-KR15** **OL-KR2** **OL-KR16-OL-KR18 (including B-holes)** **OL-KR4**	Hämäläinen 1991a, b,[1,2] Kuusela-Lahtinen & Front 1991a, b, c.[1,2] Hämäläinen 1997a, b, c, d, e, 1998, 2003a,b,c, 2004a,b[1,2] **Hämäläinen 2006a (WR 2004-42)**[1,2] **Hämäläinen 2006b (WR 2005-23)**[1,2] **Hämäläinen 2006c (WR 2006-10)**[1,2] **Hämäläinen 2006d (WR2006-04)**[1,2] **Hämäläinen 2006e (WR 2006-24)**[1,2]
Measurement of hydraulic conductivity and transmissivity by DIFF-tool[1, 2]	KR1 KR6 KR1-KR4, KR7, KR8 KR9, KR10 KR11 KR6, KR7, KR12 KR1 - KR11 KR13 and KR14 KR15 KR15-KR18 and KR15B-KR18B KR1, KR2, KR4 and KR11 **KR1, KR2, KR4, KR7, KR8, KR12 and KR14** **KR19-KR28, KR19B, KR20B, KR22B, KR23B, KR27B and KR28B** **KR29-KR33 (including B-holes)** **KR34-KR39, KR37B and KR39B**	Rouhiainen 1992, 1996[1,2], Pöllänen & Rouhiainen 1996a, 1996b, 2000, 2001[1,2]. Rouhiainen, P. 2000, 2002a.c,d,e [1,2] **Pöllänen & Rouhiainen 2005a (WR 2005-51)**[1,2] **Pöllänen & Rouhiainen 2005b (WR 2005-52)**[1,2] **Pöllänen et al. 2005 (WR 2005-47)**[1,2] **Pöllänen 2006 (WR 2006-47)**[1,2] **to be published**

Measurement of hydraulic conductivity of overburden by Slug-tool	PP2, PP3, PP5, PP7, PP9, PP10, PP31, PP32, PVP3-PVP10 PP2, PP38, PP39, PVP4A, PVP4B, PVP14	Hellä & Heikkinen 2004 **Tammisto & Hellä 2005 (WR2005-76)**
Yield of shallow holes in connection with groundwater sampling	PP1-PP3, PP5, PP7-PP10, PP31, PP32, PP34, PP35, PR1-PR4 and PVP1-PVP10	Hatanpää 2002, Backman et al. 2002
Measurement of hydraulic conductivity by slug and bail tests	Multi-level piezometers EP1-EP7	Ahokas & Oksa 1992
Long-term pumping and crosshole tests[1, 2]	KR1, KR4 KR7, KR8 KR1, KR4 KR24 KR6 KR14-KR18 **KR24** **KR14-KR18 and KR15B-KR18B**	Hinkkanen et al. 1992[1,2], Ylinen & Väätäinen 1993[1,2], Niva 1996[1,2] Jääskeläinen 1998[1,2], Vaittinen & Ahokas 2004 (in prep.)[1,2], Pöllänen & Rouhiainen 2002b[1,2], Pekkanen et al. 2004[1,2], Rouhiainen & Pöllänen 2003[1,2] **Pöllänen 2006 (WR 2006-38)[1,2]** **Ahokas & Vaittinen 2005 (WR 2005-40)[1,2], Pöllänen & Rouhiainen 2005 (WR2005-49)[1,2]** **Klockars et al. 2006 (WR 2006-01)[1,2], Hämäläinen 2006 (WR 2006-02)[1,2]**
Measurement of groundwater flow across drillhole sections by transverse flow meter	KR10 KR1-KR4, KR7-KR9	Rouhiainen 1997 Pöllänen & Rouhiainen 1997
SUMMARY AND MODELLING REPORTS	Simulation of hydraulic disturbances caused by the Underground Rock Characterisation facility in Olkiluoto Simulation of hydraulic disturbances caused by the decay heat of the repository in Olkiluoto	Löfman et. al 2005 (POSIVA 2005-08) Löfman 2005 (POSIVA 2005-07)

1 Used in hydrogeological structure model in 2006
2 Used in numerical modelling of hydrogeology in 2006

2.2.4 Hydrogeochemical and microbiological data

Groundwater sampling has continued twice a year (in spring and autumn) from shallow and deep drillholes and groundwater observation tubes. Seawater has also been

regularly sampled. The results from 2004 are reported in Hirvonen (2005). The sampling programme also included microbiological studies in 2005 and 2006, the results of which have been reported in Itävaara (2005) and Pedersen (2006). Pedersen (2006) also summarises the results of microbe sampling carried out in the deep drillholes using PAVE equipment.

Several groundwater samples from open and multi-packered drillholes have been taken regularly for monitoring purposes since 2004. The results have been reported by Hirvonen et al. (2005) and by Hirvonen and Hatanpää (2005a and 2005b). The results of hydrochemical analysis derived from groundwater sampling during the long-term pumping test in drillhole OL-KR6 have been reported by Paaso et al. (2006).

In 2005 the results of dissolved gas measurements from deep drillholes were evaluated (Hatanpää et al. 2005) and the most representative data for modelling purposes were selected. Gas results were also evaluated from the physical point of view by Gascoyne (2005). Also other chemical data have been evaluated and reported by Hellä et al. (2006, to be published).

Table 2 *List of hydrogeochemical investigations carried out at Olkiluoto. References to reports containing data collected since Site Description 2004 are shown in bold.*

Hydrogeochemical data	References
Precipitation, surface water and Baltic seawater	Honkasalo 1995a (WR PATU-95-32) Honkasalo 1995b (WR PATU-95-54, no data in OIVA) Tuominen 1994 (WR PATU-94-35) Tuominen 1995 (WR PATU-95-17, no data in OIVA) Paaso 2003 (WR 2003-18)
Shallow drillholes and groundwater observation tubes in overburden	Kröger 2004 (WR 2004-44) Backman et al. 2002 (WR 2002-41) Hatanpää 2002 (WR 2002-20) Hirvonen 2005 (WR 2005-57) Honkasalo 1995c (WR PATU-95-66) Tuominen 1998 (WR 98-07)
Groundwater sampling in deep drillholes	Helenius et al. 1998 (WR 98-23) Hirvonen et al. 2004a (WR 2004-19) Hirvonen et al. 2004b (WR 2004-34) Hirvonen et al. 2005 (WR 2005-77) Hirvonen & Hatanpää 2005a (WR 2005-75) Hirvonen & Hatanpää 2005b (WR 2005-80) Honkasalo 1995b (WR PATU-95-54, no data in OIVA) Karttunen et al. 1999 (WR 99-70) Karttunen et al. 2000a (WR 2000-47) Karttunen & Mäntynen 2001 (WR 2001-26) Kröger et al. 2004 (WR 2004-68) Kröger et al. 2003 (WR 2003-33) Paaso et al. 2003a (WR 2003-20) Paaso et al. 2003b (WR 2003-34) Paaso & Mäntynen 2002 (WR 2002-15) **Paaso et al. (2006) (WR 2006-11)**

	Rantanen et al. 2002 (WR 2002-19) Ruotsalainen & Alhonmäki-Aalonen 1996 (WR PATU-96-81) Snellman 1996 (WR PATU-96-21) Snellman et al. 1995a (WR PATU-95-57) Snellman et al. 1995b (WR PATU-95-77) Tuominen 1995 (WR PATU-95-17, no data in OIVA)
In situ electrical conductivity (EC) measurements in deep drillholes	Pöllänen & Rouhiainen 1996a (WR PATU-96-43e) Pöllänen & Rouhiainen 1996b (WR PATU-96-44e) Pöllänen & Rouhiainen 2000 (WR 2000-38) Pöllänen & Rouhiainen 2001 (WR 2000-51) Pöllanen & Rouhiainen 2002a (WR 2001-42) Pöllänen & Rouhiainen 2002c (WR 2000-29) Pöllänen & Rouhiainen 2002d (WR 2000-42) Pöllänen & Rouhiainen 2002e (WR 2002-43) Rouhiainen 2000 (WR99-72)
Summary and modelling reports etc.	Anttila et al. 1999 (POSIVA-99-10) Gascoyne 2000 (WR 2000-49) Gascoyne 2005 (WR 2005-56) Hatanpää et al. 2005 (WR2005-55) Hirvonen et al. 2005 (WR 2005-77) **Hirvonen et al. 2006 (WR 2006-67)** **Itävaara et al. 2005 (WR 2005-65)** Karttunen 2000 (WR 2000-34) Karttunen et al. 2000b (WR 2000-50) Lampén & Snellman 1993 (YJT-93-14) Luukkonen et al. 2005 (WR 2005-72) Luukkonen 2006 (WR 2006-) Mäntynen 2005 (WR 2005-29) Palmén & Hellä 2003 (WR 2003-19) Pedersen (2005) (WR 2006-09) Pitkänen et al. 1996 (POSIVA-96-04) Pitkänen et al. 1999 (POSIVA-98-10) Pitkänen et al. 2004 (POSIVA-2003-07) **Pitkänen et al. 2007 (**to be published**)** **Pitkänen & Partamies 2007 (to be published)** Posiva Oy 2003 (POSIVA-2003-02) Ruotsalainen & Snellman 1996 (WR PATU-96-91E) Snellman 1995 (WR PATU-95-18)

1 Used in geochemical modelling in 2006

2.2.5 Rock Mechanics Data

Descriptions of all the methods used to date in the rock mechanics studies are presented in Posiva (2005). Most of the measurements will in future be conducted from the ONKALO, so little has occurred in the site investigation programme since the Olkiluoto Site Description 2004 (Posiva 2005) (Table 2-5). The main data for rock mechanics modelling are collected during the mapping of the drillhole core and the ONKALO tunnel (see Sections 2.2.1 and 2.3).

2.2.5.1 Rock stress

Rock stress measurements have not been carried out since 2003; however, these will resume in the ONKALO in 2006, where it is possible to use the overcoring method in relatively short boreholes. Studies on estimating rock stresses by making use of the Kaiser Effect have been published by Lehtonen (2005), using core samples taken from about 80 m and 500 m depth in borehole OL-KR14 (Figure 2-3). A methodology for the interpretation of overcoring stress measurement data in anisotropic rock was also developed (Hakala & Sjöberg 2006).

The Kaiser effect is a phenomenon that can be used to indicate the previous maximum stress level of the specimen from the acoustic emission signatures of the rock under compressive loading. KE is detected as a rapid intensification of acoustic emission during loading at a certain stress level, which is taken as the normal component of in situ stress in the direction of the specimen axis. The three-dimensional nature of stress is addressed by re-sampling the original sample in at least six independent directions, which enables the calculation of a full stress tensor. A detailed description of the method is presented in Lehtonen (2005).

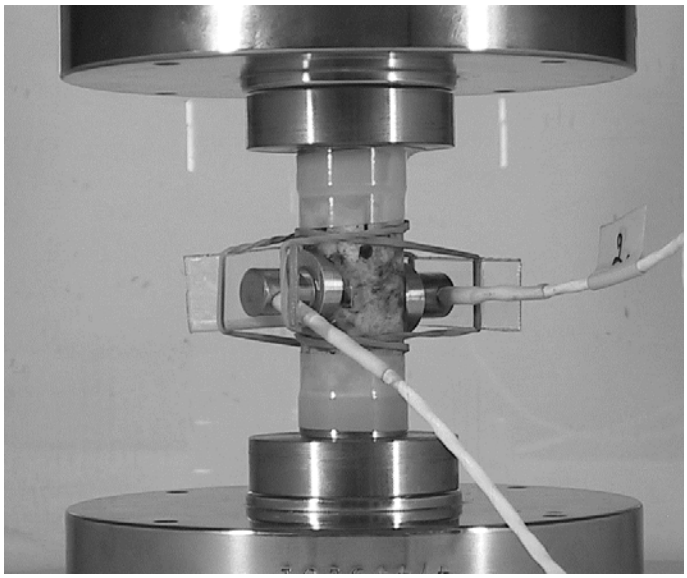

Figure 3 *A KE specimen from a depth of approximately 500 m, tested without extensometers.*

Also, the old overcoring data from OL-KR10 was reanalysed using the transient strain analysis code reported in Hakala (2006). The initial idea is to interpret the in situ state of stress based on early strains, when the core damage potential is low. The code can handle both isotropic and transversely isotropic rock conditions.

2.2.5.2 Intact rock mechanics properties

The mechanical properties of intact rocks at Olkiluoto, which are initially being considered, are the deformation properties and the critical stress state. The mechanical

properties have been studied by carrying out field loading tests with a portable test unit, by point load testing (Pohjanperä et al. 2005) and by conducting tests in the laboratory. Since Site Report 2004, additional laboratory tests have been conducted in borehole OL-KR24 (Eloranta 2006). The work also included tests to determine anisotropic rock properties.

Additional field tests have been performed in surface boreholes OL-K29-40 and in the ONKALO pilot holes OL-PH1 and ONK-PH2. Also, a programme of point load testing was conducted in boreholes OL-KR1 and OL-KR12, initially to determine the strength properties of the altered rocks (due mainly to pervasive illitisation).

All the previous mechanical test results have been revisited to ensure the rock type names are in agreement with those used in the new lithological model.

The results show that the anisotropy of the rocks at Olkiluoto has an effect on their strength, so further studies are required to establish the effect of orientation on strength. The elastic modulus and strength anisotropy of migmatitic gneisses have been studied (Hakala et al. 2005) and the overall significance of foliation in rock mechanics has also been evaluated by Milnes et al. (2006). Work has also taken place to investigate which rock mechanical properties can be estimated from a knowledge of the geological environment of the Olkiluoto area (Hudson & Cosgrove 2006).

2.2.5.3 Thermal properties of intact rock

Development work on the TERO borehole logging device has continued. The first test measurements in a borehole took place in OL-KR2 and the results compared with the laboratory measurements (Kukkonen et al. 2005). The new TERO76 (for 76 mm boreholes) has also been recently constructed and test measurements have been conducted in borehole OL-KR14.

2.2.5.4 Microseismic and GPS monitoring

Microseismic (MS) and GPS monitoring of the Olkiluoto bedrock has continued and GPS monitoring networks have been expanded (Ahola et al. 2005) - the microseismic network contains 14 stations (Figure 2-4) and the GPS 12 stations (Figure 2-5). The results from both of the monitoring networks have so far shown no unexpected observations (Riikonen 2005).

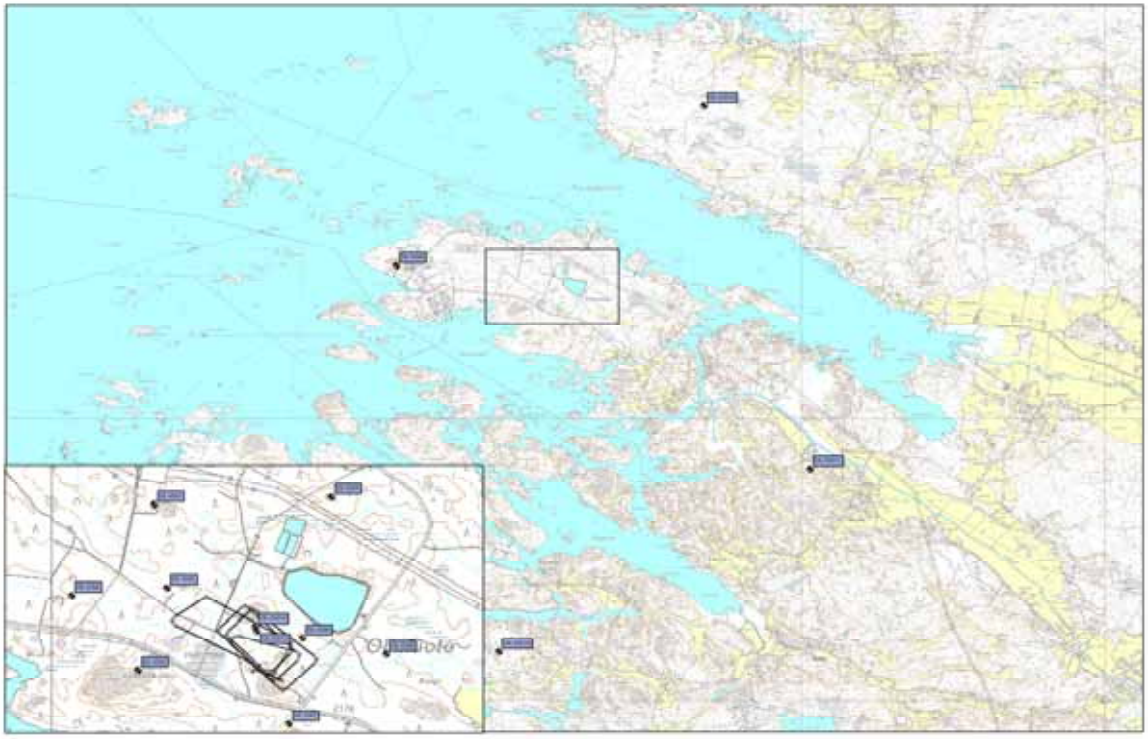

Figure 2 *The microseismic monitoring network at Olkiluoto.*

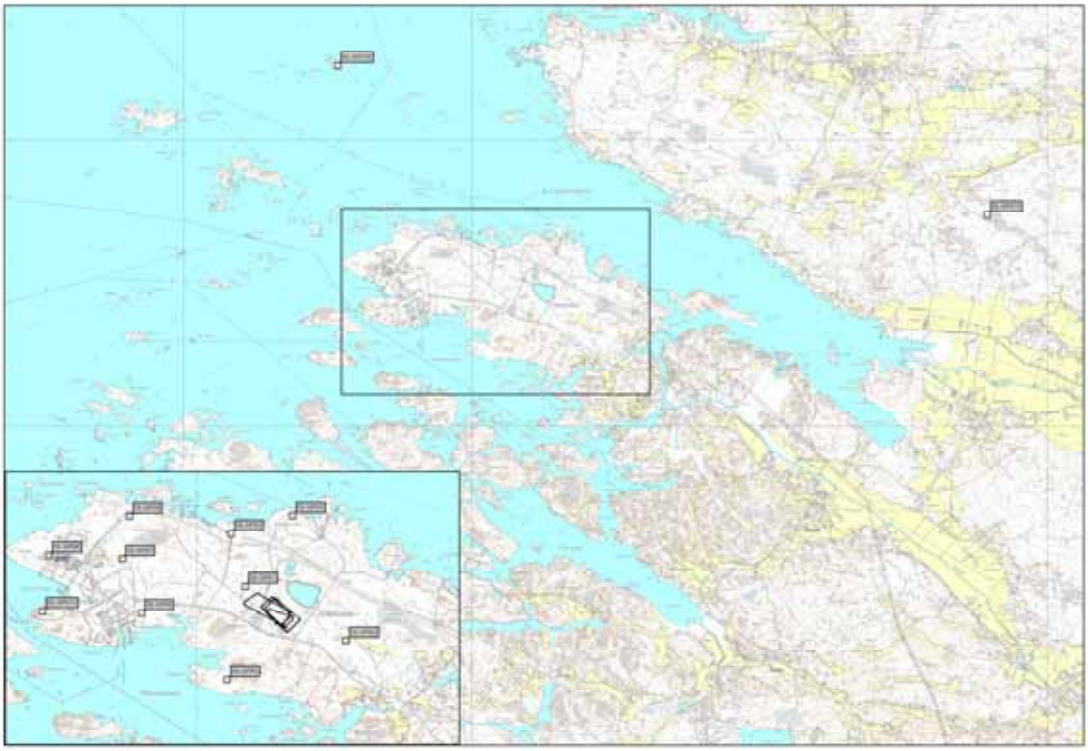

Figure 3 *GPS monitoring network at Olkiluoto.*

The thermal properties of the bedrock have now been studied with the in situ borehole logging device, TERO. The first test measurements were performed in drillhole OL-KR2 and the results are promising in comparison with the laboratory results on core samples (Kukkonen et al. 2005). Development of the TERO equipment will continue.

Table 3 *List of rock mechanics investigations carried out at Olkiluoto. References to reports containing data collected since Site Description 2004 are shown in bold.*

Investigations	References
Rock Stress measurements	Klasson & Lejon 1990 (YJT-90-18) Ljunggren & Klasson 1996 (PATU-96-26e) Malmlund & Johansson 2002 (WR 2002-47) Sjöberg 2003 (WR 2003-60) **Geological Survey of Finland 2005 (Report P 34.4.042)** **Lehtonen 2005 (WR 2005-67)** **Hakala 2006 (POSIVA 2006-03)** **Hakala & Sjöberg (WR 2006-99)**
Mechanical properties of the intact rock	Matikainen & Simonen 1992 (TVO WR 92-36) Kuula 1994 (TEKA-94-13) Johansson & Autio 1995 (TEKA-95-19) Tolppanen et al. 1995 (YJT-95-11) Hakala & Heikkilä 1997a (POSIVA-97-04) Hakala & Heikkilä 1997b (POSIVA-97-07e) Wanne 2002 (POSIVA 2002-05) **Pohjanperä et al. 2005 (WR 2005-59)** **Hakala et al. 2005 (WR 2005-61)** **Eloranta 2006 (WR 2006-80)**
Thermal properties of the intact rock	Kjorholt 1992 (TVO WR 92-56) Kukkonen & Lindberg 1995 (YJT-95-08) Kukkonen & Lindberg 1998 (WR 98-09e) Kukkonen 2000 (WR 2000-40) Kukkonen & Suppala 1999 (POSIVA 99-01) Kukkonen et al. 2000 (WR 2000-25) Kukkonen et al. 2001 (WR 2001-23) Huotari & Kukkonen 2004 WR 2004-04) Suppala et al. 2004 (WR 2004-20) **Kukkonen et al. 2005 (WR 2005-09)**
Mechanical properties of fractures	Kuula & Johansson 1991 (YJT-91-03) Hakala et al. 1993 (YJT-93-06) Rautakorpi et al. 2003 (WR 2003-09)
Mechanical properties of deformation zones	Äikäs et al. 2000 (POSIVA 2000-08)
Mechanical properties of the rock mass	Geotek 1975 (IVO Work no. 6119) Geotek 1978 (IVO Work no. 6154) Äikäs et al. 2000 (POSIVA 2000-08) Ihalainen & Lahti 2002 (WR 2002-24) Ihalainen 2003 (WR 2003-12) Lehtimäki 2003a (WR 2003-62)

	Lehtimäki 2003b (WR 2003-63) Cosma et al. 2003 (POSIVA 2003-01) Enescu et al. 2003 (WR 2003-13) Enescu et al. 2004 (WR 2004-62) Heikkinen et al. 2004 (WR 2004-16)
MS and GPS and surface levelling measurements	Chen & Kakkuri 1994 (YJT-94-02) Chen & Kakkuri 1995 (PATU-95-30e) Saari 2003 (WR 2003-37) Ollikainen et al. 2004 (WR 2004-12) Lehmuskoski 2004 (WR 2004-07) **Riikonen 2005 (WR 2005-30)** **Ahola et al. 2005 (WR 2005-41)** **Saari 2005 (WR 2005-48)**
Geological information and rock mechanics properties	**Milnes et al. 2006 (WR 2006-03)** **Hudson & Cosgrove 2006 (WR 2006-14)** **Hudson & Johansson 2006 (POSIVA 2006-04)**

2.3 ONKALO-based investigations

Excavation of the ONKALO started in September 2004 at Olkiluoto. The ONKALO is needed for the detailed site investigations to ensure that the rock quality and hydrogeological, geochemical and rock mechanical properties of the rock at the Olkiluoto are suitable for repository development The length of the ONKALO tunnel was 990 m at the end of 2005 and it has a designed gradient of 1:10.

2.3.1 Geological mapping

Geological mapping of the tunnel roof and walls took place from the outset of tunnel construction and is currently carried out in two stages and in two or three working shifts. Before 2005, mapping was carried out in three shifts and the first stage of the mapping was carried out immediately after excavation – a process that also included mapping of the tunnel face. At the beginning of 2005 the first stage mapping procedure was changed so that only basic information about rock quality, mainly for rock support and injection planning, was to be collected from the roof and walls of the previous round. The associated systematic mapping follows the construction work about 100 to 200 m behind the tunnel face. During this mapping procedure the rock is investigated more carefully and this is actually the real rock investigation phase; and the list of parameters which are mapped is presented in Table 2-6. The data are used for planning rock reinforcement, for geological and rock mechanical modelling and also for prediction-outcome studies. Initially, the mapping data are checked, approved and saved in Kronodoc and then subsequently transferred to the POTTI database. Mapping data are being reported as memos and will be published later in a Posiva Working Report series. Mapping data from chainages 0- 570 was used in the Geological Model v.0.

Table 2-6 *Mapping parameters of the round mapping (1st stage mapping) and systematic mapping (2nd stage mapping).*

1st stage – round mapping	**2nd stage – systematic mapping**
Chainage Rock type Grain size Rock Quality Designation (RQD) Joint set number (J_n) Fracturing 10-20 main fractures Length over 1 metre Orientation (dip and dip direction) Joint roughness number (J_r) Joint alteration number (J_a) Rock type Joint water reduction factor (J_w) Stress reduction factor (SRF) Provisional appraisal of rock quality	Chainage, tunnel direction and gradient Rock Quality Designation (RQD) Joint set number (J_n) Rock types Fracturing All natural fractures (>0 cm) Orientation Length, joint roughness (J_r), joint alteration (J_a), fillings, filling thickness, aperture, terminations, undulation, rock type and water leakages. Foliation Orientation Type and intensity Fold, fold axis, axial planes, lineations and faults Orientation Fault kinematics Weathering and water leakages Intersection mapping Sketch of mapped area, which includes among the others fracturing, lithological contacts

2.3.2 Pilot holes

Altogether five pilot holes (OL-PH1 and ONK-PH2-ONK-PH5) have been drilled into the tunnel profile (Table 2-7) and core logging and flow measurements using the Posiva Flow Log have been carried out. ONK-PH3, ONK-PH4 and ONK-PH5 were all planned to intersect some major water conductive features in the upper part of the bedrock. In ONK-PH3 only small fractures were found and the total water leakages from the hole was about 10 L/min. Both ONK-PH4 and ONK-PH5 intersected water conductive fractures with high flow rates, about 70 L/min and 180 L/min respectively. The high flow in ONK-PH5 prevented all other drillhole investigations, except flow measurements and groundwater sampling. The drilling of the pilot holes has provided important information to the tunnelers about the quality of the rock and the flow conditions in advance of the tunnel face, but these drillholes have also provided important information to site modelling teams and to the prediction/outcome studies. The results have been reported in several Working Reports (Niinimäki 2004, Rouhiainen et al. 2005, Julkunen et al. 2004, Öhberg et al. 2005, Öhberg et al. 2006a, Öhberg et al. 2006b, Öhberg et al. 2006c).

Table 2-7. *Information of the pilot holes OL-PH1 and ONK-PH2-ONK-PH5.*

Pilot hole	Chainages (m)	Length of pilot hole (m)	Investigations performed	References
OL-PH1	0-137	160	Standard Geophysical measurements, flow measurements	Niinimäki 2004 (WR 2004-41), Rouhiainen et al. 2005 (WR 2005-18) Julkunen et al. 2004 (WR-2004-11) Lahti & Heikkinen 2004 (WR 2004-43)
ONK-PH2	135-257	122	Standard Geophysical measurements, flow measurements, hydrogeochemical sampling	Öhberg et al. 2005 (WR 2005-63) Lahti & Heikkinen 2004 (WR 2005-04)
ONK-PH3	696-841	145	Standard Geophysical measurements, flow measurements, pressure build up test, water injection test (water loss test- Lugeon test), hydrogeochemical sampling	Öhberg et al. 2006a (WR 2006-20)
ONK-PH4	874-970	96	Standard Geophysical measurements, flow measurements, pressure build up test, water injection test (water loss test- Lugeon test), hydrogeochemical sampling	Öhberg et al. 2006b (WR 2006-71)
ONK-PH5	990-1192	202	Flow measurements, hydrogeochemical sampling	Öhberg et al. 2006c (WR 2006-72)

2.3.3 Rock mechanics data

This section provides a brief overview of the new rock mechanics data obtained from the ONKALO since Site Report 2004. The data themselves are presented in Section 5.4, since they relate to the modelling activities.

2.3.3.1 Mechanical properties of fractures

The mechanical properties of fractures have been estimated, based on the rock engineering tunnel mapping (Q-system) in the ONKALO.

2.3.3.2 Mechanical properties of brittle deformation zones

The mechanical properties of the deformation zones have also been estimated, based on the rock engineering classification (Q-system) in the ONKALO in the locations where

the tunnel has penetrated such zones. A photographic record of the deformation zones intersected by the boreholes has also been established.

One of the important rock mass features requiring rock mechanics characterization is the brittle deformation zones – because they are major discontinuities and hence weaknesses in the rock mass continuum. The brittle deformation zones have been encountered in the site investigation boreholes and, with the progressive excavation of the ONKALO, can now be studied in more detail in the ONKALO ramp. The intersections in the first 0-140 m of the ramp are shown in Figure 2-6 and an example intersection is illustrated in Figure 2-7.

As reported by Kemppainen et al. (2006), the zone illustrated in Figure 2-7 consists of multiple undulating slickensided fault planes with a dominant orientation of 87°/271°. The intersection is visible across the whole tunnel and has a trace length of approximately 15 m. The width of the zone varies from 10 cm to 80 cm and the fault planes/fractures are greenish, chlorite- and graphite-bearing slickensided surfaces.

The photograph in Figure 2-7 illustrates the significant advantage of having 'man access' to the brittle deformation zones for the purposes of rock mechanics characterization. In addition, there are photographs of all the site investigation brittle deformation zone intersections, together with the associated geological descriptions. Moreover, the site investigation cores are currently being re-logged and the Q′ values for the brittle deformation zones will become available in due course. All these data will be used in developing a methodology for rock mechanics characterization of the brittle deformation zones.

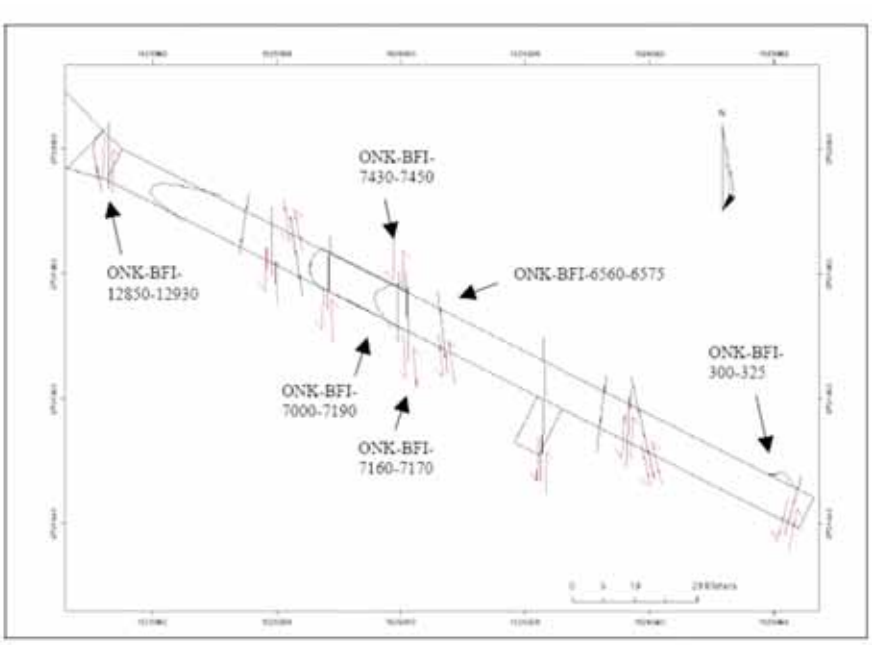

Figure 2-6. *Brittle deformation zone intersections in the first 140 m of the ONKALO ramp (from Geological Outcome from the ONKALO Underground Research Facility, Chainage 0-140. Memo from Kemppainen K, Engström J, Talikka M, Mattila J., 2006).*

Figure 2-7. *Brittle deformation zone intersection ONK-BFI-6560-6575, see Figure 2-6 for the location of this intersection (from Geological Outcome from the ONKALO Underground Research Facility, Chainage 0-140. Memo by Kemppainen K, Engström J, Talikka M, Mattila J., 2006).*

2.3.3.3 Mechanical properties of the rock mass

The mechanical properties of the rock mass have also been estimated based on the rock engineering classification (Q-system) in the ONKALO. Seismic velocity measurement data have also been used to evaluate the rock mass deformation modulus.

2.3.3.4 Impact of excavation

Data on the impact of the excavation have been received from the first 1000 m tunnel chainage of the ONKALO construction, as part of the prediction-outcome studies (see Chapter 9).

2.3.4 Hydraulic data

Systematic mapping of the inflow to the ONKALO started in summer 2005. All inflow points have been mapped and the amount of inflow has been measured whenever possible. Also groundwater sampling from the inflow points has been performed, always when the flow has been high enough for sampling. All new inflow points have been mapped every second month. Once a year the whole tunnel will be mapped to monitor the changes in inflow points. The first results from mapping will be reported in 2006 (Lehtinen 2006).

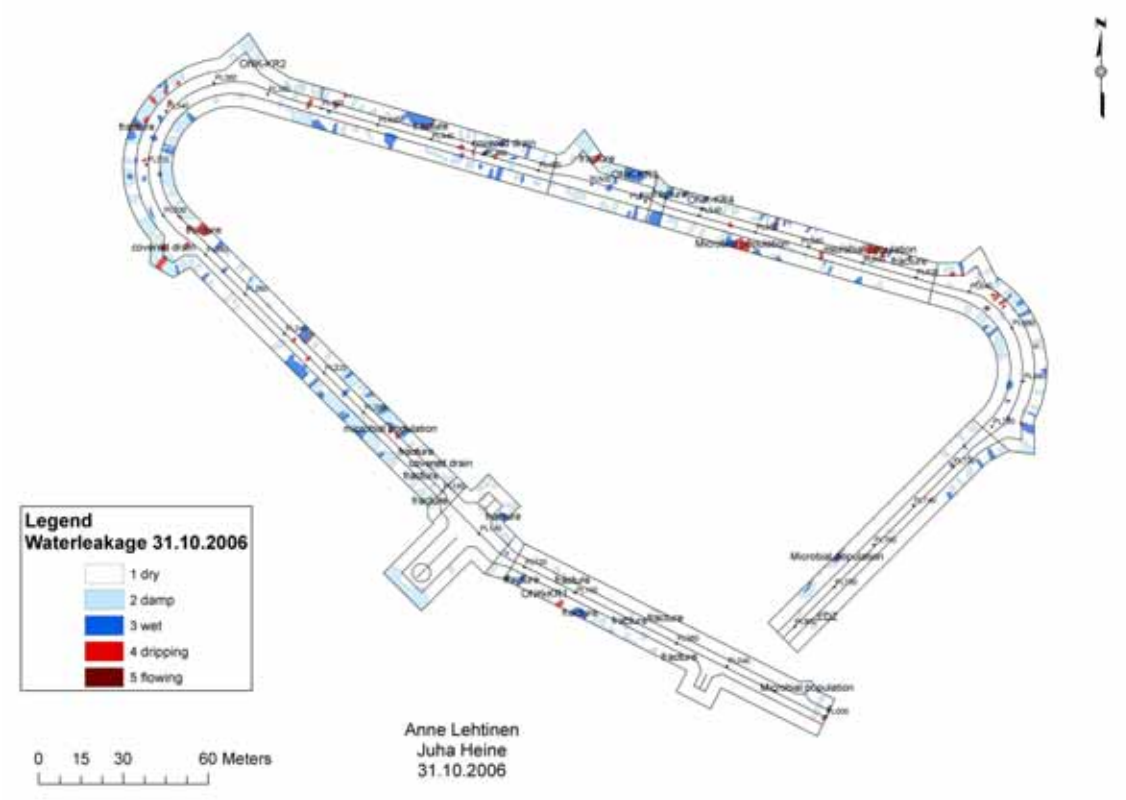
Legend
Waterleakage 31.10.2006
1 dry
2 damp
3 wet
4 dripping
5 flowing
0 15 30 60 Meters
Anne Lehtinen
Juha Heine
31.10.2006

a)

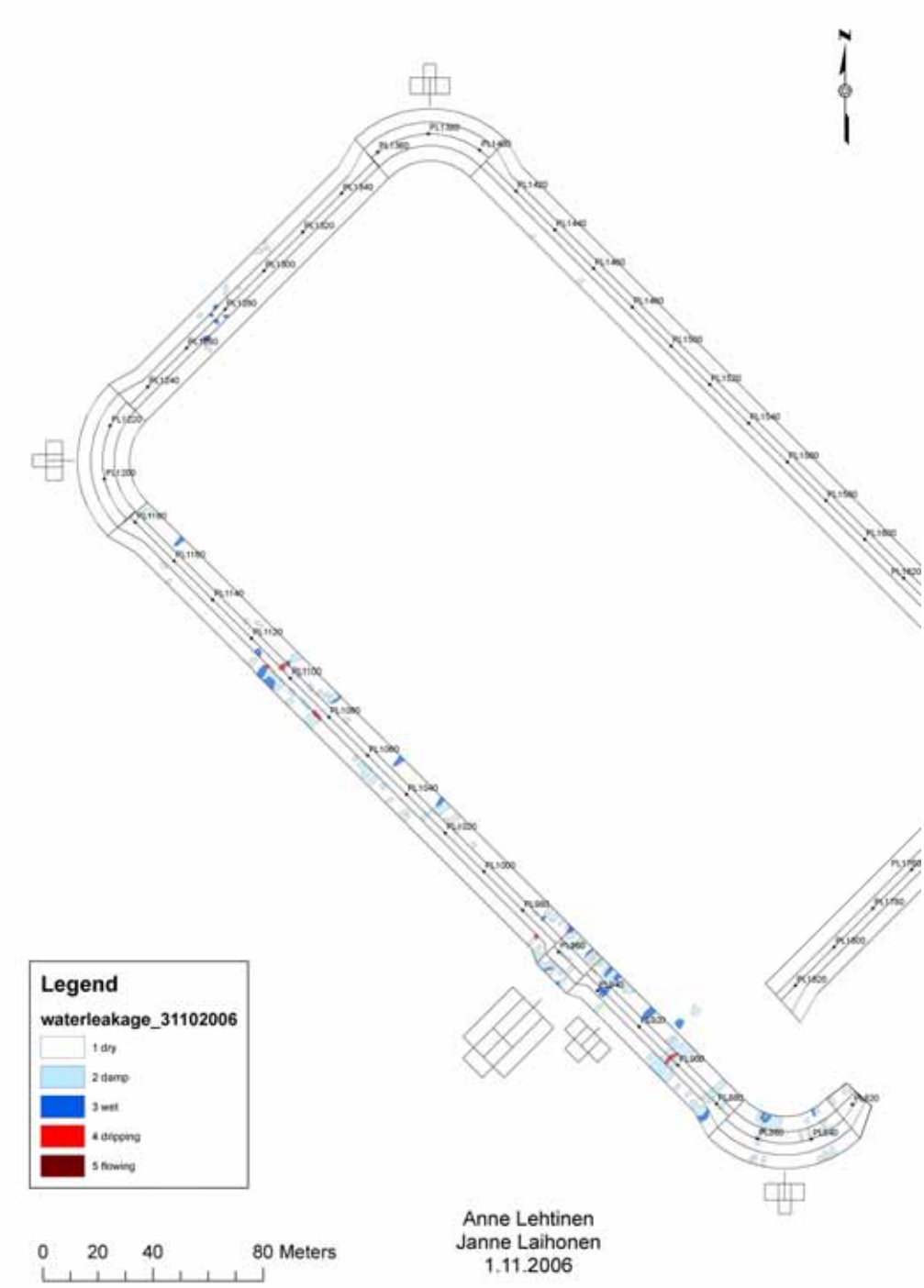

(b)

Figure 2-8. *Results of the inflow mapping carried out in October 2006 a) chainages 0-900 and b) 900-1503.*

Flow measurements from the probe holes also started in autumn 2004. All probe holes, which have been leaking have been measured after water injection tests. The results have been used in the injection planning and later they will be used in the

hydrogeological modelling. Results has been saved into the Kronodoc and they will be reported later in Posiva Working Report series.

The first groundwater station (ONK-PVA1) was installed for regular groundwater monitoring at chainage 200 which is at a depth of approximately 25 m. A second groundwater station (ONK-PVA2) has been drilled to chainage 727.5, which is at approximately 75 m depth. The first monitoring results will be reported in the monitoring report in summer 2006 (Lehtinen et al 2006). The first measuring weir was also installed at chainage 580 for total inflow measurements.

In 2005 EDZ studies started in the ONKALO tunnel. Altogether about 60 drillholes were drilled to the tunnel floor and walls and the cores were investigated in detail by geologists. The results will be reported in 2007.

3 SURFACE CONDITIONS

Previous summaries of surface conditions at Olkiluoto are presented in the Baseline report (Posiva 2003) and in the Site Description 2004 (Posiva 2005). This report presents a concise summary of the most recent studies, together with a summary of the information presented in the previous reports. The first comprehensive Biosphere Site Description report is currently being compiled as part of the Safety Case documentation (Vieno & Ikonen 2005).

Formally, the surface conditions are not within the remit of the Olkiluoto Modelling Task Force, which is concentrating on modelling the bedrock around the ONKALO and the future repository. The influence of the surface conditions on the overall system and on the conditions at depth is recognised, however, and thus a summary of climate, ecosystems and overburden properties is also included in this report.

3.1 Climate and meteorology

Currently Olkiluoto has a continental climate, with some local marine influence due to its location on the eastern coast of the Bothnian Sea, which is in the northern part of the Baltic Sea. In spring, the presence of the sea lowers temperatures somewhat compared with those inland, and correspondingly in the autumn provides warmth, so that night frosts are less frequent. The long-term statistics for Olkiluoto and the reference sites are given in Table 3-1 and Figure 3-1 (Ikonen 2007).

3.1.1 Weather statistics

These weather data have been recorded at the power plant weather mast at the western end of the island, 2-3 km from the central investigation area. In June 2004, a 20 m weather mast was erected in the southern central part of the island to provide data closer to the site investigation area and also within the forested area, sheltered from the direct influence of the sea by the highest hills on the island. Comparison of the observations between these two stations for 2005 is discussed in (Ikonen 2007) but the brevity of the time series has not allowed computation of the climate statistics.

Table 3-1. *Long-term average temperature, annual precipitation and average wind speed at Olkiluoto (1992-2005), at Kuuskajaskari Island 13 km SSW (1971-1995) and at Pori airport 30 km NE (1971-2000) (Drebs et al. 2002, Ikonen 2007).*

	Olkiluoto 1992-2005	Kuuskajaskari 1971-1995	Pori airport 1971-2000
Average temperature	5.8 °C	5.1 °C	4.8 °C
- coldest month	-4.2 °C (Feb)	-5.0 °C (Feb)	-5.6 °C (Feb)
- warmest month	17.1 °C (Jul)	15.9 °C (Jul)	16.3 °C (Jul)
Annual precipitation	517 mm	559 mm	578 mm
Prevailing wind direction	S	SE-S-SW	SE
Average wind speed	4.0 m/s	5.5 m/s	4.2 m/s

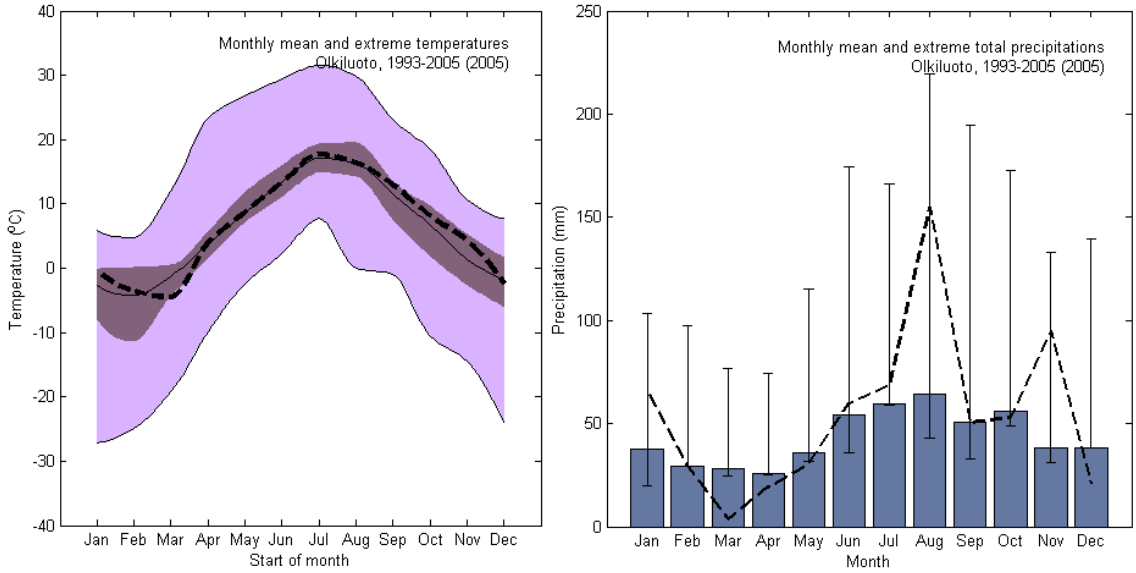

Figure 3-1. *Monthly mean and extreme temperatures (left) and monthly total precipitation (right) at Olkiluoto for the period of 1993-2005. Solid lines in the middle represents the average over the period and dashed lines are values for 2005. The darker area shows the range between average minima and maxima temperatures, and the outermost lines represent the extreme temperatures of each month during the period. In the right-hand side the columns represent the average monthly precipitation sum and the extremes over the period are shown with "error bars" (Ikonen 2007).*

3.1.2 Snow cover and ground frost

The thickness of snow cover and its water content at Olkiluoto have been measured regularly since 1990. The snow cover is usually less (less than 20 cm snow and 40 mm of water content) than at the closest reference sites (20 cm, Leinonen 2001), and the amount of snow varies during winter, with temperatures fluctuating around 0°C (Ikonen 2007).

Ground frost measurements started at Olkiluoto in December 2001. In the most recent five winters the base of the frost layer has been, at most, at a depth of 10 to 70 cm, depending on the openness and soil type at the measurement point, and at a depth less than some tens of centimetres at forested points with thick snow cover. The period with ground frost has been from December/January to April/early May (Ikonen 2007).

3.1.3 Deposition

The main chemical characteristics of precipitation, and wet deposition, have been monitored since June 2003 with a network of rainwater collectors, replaced with snow collectors during the winter (Raitio et al. 2007). The results of deposition monitoring, presented as averages, are presented for 2004 in Table 3-2, separately for open and forested terrain, and are discussed further, for example, in Haapanen (2005). The effect of the forest canopy can be clearly seen, and is in agreement with common forest processes; for example the interception fraction of annual precipitation has varied

between 20 and 43% depending on the stand and the year, being about 33% averaged over all monitoring plots and years 2004-2005 (Haapanen 2006).

Table 3-2. *Annual average results of wet deposition monitoring in open and forested terrain at Olkiluoto in 2005 and 2004 (in parenthesis) and at two other intensive forest monitoring plots in southern Finland (1998-2000) (Haapanen 2006).*

Parameter	Olkiluoto Open terrain	Olkiluoto Forest	Reference areas Open terrain	Reference areas Forest
pH	5.3 (5.1)	5.1 (5.0)	4.9	4.8
DOC (mg/m²/a)	823 (1188)	3699 (5025)	1517	5567
N_{tot} (mg/m²/a)	341 (361)	289 (262)	395	322
NH_4-N (mg/m²/a)	135 (123)	52 (51)	163	76
NO_3-N (mg/m²/a)	148 (171)	147 (105)	196	154
Ca (mg/m²/a)	159 (186)	252 (229)	71	190
Mg (mg/m²/a)	44 (75)	99 (88)	20	61
K (mg/m²/a)	88 (178)	595 (782)	42	412
Na (mg/m²/a)	182 (318)	386 (460)	136	218
SO_4-S (mg/m²/a)	158 (212)	243 (269)	247	287
Cl (mg/m²/a)	285 (460)	680 (787)	159	301

The nuclear power plant has monitored radioactivity in the environment since the 1970s. Radionuclide concentrations in direct wet deposition at Olkiluoto over recent years have been low: however, some traces of Chernobyl-derived Cs-137 are still detectable (Haapanen 2005, 2006).

On the basis of sampling in 1989-1995, the isotopic contents of H-2 and O-18 in precipitation display some seasonal variation, both being lower in winter than in summer; for example the range of $\delta^{18}O$ of annual precipitation has been –17‰ to –8‰ in snow to rain (Posiva 2003a, p. 153). A national three-year sampling programme for these isotopes in precipitation and in shallow groundwater was launched by the Geological Survey of Finland in January 2005, and Posiva provides it with regular samples collected above the ONKALO. The results are due to be reported at the end of the study.

3.2 Ecosystems and land-use

Olkiluoto Island is relatively flat and is covered by forest and shoreline vegetation which is typical of such an island in southwestern Finland. However, there are also several current construction projects, most prominently the ONKALO and the new nuclear power reactor.

3.2.1 Land-use in Olkiluoto

The western part of the island is occupied by a nuclear power plant (NPP) with its auxiliary facilities, and a new unit is currently under construction. In the central part of the island there is a site for rock storage and crushing (which serves the construction of the power plant and the excavation of the ONKALO), Posiva's main site investigation area and, of course, the ONKALO excavation site itself with its support facilities. In the

southern part of the island there is a nature conservation area consisting of old forest. The eastern part of the island consists largely of privately-owned forest, summer cottages and an area for small-scale agriculture. The different areas of land use for Olkiluoto Island are shown in Figure 3-2.

Development on the island can be followed with the help of aerial images, which so far have been taken in May 2002, May 2003, July 2004, May 2005 and June 2006; and which are to be followed by one which is scheduled for spring/summer 2007, supported by a satellite image, which is also planned for 2007. The images are archived by Posiva, but not published, since they might contain sensitive information regarding the nuclear installations.

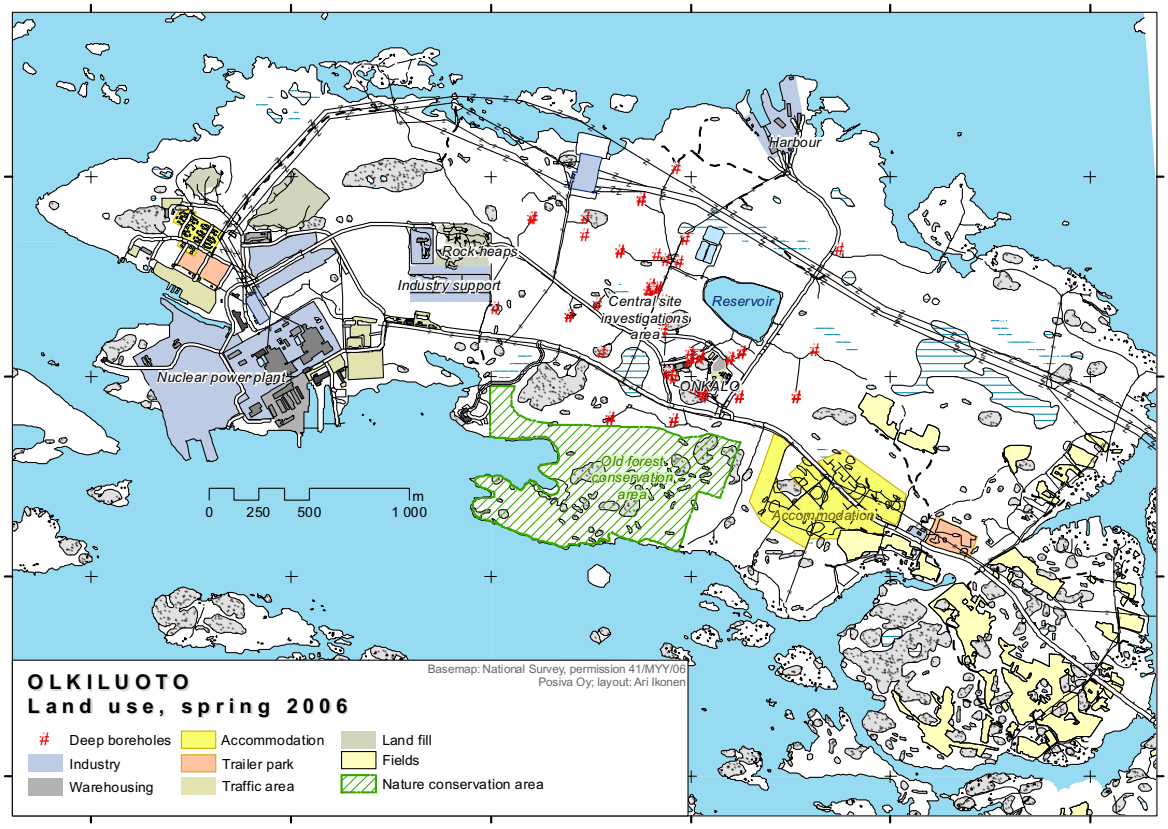

Figure 3-2. *Land use on Olkiluoto Island as of spring 2006. Industrial and site investigation activities are concentrated in the western and central part of the island, and new accommodation facilities for the power plant are being built southeast from the ONKALO. Numerous small cottages lie in the eastern part of the island, especially near the shoreline. Thial ecoe white areas are mostly forest.*

3.2.2 Terrestrial ecosystems

Commercial forests, rich in rocky soil, outcrops and rock vegetation, cover most of Olkiluoto Island, with the vegetation being quite variable in age, due to the different phases of thinning and cutting. The significant areas of natural vegetation are the Liiklanperä old spruce forest area, the Ulkopää-Tyrniemi area, with its luxuriant forests

and undisturbed shoreline, and the shore vegetation. There is frequently a sharp boundary between such natural habitats and the almost urban-like surroundings of the western and middle parts of the island, i.e. the power plant and ONKALO construction areas. The power lines from the NPP stretch across the island and form another type of vegetation - man-made grassy scrub land. At Olkiluoto, moose, hare, white-tailed deer and raccoon dogs are plentiful; and the other mammals, which are common in the region are also present. The seashore is rich in birds, typically ducks, gulls and waders. Apart from the industrial developments, the fauna on Olkiluoto Island appears not to be in any way exceptional.

The forest ecosystem on the island has been intensively catalogued over the last few years: vegetation type mapping in 2002 (Miettinen & Haapanen 2002) was complemented by tree stand measurements over the following summer (Rautio et al. 2004), and a subset from a dense plot network where trees were measured in 2004 (Saramäki & Korhonen 2005) was selected for ground vegetation mapping (Huhta & Korpela 2006) and extensive sampling from the various forest compartments in 2005. All this work will be covered in detail in the Biosphere Site Description, which is currently being compiled.

The results of the environmental monitoring programme clearly display the effects of the forest in, for example, influencing the percentage of precipitation reaching the soil and also its chemical composition. These effects, as well as the radioactivity measurements, are discussed further in Posiva (2005) and Haapanen (2005, 2006).

3.2.3 Baltic ecosystems

The waters around Olkiluoto Island are shallow, except for a few areas where sea depths reach about 15 m. There is more open sea beyond the few rocky islets at the western end of the Island. There are only a few islands to the north and the Rauma archipelago lies to the south. Due to the openness to the sea, the wind strongly affects water currents in the area (Posiva 2003).

Two of the largest rivers in the Satakunta province, the Lapinjoki and the Eurajoki, discharge to the sea north and east of Olkiluoto, increasing the concentrations of nutrient and solids, especially at their mouths. The average outflow of the Eurajoki, the larger river, is 6-12 m^3/s. The cooling water intake and discharge of the NPP significantly affect the temperature and the currents, but only in their close vicinity. The cooling water flow is about 60 m^3/s (Posiva 2003).

In general, the nutrient and solids content of the sea around Olkiluoto Island is characteristic of the coastal waters of the Bothnian Sea, with the relatively high concentrations of phosphorus reflecting the overall eutrophication of the coastal areas. The salinity (TDS) of the seawater is about 6 g/dm^3, and can be described as a brackish Na-Cl type water (Posiva 2003). The area is monitored as part of the surveillance programmes of the NPP, and the most recent water quality results are presented in Haapanen (2005, 2006). In addition, as a part of Posiva's environmental programme, hydrochemical parameters were analysed from 4 samples in summer 2005 to provide more comprehensive monitoring data for hydrogeochemical modelling; see Table 3-3.

The aquatic fauna and flora typical of the region and the radioactivity in the marine ecosystems are summarised in Posiva (2005) and presented in detail in its references. They do not significantly affect the bedrock conditions and are, therefore not discussed in this report.

Table 3-3. *Some hydrochemical parameters of seawater samples in 2005.*

Parameter	OL-SEA01 Eteläriutta	OL-SEA02 Puskakari	OL-SEA03 Susikari	OL-SEA04 Pitkäkarinkulma
TDS (mg/dm³)	6060	5680	5760	5640
Bromide (mg/dm³)	10	10	10	10
Chloride (mg/dm³)	3390	3120	3170	3080
Sulphate (mg/dm³)	440	440	450	440
Potassium (mg/dm³)	61	59	60	58
Calcium (mg/dm³)	97	93	93	92
Magnesium (mg/dm³)	220	210	210	200
Sodium (mg/dm³)	1750	1660	1680	1660
Strontium (mg/dm³)	1.4	1.2	1.3	1.2

3.3 Overburden

Olkiluoto is a relatively flat island with an average height of 5 m above sea level (m a.s.l), with the highest point at 18 m a.s.l. The sea area around the island is shallow: mainly less than 12 m within 2 km from the shoreline. The elevations relative to sea level are continuously changing, since the apparent uplift rate is significant at 6 mm/y, mainly due to the isostatic adjustment of the bedrock.

The overburden, both onshore and offshore, is usually till. The other terrestrial sediment types are, in order of abundance, fine sand, sand and silt; with the thickness of the overburden usually being 2-4 m. On the sea bed, non-glacial sediments are usually stratified but, in general, such sediments are lacking and the rock is overlain solely by till, or is exposed. Some areas of Littorina and Ancylus clay are present in addition to the areas of (sub-)recent mud on the northern and southern sides of the island.

The terrestrial overburden is discussed rather extensively in Posiva (2005) and further in Lahdenperä et al. (2005). It will also be included in the Biosphere Site Description currently in preparation; thus here only a summary is presented.

3.3.1 Terrestrial overburden

In the soil test pits at Olkiluoto the till is sandy, and contains some clay, silt, sandy and gravel layers. In some isolated depressions fine-grained glacilacustrine sediments are also observed. The till is weakly laminated and rich in fines and the clay content generally varies from 7-14%. Observations of clay and silt layers are important, because they are the most active fraction in till soils due to their large reactive surface area. Slightly chemically altered disintegrated rock layers (so called “palarapakallio”) were found in most of the test pits along research trenches TK8 and TK9, with the thickness of such layers varying from some centimetres to 2-3 m. In refraction seismic studies only a few large areas with a heavily fractured bedrock surface have been observed. The only large areas of peat not significantly affected by the construction work, the

Olkiluodonjärvi wetland area, has formed only over the last few hundred years due to the effects of uplift, however, the peat and mire layers were found to be too thin for developing distinct parameter distributions. Peat mainly contains weakly decomposed Common Reed-Carex-Spaghnum peat (Lahdenperä et al. 2005).

Olkiluoto Island forms a hydrological unit of its own, with the surface waters flowing directly into the sea. The island can be divided into several local catchment areas, on the basis of topography and flow directions in ditches. Surface runoff varies spatially and temporally and is affected by both meteorological factors and by the geology and topography of the overburden. On Olkiluoto Island, over 60% of precipitation evaporates, directly or through transpiration, with the majority of the remainder as direct surface runoff and near-surface groundwater in the overburden. Only a few percent, at most, infiltrates into the deeper parts of bedrock. The extensive construction activity has altered the runoff and infiltration patterns and decreased the level of transpiration (Posiva 2005).

3.3.2 Hydrogeochemistry of overburden groundwater

The shallow groundwater is mainly fresh and locally brackish, with the corresponding water types being Ca-HCO_3 and Na-Cl. The pH (mainly measured in laboratory) of the samples varies from 5.1 to 8.0 and updated distribution contours for pH and concentrations of Cl are shown in Figures 3-3 and 3-4. The samples collected since the earlier reports (Posiva 2003, 2005) confirm the previous understanding of the hydrogeochemical system, and also show evidence of fresh water leakage from the Korvensuo reservoir.

Seasonal trends in pH and alkalinity are observed - for example all pH values measured in spring 2002 were slightly lower than the values in corresponding samples in autumn of the same year. Clear seasonal changes were not, however, observed for any other chemical parameters (Posiva 2003). The latest samples also show a similar seasonal behaviour.

The prevailing oxic conditions of recharging groundwater change directly to sulphidic close to the surface with a short residence time. In the overburden and shallow bedrock (< 10 m depth) the solid-water interactions neutralise infiltrating meteoric water without any notable mixing with older groundwater types. Salinity clearly increases in shallow groundwaters in the low-lying southern parts of the site (Figure 3-4) where sampling points are situated in the vicinity of bedrock depressions and interpreted fracture zones, thus indicating possible discharge areas (Posiva 2003, Pitkänen et al. 2004). Similar tendency is observable in the vicinity of PVP17 and PVP18.

The chemical evolution of infiltrating groundwater is characterised by biogenic respiration of organic carbon in the thin overburden, with possible calcite dissolution and some silicate hydrolysis. Initial oxidation of sulphide minerals to dissolved SO_4 is also thought to be possible. In the overburden the water type changes to HCO_3-rich, and the pH rises above 7 (Posiva 2003, Pitkänen et al. 2004). Overburden groundwaters are also examined together with shallow groundwaters from the bedrock in Chapter 7.

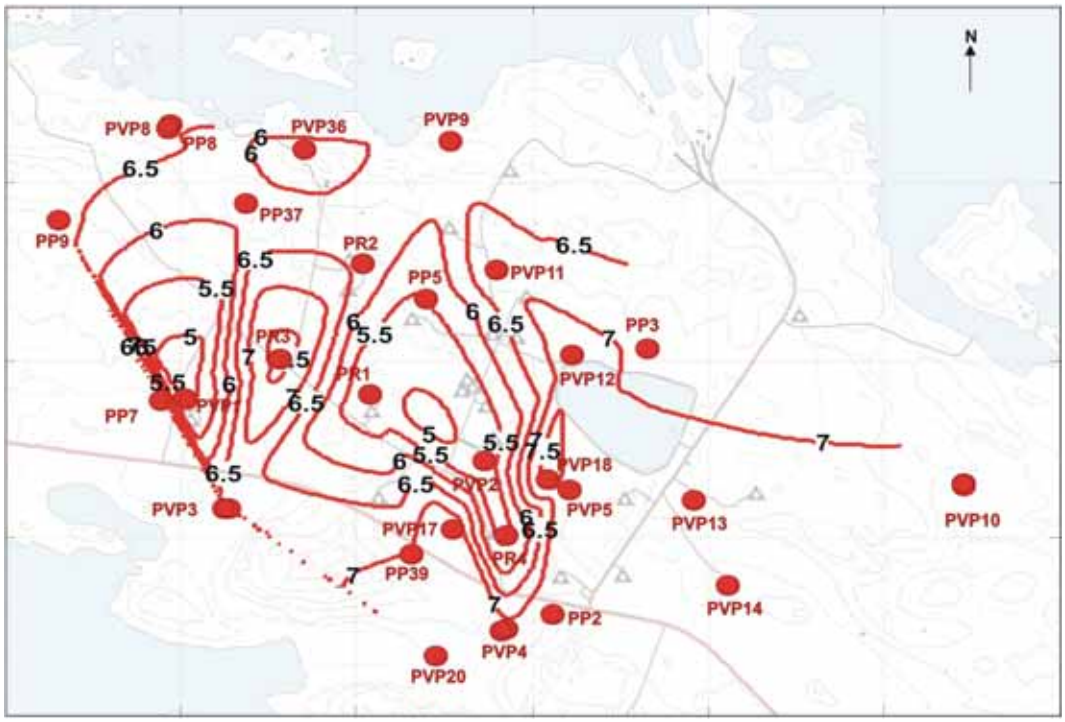

Figure 3-3. *Distribution of pH in shallow groundwater sampled from groundwater observation tubes (PVP) and shallow wells in bedrock (PP, PR) at Olkiluoto (updated from Posiva 2005).*

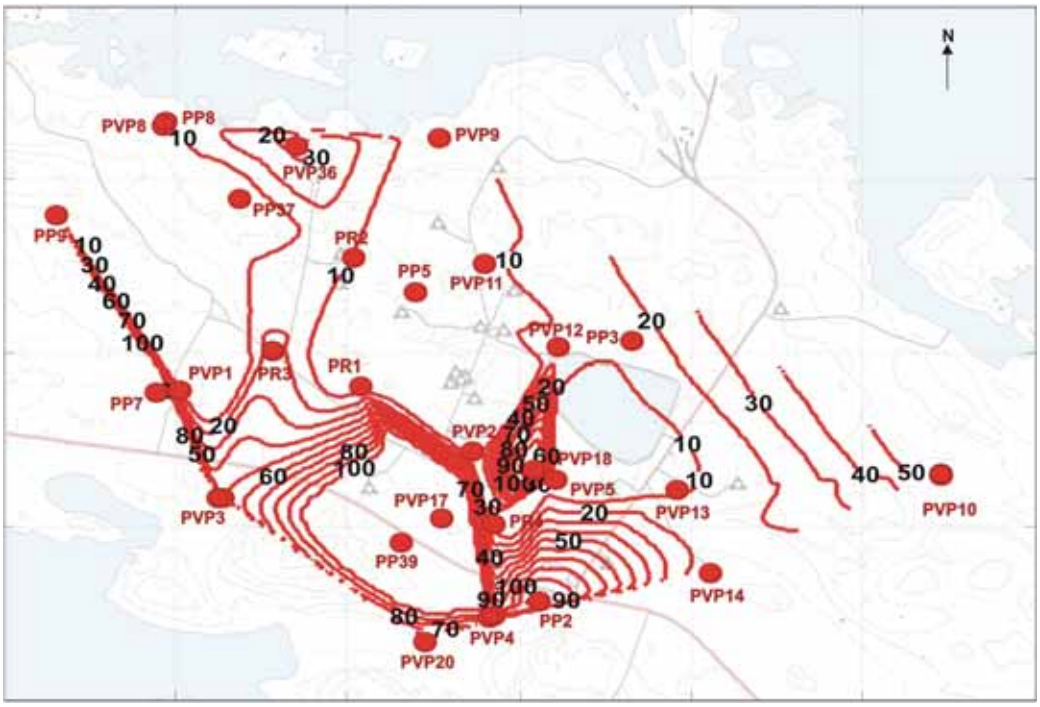

Figure 3-4. *Distribution of Cl concentration (mg/l) in shallow groundwater sampled from groundwater observation tubes (PVP) and shallow wells in bedrock (PP, PR) at Olkiluoto (updated from Posiva 2005).*

3.3.3 Sea bottom sediments

In general, the sea floor deposits present a very fragmentary pattern around Olkiluoto Island, most of the sea floor being exposed bedrock or bedrock covered solely by till. Seven different geological units were interpreted from a survey of the Olkiluoto sea floor based on acoustic-seismic sounding data and related calibration sampling (Rantataro 2001, 2002, Posiva 2003). The most common Quaternary sediment on the sea floor is till covered by post-glacial clays, mainly Ancylus clays (Rantataro 2001).

Caution is needed in interpreting these surveys, however, because it is well known that acoustic and stratigraphical boundaries do not necessarily coincide. The distribution of the various sedimentary units (from bottom to top) deposited on the Precambrian basement and sedimentary formations is illustrated in Figure 3-5 and a cross section in Figure 3-6:

- Till, sand and gravel
- Washed surficial/erosion remnant sand (limited extent)
- Proximal varved clay
- Glacial silt or clay (limited extent)
- Ancylus (varved) clay and sulphide clay
- Littorina clay
- Recent black mud and /or clay

All these offshore sediments were deposited during late-glacial or post-glacial times, following the retreat of the last continental ice sheet. The shallow water environment surrounding Olkiluoto has a maximum depth of 15 m (Rantataro 2001), but during the retreat of the last ice sheet, about 11 000 years ago, the depth of water was over 150 m, due to the extensive isostatic depression of the ground surface and the lack of any equivalent sedimentary deposition (Kotilainen & Hutri 2004).

The lowermost layer of the Quaternary sequence in the Olkiluoto region consists of till, sand or gravel, deposited directly on either Precambrian basement or sedimentary rock. Where these deposits overlie the basement their usual thickness is 2-4 m, whereas on the areas of sedimentary rock, as much as 10-15 m can be found (Rantataro 2001).

Washed surficial/erosion remnant sand, some centimetres thick, accumulates on the top of older sediments due to wave and current action and, as a result of land uplift, this unit is continually being recycled (Ekman & Mäkinen 1996). Erosional forces disturb fine-grained particles and re-sedimentation takes place in a less dynamic depositional environment, such as in a deep basin or sheltered bay. As a consequence of this washing effect, heavier particles stay in place as erosional remnants (Rantataro 2001).

Ancylus phase (late-glacial) varved clay is usually deposited disconformably on the underlying Precambrian basement and sedimentary rock, till/sand/gravel and proximal clay. The Littorina clay, as well as any younger sediment, is deposited as basin-fill, thus differing from older clay sediments that were deposited more or less conformably (Winterhalter 1992).

Late glacial, varved and sulphide-rich Ancylus clays are typically present in basins and outside the archipelago in the open sea areas west of Olkiluoto. Post-glacial Littorina clay/mud as well as recent/sub-recent mud/clay covers the sea floor in sheltered near-shore basins and in the inner archipelago. Present day areas of active sedimentation are situated in the inner archipelago south/southwest and northeast from Olkiluoto (Rantataro 2001).

A Precambrian sedimentary formation, west of Olkiluoto, was known to exist from previous investigations, but its precise location was unknown (Winterhalter 1972, Koistinen 1996). During the interpretation of acoustic-seismic sounding data it became clear that this formation could be much closer to Olkiluoto than previously thought, at a distance of only 5-6 km (Rantataro 2002, Kuivamäki 2001), as shown in Figure 3-5. The topographic variation of the rock surface where this formation is thought to be present is subdued (Rantataro 2002).

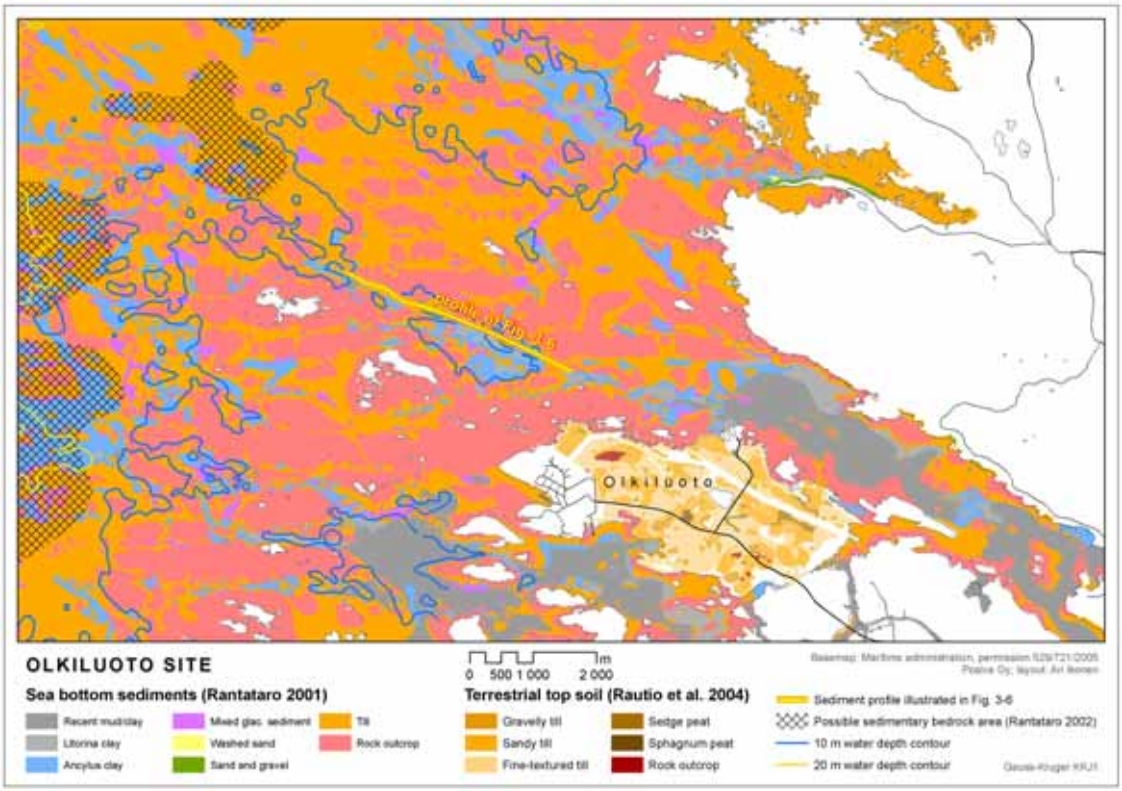

Figure 3-5. *Sea bottom sediment and terrestrial soil types at Olkiluoto based on data from Rantataro (2001, 2002) and Rautio et al. (2004).*

3.4 Interaction with other disciplines

Climate

Climate and weather conditions provide input to the modelling of groundwater evolution and flow as the time-dependent boundary conditions for the system. Weather

conditions also have a great influence on the vegetation and animal life on the site, further affecting conditions at depth.

Ecosystems

The processes maintained by living organisms and other organic matter on the surface, in soil, or in the sea, have a significant effect on the amount and composition of groundwater infiltrating the bedrock. In addition, seawater is used as a reference to help estimate the geochemical evolution and the mean residence times of deep groundwaters.

Overburden

The overburden alters the chemical composition of the precipitation that infiltrates to greater depths and affects the extent of surficial turnover and runoff. In addition, the vegetation takes up nutrients and water from the soil.

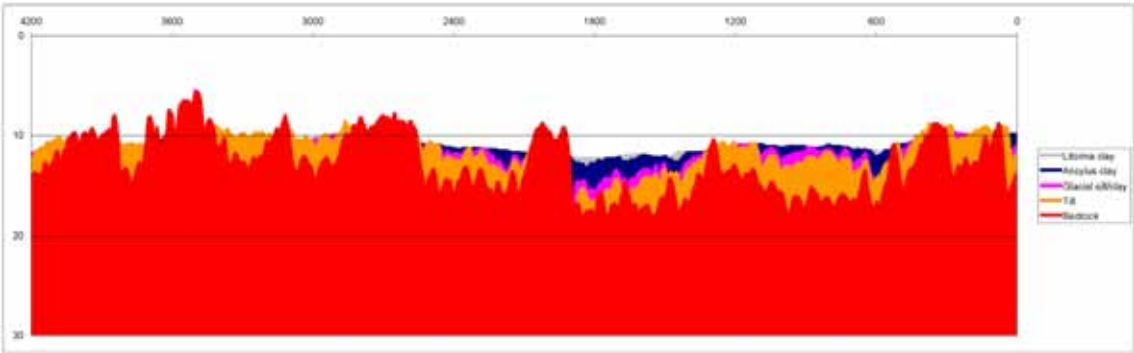

Figure 3-6. *Sea bottom sediment profile northwest of Olkiluoto based on data from Rantataro (2001). Location of the profile is indicated in Figure 3-5, NW of Olkiluoto. Note the different scales on the horizontal and vertical axes (4200 and 30 m, respectively).*

4 BEDROCK GEOLOGY

4.1 Objectives of and approaches to the geological modelling

4.1.1 Purpose and uses of the Geological Site Model

The objective of the work leading to the current Geological Site Model (Paulamäki et al. 2006) has been to develop an "initial version" (version 0) of the geological model of the Olkiluoto site area, based on the state of geological knowledge at the beginning of the underground investigations from the ONKALO at Olkiluoto, in a format that could be later used to create updated and revised versions as excavations and investigations proceed. The purpose of the Geological Site Model is to evaluate the geological properties and conditions of the rock mass in the modelled area and as such, the model acts as an important background reference for the construction, layout design, safety assessment and hydrogeological and geomechanical models (See Figure 4-1). In contrast to the published ONKALO area model (Paananen et al. 2006), which focuses mainly on the needs of the ONKALO tunnel construction, in the presentation of the Geological Site Model (and in the forthcoming Geological Site Model report (Geological Site Model version 1.0)) there is greater focus on the description of the applied modelling methodology and on the estimation of uncertainties.

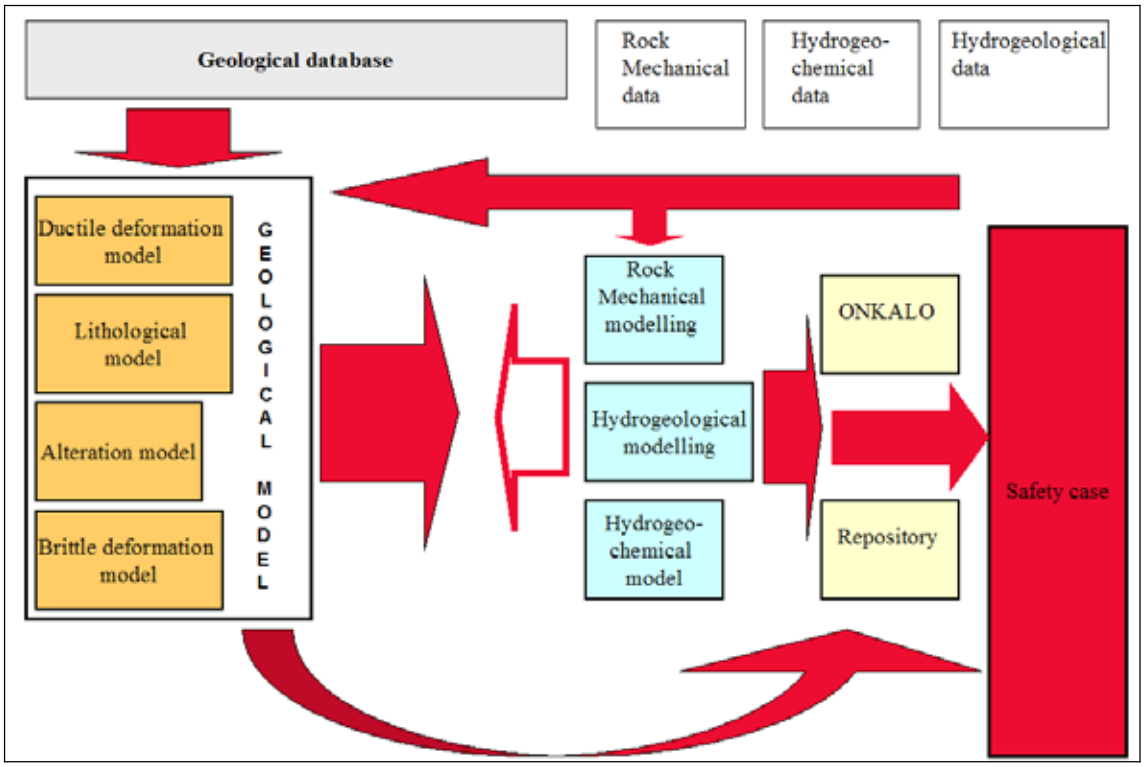

Figure 4-1. *Flow chart of the interaction between the Geological Site Model and other disciplines.*

The geological database used in the modelling has largely been collected and analysed since the production of the most recent version of the bedrock model from the site investigation phase (Vaittinen et al. 2003) and it is emphasised that, at this stage, the Geological Site Model is partly tentative, as much of the geological data has been acquired only a few months prior to the release of this report. Accordingly, the results and conclusions of this report reflect the current stage of the learning process of understanding the site-specific geological features. The quality and accuracy of the Geological Site Model will improve as knowledge of the geology evolves through prediction-outcome studies and the acquisition of an increasing number of data.

The modelled bedrock volume covers an area of 2 x 2 x 1 km, which is referred to as the Olkiluoto site area (Figure 4-2). The Geological Site Model combines the geological surface and drill core studies and interpretations of geophysical airborne, ground survey, and drillhole measurements.

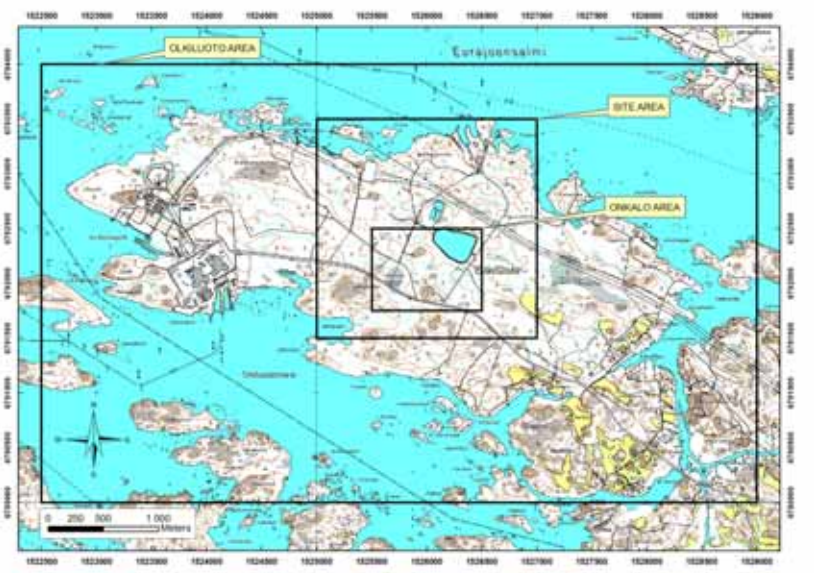

Figure 4-2. *Nominal model areas used at Olkiluoto, including the Olkiluoto Site Area.*

4.1.2 Conceptual model

The main approach in the construction of the current Geological Site Model has been the development of an understanding of the geological processes, which have created the observed geological features at the Olkiluoto site, and which have been subsequently applied in the construction of the deterministic model. A thematic approach has been taken, for the sake of convenience when describing the model, which is composed of four submodels (see Figure 4-3): the ductile deformation model, the lithological model, the alteration model and the brittle deformation model. It is emphasized that these submodels are not independent entities, as the geological

processes are closely interrelated - for example, the ductile deformation is an important precursor to the subsequent brittle deformation.

The ductile deformation model describes and models the products of polyphase ductile deformation, which makes it possible to define the dimensions and geometrical forms of individual lithological units determined in the lithological model and also to assess the orientation and effects of the lithological anisotropy.

The lithological model provides a general view of the lithological properties of definite rock volumes or units that can be defined on the basis of a set of parameters. The goal of the model is to represent the spatial distribution of lithologically-fixed and genetically-related bedrock units, which, from the perspective of underground construction, have uniform properties.

The alteration model deals mainly with the products of hydrothermal alteration, but retrograde metamorphism and subsequent low-temperature weathering, which have also affected the lithological units in the site area, are also considered as a part of the long-term alteration history. These processes have transformed the physical and chemical properties of rock material, and altered rocks may have physical properties which are notably different from those of primary, fresh rocks. Thus the degree and type of secondary alteration and retrogressive metamorphism are important parameters in evaluating, for example, the mechanical strength of the rocks. The goal of the alteration model is to present the shapes and volumes of altered bedrock units as well as the types of altered rocks.

The brittle deformation model describes the large-scale structures produced during the long history of brittle deformation, i.e. the fault zones and joint cluster zones. Brittle deformation products may have important implications for construction and long-term safety, and an initial attempt at evaluating their properties is presented. In the current Geological Site Model report, focus is on the description of the deterministic features of the brittle deformation; the results of discrete fracture network (DFN) modelling will be presented in a separate report.

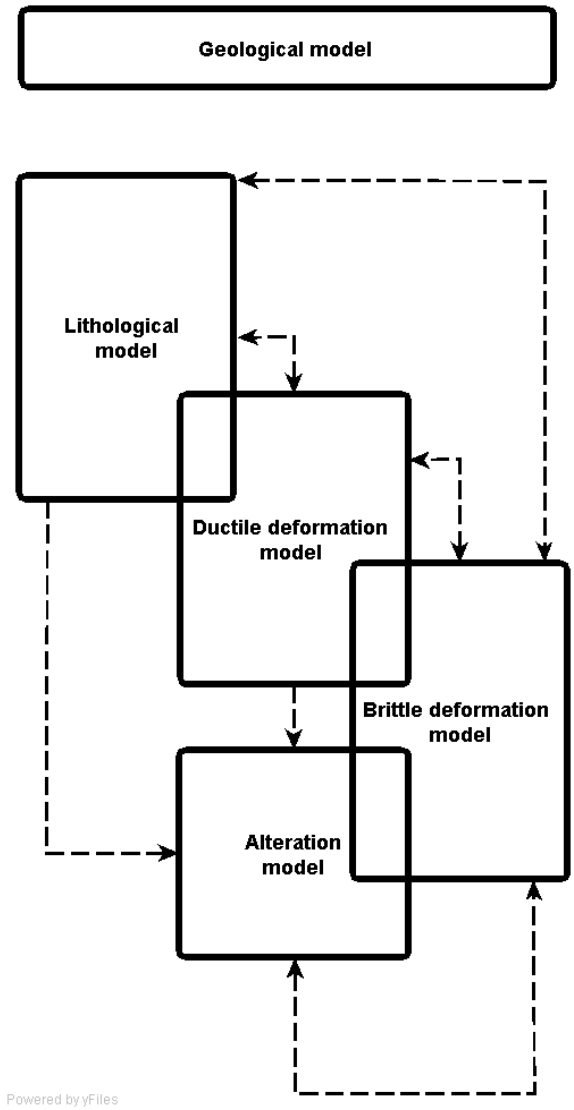

Figure 4-3. *Thematic submodels of the current Geological Site Model.*

Table 4-1 combines the current understanding of the geological history of Olkiluoto, using data from outcrops, drillcores, investigation trenches and the ONKALO tunnel. Studies are currently taking place regarding the development of concepts and suitable submodels for use in this area; the results of these studies will be summarised in more detail in the forthcoming Geological Site Model report (Geological Site Model version 1.0).

Table 4-1. *Simple integration of petrological, structural processes and products over geological time.*

Crd=Cordierite, Sil=Sillimanite, Bt=Biotite, Grn=Garnet, Oliv=Olivine, Phlog=Phlogopite, Pyr=Pyroxene, Amph=Amphibole

Time/Age (Ma)	**Petrological evolution**		**Structural evolution**	**Structural elements**
> 1900	Turbidite sediments Volcanic interlayers (Protolith) Carbonaceous beds		S_0	
	(Leucosome?)		D_1	S_1 banding
	Pegmatite Leucosome	Crd-Sil-Bt (T series) Grn-Bt (P/S series) Oliv-Phlog-Pyr Pyr-Amph (S series) Granitic and tonalitic gneisses	D_2 thrusting (to NE), F_2 folding, D_2 shearing	F_2 isoclinal to tight folds, S_2 foliations, ductile – semiductile shear zones Migmatite structures Blastomylonitic foliation in TGG gneisses
	Pegmatite Leucosome	Late muscovite, products of the waning stage of metamorphism	D_3 thrusting (to N - NW), F_3 folding, D_3 shearing	F_3 tight folds, rare S_3 foliation, ductile – semiductile shear zones Migmatite structures
	Pegmatite (?)		D_4 deformation in E-W compression	Small, open folds
			D_5	Small scale flexures
~ 1600	(Meta)diabase			
	Hydrothermal stage Epidote-Calcite-Phengite, Sulphides, Illite Quartz, Calcite, Kaolinite		Brittle deformation, faulting	Faults, fractures, tension cracks, slickensides
	Weathering Late Clay			

4.1.3 Modelling methods

The applied modelling methods are discussed only briefly here; for a more thorough description, reference is made to Paulamäki et al. (2006) and references therein. The 3D models have been constructed with Surpac Vision 3D modelling software.

The ductile deformation model

The study of ductile deformation commences initially with a description of the geometrical and petrographical features and a determination of the orientation of every single deformation structure. A detailed study of outcrops, trenches and drill core samples yielded a comprehensive data set, in which the various elements of the ductile deformation, their locations and their orientations are described. Currently, the ductile deformation model is mainly conceptual in nature, in which different deformation phases and their products are described. In addition, ductile deformation zone intersections have been defined and this provides further input for the development of deterministic models. The final structural interpretation will be a summary of knowledge obtained from the initial geometrical analysis and subsequent evaluation of the dynamic elements and cogenetic metamorphic evolution of every individual stage of the ductile structural evolution. The effects of tectonic forces, and thus the consequences of the ductile deformation, are not homogeneously distributed and, as a result, the final structural interpretation must take into account the regional variation in the strength of every deformation process. The final phase of the structural interpretation is the evaluation of the variation in strain rate, or strain partitioning, and its effect on the bedrock at Olkiluoto.

The lithological model

The 3D lithological modelling mainly comprises spatial descriptions of the tonalitic-granodioritic-granitic gneisses and the pegmatitic granites. In addition, the contact of the diatexitic gneisses and veined gneisses has been modelled, as well as the narrow diabase dykes. The veined gneisses form the main volume of the model area. Both the surface and drillhole studies clearly indicate that, within the site area, the composite foliation is fairly constant over large areas, the dip direction being to the southeast. The strike and dip of the foliation has served as a guide for correlating the various lithologies between the drillholes and from the surface to drillholes, and has been the basic principle behind the 3D lithological interpretation (see Figure 4-4 and Figure 4-5)

In the 3D lithological modelling, tonalitic-granodioritic-granitic gneiss and pegmatitic granite intersections in drillholes more than ca. 10 m in thickness have been distinguished as separate units. Adjacent pegmatitic granite sections less than 10 m in length, and separated by only short gneiss and migmatite sections, were combined into larger units, with the assumption that the gneisses represent inclusions within the pegmatitic granite. All the observed and interpreted diabase dykes have been modelled regardless of their width.

Figure 4-4 presents a N-S trending vertical section illustrating how the pegmatitic granite units have been connected between the drillholes. The units were first digitized at one or two profiles, using the data from several drillholes (Figure 4-4). These interpretations were then extrapolated to neighbouring profiles, and edited there with respect to the available drillhole and surface data, and the resulting modified interpretation again extrapolated to the next profile. This procedure resulted in several or tens of vertical profiles (Figure 4-5a), which were connected so as to produce one continuous unit (Figure 4-5b).

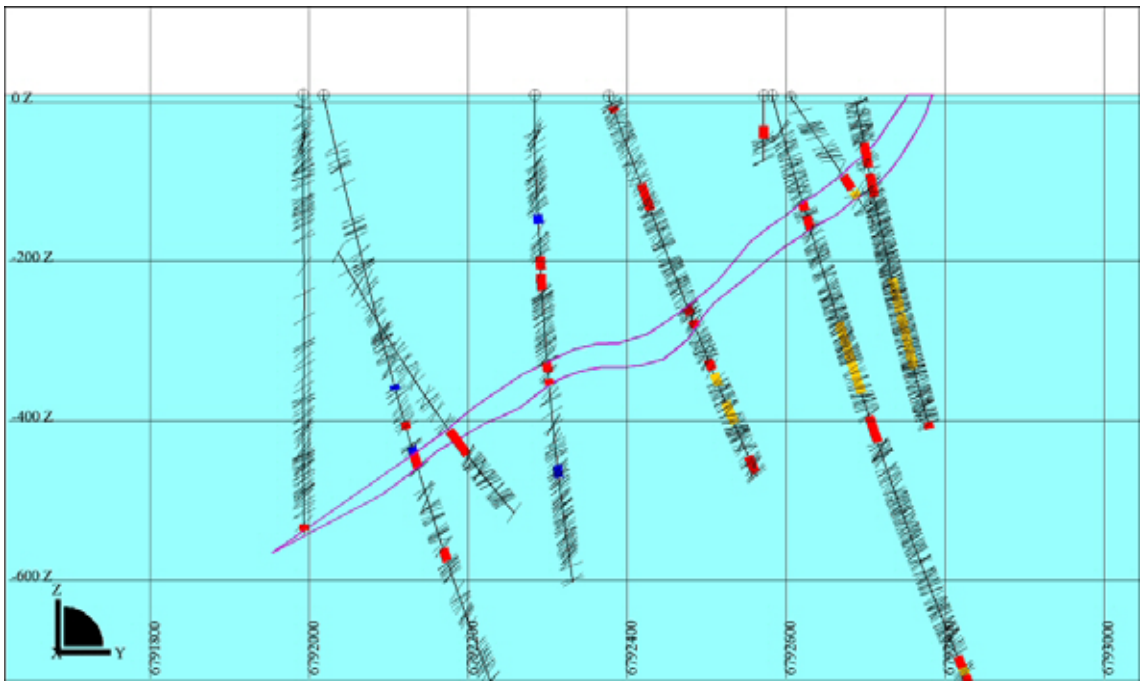

Figure 4-4. *N-S trending vertical section with lithological and foliation data from the drillholes and digitised pegmatitic granite unit (magenta). The pegmatitic granite unit on the surface (upper right corner) is connected to the drillholes using the foliation measurements as a guide.*

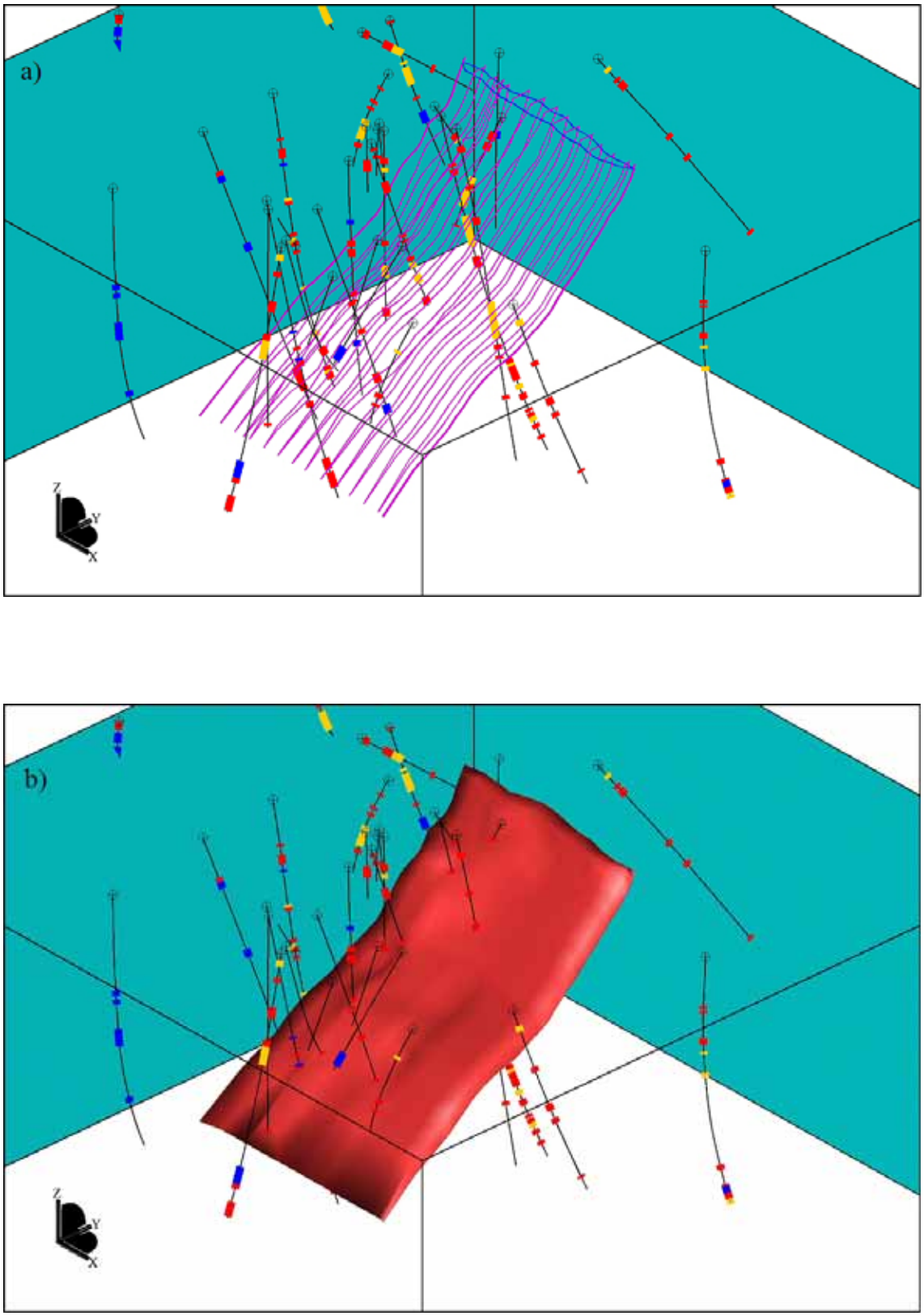

Figure 4-5. *a) Digitised sections of the modelled pegmatitic granite unit, b) completed 3D solid object. View from above towards the SSE. The frame indicates the Olkiluoto site volume.*

The alteration model

Secondary hydrothermal alteration is associated with the late stages of metamorphism and igneous activity, which involve heated or superheated water. Two types of alteration are recognised: fracture-controlled and pervasive. The drill core samples were logged in order to determine the most typical alteration minerals or mineral assemblages and the location and length of the most altered sections, in order to study the style and intensity of hydrothermal alteration. The geological information obtained from the state of alteration has been obtained solely from visual mapping.

Volumetric models of the alteration were constructed from the kaolinisation and sulphidisation data by interpolating and triangulating the lower surfaces of the models (the upper surfaces of the models coincide with the ground surface). Subsequently, triangulation was carried out between the boundary polygons of the top and bottom surfaces of both models (Figure 4-6b). Illite alteration was modelled as a dome-like volume of increased occurrence of illite and, as such, is a generalisation of the distribution of strongly illitised domains.

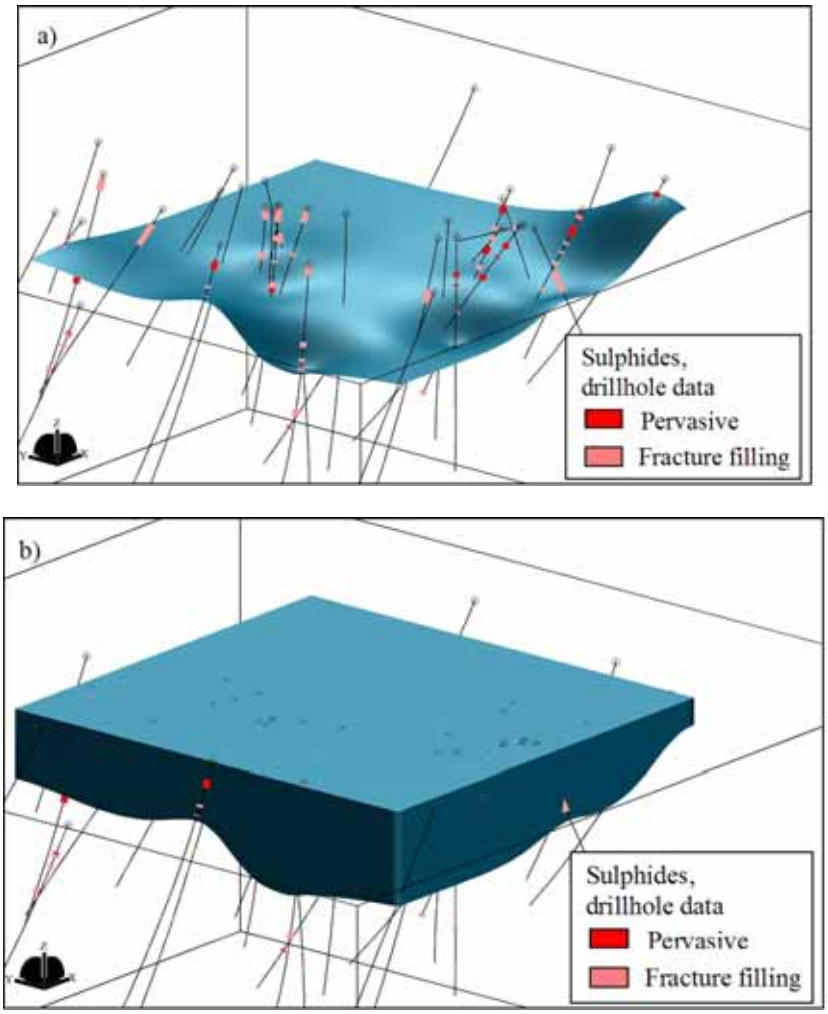

Figure 4-6. *a) The bottom surface of the sulphidisation model, b) completed volumetric model. View from the SW. The frame indicates the Olkiluoto site volume.*

The brittle deformation model

Faults usually show evidence of the most recent increment of slip and the displacement can often be inferred, for example, from the offset of lithological layering, crosscutting veins and older fractures. From the perspective of a more detailed analysis of faults, the orientation of the fault planes and associated slip striations (slickenlines and fibrous growth of minerals) on the fault surfaces provide important tools for the characterisation of the faulting and for fault-slip analysis. This analysis assumes that the slip striation corresponds to the formation of the fault, and not to the most recent increment (an assumption, which is not likely to be valid in complexly deformed areas where reactivation of older deformation zones is probable). By proper kinematic analysis, using the fault plane and slip striation orientations, kinematically-compatible sets of faults can be identified and classified into groups. Simple use of fault plane orientations alone does not provide proper tools for the identification of the cogenetic faults, as different orientations of faults may still be kinematically compatible. In the current

modelling, a very simple classification of faults is made on the basis of orientation of their slip striations, with the assumption that faults with similar slip orientations are cogenetic. It should be emphasised however, that this approach does not exclude the possibility that highly variable slip-striation orientations may have been formed in the same faulting (deformation) phase. Possible slip-compatibility will be validated later by a proper kinematic analysis.

The starting point for brittle deformation modelling was the observed intersections of deformation zones in the drillholes, including their kinematic data and geophysical indications. The most continuous brittle features were assumed to be brittle fault zones (BFZs) and were, therefore, the focus of the modelling. Brittle joint zones (BJZs) are probably more local in extent and lacking in kinematic evidence.

A statistical examination of the slickenlines revealed five separate kinematic fault groups (designated Groups A – E), which were modelled separately. The orientation of the modelled zone was assumed to be the same as the average orientation of the fault planes within that zone, and to possess the same fault-slip orientation and sense-of-shear. As a consequence, the actual cross-hole correlation was performed by extending the average fault plane orientation to neighbouring drillholes and assessing whether correlative fault group intersections and orientations could be defined within them. In addition to the fault plane data, geophysical data were also used for cross-hole-correlation. If the same brittle fault intersection in the drillhole had two (or more) distinctly separate fault orientations, each belonging to a different fault group, two (or more) brittle fault zones were assigned to the same drillhole intersection. Drillhole intersections lacking kinematic data (i.e. brittle joint intersections) were generally not modelled, as the current modelling method does not provide sufficient tools for cross-hole correlation of purely extensional fractures. However, if there had been supporting data, brittle joint intersections could have been connected to the modelled brittle fault zones (for example by using geophysics).

In the modelling work, the drillhole intersections of each fault group were viewed separately in 3D and in 2D vertical sections. The orientation of the faults is based on the orientations of slickensided fractures, geophysical data and crosshole correlation, and an example of a construction of a solid representation of a fault zone is given in Figure 4-7.

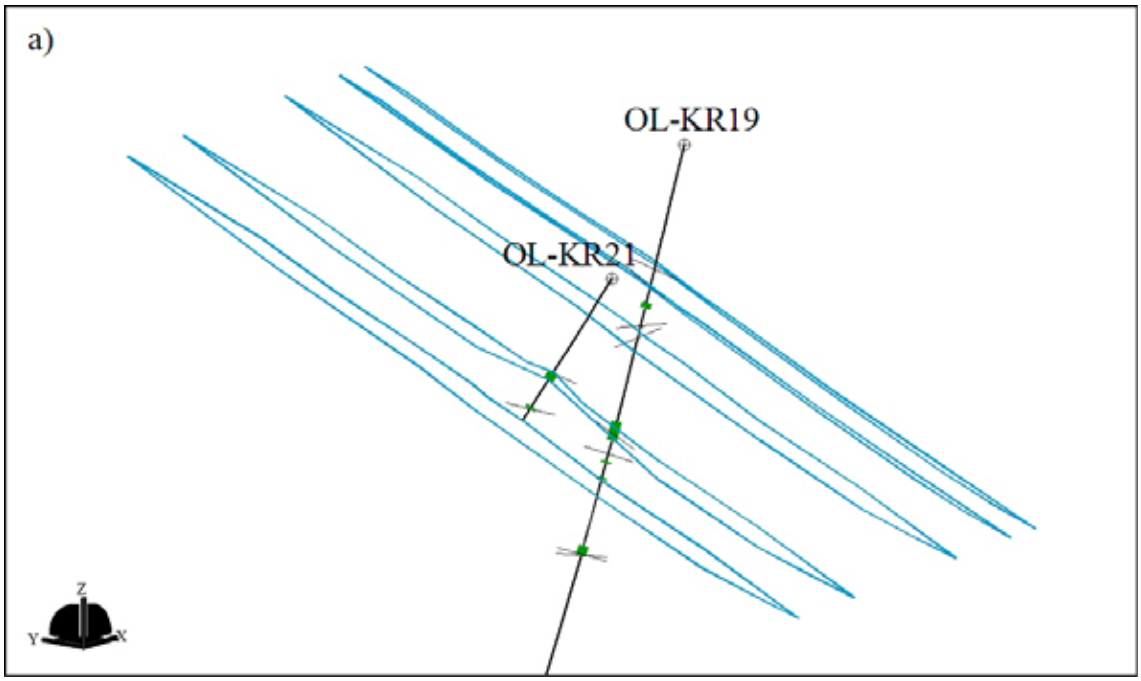

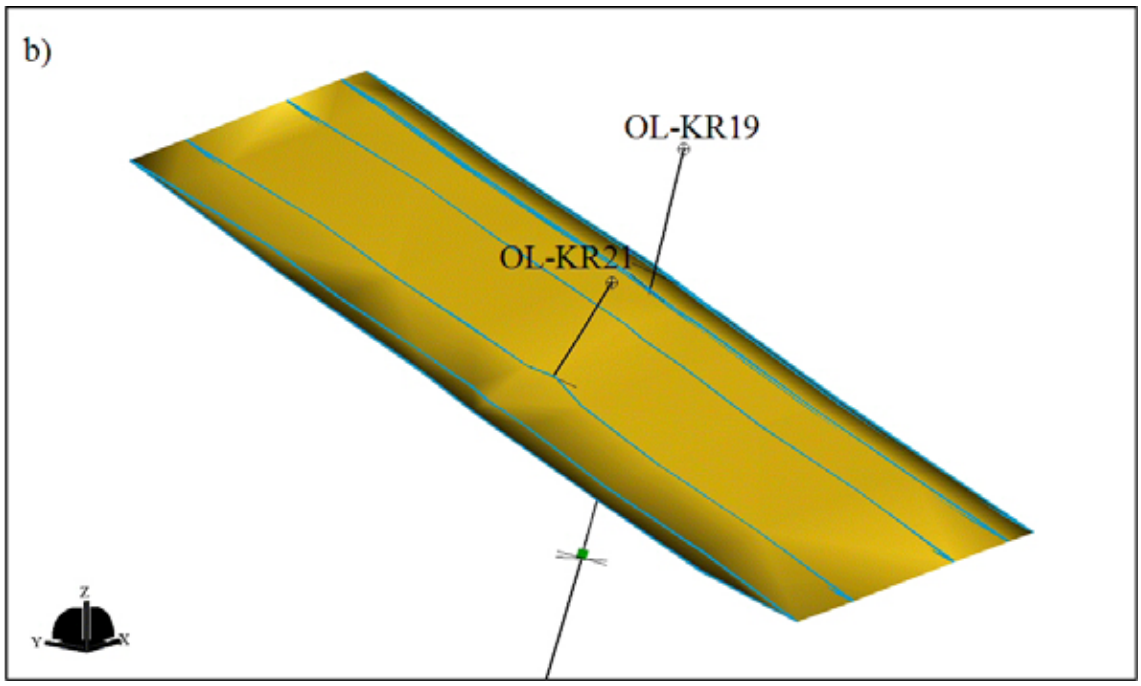

Figure 4-7. *Construction of fault OL-BFZ-009, a) digitised vertical polygons, b) completed solid representation of a fault zone. Intersection OL-KR21-BFI-20484 – 22070 (single fault plane at OL-KR19 89.58 m). Dip /dip direction 26°/173°. View from SW.*

4.2 Data Evaluation

4.2.1 Surface geological data

Geological mapping of outcrops has been carried out on several occasions during the site investigations. The first general geological mapping of the outcrops in 1989 (Paulamäki 1989) was followed a few years later by detailed structural geological mapping (Paulamäki & Koistinen 1991). Ismo Aaltonen and Jussi Mattila of Posiva Oy have made additional lithological and structural observations from outcrops at Olkiluoto, during investigations in 2003 and 2004, and the geological mapping of the Olkiluoto 3 construction site was performed in 2004 (Talikka 2005).

Several investigation trenches have been excavated and investigated in the Olkiluoto site area (Paulamäki 1995, 1996; Lindberg & Paulamäki 2004; Paulamäki & Aaltonen 2005; Paulamäki 2005a; Paulamäki 2005b; Engström 2006; Nordbäck & Talikka 2006, Mattila et al. *in prep*). The trench mapping comprises the observation of ductile and brittle deformation and the macroscopic determination of lithologies from the bedrock surface, after the removal of the remaining loose soil with compressed air and cleaning with a high-pressure washer. The total length of the trenches is ca. 3500 m and they range in width from 0.5 m to 5 m. Additionally, in the area of the Korvensuo reservoir, the exposed surfaces of two sediment-filled basins, each measuring 30 m x 85 m, have been mapped (Äikäs 1995).

A total of 14 321 tectonic measurements have been made, both at outcrops and in the investigation trenches, including 2827 measurements of ductile deformation (foliation, fold axis, axial plane, fault plane and lineation) and 11 494 fracture measurements. Additionally, detailed fracture mapping was carried out in the area of the Ulkopää cape, as part of the investigations for the repository for low- and intermediate-level waste, which included a further 1700 fracture measurements.

4.2.2 Drill core investigations

Deep cored drillholes have been drilled since 1988, and the total number of such holes now exceeds 40; however, only the data from drillholes KR1-KR33 were available for the development of the Geological Site Model. Preliminary descriptions of all drill cores have been published as Posiva Working Reports and the most recent ones (drillholes KR15-KR33), which are written in English, are included in the list of references (Niinimäki 2002a-h, 2003a-d, Rautio 2002, 2003, 2004a-c, 2005a-b). The drill cores are mostly 300 – 1000 m in length, and their combined length is 17 000 m. Gehör et al. (1996, 1997, 2000, 2005) and Lindberg & Paananen (1991, 1992) have presented the results of petrological studies from drillholes KR1-KR28. These reports include the results of visual drill core logging, polarization microscope examinations and whole rock chemical analyses of ca. 250 samples.

During the spring and summer of 2005, a drill core investigation programme was carried out to gather the necessary basic structural data for both ductile and brittle deformation models. Different elements and kinematic features of structural geological

evolution were systematically logged along cored samples of drillholes OL-KR1 to OL-KR33B and a total of ca. 1700 fault plane and fault vector directions were measured.

In parallel with the kinematic study, deformation zone intersections were observed from the drill core samples and divided into five classes: *High-grade ductile shear intersection (HGI), Low-grade ductile shear zone intersection (DSI)*, *Semi-brittle fault zone intersection (SFI)*, *Brittle joint intersection (BJI)* and *Brittle fault zone intersection (BFI).* Each intersection was assigned a unique label, which defines the type of deformation product and also the observed intersection interval in the drill core sample.

Indicators of intense ductile shear in samples would need to be detected to indicate a HGI. The small sample size made it difficult to identify ductile zones, and, so far, no low-grade ductile shear intersections (DSIs) (mylonites, phyllonites etc.) have been observed at Olkiluoto. During the transition from ductile to brittle deformation the rock was sheared and deformed in a semi-brittle manner, and evidence of such deformation was used to define SFI sections. In the Geological Site Model only semi-brittle and brittle deformation zone intersections were used. A BJI is a section with higher fracture frequency compared with the surrounding rock, but where no evidence of faulting exists. If at least one slickensided fracture surface is observed, the section is classified as a BFI. The determination of a BFI or BJI was based not on a set fracture frequency limit (e.g. 10/m), but on expert judgement[1] as there can be large variation of thickness, fracture number, etc. within such a zone. Generally, brittle joint sets include intersections of fracturing that do not show traces of faulting and fractures that are more or less parallel. In the case of BFIs, fracturing is generally more intense, and faulting and cataclastic features are obvious, but in some cases BFIs may show only one or a few slickensided fracture surfaces. The logging of brittle fault intersections consisted of observations on rock type, and especially fracture types, the orientation of fractures and fracture sets, and the relation of fractures to ductile features (foliation, schistosity, shearing), cataclastic features, breccias, fault gouges. A note on drilling-induced fracturing was also provided, as well as an estimation of traces of water flow on fracture surfaces. From drillholes KR1 to KR33, 42 high-grade ductile shear intersections, 8 semi-brittle fault intersections, 125 brittle fault intersections and 82 brittle joint intersections were determined.

Foliation and ductile shear zones were systematically logged at 1 m resolution. All 1 m sections were systematically characterised according to the type and degree of foliation using the procedures outlined in Milnes et al. (2006), small-scale fold axes, axial planes and lineations were also observed. OPTV drillhole images and WellCAD software were used for determining the orientation of the foliation and, in some cases, measurements

---

[1] *Here expert judgement refers to the subjective decision during the mapping as to whether a mapped section could be a part of a deformation zone. The judgement is based on characteristics, such as increased fracturing, increased number of slickensides, occurrence of crushed rock etc., that may indicate connection to a larger deformation zone. During the actual modelling, assessment is made as to whether the mapped intersections actually are part of a deformation zone, and, during this process, some of the mapped intersections may be discarded due to a lack of supportive data, and are thus considered as sections of localised deformation.*

were made on oriented core. Altogether more than 17 000 observations and measurements were made on ductile features.

The research on hydrothermal alteration benefited significantly from the very detailed study of fracture mineralogy and the newly-redeveloped fracture database, which currently consists of more than 40 000 fracture records. Simultaneously with the re-logging of fractures, drill cores from OL-KR1 to OL-KR33 were studied to find out those sections where hydrothermal alteration is clearly observable to the naked eye. Alteration products were detected, at least in small amounts, in almost every drillhole and throughout the site volume.

In addition to the deep drillholes, 36 shallow (10-20 m) drillholes have been drilled to supplement the bedrock mapping (Suomen Malmi 1989). In the site area, there are also 16 shallow drillholes with a range of depths of 14-36 m, which were drilled in the 1970s and subsequently re-logged in 1990 (Jokinen 1990).

Pilot holes ONK-PH1 to ONK-PH5 have been drilled down the centre line of the ONKALO access tunnel, as part of the ONKALO investigations. In addition, 7 shallow (15.2-45.80 m) drillholes OL-PP40 - OL-PP41 and OL-PR5 – OL-PR9 have been drilled directly above the access tunnel.

4.2.3 ONKALO underground rock characterisation facility

The excavation of the ONKALO was started on the 22nd of September 2004 and in January 2006 the access tunnel had reached a length of 990 m (corresponding to a depth of 90 m below sea level, approximately). Geological mapping of the ONKALO tunnel has been performed systematically at intervals of 5 m, corresponding to the length of one excavation round. The mapping includes the determination of rock types, the measurement of structural features (foliation, fold axis, axial planes, slip lineation and the sense of slip of brittle deformation features) and detailed mapping of fractures of all trace length distributions.

Sections of increased fracturing and/or with occurrences of slickensides in the ONKALO tunnel were mapped and subdivided into *brittle joint intersections* (BJI) and *brittle fault intersections* (BFI). Sections showing evidence of high strain, without the development of specific rupture surfaces, were mapped as *high-grade ductile shear intersections* (HSI), a classification that corresponds to the system used in the logging of brittle deformation products from the drill cores. The results of the geological mapping of the first 840 m of the tunnel were used in the modelling.

4.2.4 Geophysical data

Geophysical airborne data have been available from two separate survey campaigns carried out by GTK and Scintrex (Suomen Malmi 1988). The airborne surveys include the following: magnetic (total field and vertical gradient), multifrequency EM at 888, 3113 (GTK) 7837 and 51250 Hz, VLF and radiometric (K, U, Th, total intensity). The first interpretations of the data were carried by Paananen and Kurimo (1990), followed by two lineament interpretations (Paulamäki & Paananen 2001, Paulamäki et al. 2002).

The most recent lineament interpretation, combining systematically topographic and geophysical data, was carried out by Korhonen et al. (2005).

Geophysical ground surveys consist of magnetic and horizontal-loop EM measurements (Suomen Malmi Oy 1989), seismic refraction (Lehtimäki 2003a,b) and wide-band electromagnetic soundings (Jokinen 1990, Jokinen & Jokinen 1994; Ahokas 2003; Jokinen & Lehtimäki 2004).

The magnetic data have been used in delineating the most intensely magnetized rock types. According to petrophysical data (Lindberg & Paananen 1991a, 1991b, 1992; Paananen & Kurimo 1990; Paananen 2004), susceptibility cannot be used directly to indicate different rock types, however, the most significant magnetic anomalies are related to ferrimagnetic, pyrrhotite-bearing gneisses (vein gneisses, mica gneisses, diatexite). According to the most recent systematic 3D profile modelling, the dips of the magnetized units become gentler with depth, agreeing well with the foliation observations in the drillholes.

SAMPO Gefinex wide-band electromagnetic soundings have been carried out at Olkiluoto in four separate campaigns in 1990, 1994, 2002 and 2004 (Jokinen 1990; Jokinen & Jokinen 1994; Ahokas 2003; Jokinen & Lehtimäki 2004). They have been used in mapping deep saline groundwaters, but also provide information on sulphide minerals and possible deformation zones related to sulphide-rich locations. Previous interpretations were performed as part of each campaign (Paananen et al. 1991; Jokinen et al. 1995; Heikkinen et al 2004a), but were all separate pieces of work, and the assumptions used in the interpretations were not fully consistent. All the data were subsequently collectively interpreted, taking into account also the known electric conductors (Paananen & Jääskeläinen 2005; Paananen et al. 2006).

The single-hole data from the following drillholes within the site area were re-interpreted: OL-KR1 to OL-KR28 (Niva 1989; Suomen Malmi Oy 1989, 1990; Julkunen et al. 1995, 1996, 2000a,b, 2002, 2003, 2004a,b; Laurila & Tammenmaa 1996; Lowit et al. 1996; Lahti et al 2001, 2003; Heikkinen et al. 2004b). Hydraulic data were obtained from Pöllänen & Rouhiainen (2000a,b, 2001, 2002a,b). The interpretation is purely based on geophysical data; no geological logging information from the drill cores was used.

The single-hole data gathered comprises different seismic (P-wave and S-wave velocity, P-wave and tubewave attenuation), radiometric (gamma-gamma, neutron-neutron), electric (long normal, short normal/Wenner), magnetic and caliper data. Also, hydraulic and thermal data (from drillholes KR1 – KR11) were used to map the locations of hydraulic fractures or the distribution of hydraulic conductivity. The seismic, radiometric, electric and hydraulic parameters have been mainly used in determining the locations of the deformation zones (however sulphides also have a strong effect on electric measurements). The magnetic data are mainly used in locating ferrimagnetic, pyrrhotite-rich sections.

Petrophysical measurements have been made from drillholes OL-KR1 – OL-KR6 (Lindberg & Paananen 1991a, 1992), bedrock outcrops and shallow drillholes (Paananen & Kurimo 1990) and the VLJ repository (Lindberg & Paananen 1991b).

Recently, the data have been supplemented by the results from OL-KR8, OL-KR15, OL-KR19 – OL-KR23 and 24 minidrill samples from the ground surface (Paananen 2004).

Several charged potential cross-hole measurements have been carried out in Olkiluoto (Lehtonen & Heikkinen 2004; Lehtonen 2006), with the earthings being located in drillholes OL-KR4, 7, 25, 28 and 29. The locations of the current groundings are based on the previous bedrock model of Olkiluoto (Vaittinen et al. 2003). With the charged potential measurements, it has been possible to define mostly gently-dipping, electrically conductive horizons that occasionally coincide with the deformation zones.

Vertical seismic profiling (VSP) surveys have been carried out several times at Olkiluoto, starting in 1990 and, over the years, there have been significant developments in the survey technique as well as in the interpretation procedures. In this study, the VSP interpretation results from each drillhole in the Geological Site Model area have been examined and correlated with the geological data. The most recent VSP results are from drillholes, OL-KR7, 8 (Cosma et al. 2003, Heikkinen et al. 2004), and 4, 10, 14 (Enescu et al. 2004, Heikkinen et al. 2004), which are located in the ONKALO area.

VSP results from the Korvensuo reservoir (Cosma et al. 2003), crosshole surveys between OL-KR14 and OL-KR15 (Enescu et al. 2003) and OL-KR4 and OL-KR10 (Enescu et al. 2004), and the results of the Walkaway Vertical Seismic Profiling (WVSP) from drillholes OL-KR4, 8, 10 and 14 (Enescu et al. 2004, Heikkinen et al. 2004) were available.

4.3 The Geological Site Model

4.3.1 Lithology

The rocks at Olkiluoto can be divided into high-grade metamorphic rocks and igneous rocks on the basis of texture, migmatite structure and major mineral composition. The metamorphic rocks include various migmatitic gneisses and homogeneous, banded or only weakly migmatised gneisses, such as mica gneisses, quartz gneisses, mafic gneisses and tonalitic-granodioritic-granitic gneisses. The igneous rocks comprise abundant pegmatitic granites and sporadic narrow diabase dykes (Kärki & Paulamäki 2006). Within the metamorphic rocks, the change from certain gneiss variants to migmatitic gneisses takes place gradually, so that no distinct contacts between these end members can be defined. Consequently, an artificial boundary between the gneisses and migmatites has been set at a 10% or 20% proportion of the leucosome.

The migmatitic gneisses of Olkiluoto can be divided into three subgroups in terms of the type of migmatite structure: veined gneisses, stromatic gneisses and diatexitic gneisses. The transition from one migmatite type to another takes place gradually.

Migmatitic gneisses are composed mostly of a mica-rich older component, or palaeosome and a younger component, the neosome. The neosome is composed of granitic material that can also be referred to as a leucosome due to its light colour and

lack of mafic minerals. The typical migmatites of Olkiluoto contain 20 – 40% leucosome on average, but the proportion can be less than 20% or in excess of 80% in individual samples.

Veined gneisses contain elongated leucosome veins, which show a distinct linear symmetry and appear as swellings in the dykes or roundish quartz-feldspar aggregates that may be composed of augen-like structures with diameters varying between 1 and 5 cm. The palaeosome is often banded and can show an intense shear deformation, e.g. asymmetric mylonitic foliation. Veined gneisses form the dominating migmatite type in the central part of the Olkiluoto site and make up 43% of the drill core samples studied so far (Figure 4-8).

Stromatic gneisses include migmatites with plane-like, linear leucosome dykes or layers varying in width from several millimetres to 10 – 20 cm. The palaeosome is often well foliated and shows a linear metamorphic banding or schistosity. Planar symmetry is typical of all the physical parameters of bedrock units dominated by stromatic gneisses. Stromatic gneisses represent only 0.4% of the length of the drill cores studied so far.

Diatexitic gneisses (See Figure 4-8) include migmatites that may contain more than 70% leucosome. The palaeosome occurs as fragments of different shape and size, or they can be totally assimilated into granitic vein materials, or the border zones of these may be gradual. In general, all the migmatite variants, in which the shapes of the palaeosome and leucosome are random and which are structurally asymmetric in their entirety, have been classified into this group. Diatexitic gneisses comprise 21% of the total length of the drill cores studied so far.

Fine-and medium-grained *mica gneisses* with less than 10% leucosome material are quite common and make up ca. 7% of the total length of the drill cores. They contain more than 20% micas or their retrograde derivatives. Cordierite, or its retrograde derivative pinite, is a typical constituent, occurring often as porphyroblasts ca. 5 – 10 mm in diameter. The fine-grained mica gneisses are typically schistose, whereas the medium-grained variants show a distinct metamorphic banding.

Quartz gneisses are fine-grained, homogeneous, typically poorly foliated and contain more than 60% quartz and feldspars, but not more than 20% micas. Certain variants may contain some amphibole and in places some pyroxene in addition to amphibole. Garnet is also typical of one subgroup of the quartz gneisses. The quartz gneisses comprise less than 1% of the total length of the drill cores.

Mafic gneisses occur sporadically and make up less than 1% of the total length of the drill cores. Hornblende or chlorite is the dominant mafic mineral, but some mafic gneisses may exceptionally contain some pyroxene or olivine in addition to mica and hornblende.

The tonalitic-granodioritic-granitic gneisses (TGG, See Figure 4-8) are medium-grained, rather homogeneous rocks, which typically form weakly-fractured units. In places, they have an appearance of plutonic, non-foliated rocks but in places resemble coarse-grained mica gneisses, showing a weak metamorphic banding or mylonitic foliation. Their contacts can be gradual, varying in width from several tens of

centimetres to several metres, but they may locally resemble the sharp, intrusive contacts typical of igneous rocks. Leucosome-like granitic veins and crosscutting pegmatitic granites can locally comprise up to 20% of the volume of the gneisses. The proportion of tonalitic-granodioritic-granitic gneisses in the drill cores studied so far is 8%.

The *pegmatitic granites* (Figure 4-8) are leucocratic and very coarse-grained rocks, which occur as dykes ranging in width from a few tens of centimetres to tens of metres, or as large, uniform intrusions. Large garnet phenocrysts, or tourmaline and cordierite grains of variable size, are present in places. Mica gneiss inclusions are typical within the wider pegmatite dykes. Pegmatitic granites constitute a fairly large proportion of the bedrock of Olkiluoto, the pegmatite sections representing 20% of the total length of the drill cores studied so far.

Diabases (Figure 4-8). appear as very narrow (5-50 cm) dykes, which have very sharp contacts without chilled margins. They are typically blackish, fine-grained and thoroughly altered, the original mafic minerals being replaced by microcrystalline saussurite (epidote, calcite and sericite), and the plagioclase has recrystallised into pure albite. They contain quartz- and carbonate-filled amygdales, 0.1- 0.3 mm to ca. 2 mm in diameter. The geochemical, petrological and U-Pb age data of the dyke in TK3 (Mänttäri et al. 2005) indicate that the Olkiluoto diabase dykes are probably Mesoproterozoic (ca. 1600 Ma) in age.

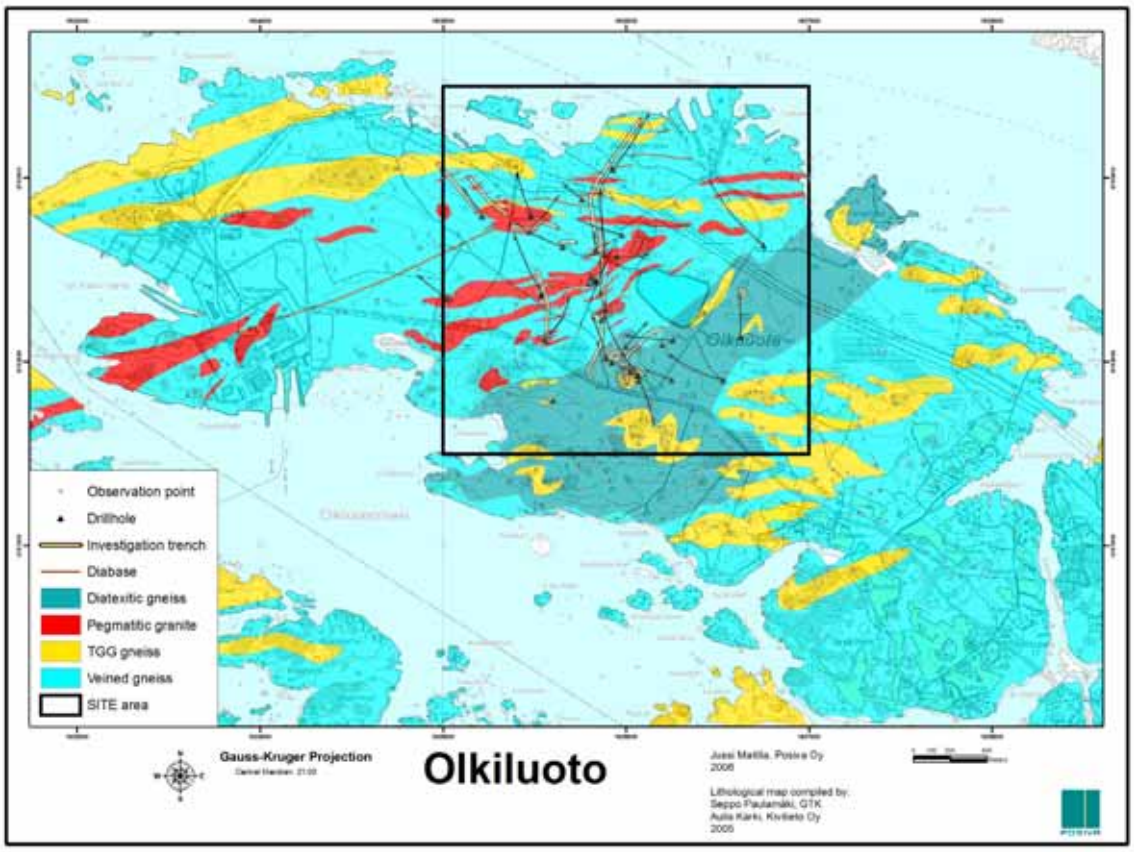

Figure 4-8. *Lithological map of Olkiluoto. The Olkiluoto site area is marked with a black box.*

The lithological 3D modelling mainly comprises modelling of the tonalitic-granodioritic-granitic gneisses and the pegmatitic granites. In addition, the contact of the diatexitic gneisses and veined gneisses has been modelled, as well as the narrow diabase dykes. The veined gneisses form the main volume of the model area. Both the surface and drillhole studies clearly indicate that, in the site area, the composite foliation is fairly constant over large distances, the dip direction being to the southeast. Thus, the strike and dip of the foliation has served as a guide for the correlation of the lithologies between the drillholes and from the surface to the drillholes – and this has been the general approach behind the 3D interpretation of the lithologies.

The 3D lithological model is composed of 17 units of tonalitic-granodioritic-granitic gneisses, 35 units of pegmatitic granite, one diatexitic gneiss unit and six diabase dykes and these are shown in Figure 4-9 - Figure 4-12.

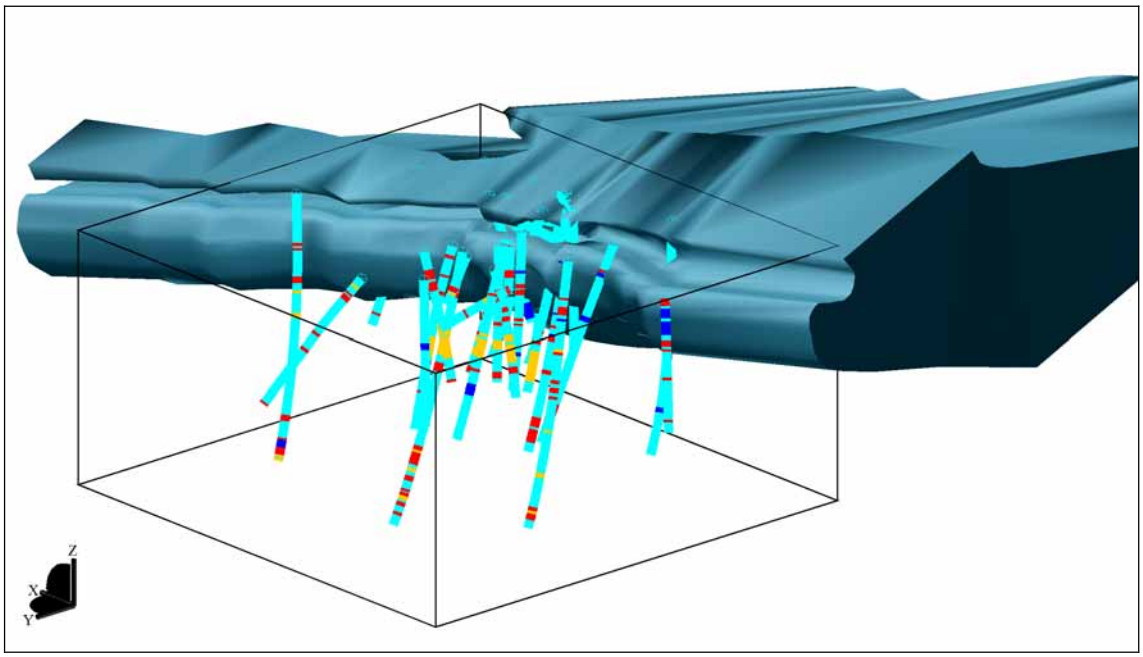

Figure 4-9. *Diatexitic gneiss unit. View from the NW. The black frame indicates the Olkiluoto site volume.*

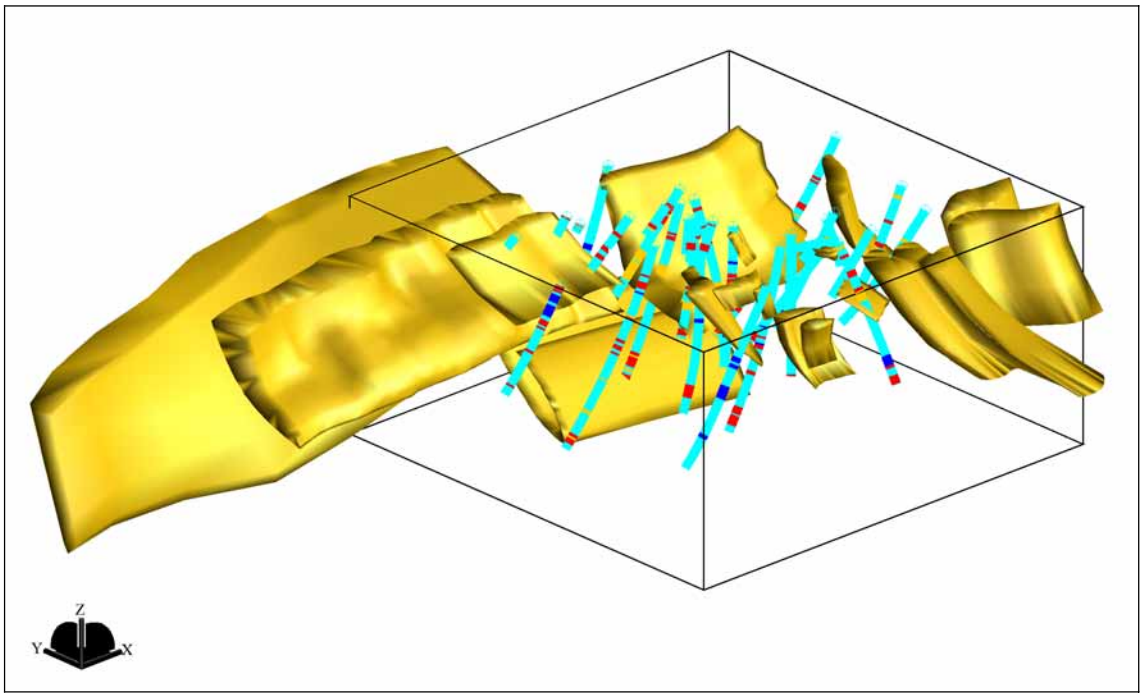

Figure 4-10. *Modelled tonalitic-granodioritic-granitic gneiss units. View from the SW. The black frame indicates the Olkiluoto site volume.*

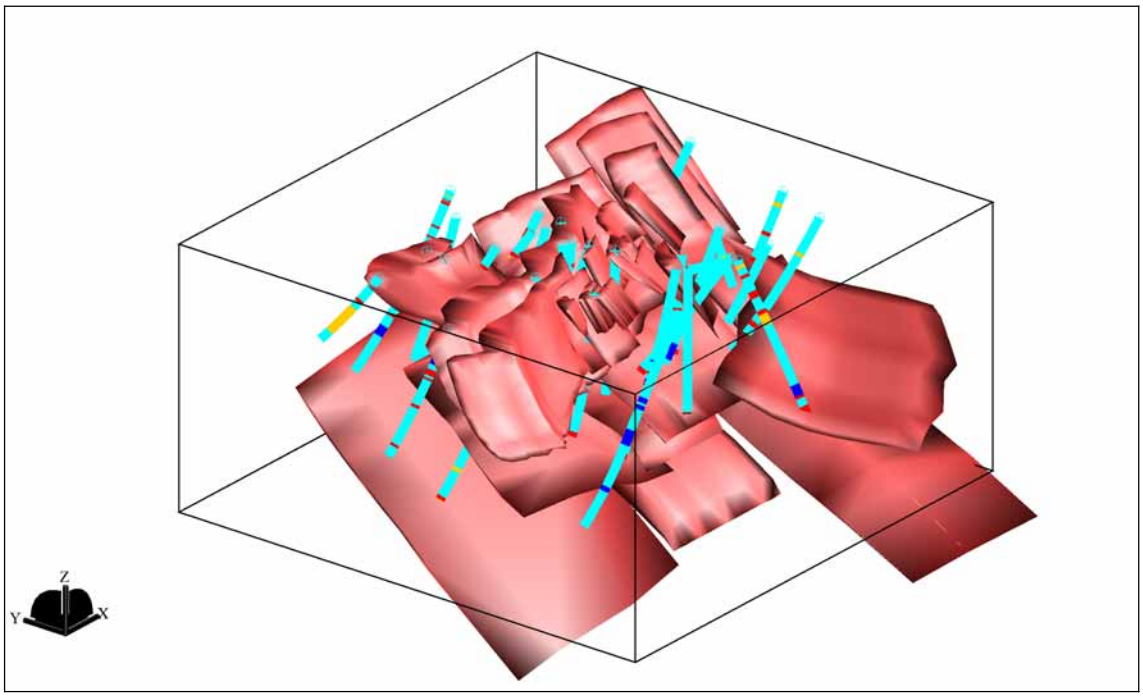

Figure 4-11. *Modelled pegmatitic granite unit. View from the SW. The black frame indicates the Olkiluoto site volume.*

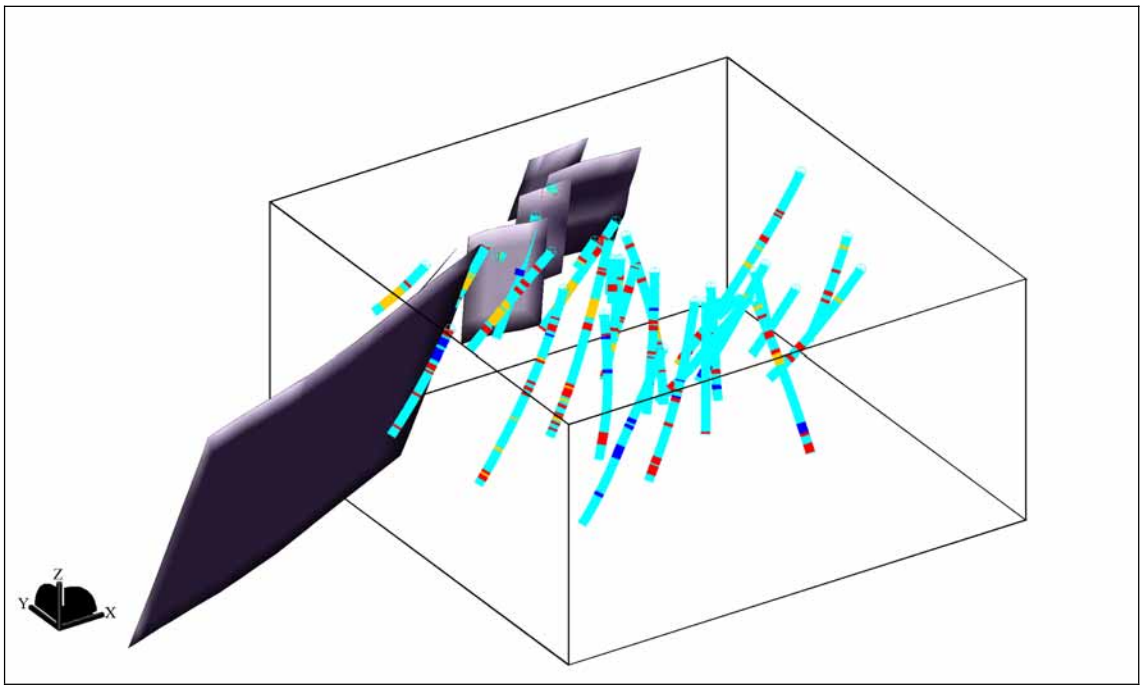

Figure 4-12. *Modelled diabase dykes. View from the SW. The black frame indicates the Olkiluoto site volume.*

4.3.2 Alteration

Three different alteration episodes can be identified at Olkiluoto, which can be distinguished from one another on the basis of a characteristic alteration assemblage (Paulamäki et al. 2006). The alteration events have affected the whole chemical composition and the mineralogical character of the altered rocks and, as a consequence, the physical properties of the bedrock.

A retrograde phase of metamorphism affected the rock ca. 1900 - 1800 Ma ago, and includes sericitisation and saussuritisation of feldspars, and chloritisation and pinitisation of mafic minerals. Temperatures were significantly higher than during the later hydrothermal alteration event. The products of the retrograde metamorphism represent a common regional metamorphic condition in Finland and they can be observed throughout the Olkiluoto bedrock. In terms of construction and long-term safety, they are considered insignificant.

Hydrothermal alteration processes are estimated to have taken place at temperatures from 50°C to slightly over 300°C (Blyth et al. 1998, Gehör et al. 2002, Gehör, *in prep*). At Olkiluoto, these processes are assumed to be related to the late stages of metamorphism and to the emplacement of the rapakivi granites 1580 - 1570 Ma ago and intrusion of the olivine diabase dykes 1270 - 1250 Ma ago (Paulamäki et al. 2006). Typical products of hydrothermal alteration are Fe-sulphides (pyrrhotite, pyrite), clay minerals (illite, smectite-group, kaolinite group) and calcite.

Surface weathering is a process that affects rocks in situ, mechanically or chemically, and where they are close to the surface. In general, weathering is restricted to destructive processes caused by temperature changes and corrosion by surface waters and by atmospheric oxygen. This is the youngest of the alteration processes at Olkiluoto and is still active. It is probable that it has its roots back to at least tens of millions of years ago and has a spatial relationship with the locations of strong hydrothermal alteration.

Hydrothermal alteration

Two different varieties of hydrothermal alteration have been distinguished: a fracture-controlled type and a pervasive (or disseminated) type. The presence of fracture-controlled alteration indicates that hydrothermal fluids have passed through the rock along planar features and alteration is restricted to incipient fractures or narrow zones adjacent to them. The presence of pervasive alteration indicates a stronger type of alteration, which exists pervasively or is disseminated in the rock, in addition to alteration associated with fractures.

There are three main types of hydrothermal alteration: sulphidisation, kaolinisation and illitisation. In addition, the occurrence of calcitic fracture fillings and sets of calcite stockworks have been evaluated in the model.

Sulphidisation consists of the dissemination of pyrrhotitic and the occurrence of pyritic stockworks of considerable dimensions. Disseminated pyrrhotite is associated with mica gneisses and migmatites and has a particular affinity with graphitic occurrences. The

sulphidisation reaches its greatest depth, -250 to -300 m, on the SW margin of the modelled bedrock volume (Figure 4-13).

The kaolinitic alteration zones consist of numerous spots and lenses at irregular intervals, which have thicknesses from tens of centimetres to tens of metres in drill cores. The most intensively kaolinised zones appear as strongly-weathered and softened sections, and kaolinised zones contain illite on slickensides and as fracture fillings. Kaolinite occurs as spots, either as a single phase, or together with illite. In addition, kaolinite forms powdery, disseminated white coatings that may be several millimetres thick.

The kaolinised sections are located in the upper part of the modelled volume, varying in thickness from 100 to 200 m. Where present, kaolinite appears to be an important constituent of the rocks, forming 5 - 30% or locally even more of the volume. In the alteration model (Figure 4-14), the kaolinised wedge becomes deeper in the northern part of the target area, where the kaolinised block reaches a depth of 250 m.

Illite alteration zones are present as green, transparent, soap-like masses or grey to green and waxy or powdered coatings on fracture planes. In drill cores, the illitised zones are characteristically 5 to 20 m thick. Illite may occur as a single alteration product, but generally it is associated with calcite and sulphide precipitates and with the other clays, such as other members of the kaolinite group, or from the smectite or chlorite groups. The illite alteration forms a block, which is located to the north of the ONKALO volume (Figure 4-15) and the drillhole data indicate that this block encloses the eastern repository panel. In the zones of advanced illitisation, illite has replaced most of the previous minerals and the rock has adopted to a totally new chemical composition and has approached the equilibration with its new environment, which is related to the chemical state generated by the fluid-rock interaction. This process has typically resulted in rock with a lower mechanical strength. The process of illitisation has been more effective than that of kaolinisation and it is assumed to have had a greater influence on the host rock.

The occurrence of calcite as infillings on the walls of fractures and as planar and irregular veinlets is a special feature of the drillholes, but has had only a minor affect on the rock, and there is hardly any evidence of penetrative carbonatisation of the bedrock itself. Instead, calcite may have an important role in hydrothermal-derived fractures and zones of brittle deformation and, similarly, calcite precipitates are widely observed in the matrices of breccia fragments and in thick clay fracture infillings. The fluid inclusion study of the fracture calcites has demonstrated that calcite precipitation took place at a temperature which was initially 300°C, and later reduced to less than 100°C.

There is evidence that the distribution and density of calcitic fracture sets is increased in the zones where hydrothermal fluid flow has chemically and physically reworked the bedrock. In line with the three other alteration processes, carbonatisation has a significant role in alteration, and the total volume of calcite in the hydrothermally altered zones appears to be significant. The reaction kinetics for calcite precipitation-dissolution reactions are known to be rapid, and for that reason calcite may well have had several phases of precipitation and dissolution. Since hydrothermal activity started,

the precipitation of calcite has continued up until the present whenever calcite has reached saturation level in the groundwater system.

The grade of carbonatisation has been estimated by mapping the frequency and thickness of the calcitic fractures in the drillholes. When the recurrent calcite-filled fractures are combined into zones, the carbonatised sequences appear to be located in the same positions as the other alteration types. The drillhole lengths of the fracture-connected calcitic zones vary from few metres to tens of metres.

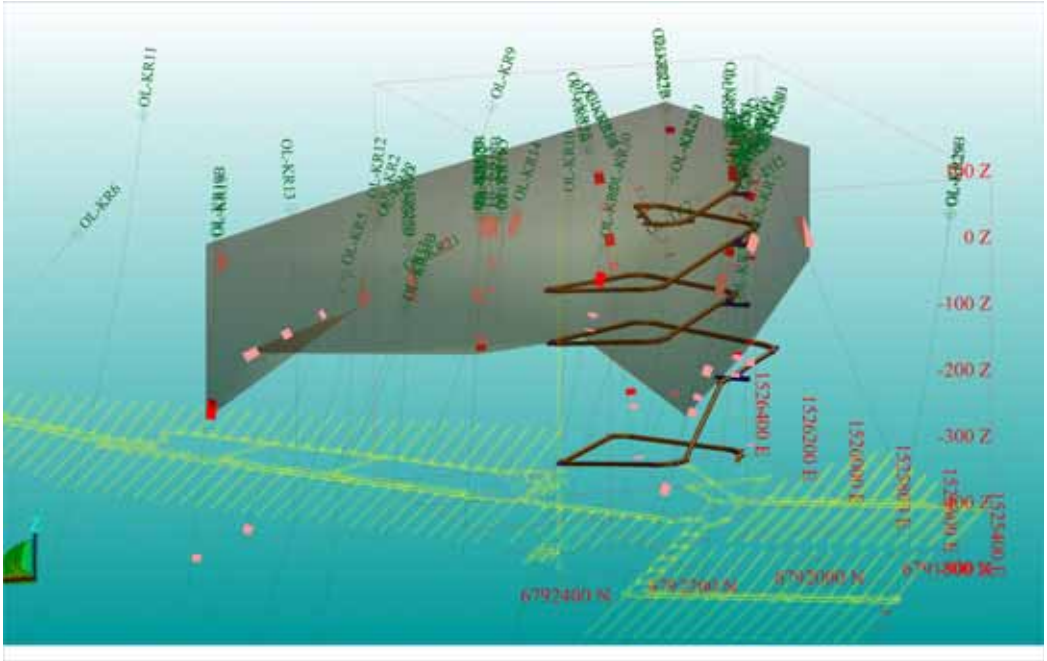

Figure 4-13. *Sulphides are located in the uppermost part of the model volume and their distribution roughly follows the lithological trend (dipping slightly to the SE). A view towards the SE. Red = pervasive sulphidisation, light red = fracture-controlled sulphidisation. The currently suggested repository layout is shown for reference.*

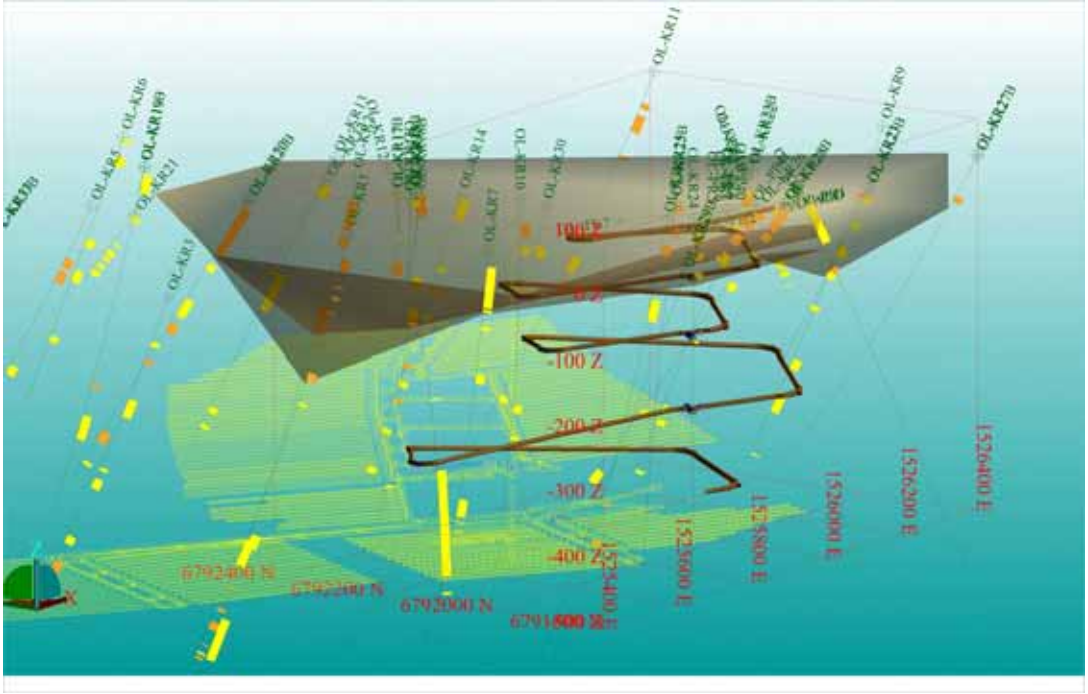

Figure 4-14. *Kaolinised domain located in the uppermost part of the site volume. View towards the NE. Yellow = pervasive kaolinitisation, orange = fracture-controlled kaolinisation. The currently suggested repository layout is shown for reference.*

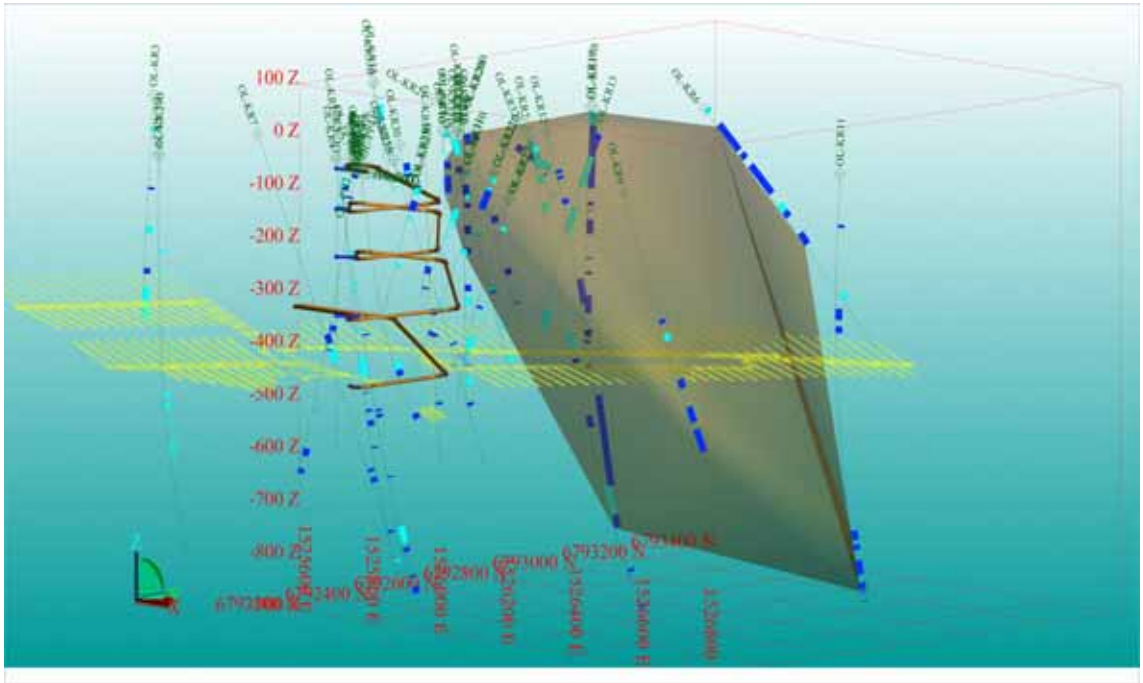

Figure 4-15. *Domain of pervasive (dark blue) and fracture-controlled (cyan) illitisation. A view towards the NW. The currently suggested repository layout is shown for reference.*

4.3.3 Ductile deformation

The bedrock at Olkiluoto belongs to the Svecofennian domain of Southern Finland, which was deformed in a ductile manner during the Svecofennian Orogeny ca. 1.91 – 1.80 Ga ago (e.g. Gaál & Gorbatsvhev 1987, Nironen 1997). The bedrock, except for the diabases and certain pegmatitic granite dykes, has been affected by five stages of ductile deformation, as determined on the basis of refolding and crosscutting relationships (Paulamäki & Koistinen 1991, Aaltonen 2005, Kärki & Paulamäki 2006).

The lithological layering (S_0) and penetrative, slightly segregated foliation S_1 of deformation phase D_1, which is mostly (sub)parallel to S_0, are the oldest observed structural features at the site. Structures of this deformation phase have been detected only sporadically within the hinges of isoclinal, intrafolial folds.

The subsequent deformation phase D_2 is a complex chain of events, characterised by intense thrust-related folding and leucosome production. During the D_2 deformation the earlier structures were overprinted by a penetrative S_2 schistosity or metamorphic banding, associated with strong migmatisation and the abundant production of leucosome veins parallel to the F_2 axial surface. Due to the tightness of F_2 folds and the intensity of the D_2 deformation, the lithological layering and earlier foliations have been often rotated parallel to the S_2 foliation which can, in fact, be expressed as a composite $S_{0/1/2}$ structure.

During the course of progressive D_2 deformation, the production of leucosome veins continued and the veins formed earlier were folded isoclinally and accompanied by semiconcordant shearing. Shear-related structures have been observed as the most important D_2 elements in certain zones or lithological units. Some fragmentation of the migmatitic gneisses and rotation of the fragmented blocks occurred in the waning stage of the D_2 deformation. The D_2 deformation is assumed to be the most intense ductile deformation event in the structural evolution of the Olkiluoto area (Paulamäki et al. 2006) - it has pervasively deformed the whole gneiss complex simultaneously with upper amphibolite facies metamorphism.

In deformation phase D_3, the migmatitic gneisses deformed during D_1 and D_2 were refolded or rotated. Zones dominated by ductile D_3 shears and folds were formed, and the S_2 foliation was reoriented parallel to the F_3 axial plane (S_3), so that the foliation can be described as a $S_{2/3}$ composite structure (Figure 4-16). Typically no new foliation was created, but new granitic leucosome was intruded parallel to the F_3 axial planes. The fold axes of the F_3 folds usually plunge gently to the NE or SW, indicating the subhorizontal orientation of previous planar structural elements. Overturned F_3 folds with axial planes dipping to the SE have been mapped in the eastern part of the Olkiluoto area.

The D_3 elements and earlier structures were again redeformed in the following deformation phase D_4, which produced close to open F_4 folds with axial planes trending ca. NNE -SSW and dipping to the ESE (Figure 4-16). The central and southeastern parts of the Olkiluoto site, the ONKALO area and the regions eastward from that, have been more strongly affected by this deformation phase. Due to D_4 deformation, the $S_{2/3}$ composite structures were zonally reoriented towards the trend of the F_4 axial planes

(S_4). Locally, ductile D_4 shear zones subparallel to the regional S_4 plane have been observed.

The latest identified ductile structures are very open F_5 folds, the fold axes plunging gently to the ESE and axial planes to the SSW (Figure 4-16).

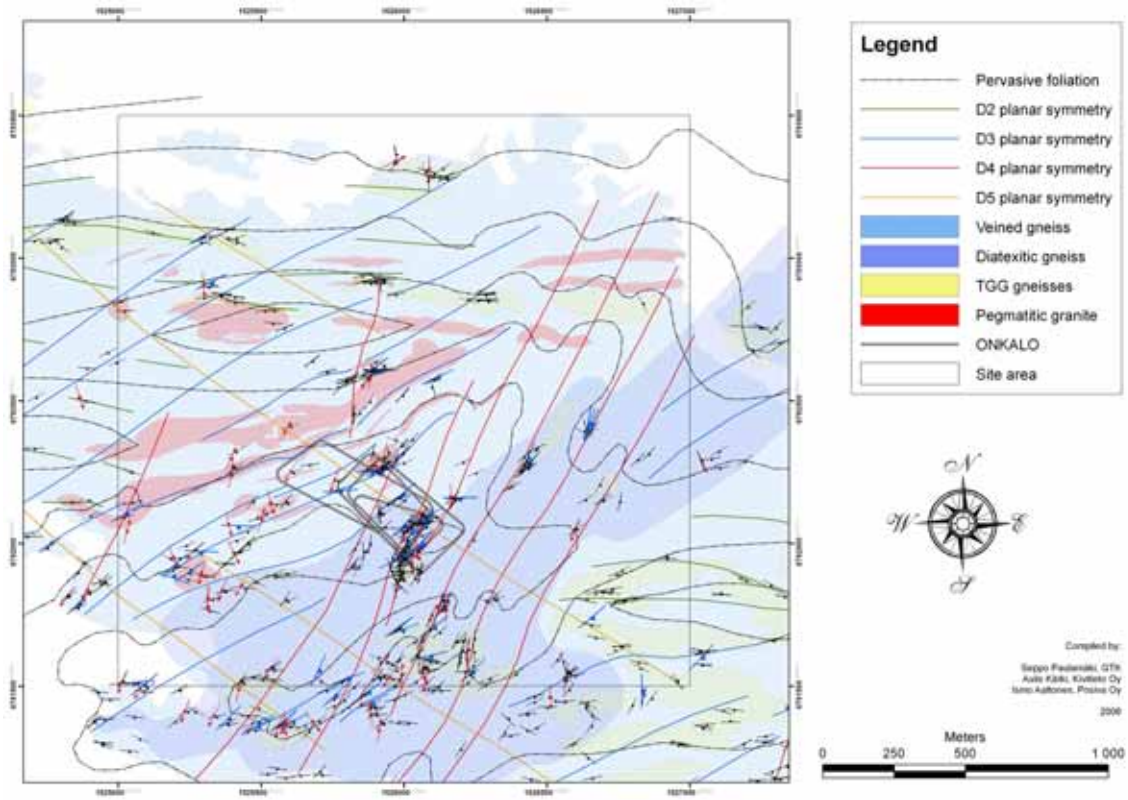

Figure 4-16. *General trends of planar D3 – D5 ductile deformation elements. Tentative form lines of the pervasive foliation by (Paulamäki et al. 2006).*

The 3D ductile deformation model (Figure 4-17) is extended downward from the 2D model shown in Figure 4-16. The trends of structural symmetry, i.e. the orientations of axial surfaces and rarely-developed axial surface foliations and the domains of the most intense D_3 and D_4 deformation, are determined on the basis of drill core sample investigations. The 3D model visualizes the domains affected most intensively by these late-stage deformations. The model also shows the anticipated orientations of S_3 and S_4 axial surfaces down to a depth of 500 m.

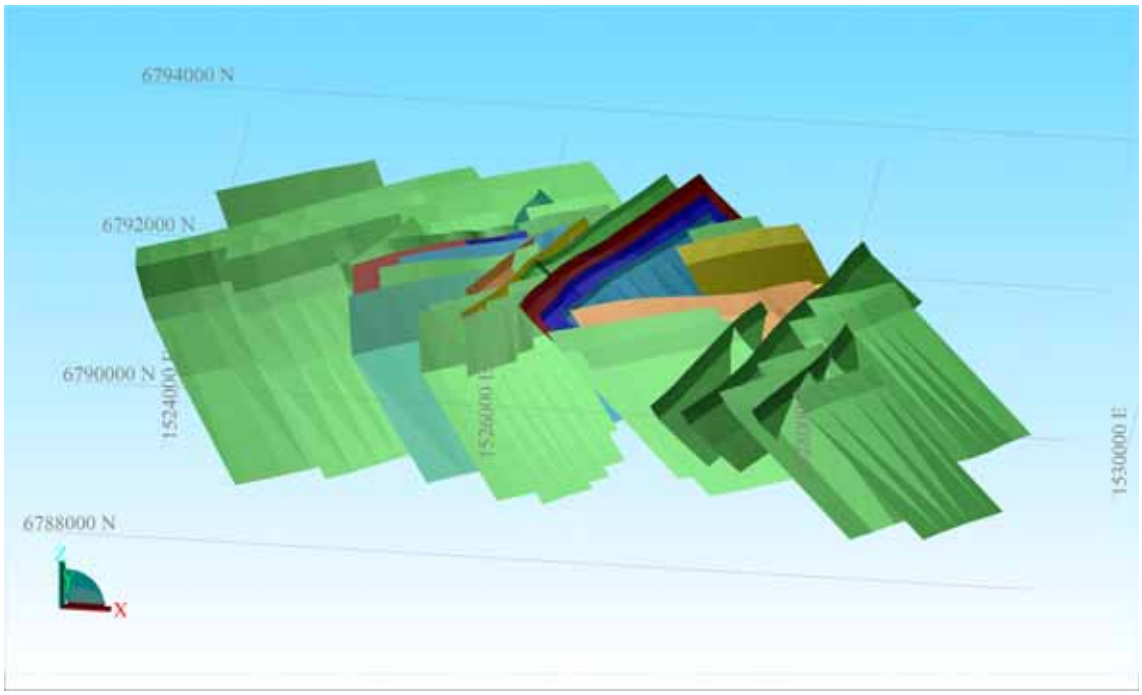

Figure 4-17. *The 3D model of the orientation of the composite foliation $S_{2/3/4}$ dipping gently to the S and SE. The colours are from the Surpac software and do not refer to any specific foliation (Paulamäki et al. 2006).*

4.3.4 Brittle deformation

After the Svecofennian Orogeny ca. 1910 – 1800 Ma ago, the Fennoscandian shield was dominated by the following tectonic events (Kohonen & Rämö 2005; Paulamäki & Kuivamäki, 2006):

- Intracratonic rift basin stage at ca. 1600-1300 Ma, associated with the intrusion of rapakivi-granites and the formation of the Satakunta graben
- Sveconorwegian orogeny at ca. 1250 - 900 Ma, which mainly affected the present southwest of Sweden and southern Norway. In Finland, the 'Postjotnian' olivine diabases, dated at 1270 - 1250 Ma, and which also occur close to Olkiluoto, are considered to be connected to the initial rifting prior to the onset of the orogeny
- Break-up of the supercontinent Rodinia at ca. 620 - 600 Ma, opening of the Iapetus Ocean
- Caledonian orogeny at ca. 430-350 Ma ago
- Opening of North Atlantic during Tertiary (at ca- 65-1.6 Ma ago) and associated substantial tectonic uplift (1-2 km) in northwestern Scandinavia

Currently, the connection of these main tectonic events in the Fennoscandian Shield to the brittle deformation zones observed in Olkiluoto is poorly understood, but, nevertheless, these events do provide the framework for further constraint on the timing and development of brittle structures in Olkiluoto. There will be more focus on this topic in the Geological Site Model report (version 1.0).

A total of ca. 1700 fault plane and fault vector directions were measured. The most common population of fault planes dips gently to the SE, but statistical evaluation of fault plane orientations does not provide any useable basis for a further subdivision of these structures. Detailed analysis of fault-slip data, however, shows that more than 20 groups of kinematically-similar brittle faults can be detected on the site. Evaluation of their real impact on the bedrock structure is a challenging exercise and, for that reason, this initial modelling is based on the result of a simplified and generalised classification of fault-slip data. Tentatively, five groups of brittle faults (Groups A to E) can be defined from the total number of brittle faults. Fault-slip directions are subhorizontal, N-S trending for group A, gently NE or SW plunging for group B, gently SSE plunging for group C, gently ENE plunging for group D and gently SE plunging for group E. In all of the groups, most of the fault planes dip gently to the SE. In fault groups A and B there are also fault planes dipping steeply to the E and SE, respectively.

Recent studies of the structural evolution of the Olkiluoto bedrock have shown the obvious statistical similarity between the orientation of the regional, composite, pervasive foliation and the slickensided fracture surfaces, measured from the drillholes. One explanation for this relation is that the faults appear to have exploited the planes of weakness imposed by the pervasive foliation. The products of ductile deformation seem, therefore, to be important precursors for subsequent brittle deformation; however, many brittle fault structures are not controlled by any older deformation elements.

The starting point for the brittle deformation modelling was the observed intersections of deformation zones (brittle fault intersections and brittle joint intersections) in the drillholes, their kinematic data and geophysical indications. Since the brittle fault zones were supposed to be the spatially most continuous brittle features, the modelling work was strongly focussed on them.

All five fault groups were modelled separately. The modelled brittle fault zones are shown in Figure 4-18 - Figure 4-22.

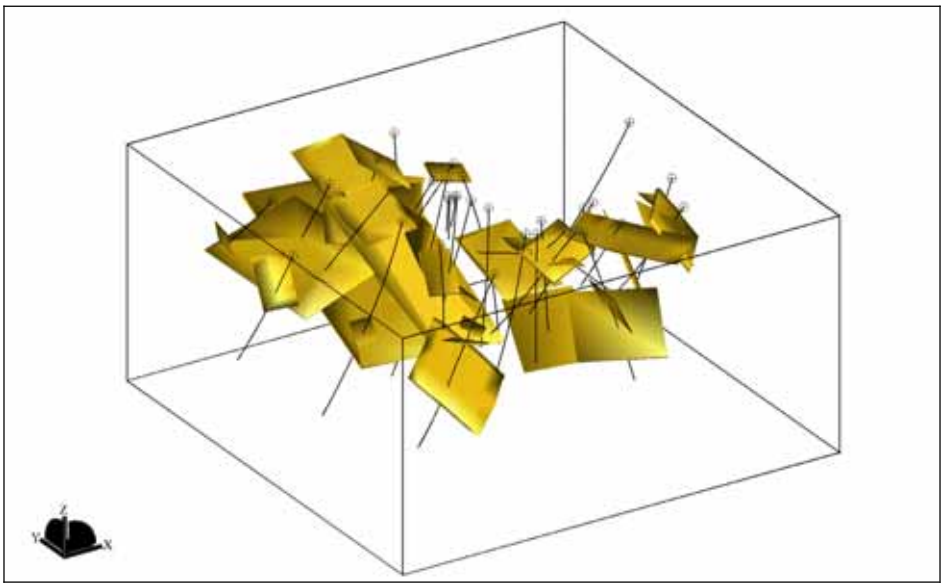

Figure 4-18. *Fault zones of fault group A. View from the SW.*

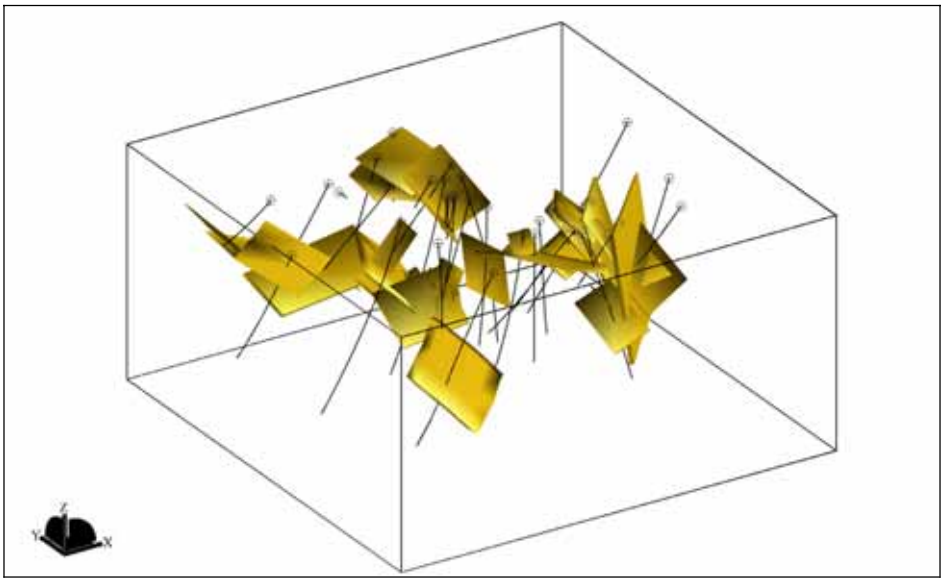

Figure 4-19. *Fault zones of fault group B. View from the SW.*

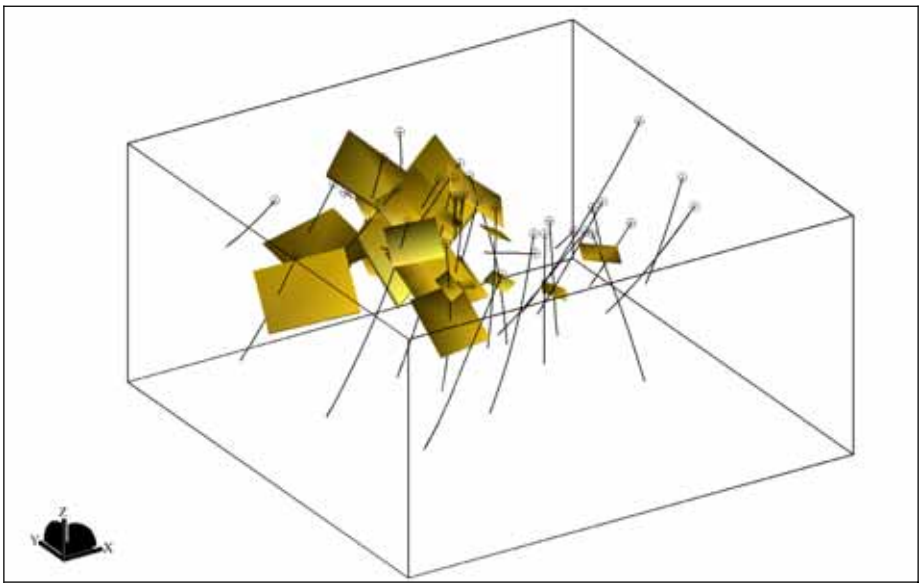

Figure 4-20. *Fault zones of fault group C. View from the SW.*

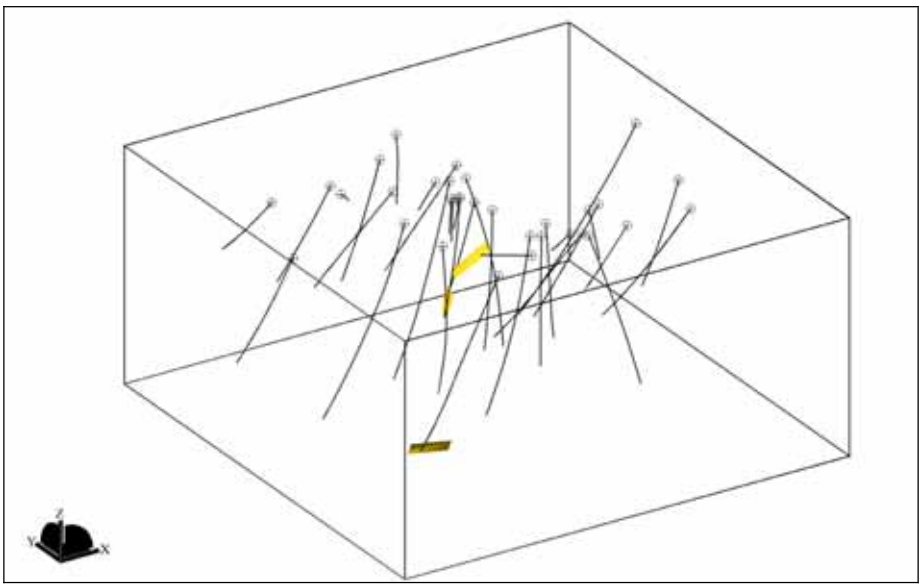

Figure 4-21. *Fault zones of fault group D. View from the SW.*

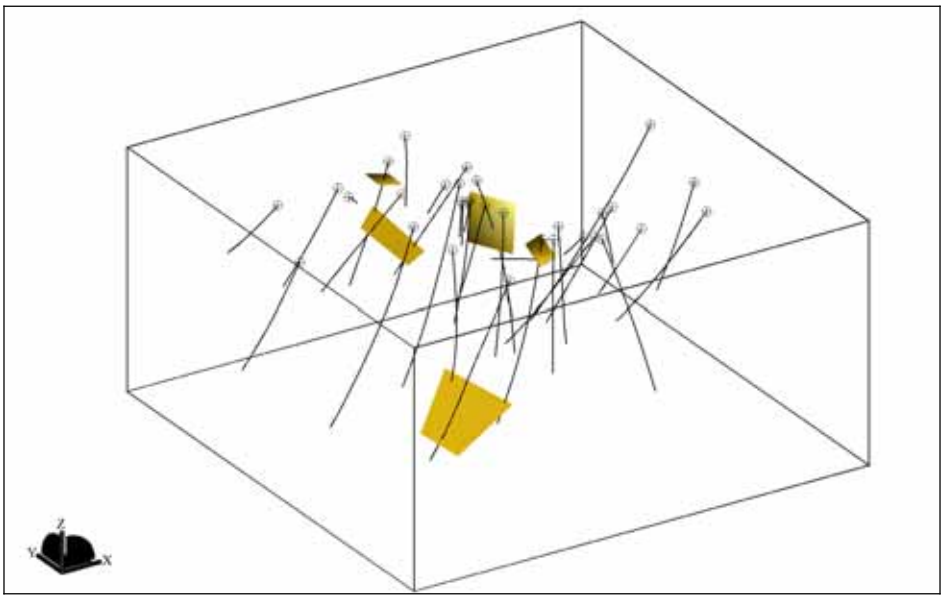

Figure 4-22. *Fault zones of fault group E. View from the SW.*

4.3.5 Fracturing (DFN-model and fracture characterisation)

A preliminary statistical model of fractures, based on all fracture data from investigation trenches OL-TK7 and OL-TK11, drillholes OL-KR24 and ONK-PH1 and ONKALO chainage PL0 – 140 m, has been developed by Tuominen et al. (2006) for DFN modelling of the ONK-PH2 area. Fractures were assigned to three sets based on their orientation: a sub-horizontal set dipping towards the SE, and two vertical sets with N-S and E-W strike. The mean orientations of the sets are 139°/18°, 089°/89° and 177°/86°, with the first set having clearly the smallest dispersion. The size distribution and intensity were defined for each set and the influence of the data source and the geological setting, such as the effects of rock types and the presence of deformation zones, were analysed. The DFN parameters were defined for migmatites, excluding fractures within any deformation zone.

The work of Tuominen et al. (2006) was a first attempt to statistically describe fracture data mapped from the ONKALO, from drillholes and from investigation trenches and, as such, the model is representative of the near-surface parts of the ONKALO access tunnel. The resulting parameters are presented in Table 4-2 and an example of the simulated fracture map is presented in Figure 4-23.

Table 4-2. *Summary of simulation parameters in Tuominen et al. (2006).*

		P_{32}	r_{min}	k_r
Set 1	Dipdir = 139 Dip = 18 Disp. 7,9	**0,87**	**0,52**	**3,33**
Set 2	Dipdir = 89 Dip = 89 Disp. 16,7	**0,47**	**0,22**	**3,11**
Set 3	Dipdir = 177 Dip = 86 Disp. 16,6	**0,45**	**0,47**	**3,5**

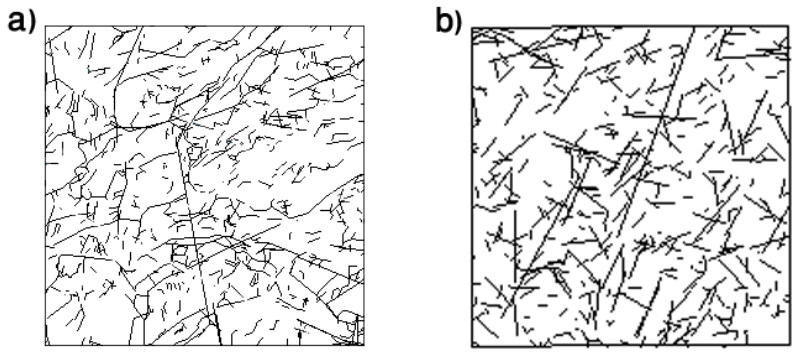

Figure 4-23. *Trace map of a 20 m x 20 m area of OL-TK11 (a) and trace map of 20 m x 20 m sampling trace plane from the simulation (b) (Tuominen et al. 2006).*

4.4 Interaction with other disciplines

The Geological Site Model is constructed using purely *geological* data, as this provides the basic framework for the models from other disciplines and also indications as to the probable locations of incohesive rock, which are the potential flow routes for groundwater and one of the main reasons for local perturbations in the existing stress field. Therefore, integration with other disciplines (rock mechanics, hydrogeology and hydrogeochemistry), following the completion of the Geological Site Model, is a vital phase of the modelling, as the subsequent integrated model provides the basic background for the assessment of long-term safety and the estimation of the suitability of bedrock for repository development.

During the latest phase of modelling, initial steps were taken towards building an integrated bedrock model – the modelled geological objects were used as input for the hydrostructural model and the interrelationships between the brittle deformation zones and measured hydraulic connections were closely assessed during integration meetings, with participants from both the geological and hydrogeological modelling teams. The

purpose of this approach was to develop a formalised methodology for the integration and also to enhance active discussion between different disciplines. In the future, there will be further such meetings and the resolution of the integration will be increased from the zone-scale to the fracture-scale. In addition, feedback from the end-users provides the necessary tool for the continuous development of the Geological Site Model and, therefore, the whole concept of integration can be thought of as a continuous, iterative process.

4.5 Uncertainties

Uncertainties in the lithological and ductile deformation models

One of the main uncertainties in the lithological 2D model is due to the incomplete coverage of available data. The bedrock is rather poorly exposed, which causes difficulties in determining the location of lithological boundaries. In the central investigation area where outcrop is limited, the mapping has been supplemented by the results from deep and shallow drillholes, ten investigation trenches and the interpretations of the geophysical investigations. However, the contacts between the rock types are visible only occasionally, and, thus, the bedrock map is largely an interpretation, which combines the direct observations of the rock types and their contacts in outcrops, investigation trenches and in drillholes with the interpretation of the geophysical investigations and the tectonic structure of the area.

During the site investigations, a number of different geologists have carried out the outcrop and trench mappings at Olkiluoto. Since the outcrop data are largely descriptive in character and based on the interpretations of individual geologists, they are rather heterogeneous. Moreover, the names given to the rock types during the early mapping in 1988 and 1991 were different from those adopted later in the drill core studies. Although the nomenclature has recently been standardised (see Mattila 2006 and Kärki & Paulamäki 2006), uncertainties may still exist, especially regarding the naming of different migmatite types. The gneisses and migmatites of Olkiluoto form a transitional series and it is not possible to define any clear contacts between the rock types, as the change from one type to another takes place gradually. An artificial border between the gneisses and migmatites has been set at 10% or 20% of granitic leucosome. Within the migmatites the proportion of the leucosome varies from about 10% to more than 80%.

Although lithological data from 33 drillholes have been available in preparing the 3D lithological model, they are, however, rather limited in number and the distance between the drillholes is relatively large. Consequently, there are uncertainties concerning the geometry and extension of the various rock units at depth - uncertainties remain, especially with regard to the size and extension of the pegmatitic granites. In the lithological model, the granite pegmatite sections in drillholes more than 10 m in length have been distinguished as separate units. In addition, pegmatite sections which are less than 10 m in length, if separated only by short sections of migmatitic mica gneiss, are combined into larger units. It is known that the pegmatitic granites are not as continuous and coherent as modelled, but exist in reality rather as volumes of rock where granite pegmatite veins are more common than outside these units.

The complexity of the ductile deformation is an important source of uncertainty in the bedrock modelling. The bedrock has been interpreted as having been subjected to five successive ductile deformational phases. The actual measurement of the various ductile deformation structures (foliation, folds, lineations etc.) can be rather exact, although errors certainly occur, for instance, in the measurement of dip values. The complexity of the deformation leads to difficulties in determining the distribution and form of the different lithologies occurring at the surface or at depth.

The effects of folding, especially during D_3, have not been visualised in the 3D lithological model, except in the case of veined gneiss/diatexite contact, but an assumption was made that the foliation is rather constant over large distances between drillholes and that lithological correlations from drillhole to drillhole and from the drillhole to surface can be made in accordance with foliation measurements. Thus, the current model must be seen as a simplified representation of probable complex geological structures. Although we have rather a good understanding of the larger-scale folding in the site area, presenting it in 3D is difficult because of the lack of proper larger-scale marker horizons. The migmatites, which in the present lithological model form the main volume of the rock mass, have been divided into different migmatite types. Their use in the modelling is uncertain, however, because the classification is based solely on a visual inspection of rock types in outcrops and drill cores by a number of individuals, independently of each other. More detailed petrological and lithogeochemical studies of the drill core samples have shown that the metasedimentary and metavolcanic rocks of Olkiluoto can be subdivided into four different series This new classification of the migmatitic mica gneisses may provide a way of incorporating the folding into the lithological model. However, information on the distribution of these series is, at present, far too sparse to be used in the modelling.

Uncertainties in the brittle deformation model

In general, one important source of uncertainty in geological modelling is the small number of drillholes, their uneven distribution and the distances between them. At Olkiluoto, the ONKALO area is well covered with drillholes and here the confidence in the model is higher; nevertheless, within the modelled area, there are still a few "white areas" (See Figure 4-24), where the drillhole density is very low which, in turn, affects the confidence of the model, at least locally. In addition, in places where there are no drillholes, deterministic modelling is impossible, due to lack of proper data and, as a consequence, these areas are likely to be underrepresented by geological features in the model. Another cause of uncertainty is the relatively uniform drilling orientation that results in bias, as it masks the occurrence of possible N-S trending features.

Modelling the brittle phase of deformation is associated with two types of uncertainty. The first of these is a measurement-related problem, i.e. how to identify and measure brittle elements and their kinematic features (e.g. fractures, slickensides, fault slip direction, sense of slip direction) correctly and the second is data analysis-related or associated with conceptual uncertainty.

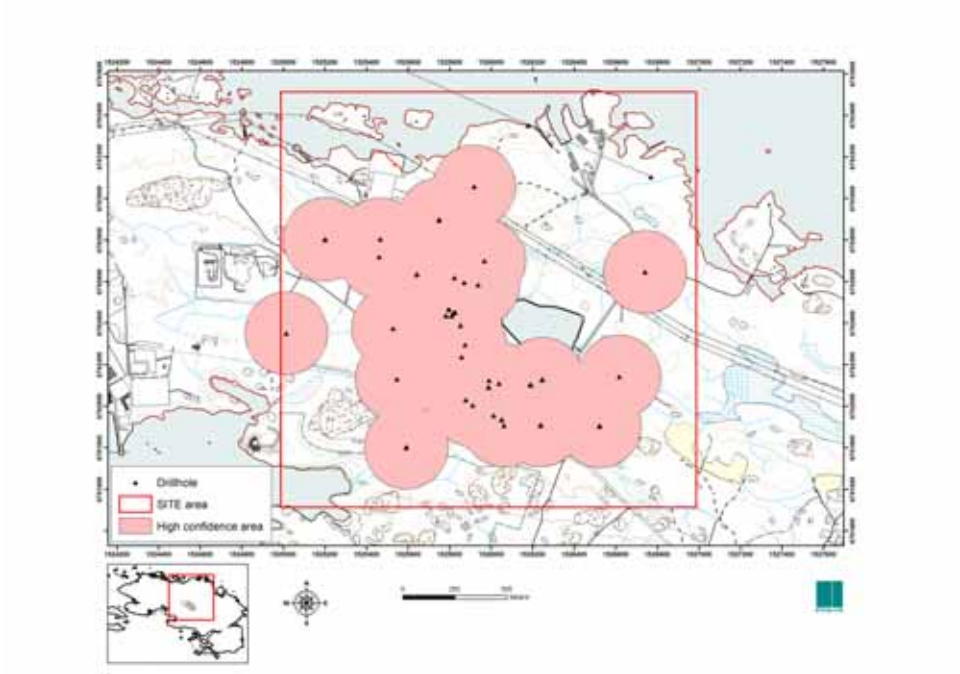

Figure 4-24. *The location of drillholes 1-33 (black triangles) and the area of higher confidence, presented as a cluster of light-red circles. The area adjoining the high confidence area within the site area (red rectangle), depicts an area with lower data density and thus the confidence of the model is lower in this region. Note, that the Figure refers to the conditions at the surface.*

Modelling requires a large number of oriented data from drill core samples. The insufficiency of oriented core and in places the lack of core due to core loss, together with the increasing need for accurate orientation data on kinematic elements and fractures at depth, resulted in the substantial use of drillhole TV. The analysis of the TV imagery is associated with similar uncertainties as that of the drill core samples, as it makes use of the same deviation data. The other uncertainties are related to the disturbance or to the inadequate quality of the TV imagery, and sometimes to the difficulty in identifying the planar features in the imagery (i.e. the fractures). In the TV image analysis the core sample is also examined, if available, to compensate, for problems, such as the low quality of the TV imagery, and to minimise errors in the interpretation of planar elements.

Data analysis-related and conceptual uncertainties regarding the brittle deformation modelling are, for example:

- Orientation of the fault zones
- Length and down-dip extent of the zones
- Strong spatial variation in properties (width, fracturing, hydraulic conductivity) within the same modelled brittle fault zone

- Large number of modelled zones intersected by only one drillhole and presented as rectangular bodies, extending about 50-300 m from the drillholes
- Surface exposure of the fault zones
- Termination of the fault zones (in the present model, almost all the modelled zones are presented as individual zones)
- Lack of possible N-S and NW-SE-striking fault zones, which may exist between the drillholes (which tend to have been drilled with similar orientations)

There are large uncertainties in the orientations of the modelled zones, since the majority of such orientations are based on a few striated fault surfaces, which are assumed to reflect the orientation of the zone. In some zones the orientation is determined by just one or two faults. With regard to the certainty of the orientations, 8 zones are associated with a high level of confidence, 25 a medium level of confidence and 70 a low or very low level of confidence. As the orientation of the modelled fault zones is normally based solely on the kinematic data, errors in the data may have a significant impact on the orientation of the zone. Moreover, even if the data are correct, there can be several different fault orientations in one drillhole intersection, resulting in other interpretations of the orientation of the whole fault zone. By using fault plane orientations as a tool for cross-hole correlation, the effect of secondary shear fractures is neglected, i.e. the modelled orientation of the zone may correspond to the "local" small-scale orientation of the fractures within a zone (i.e. internal geometry) and not to the large-scale orientation of the actual zone. The role of reactivation, producing various slip-directions even within a one single zone, is also neglected, and this may effectively hinder cross-hole-correlation. Drillhole intersections lacking kinematic data (i.e. brittle joint intersections) were generally not modelled, as the current modelling method does not provide sufficient tools for the cross-hole correlation of purely extensional fractures. This is likely to cause some uncertainties in the integration with hydrogeological models, as extensional fractures are likely candidates for transmissive features.

Both the horizontal and down-dip continuities of the modelled fault zones are uncertain. Although 33 drillholes have been drilled at the site area, it is, however, a rather small number considering the dimensions of the area, and the distances between the drillholes are quite large. This causes uncertainties in connecting the individual brittle fault and joint intersections in one drillhole to another over large distances, and has led to a large number of zones extending only about 50-300 m from the drillhole. However, it should be borne in mind that these rather limited dimensions are not necessarily incorrect, since the fault zones may actually be discontinuous, as noticed in areas where many drillholes are closely spaced.

There are uncertainties in measuring the dip of fractures accurately, as the outcrops lack much relief, and, at the very least, horizontal or subhorizontal fractures are underrepresented in the surface fracture data. There are considerable uncertainties in the distribution of the fracture trace lengths, since only about one-third of the measured

fractures in the outcrops and investigation trenches can be seen over their full length (i.e. terminations of both ends of a fracture are visible).

Uncertainties exist regarding the relationship between the surface fracture data and the drill core data. There are, for example, differences in the distribution of fracture sets. For example, the ca. N-S striking fracture set, which is one of the two main fracture sets in outcrop, is commonly only poorly represented in the drill core fracture data, probably due to the unfavourable orientation of many of the drillholes. In the previous phase of the site investigations, the outcrop data and the drillhole data were combined and a correction method was used to reduce the bias by compensating for the under-represented fractures (see Paulamäki & Paananen 1996).

Although most of the modelled fault zones strike E-W or NE-SW, i.e. follow the general trend of the ductile deformation, the existence of N-S and NW-SE striking zones cannot be overlooked. The N-S striking fractures form a very distinct fracture cluster in the outcrop data and all the brittle faults observed at outcrop strike either N-S or NW-SE. Moreover, NW-SE trending lineaments are very common in the Olkiluoto area.

Uncertainties in the alteration model

The alteration study benefited from data collected in the pilot study from deep drillholes OL-KR1 to OL-KR33 and the visual assessment of the alteration was supported by the preparation of a small number of thin sections. At the moment, the mapping method is one of the main limitations of the alteration study, because it is mineralogically overly simplistic, with the result that uncertainties are introduced. For example, all greenish, soft clay-type material is classified as illite, although illite is known to occur together with a variety of other minerals, such as those of the smectite group, chlorite, montmorillonite, etc. In thin sections, it was impossible to separate the above minerals from each other, or illite from fine-grained muscovite or sericite; however, the mode of occurrence of illite or illite-like material shows clear replacement of older silicate minerals, often plagioclase. Considerable instrumental analytical work would be required to distinguish and identify different mica and clay species, but any of these minerals may have the same impact on the safety case or construction, as they are present as a soft, soap-like mass, which may form 5 - 10% by volume of the rock at Olkiluoto, locally even greater. Kaolinite forms very fine-grained, pure white, soft and powdery masses and coatings which, in some places could be mistaken for fine-grained calcite, which, however, can be identified by using dilute hydrochloric acid. The configuration and number of the drillholes, in particular, limit the evaluation of the size of the illitic body and its continuation to the NE and E.

5 ROCK MECHANICS

This Chapter provides an overview of the rock mechanics aspects of the Olkiluoto site characterization. The objectives and approaches of the rock mechanics site modelling are presented first in Section 5.1; this is followed by an evaluation of the available investigation data and comments on the utilisation of the data in Section 5.2; then the interaction with the other disciplines is described in Section 5.3. The rock mechanics modelling itself is described in the Section 5.4 and comprises separate sub-sections on in situ stress, intact rock properties, thermal properties, drilling properties, fracture properties, brittle deformation properties and mechanical properties of the rock mass. Section 5.4 concludes with a description of the bedrock stability measurements. Finally, Section 5.5 describes the evaluation of uncertainties relating to rock mechanics properties.

5.1 Objectives of and approaches to the rock mechanics modelling

5.1.1 Purpose and uses of the rock mechanics model

In order to characterize the Olkiluoto rock mass for the purpose of hosting a radioactive waste repository, it is necessary to have a rock mechanics model in order to be able to predict the consequences of various repository design options, including the repository depth and deposition tunnel orientations. If the rock stresses are too high, due to the repository being located at too great a depth, damage or even spalling can occur in the deposition tunnels and emplacement boreholes. If there are too many fractures forming rock blocks, there can be block fallout from the tunnel roof. The extent to which these problems might occur is a function of the stress state, the intact rock and fracture properties, and the location and orientation of the excavations.

Thus rock mechanics modelling is required, both in the sense of having a rock mechanics model describing the site and in the sense of undertaking numerical computer simulations to establish the impact of excavation for various conditions. With this modelling capability, the repository can be coherently designed from a mechanical point of view. If there are dominating criteria from other disciplines which dictate the design, then the mechanical consequences of a given repository design can be evaluated.

Although the principles of rock engineering and the necessary associated modelling for civil engineering are well known for general purpose underground construction, there are aspects of a radioactive waste repository which require special attention. These relate to the fact that the repository will be at a significant depth (ca. 400-500 m) compared to the usual depths for civil engineering structures, the repository function is waste isolation, and the design life far exceeds the conventional civil engineering design life of ~120 years. So, in addition to the need to provide site-specific information for input to the discrete element programs supporting the rock mechanics modelling, there is also the need to consider other aspects, such as the very long-term behaviour of stressed rock, the thermal properties of the rock mass, the interaction between rock mechanics and hydrogeology with regard to fracture flow, and auditing any uncertainties in the modelling data and procedures.

To put the rock mechanics contribution to the Olkiluoto Site Model and the interactions with other disciplines in context, the three separate areas of rock mechanics work are:

- rock mechanics characterisation of the Olkiluoto site;
- studies supporting the ONKALO and repository design and operations; and
- studies supporting the Safety Assessment.

This context is illustrated by the flowchart (Figure 5-1).

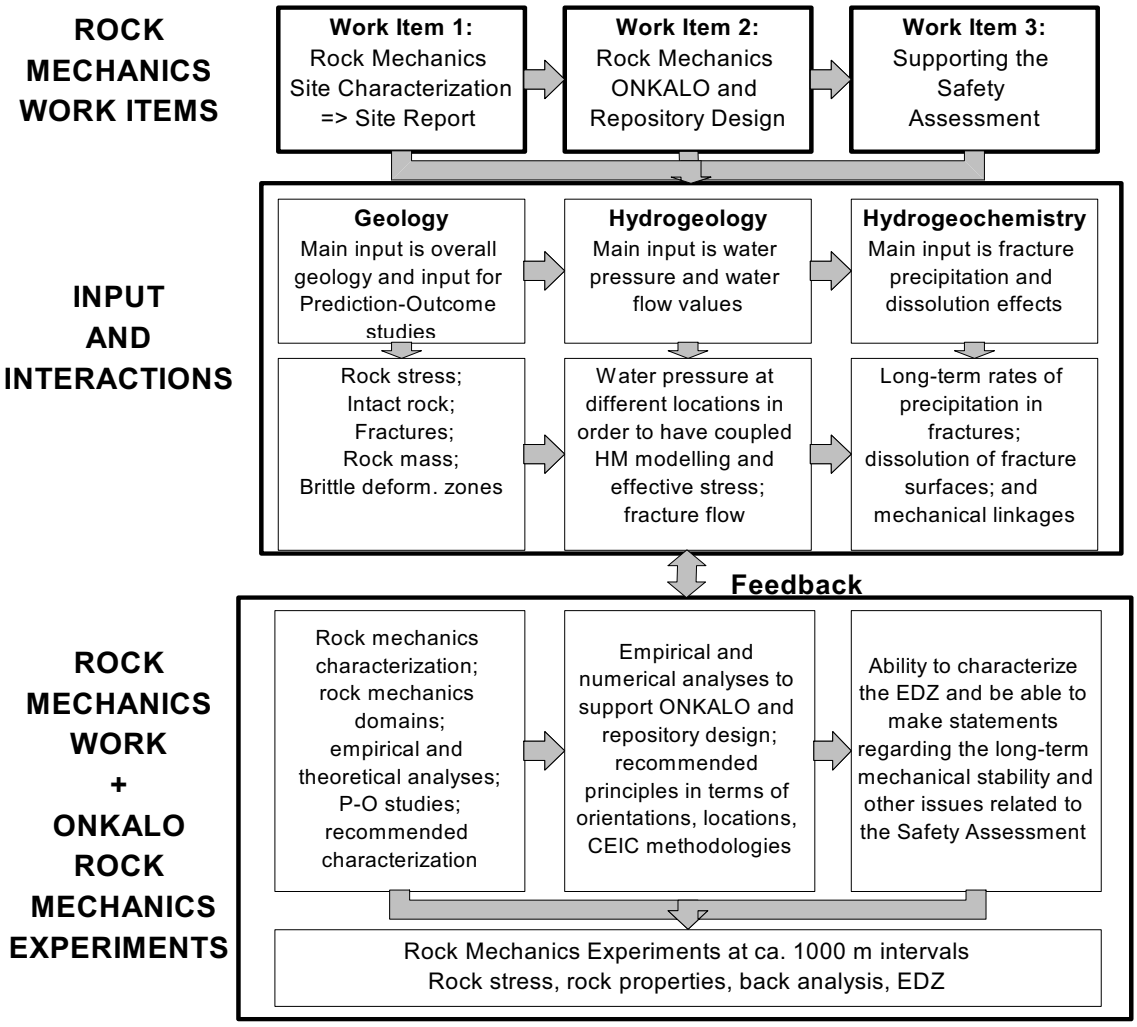

Figure 5-1. *Composite flowchart summarising Posiva's rock mechanics work.*

5.1.2 The rock mechanics conceptual model

In a general mechanics problem, the boundary conditions and geometry are specified, together with the material properties. A perturbation is then applied to the system in the form of changes to the boundary conditions, geometry, or material properties. The consequences of the perturbation are then evaluated. When the material involved is rock, it is a rock mechanics problem, as illustrated in Figure 5-2 This is the general conceptual model. A more extended conceptual model is shown in Figure 5-3.

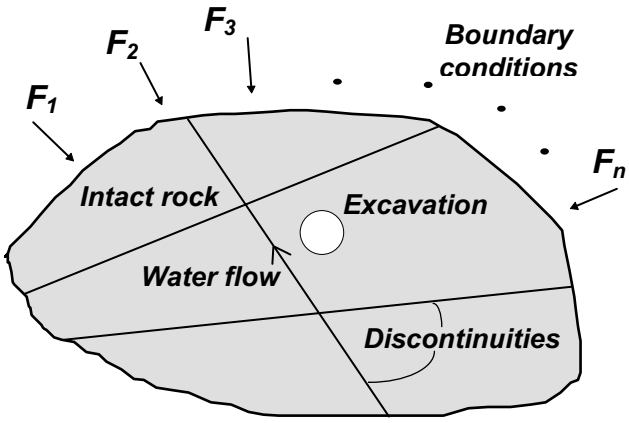

Figure 5-2. *The general conceptual rock mechanics model and its components.*

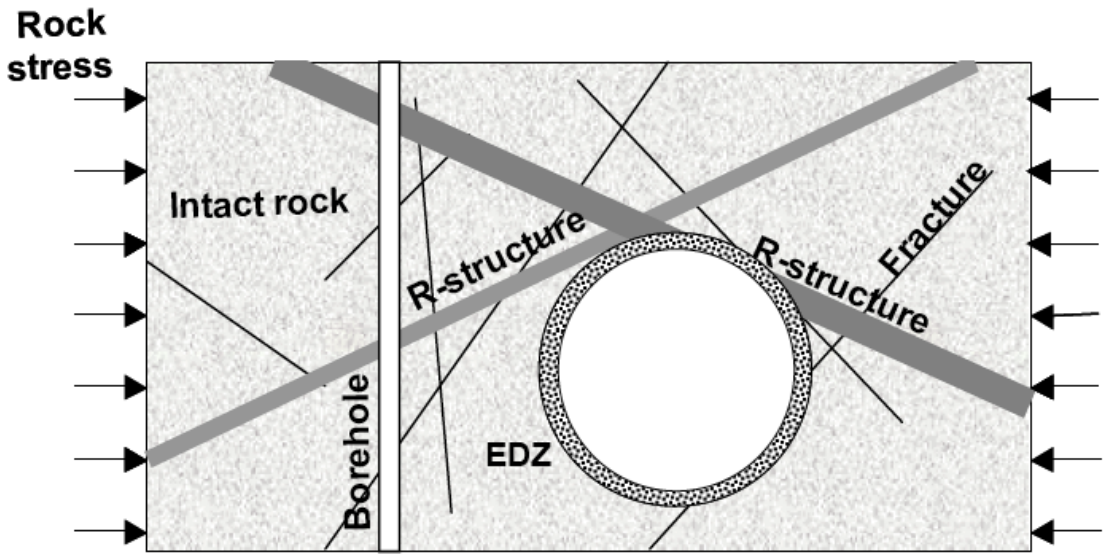

Figure 5-3. *Extended conceptual rock mechanics model.*

A change to the boundary conditions would involve alteration of the forces, F_i, illustrated in Figure 5-2 These force boundary conditions are usually expressed via the principal stresses (Figure 5-3), and so a change in the boundary conditions would involve a change in the far-field natural stress state. This is unlikely during the construction and operation of the ONKALO and repository and especially before the next glaciation period, except for the case of dynamic changes resulting from earthquakes. In the longer term, glacial loading and unloading will alter the vertical stress component and, to a lesser extent, the horizontal stress components.

A change in the geometry occurs, however, when an excavation is made, for example the tunnel excavation illustrated in Figure 5-3. Such an excavation could be the ramp of

the ONKALO, a shaft, or the deposition tunnels and holes. When an excavation is made, there are inevitable effects because:

- the stiffness of the rock in the tunnel volume has been reduced to zero,
- the stresses have been locally realigned to be parallel and perpendicular to the excavation surfaces, having passed along a stress path, and there have also been changes in magnitude,
- the hydraulic pressure in the tunnel has been reduced to atmospheric pressure.

In the immediate vicinity of the excavation (due to blasting and stress concentration), there is an excavation *damaged* zone, EDZ, in the sense that irreversible changes have occurred, e.g. the formation of microcracks. Further away from the excavation, there is an excavation *disturbed* zone, where the changes can be reversed, e.g. elastic displacements.

A change in the material properties can occur as a result of excavation, e.g. damage (spalling) of rock around the excavation when the secondary stresses become too high. There can also be long-term (creep) effects, i.e. continuing displacement as a result of the application of a constant stress. Additionally and in the longer term, there can be changes to the rock fractures and deformation zones as a result of groundwater flow, e.g. calcite precipitation in the fractures, which not only affects their hydraulic properties but also their fracture stiffness and strength. This is why there are strong links between rock mechanics and the sister disciplines of hydrogeology and hydrogeochemistry (cf. the flowchart in Figure 5-1).

5.1.3 Modelling methods

As indicated in the bottom left-hand box of the flowchart in Figure 5-1, the modelling methods include the direct characterization of the rock mechanics properties, consideration of rock mechanics domains in the rock mass (i.e. zones having similar rock mechanics properties), analyses based on both the empirical rock characterization approach and the theoretical computer-based approach. The Prediction-Outcome studies in the ONKALO enable these methods and the overall predictive approach to be refined, by repeated comparison with the outcome measured during the ONKALO excavation.

Additionally, the modelling methods will incorporate the interactions with other disciplines, as indicated in the flowchart in Figure 5-1.

5.1.4 Rock mechanics model components and parameters

Given the subject matter described above and the illustration of the rock mechanics conceptual model in Figure 5-2 and Figure 5-3, the key model components are as follows:

- the boundary conditions expressed as the pre-existing primary stresses in the rock mass;

- the unfractured intact rock;
- the individual fractures;
- the brittle deformation zones;
- the operating rock mechanics mechanisms, e.g. elastic deformations, and the mechanisms which are coupled with other processes and interact with other disciplines, e.g. the changes in effective stress caused by changes in the hydraulic pressure;
- the perturbations introduced by changes in boundary conditions, geometry and/or material properties; and
- evaluating the effects of the perturbations.

The salient points associated with these seven aspects of the conceptual model, together with the associated parameters, are briefly described in the following paragraphs.

The boundary conditions expressed as the pre-existing primary stresses in the rock mass. The in situ rock stress state is expressed via the magnitudes and orientations of the three mutually orthogonal principal stresses, i.e. σ_1, σ_2, σ_3. In Fennoscandia, the major principal stress, σ_1, tends to be sub-horizontal and oriented NW-SE. However, the rock stress is affected by the geological conditions, especially the major lineaments and brittle deformation zones, which can locally affect the principal stress magnitudes and orientations. There could well be significant differences in the stress states between various locations within the Olkiluoto site. Thus, the stress state cannot be assumed: it has to be established through measurements. The potential stress state variations through the rock mass can be determined through numerical models, such as the distinct element code 3DEC.

The intact rock. The key rock mechanics properties of the intact rock, i.e. the rock without visible fractures, are its stiffness (E) and uniaxial compressive strength (UCS). The stiffness determines how much strain will occur as the result of stress changes induced by excavation, and the strength determines when damage/failure will occur as the result of the applied secondary stresses, particularly in the EDZ region.

Key aspects of the intact rock properties are whether the rock is inhomogeneous (having different properties in different locations) and/or anisotropic (having different properties in different directions). The inhomogeneity can be taken into account via changes in the lithology and the establishment of rock mechanics domains, but the anisotropy requires an understanding of the foliation. In certain directions, the stiffness and especially the strength will be a function of the applied stress relative to the orientation of the foliation. In this case, a fully transversely anisotropic characterization is required with five elastic parameters, see Hakala et al. (2005) and Milnes et al. (2006).

The interaction between the stress field, the anisotropy of the intact rock and the excavation is illustrated in Figure 5-4. The magnitudes of the local circumferential stresses (stresses denoted by the white arrows) depend on the regional stress field. The direction of the foliation is indicated by the shading in the samples being considered around the excavation. Thus, the location of any stress-induced failure will be a function of these parameters in combination. Cracking induced by excavation is being studied via a Posiva EDZ programme, but not results are yet available.

The individual fractures. This refers to the individual fractures within the rock mass, which are not part of the brittle deformation zones. Because the rock stress has been applied through geological history via the three principal stresses, these fractures tend to occur in certain preferred directions, i.e. to be clustered into sets. One corollary is that the rock mass mechanical properties will be a directionally-dependent function of both the intact rock properties and the fracture properties. Another corollary is that the influence of the fractures will be a function of their orientation with respect to the excavation orientation.

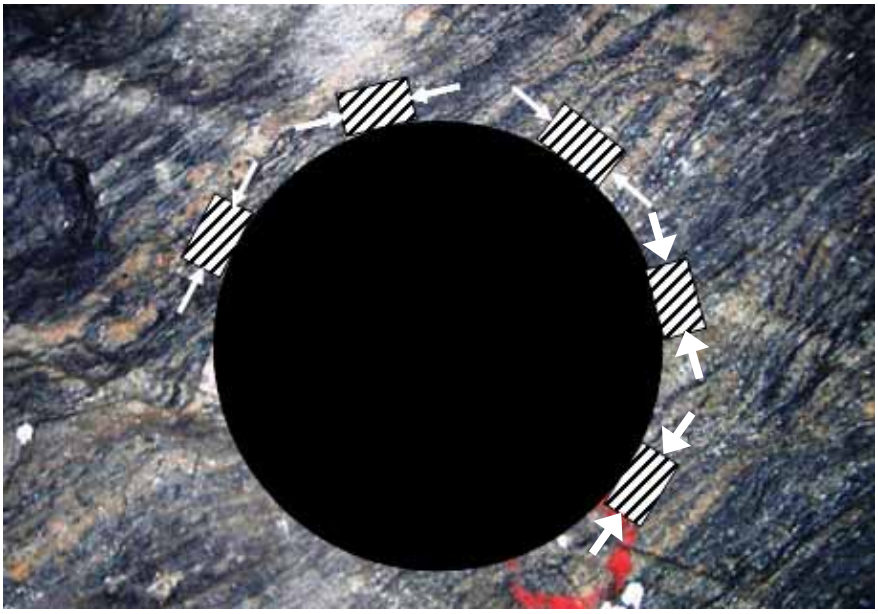

Figure 5-4. *The secondary stress field around an excavation in the anisotropic Olkiluoto rock mass.*

There are many characteristics of fractures, of which the most important are their frequency, orientation, trace length, stiffness and strength. In terms of block fall into excavations, the minimum number of faces that a rock block can have is four: i.e. a tetrahedral-shaped block. If the excavation surface forms one of these faces, there have to be three fractures at different orientations to form a rock block. Whether such a block will fall or slide into an excavation is a function of both the location and size of the block together with the orientation of the excavation surfaces.

The deformation zones. The brittle deformation zones are major zones of fracturing characterized by a large geometrical extent and a much greater width (in metres) than individual fractures (in millimetres). It is evident from Figure 5-3 that the brittle deformation zones will have a greater mechanical effect than an individual fracture.

Compared to the properties of the in situ stress, intact rock and individual fractures previously described, the brittle deformation zones are difficult to characterise, as illustrated in Figure 5-5 (also shown in this Report as Figure 2-7). This is because the intersections manifested via site investigation boreholes are specific, small samples through large inhomogeneous geological structures and cannot be considered as representative. A much better evaluation can be obtained via inspection of the

ONKALO tunnel intersections, which will be described later. The key parameters are the geometry, stiffness and strength characteristics.

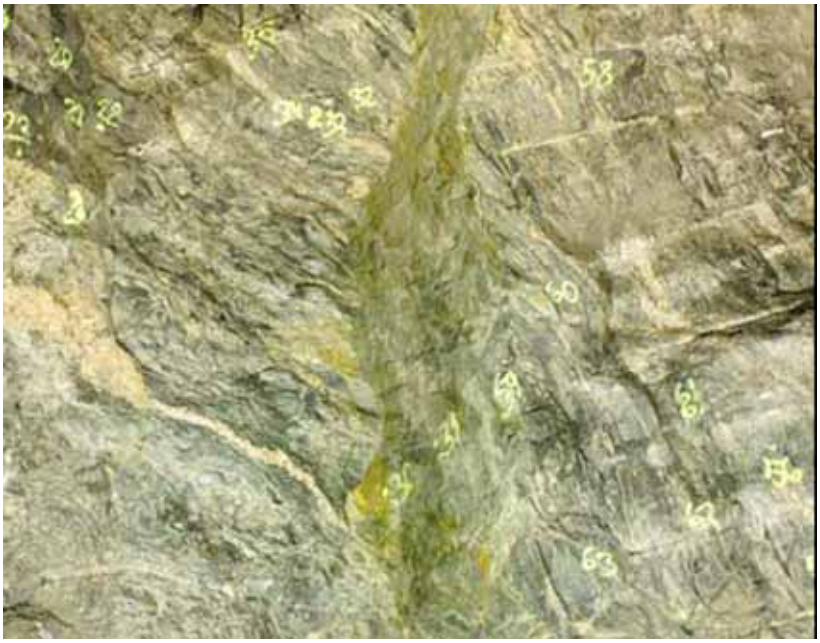

Figure 5-5. *Part of a brittle deformation zone intersection (ONK-BFI-65.60-65.75 m) in the ONKALO, from the top to the bottom of the central part of the photograph. (from Geological Outcome from the ONKALO Underground Research Facility, Chainage 0-140. Memo by Kemppainen K, Engström J, Talikka M, Mattila J.)*

The operating rock mechanics mechanisms. The operating mechanisms are elasticity, fracture and flow and their interactions with other processes and changes.

Elastic deformation occurs when the stresses are changed – but elastic deformation is fully recoverable; also, all the energy involved in elastic deformation is fully recoverable, by definition. Fracture occurs when the stresses are increased further. Microcracking can in principle occur right from the onset of applying stress, but it is generally assumed that microcracking starts at about 40-50% of the compressive (peak) strength in crystalline rock. Flow or creep refers to continuing displacement at constant stress. For example, the rock may initially crack around a tunnel as it is being excavated because of the increased stress, but it can also deform and crack further over time as the high stress is maintained.

Mechanisms, which are coupled with other processes and disciplines are alterations to the effective stress when the water pressure changes, and changes to fracture hydraulic conductivity when stress magnitudes change close to an excavation. The chemical erosion of fractures or the precipitation of minerals on fracture surfaces can also affect their mechanical properties.

The introduced perturbations. The initial perturbation is the excavation itself. This is followed by the thermal load as a result of emplacement of the canisters. There are consequential thermal, hydrogeological (H), mechanical (M) and chemical effects (C). The latter three are illustrated in Figure 5-6.

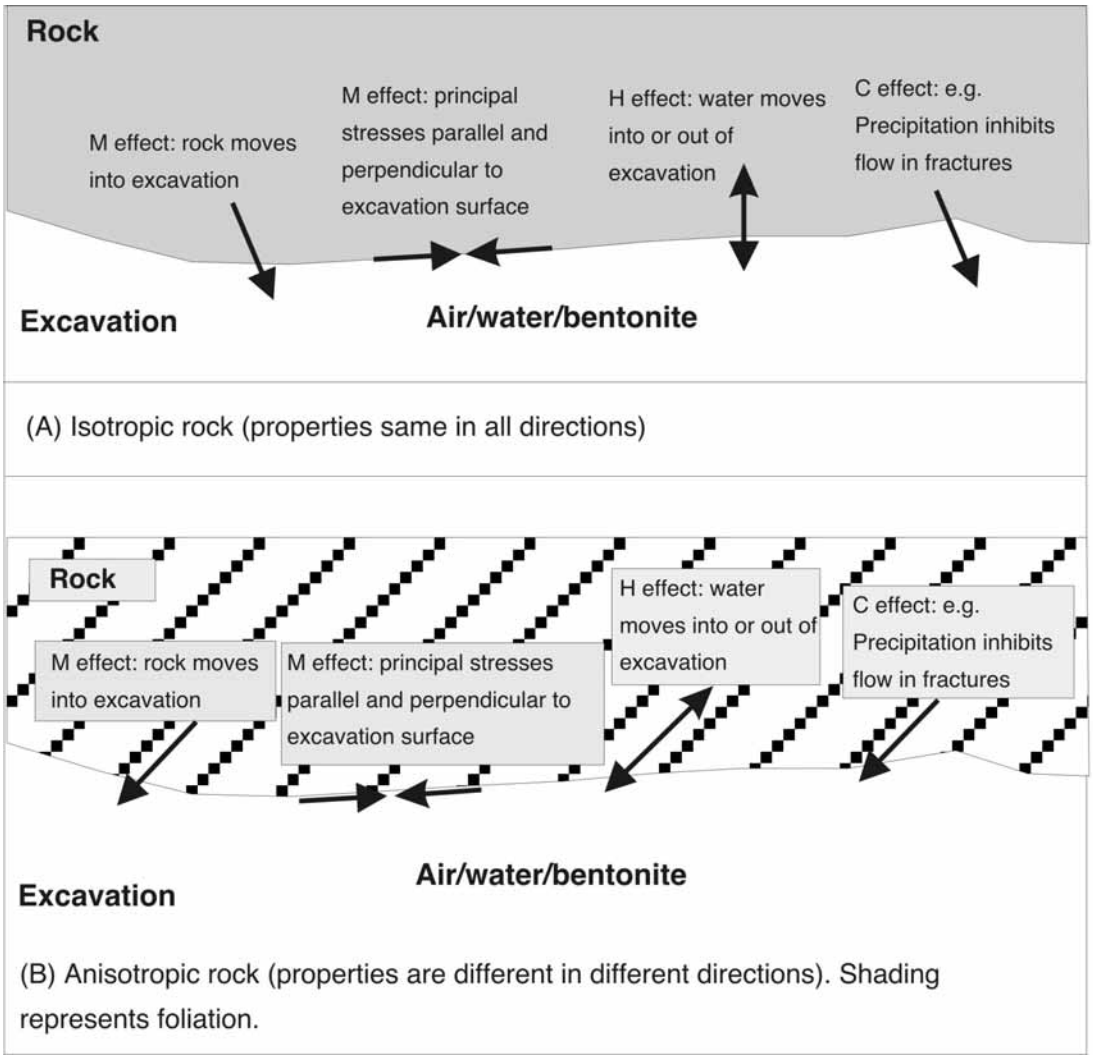

Figure 5-6. *Examples of mechanical, hydrogeological and hydrogeochemical effects resulting from deposition tunnel and hole excavation.*

Thus, not only must the 'purely rock mechanics' perturbations be evaluated but also the coupled mechanisms involving the other disciplines.

Evaluating the effects of perturbations. There are two main ways of evaluating the effects of the engineered perturbations: empirical assessments and numerical modelling. Both should be used but, of the two, numerical modelling is preferred because of its flexibility and ability to predict conditions for a variety of circumstances and to incorporate the interactions mentioned in the previous paragraph. This is especially true for radioactive waste disposal, where we do not have the precedent practice information which is required to fully implement the empirical approaches.

5.2 Evaluation of information

The rock mechanics data presented in Section 2.3 have been collected over a long time and many of these data have been analysed in various published studies. In order to establish all the direct rock mechanics knowledge that is available with reference to the Finnish waste disposal programme, a review has been conducted summarizing all the rock mechanics work completed for Posiva before 2005 (Hudson & Johansson 2006). This report provides a tabular description of each report with highlighted diagrams from the reports. The previous work has been extensive, with over 80 projects, and covers: baseline conditions, in situ stress state, strength and deformation properties of intact rock, mapping of stress damage, long-term behaviour of rock, fracture properties, thermal properties of rock and thermal analyses, EDZ (both the excavation damaged and disturbed zones), rock mass classification, rock mechanics studies elsewhere, but of relevance to Olkiluoto, non-Olkiluoto specific studies, but of relevance to Olkiluoto, Olkiluoto site-specific analyses, rock monitoring, and planning of rock mechanics investigations

Although further information is always helpful, the assessment of the Chapter 2 applied investigation data is summarised in the context of the 2005 conditions (i.e. the currently existing data) as follows.

In situ stress: The spatial variability of the in situ stress orientation and magnitudes is not known with sufficient accuracy and further measurements will be required, as anticipated for the ONKALO niches. A report on the influence of the geology of Olkiluoto on the rock mechanics properties, and especially the likely stress state, has being prepared (Hudson & Cosgrove, 2006). The future rock stress plan has been established through discussions within the Rock Mechanics Group (part of the OMTF). Anisotropy of the intact rock affects the interpretation of rock stresses and this effect can now be taken into account (Sjöberg & Hakala 2006).

Thermal rock properties: These are well established and an in situ probe has been developed and is being used. However, the anisotropy of the intact rock also affects the thermal properties and there is a need to appropriately upscale the laboratory properties to the rock mass thermal properties.

Intact rock properties: The intact rock refers to the rock without visible fractures. Its properties are also well established, although the factors of inhomogeneity and anisotropy have not been fully addressed across the site. Another issue is the long-term mechanical properties, e.g. the susceptibility of the rock to creep, fatigue and other time-dependent mechanisms. A literature review on this subject is currently in progress.

Fracture properties: These have not been very well established because of the difficulty of direct measurements. Some geological information and other information from the VLJ repository has been used via rock mass classification schemes to estimate the fracture properties. Further anticipated work will include direct testing of fracture properties from samples obtained from drill cores in the ONKALO niche boreholes.

Deformation zone properties: These properties require further work and are the least understood of the rock mechanics properties. Rock mass classification systems have

been used to estimate the properties, but further effort is required in this area, and a report is currently being written on a newly-developed methodology (Hudson et al. 2007, in preparation).

Rock mass properties These have to be estimated via geophysical measurements and empirical and/or numerical modelling, based on the properties of the rock mass components, i.e. intact rock, fractures and the deformation zones. Further work is required to analyse the investigation data.

Impact of excavation: The information is being made available as the ONKALO tunnel ramp proceeds and will be of major use in the future. Preliminary estimations of the effects have been made and evaluated for the 0-1170 m outcome and are reported in Chapter 9 concerning the Prediction-Outcome studies.

Utilization of the data. The data have been used appropriately for the modelling presented in Section 5.4 and also in the production of the Predictions (see Chapter 9).

5.3 Interaction with other disciplines

There are a considerable number of interactions between the component disciplines supporting the Site Model. These are illustrated in Figure 5-7.

5.4 Rock Mechanics Modelling

In this section, the modelling of the component parts of the rock mechanics model is described in detail. The uncertainties in the modelling are discussed in the next section.

5.4.1 In situ stress

Regional stress data include information from focal mechanisms, borehole breakouts etc., as well as from direct measurements of the stress state. Compilations by the World Stress Map Project (Reinecker et al. 2005) show that the regional stress field in Fennoscandia, and in particular in the region around Olkiluoto, is characterized by larger horizontal than vertical stresses (a so-called thrust faulting stress regime; $\sigma_H > \sigma_h > \sigma_v$), where σ_H = the maximum horizontal stress, σ_h = the minimum horizontal stress and σ_v = the vertical stress. The vertical stress component is often assumed to equal the overburden pressure. The major stress orientation in the regional vicinity of Olkiluoto is primarily E-W to NW-SE, see Figure 5-8.

The major stress orientation in Fennoscandia is normally believed to be attributed to an E-W direct compression from the mid-Atlantic ridge push and a N-S compression from the Alpine margin. Relative plate motions can be taken as indicators of the regional stress direction. These are often considered to be more reliable compared to, for example, focal mechanisms. (Furthermore, there are no data on focal mechanisms from the area near Olkiluoto in the World Stress Map database.) Since the European plate is moving quite slowly, the motion relative to other continents (e.g. Africa) may be taken as a regional stress indicator. Using these data, the relative plate motion at Olkiluoto is

approximately 146° (see e.g. UNAVCO, 2005), which would correspond to the orientation of σ_H.

A study of the regional stress field in the Satakunta area (the regional area around Olkiluoto) was published in 2005 (Huhta & Korsman 2005). This study reports data from earthquake focal mechanisms in Finland, indicating a NW-SE orientation of the maximum horizontal stress. In addition, direct stress measurement data away from Olkiluoto were referenced, but no site-specific stress profiles were given. The factors possibly affecting the stress field (deformation zones, glacial uplift, etc) were discussed but not quantified in this report.

1,1 Geology	1,2 Rock inhomogeneity and anisotropy & fractures (geometry, etc.) affects rock properties/stresses	1,3 Rock porosity, rock mass permeability and water-rock interaction affects water flow	1,4 Rock mineralogical compositional and geometry of factures affects hydro-geochemistry	1,5 Mineralogical composition, porosity, textural and structural anisotropy effects
2,1 Stress data affecting the geo-interpretation of facture systems and rock mass	2,2 Rock Mechanics	2,3 Spatial distribution of in situ stresses and EDZ influences the hydrogeological regime	2,4 Stress changes near fracture zones affecting flow may change precipitation	2,5 Rocks & fracture zones subjected to higher stresses may be more thermally conductive
3,1 Hydrogeological tests and measures can affect the geo-interpretation of permeable features	3,2 Water pressure changes the effective stress	3,3 Hydro-geology	3,4 The flow pattern affects dilution and mixing	3,5 The flow pattern will affect the temperature due to convection effects
4,1 Hydrogeochemistry interpretation affecting the interpretation of fracture mineral relationships	4,2 Precipitation and dissolution in fractures affects their mechanical properties	4,3 Effects of groundwater age, density, viscosity and dissolution and precipitation	4,4 Hydro-Geochemistry	4,5 No interaction
5,1 Thermal anisotropy and measurement affecting the geo-interpretation	5,2 Change in temperature can change the local stress, possibly leading to failure	5,3 Temperature gradients and thermal expansion in rock/fractures affect the water flow	5,4 Dissolution and precipitation enhanced by thermal gradients	5,5 Thermal properties

Figure 5-7. *Interaction matrix illustrating the way rock mechanics affects the other disciplines (interactions in the yellow row) and how they in turn affect rock mechanics (interactions in the yellow column). Note that the binary interactions listed in the off-diagonal boxes are through a clockwise convention, e.g. Box 1,2 is the influence of Geology on Rock Mechanics, whereas Box 2,1 is the influence of Rock Mechanics on Geology.*

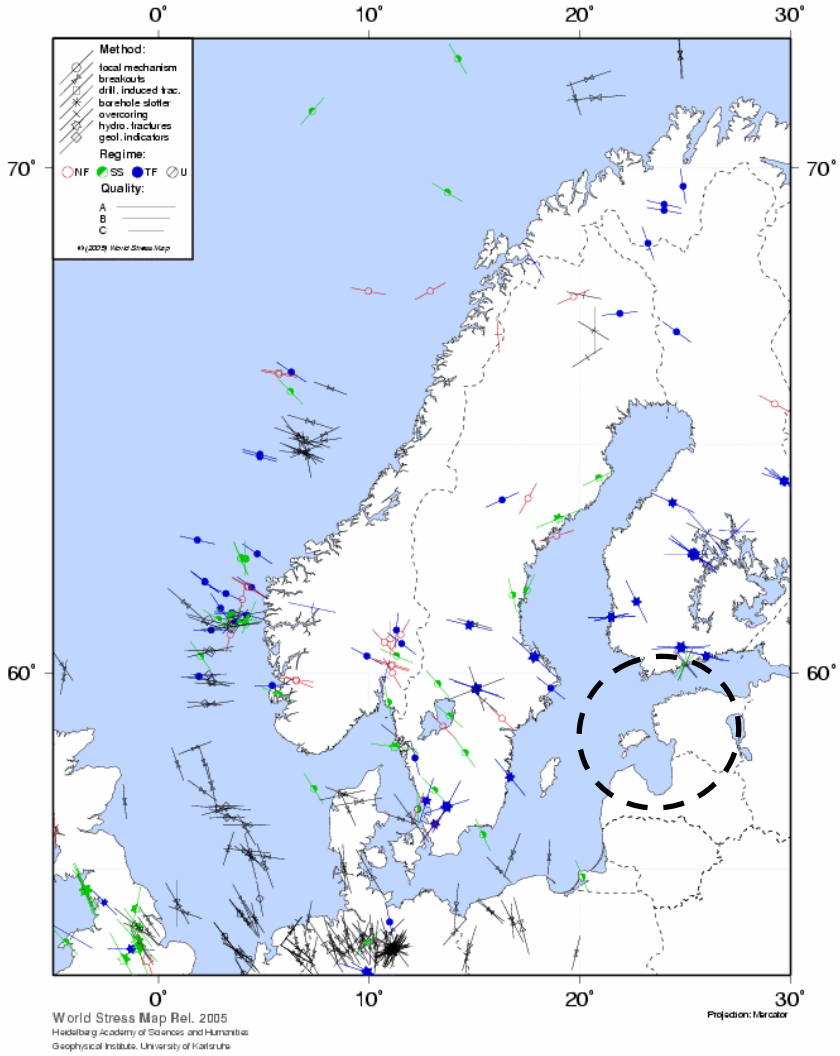

Figure 5-8. *Stress data from the World Stress Map Project for Fennoscandia (Reinecker et al., 2005), with the region of interest marked.*

On a site scale, in situ stresses have been measured at Olkiluoto over a depth range of 300 to 800 m. All these measurements have been made in vertical boreholes drilled from the surface, using either overcoring or hydraulic fracturing as the measurement method (see Chapter 2.3.1). Overcoring was used in two boreholes (OL-KR10 and OL-KR24), yielding a total of 18 measurements, whereas hydraulic fracturing was used in four boreholes (OL-KR1, OL-KR2, OL-KR4 and OL-KR10) resulting in 31 measurement points.

Using overcoring, the full, three-dimensional stress tensor can be determined; however, hydraulic fracturing only can be used to assess the horizontal stress components when used in deep vertical boreholes, as was the case at Olkiluoto. The original results from all the overcoring measurements are summarized in Figure 5-9 and results from both overcoring and hydraulic fracturing (shown as horizontal and vertical stress

components) are shown in Figure 5-10, using data from Klasson & Leijon (1990), Ljunggren & Klasson (1996) and Sjöberg (2003).

The original results show increasing stress magnitudes with depth. The vertical and minimum horizontal stress components are fairly equal in magnitude, whereas the maximum horizontal stress is distinctly larger. The measured vertical stress is approximately equal to, or slightly lower than, the theoretical value corresponding to the overburden pressure. The orientation of the major principal stress (evaluated from overcoring) varies significantly between the boreholes, as well as between measurement levels and individual measurements in each borehole, although it is generally oriented sub-horizontally. There is thus a large uncertainty in the stress orientations from direct measurements.

The overcoring stress measurement data were re-analysed to better assess the reliability of individual measurements. This involved transient strain analysis (Hakala et al. 2003, Hakala 2006), to study the behaviour of individual strain gauges, as well as the potential for core damage during overcoring. The re-analysis also made use of newly-developed tools to calculate stresses for anisotropic materials. In this case, transverse isotropy was assumed, and the corresponding elastic constants determined from biaxial tests conducted in conjunction with the overcoring measurements (Hakala & Sjöberg, 2006). Based on these analyses, the overall reliability of the measurements was ranked with respect to: (i) overcoring strain response, (ii) biaxial strain response, (iii) transient strain behaviour, and (iv) potential for core damage induced during overcoring. The measurements were ranked with the following qualitative ratings: *good*, *moderate*, *poor*, and *rejected.* When considering all the criteria (i) through (iv) listed above, only two measurements were ranked as *good* and/or *moderate*. If the potential for core damage was ignored (if e.g. the assumed tensile criterion is incorrect), 12 (out of 18) measurements were ranked as *good* and/or *moderate*. The resulting principal stresses for this data set (calculated assuming transverse isotropy when applicable) are shown in Table 5-1. The corresponding horizontal and vertical stress components are presented in Figure 5-11, Figure 5-12 and Figure 5-13. The resulting re-analysed stresses are, in general, slightly lower in magnitude than the original values, whereas the differences in stress orientations are small.

Additional stress estimation has been conducted using the so-called Kaiser Effect (Lehtonen, 2005). These tests were conducted on samples from borehole OL-KR14 from two depths: about 80 and 500 m, respectively. The resulting stresses are shown in Table 5-2, and their magnitudes against depth and their orientations shown in Figure 5-14, Figure 5-15 and Figure 5-16. Comparing these data with those obtained from overcoring and hydraulic fracturing, similar results are found for the 500 m depth. For the 80 m depth, no comparison was possible, due to lack of measurements at this level, however, the vertical stress is clearly larger than the overburden pressure at both depth.

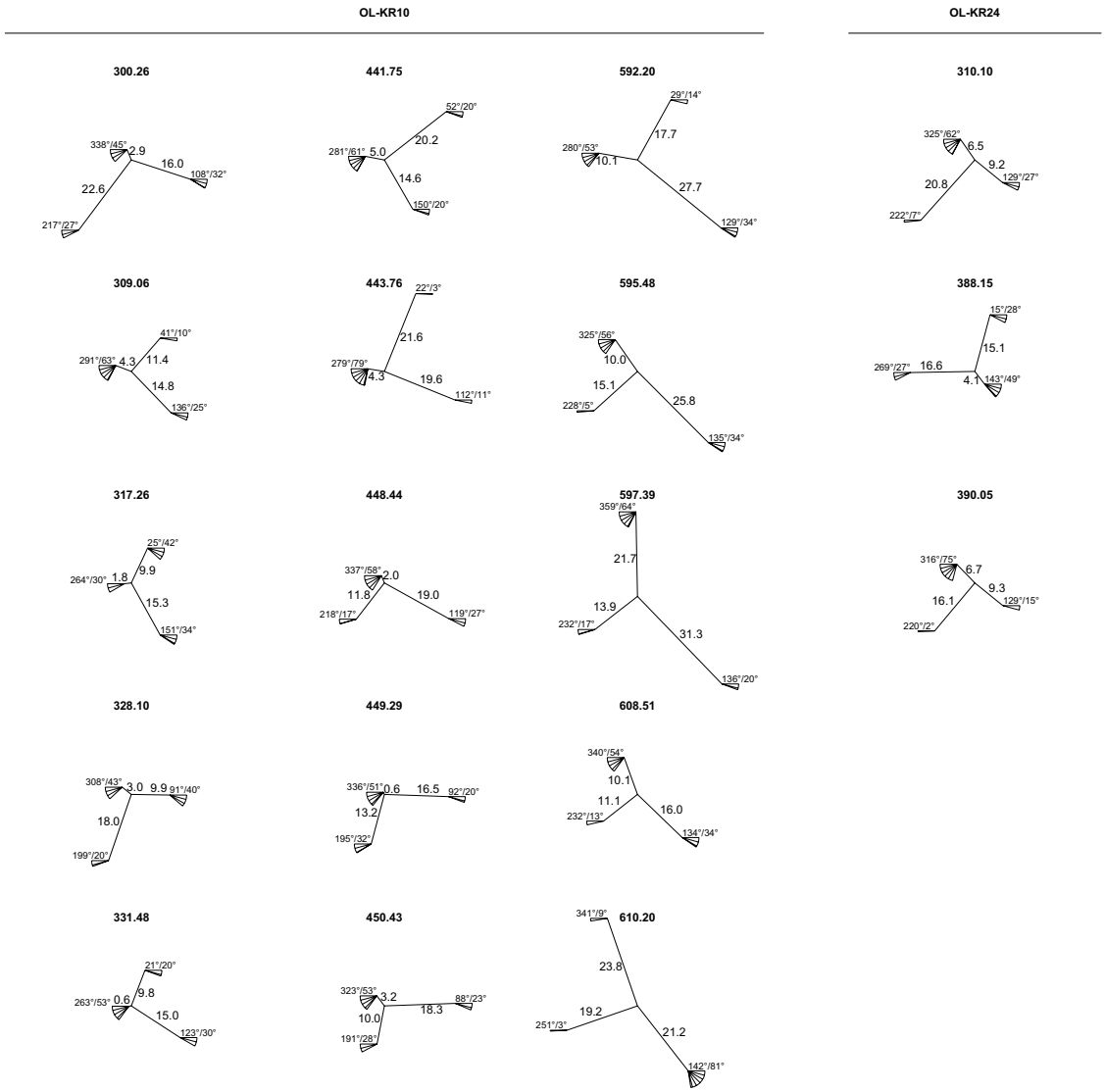

Figure 5-9. *Measured principal stresses using overcoring at the Olkiluoto site. Each principal stress is represented by magnitude (length of vector; rotated onto the horizontal plane), trend (orientation of vector relative to north) and plunge (fan-shaped symbol; each fan-slice corresponds to 15° of dip from the horizontal).*

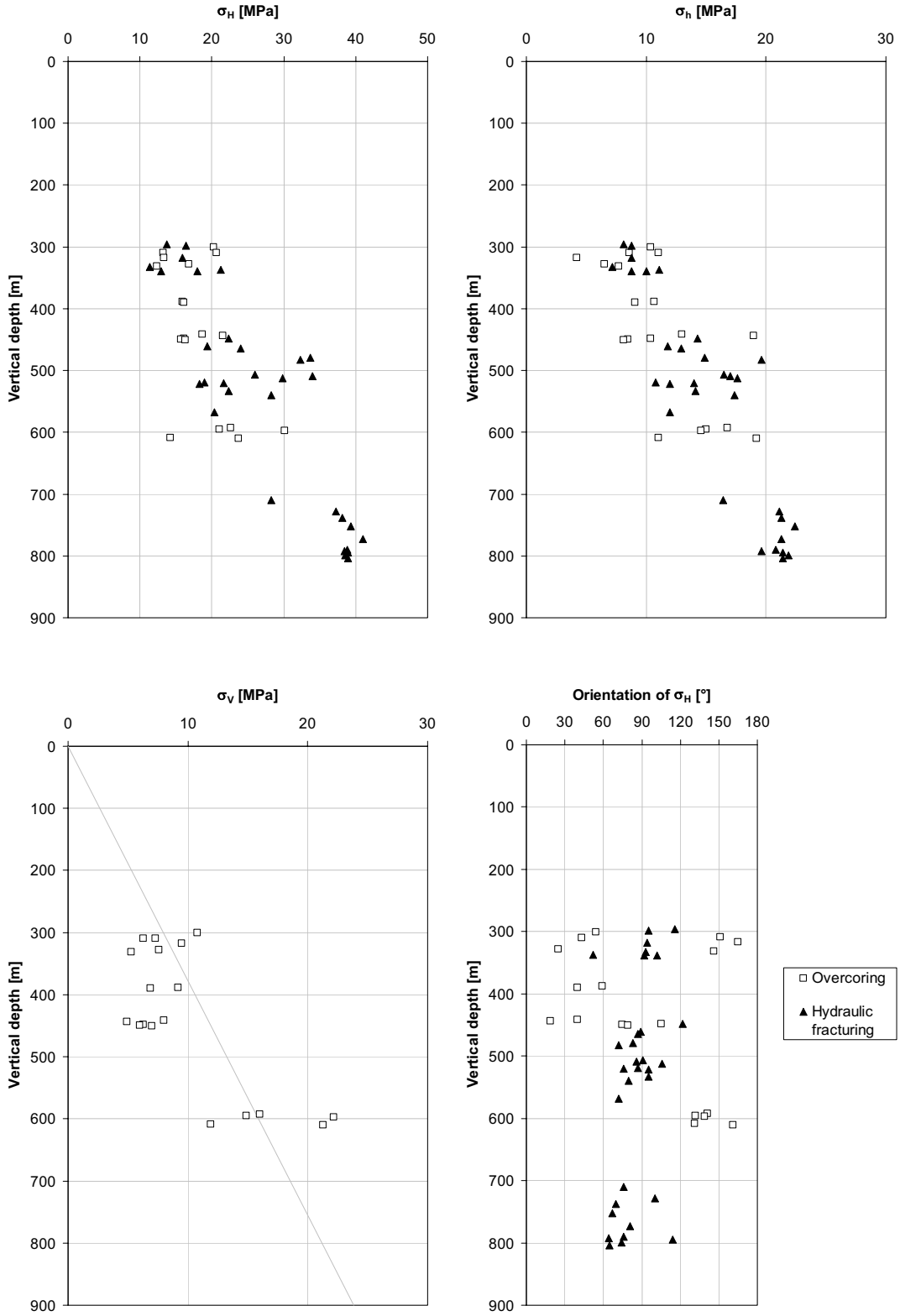

Figure 5-10. *Magnitudes of the horizontal and vertical stress components, and orientation of the maximum horizontal stress, as inferred from overcoring and hydraulic fracturing measurements. (For the vertical stress, a theoretical line corresponding to the overburden stress is shown for reference.)*

Table 5-1. *Magnitudes and orientations of principal stresses as determined from re-analysis of overcoring stress measurement data from Olkiluoto. Only data, which were ranked as "good" and/or "moderate", are presented.*

Borehole no.	Vertical depth [m]	Magnitude and Trend/Plunge of principal stresses					
		σ_1		σ_2		σ_3	
		[MPa]	[°]	[MPa]	[°]	[MPa]	[°]
OL-KR10	309.06	13.0	134/25	10.8	012/38	5.7	285/62
OL-KR10	328.10	18.1	199/22	10.0	090/40	3.1	311/42
OL-KR10	331.48	17.5	122/37	11.5	018/17	1.6	268/48
OL-KR10	441.75	19.8	069/27	14.8	167/15	6.2	282/58
OL-KR10	443.76	19.7	186/07	17.4	094/13	1.3	304/75
OL-KR10	448.44	27.2	121/37	17.5	232/25	8.0	348/43
OL-KR10	449.29	14.8	092/21	12.0	197/33	0.5	335/49
OL-KR10	592.20	28.3	125/30	17.8	029/11	5.6	282/57
OL-KR10	597.39	22.8	134/32	13.2	230/10	4.4	334/56
OL-KR10	608.51	17.7	136/29	11.9	237/18	7.6	355/55
OL-KR24	388.15	16.7	271/27	13.3	015/27	2.4	143/51
OL-KR24	390.05	14.4	222/00	8.8	132/07	2.8	315/83

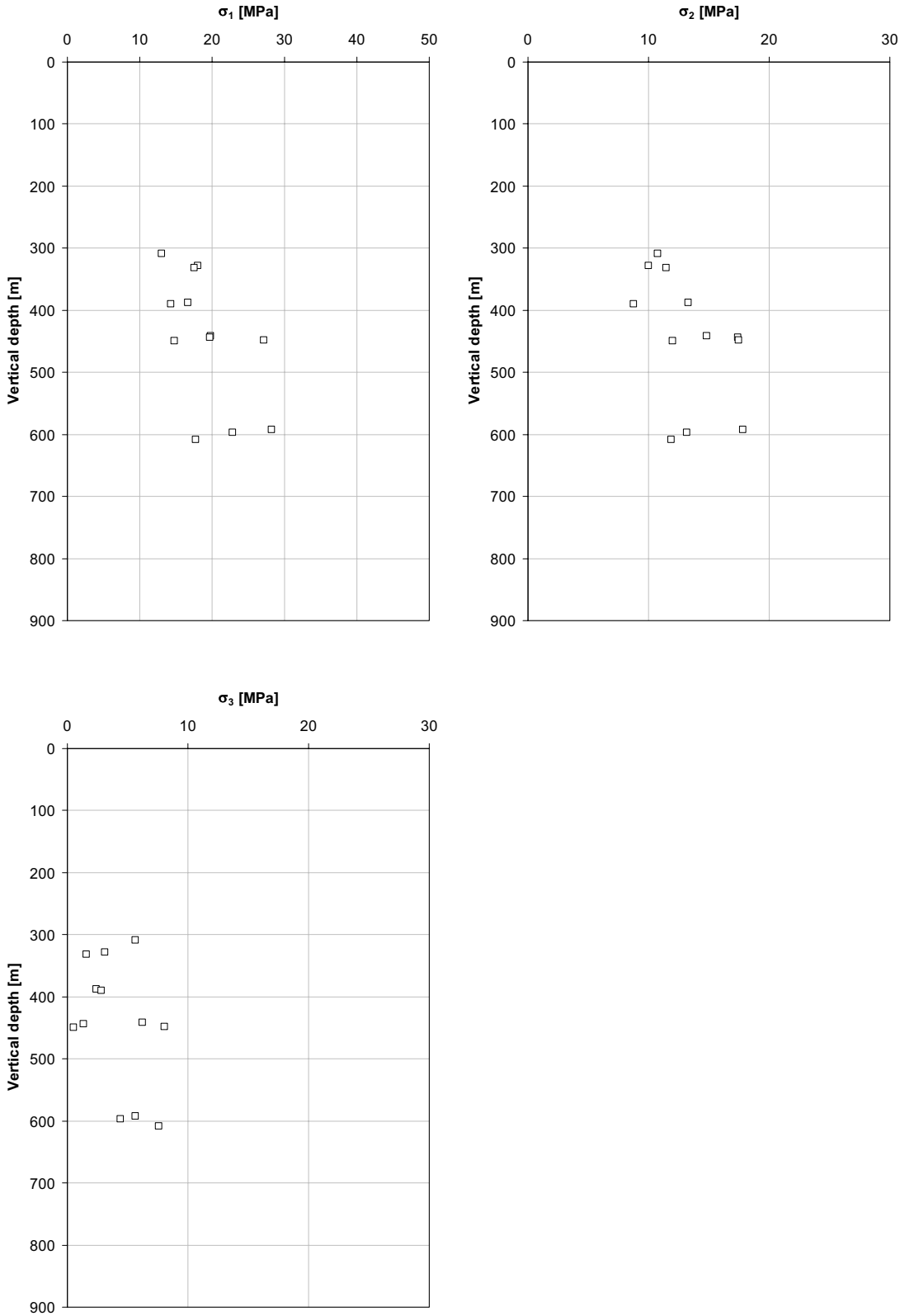

Figure 5-11. *Magnitudes of the three principal stresses from selected and re-analysed overcoring measurements, ranked "good" and/or "moderate".*

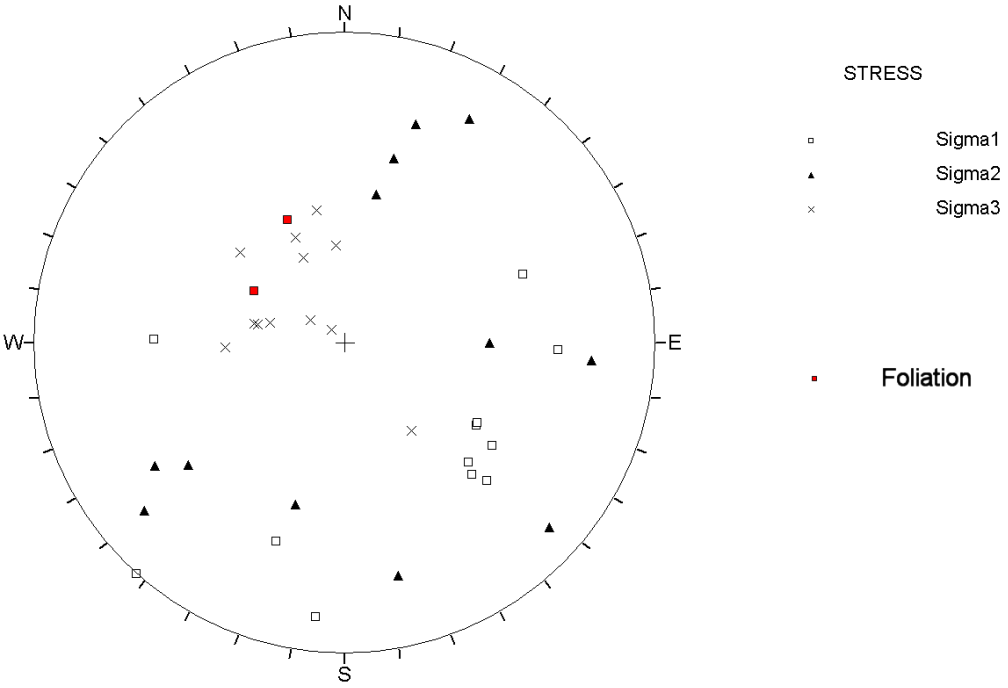

Figure 5-12. *Orientations of the principal stresses from selected and re-analysed overcoring measurements, ranked "good" and/or "moderate", shown together with the poles of major foliation orientations at Olkiluoto.*

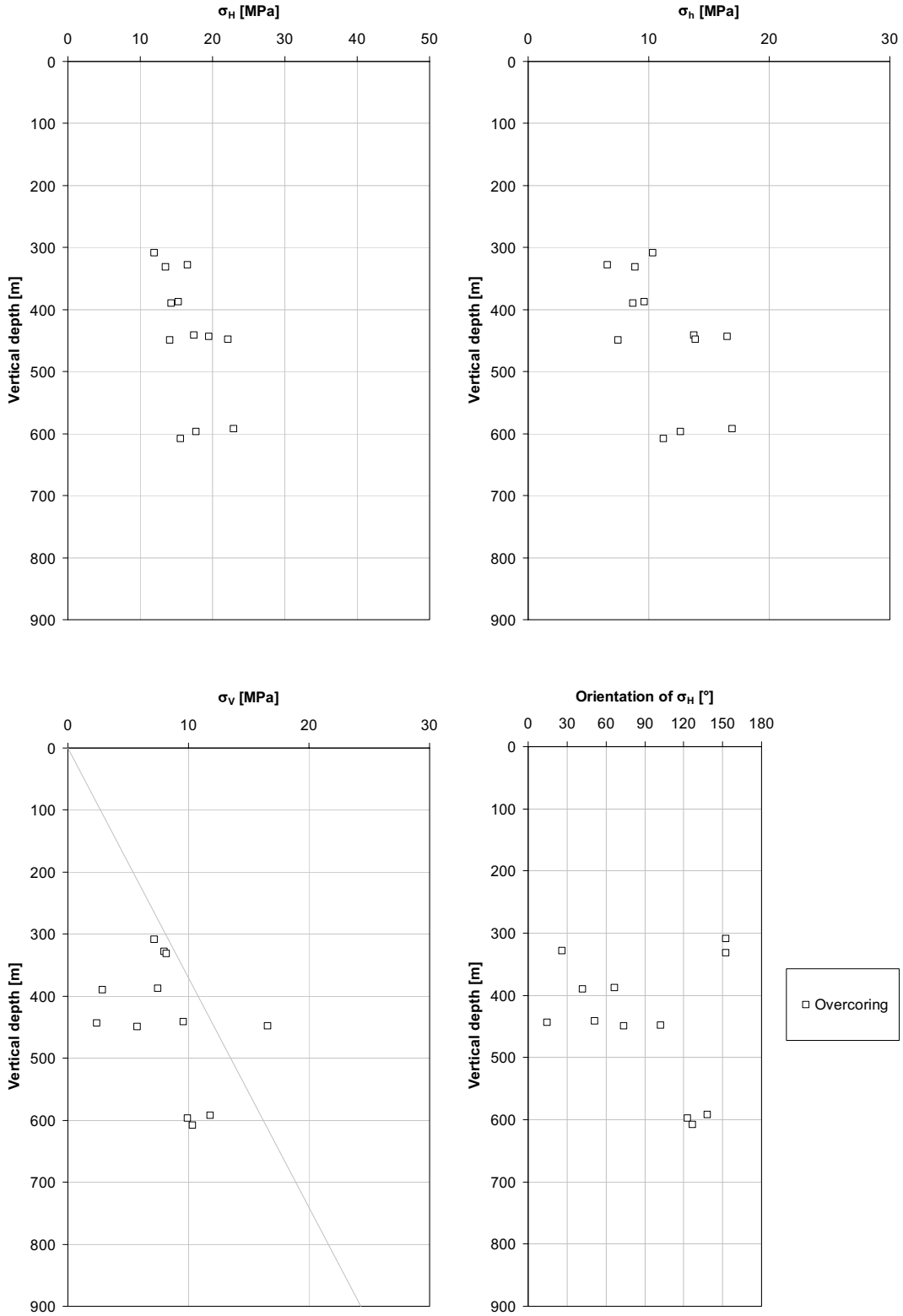

Figure 5-13. *Magnitudes of the horizontal and vertical stress components from selected and re-analysed overcoring measurements, ranked "good" and/or "moderate". (For the vertical stress, a theoretical line corresponding to the overburden stress is shown for reference.)*

Table 5-2. *Magnitudes and orientations of principal stresses as inferred from measurements of the Kaiser Effect on drill cores from Olkiluoto (see following text).*

Borehole no.	Vertical depth [m]	Magnitude and Trend/Plunge of principal stresses					
		σ_1		σ_2		σ_3	
		[MPa]	[°]	[MPa]	[°]	[MPa]	[°]
OL-KR14	80	14.4	085/37	12.1	195/25	2.6	311/43
OL-KR14	500	26.8	289/31	17.2	150/52	10.2	032/20

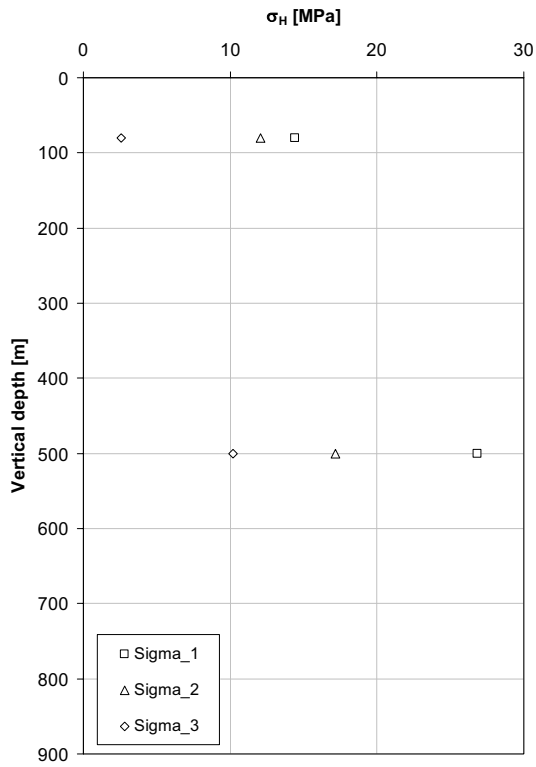

Figure 5-14. *Magnitudes of the three principal stresses, as inferred from measurements of the Kaiser Effect on drill cores.*

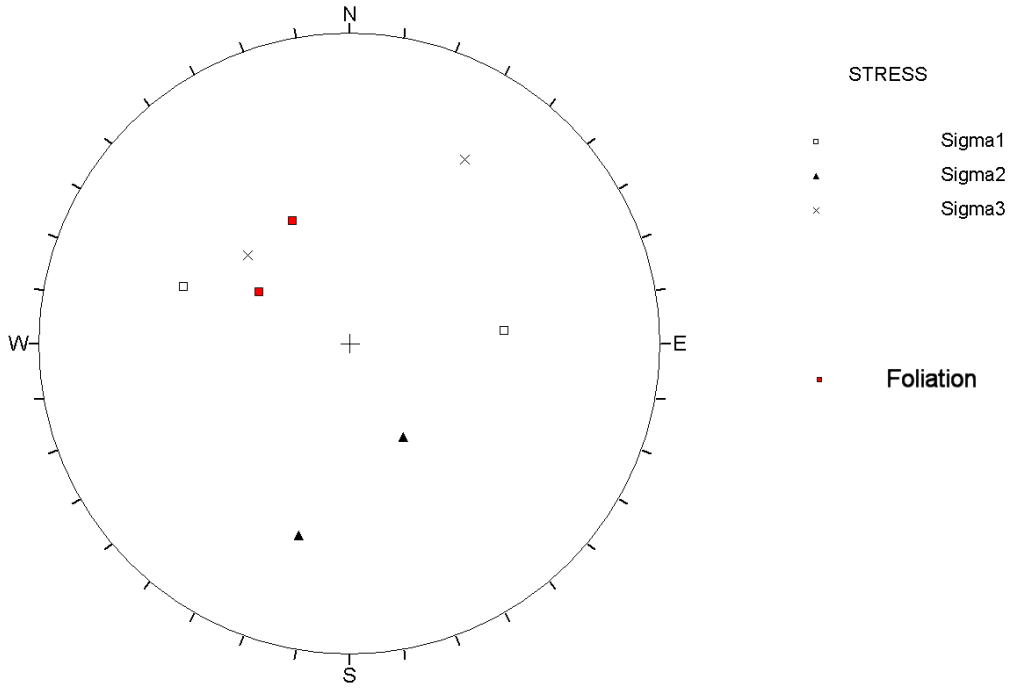

Figure 5-15. *Orientations of the principal stresses as inferred from measurements of the Kaiser Effect on drill cores, shown in a lower hemisphere projection together with the poles of major foliation orientations (bottom red).*

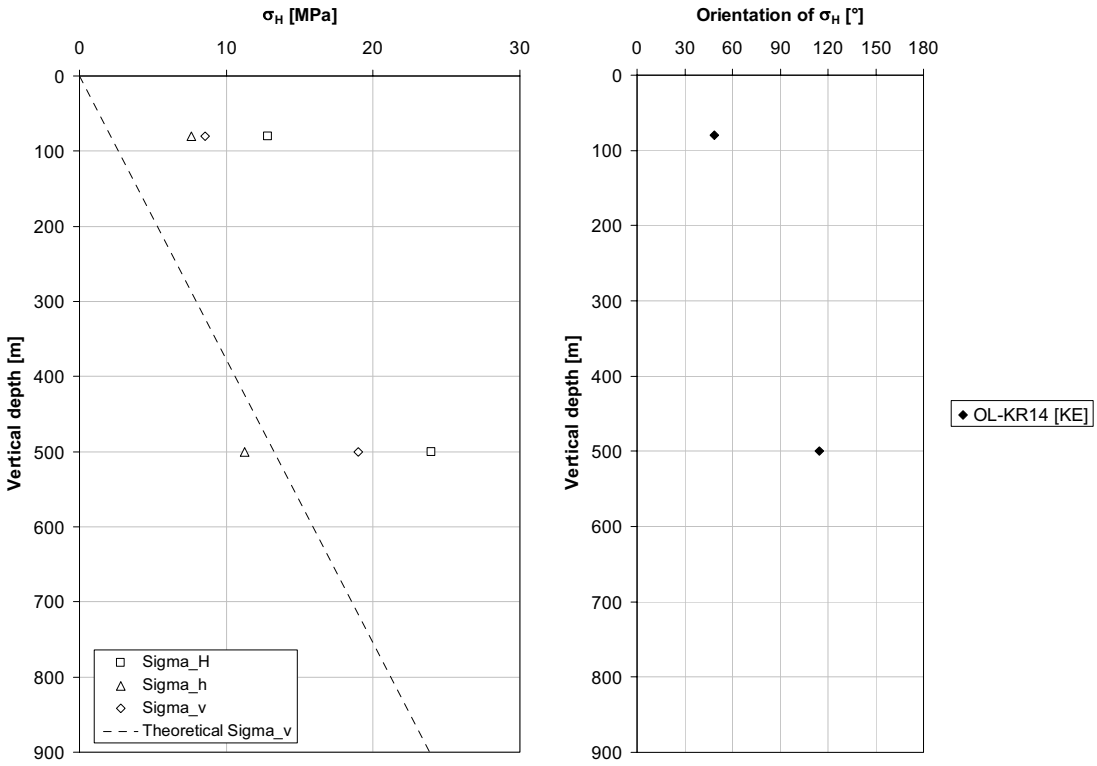

Figure 5-16. *Magnitudes of the horizontal and vertical stress components, and orientation of the maximum horizontal stress, as inferred from measurements of the Kaiser Effect on drill cores (For the vertical stress, a theoretical line corresponding to the overburden stress is shown for reference.)*

The current data do not permit more elaborate interpretation with respect to geology and/or geological structures and to arrive at representative, and useable, stress values, the horizontal and vertical stress components were used. The varying orientation of the horizontal components was not accounted for in this simplistic analysis, rather linear stress profiles were assumed for each of the stress components. Data from re-analysed overcoring measurements, original hydraulic fracturing stress data, and results from the Kaiser Effect measurements were used. The scatter in the data made it difficult to determine a single, representative, stress profile for each stress component, rather, estimated lower and upper limits were defined. When determining these, it was assumed (as is often inferred from actual near-surface measurements in Fennoscandia) that the stress state comprises a significant non-zero horizontal component near the ground surface, whereas the vertical stress is governed primarily by the overburden pressure (zero at ground surface). These linear profiles were subjectively defined to encompass the majority (but not all) of the data, thus providing reasonable input data for future work. The obtained stress profiles equations are shown in Table 5-3, and in Figure 5-17. The orientations of the maximum horizontal stress show a larger scatter, but are generally in the interval of 050–130°.

Table 5-3. *Estimated lower and upper limits for the horizontal and vertical stress components at the Olkiluoto site.*

Range	Stress component	Vertical depth range [m]
	σ_H [MPa]	
Lower limit	$\sigma_H = 5 + 0.021z$	300 < z < 800 m
Upper limit	$\sigma_H = 10 + 0.042z$	
	σ_h [MPa]	
Lower limit	$\sigma_h = 0.021z$	300 < z < 800 m
Upper limit	$\sigma_h = 5 + 0.027z$	
	σ_v [MPa]	
Lower limit	$\sigma_v = 0.015z$	300 < z < 800 m
Upper limit	$\sigma_v = 0.030z$	

z = depth below ground surface [m]

In summary, the current knowledge implies the following for the in situ stress state at Olkiluoto:

- Data from relative plate motions indicate a regional maximum stress direction of 146°. Stress orientations from local measurements display a large scatter, but the mean orientation of the maximum horizontal stress is nearly E-W. It is thus difficult to state whether the stress orientation at the site differs from the expected regional orientation.

- The site data support the notion of a thrust faulting stress regime at Olkiluoto, i.e. $\sigma_H > \sigma_h > \sigma_v$. For a target depth of 500 m, the maximum horizontal stress is estimated to be between 15 and 31 MPa, whereas the minimum horizontal stress is estimated to be in the range of 10 to 18 MPa. The vertical stress is estimated to be between 7 and 15 MPa at 500 m depth.

- The major principal stress (σ_1) is sub-horizontally oriented, thus being slightly larger in magnitude than the maximum horizontal stress. The other two principal stress components vary significantly in magnitude and orientation for the different measurement locations. This indicates the need to relate the stress field to the geological structure and to conduct associated numerical analyses.

- The scatter in orientation is troublesome as it, in theory, inhibits any derivation of stress profiles for the horizontal and vertical stress components. Future efforts should focus on determining the stress orientation with better confidence.

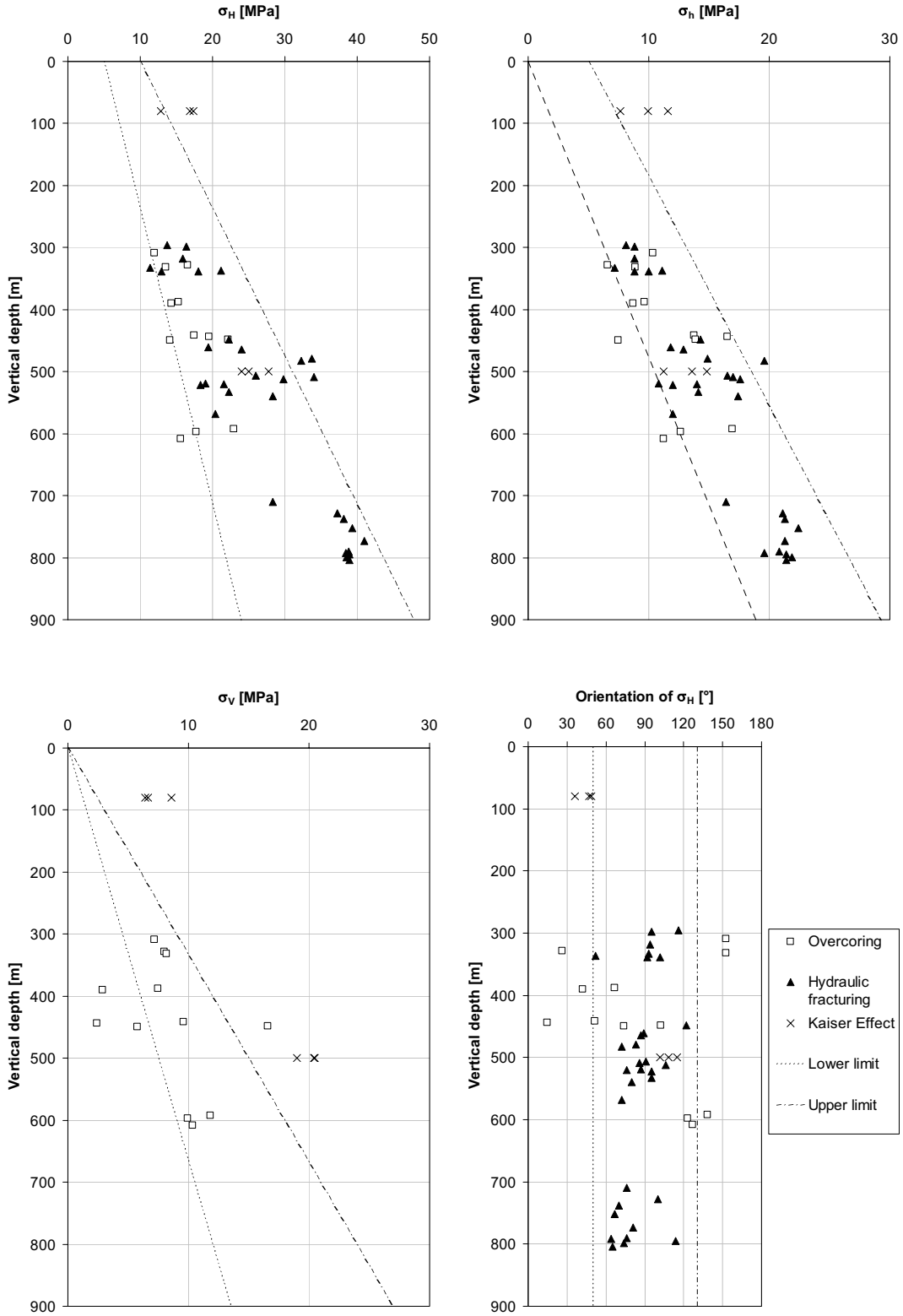

Figure 5-17. *Magnitudes of the horizontal and vertical stress components, shown with linear regression lines based on both overcoring and hydraulic fracturing measurements. (For the vertical stress, only overcoring data was used in the regression.)*

5.4.2 Intact rock properties

The mechanical properties of intact rock can, in general, be characterized by the complete stress-strain curve. This curve is obtained by compressing a cylindrical specimen, sawn from a diamond drilled core, in a servo-controlled testing machine. The stress-strain curve is used to select the appropriate conceptual model for intact rock and to define the associated parameter values (Figure 5-18).

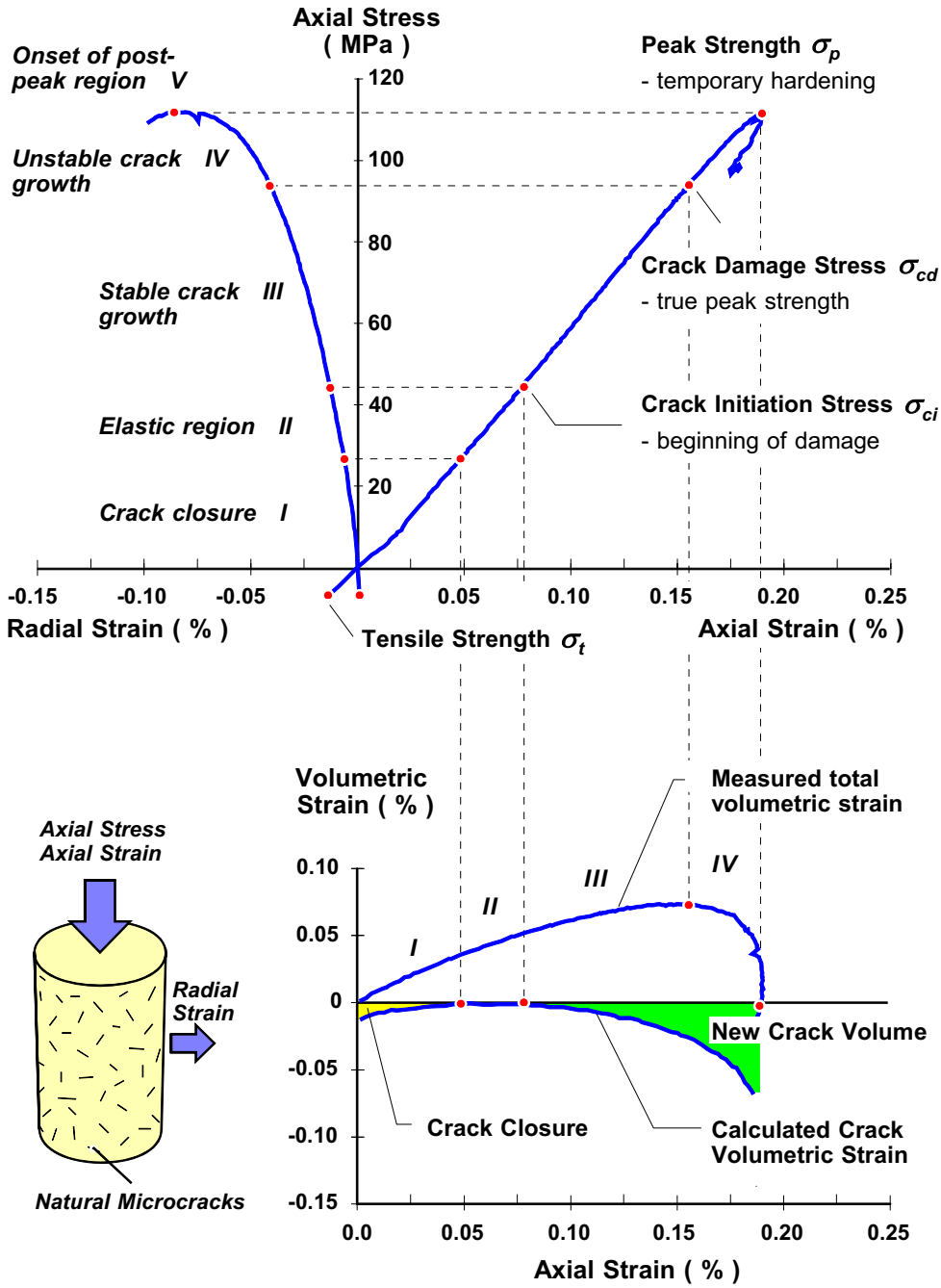

Figure 5-18. *Characteristic stress-strain behaviour of brittle rock (according to Martin 1994).*

The stress-strain curve is divided into the pre-peak strength and post-peak strength regions. The pre-peak region for crystalline rock, as for the Olkiluoto rock types, is conceptualized to be mainly linearly elastic and isotropic or transversely isotropic; other assumptions are the continuity and homogeneity of the rock. The post-peak region, describing the microstructural breakdown of rock, is characterized by Classes I and II, depending on whether the strain increases monotonically (I) or not (II) with loss of bearing capacity. Since rock types do not behave ideally, two critical stress states are normally defined: the crack initiation stress when new stable microfracturing initiates; and crack damage strength when the extension of microcracking is unstable.

The critical stress states are stress state dependent, and normally they are assumed to be a function of the minor principal stress (Figure 5-19). The strength envelopes are commonly described by the Hoek-Brown criterion, the Mohr-Coulomb criterion, or by other criteria. In addition to the compression test, other commonly used tests are the indirect tensile test, the fracture toughness tests, the bending test, the point load index test and drilling parameter tests. The test should be conducted according to the ISRM Suggested Methods, because the specimen size and shape, saturation, loading control method and loading rate affect the results. With the majority of these tests, acoustic emission measurements can also be used to obtain direct information on the microcracking (i.e. the total development of microcracking: its initiation, stable increase, unstable increase, larger occurrences).

In total, 221 laboratory test samples and 1208 point load field tests have been carried out to date, with 95% of the laboratory test samples representing metamorphic rocks and 5% igneous rocks (Table 5-4). The majority of the laboratory testing has been carried out on veined gneiss.

All metamorphic rocks (VGN, DGN, MGN and TGG) that have been tested are strongly heterogeneous and the type and amount of heterogeneity changes rapidly. The structural heterogeneity, especially the mica content and the concentration of mica in planes of weakness, in relation to the geometry of the test specimen, produces large deviations of stress-strain behaviour and strength (Tables 5-5 to 5-8 and Figure 5-20 to Figure 5-26). In addition, the loading conditions also have a considerable effect on these parameter values. The latest laboratory test results on veined gneiss samples show both clear deformation and strength anisotropy see Figure 5-29 to Figure 5-34).

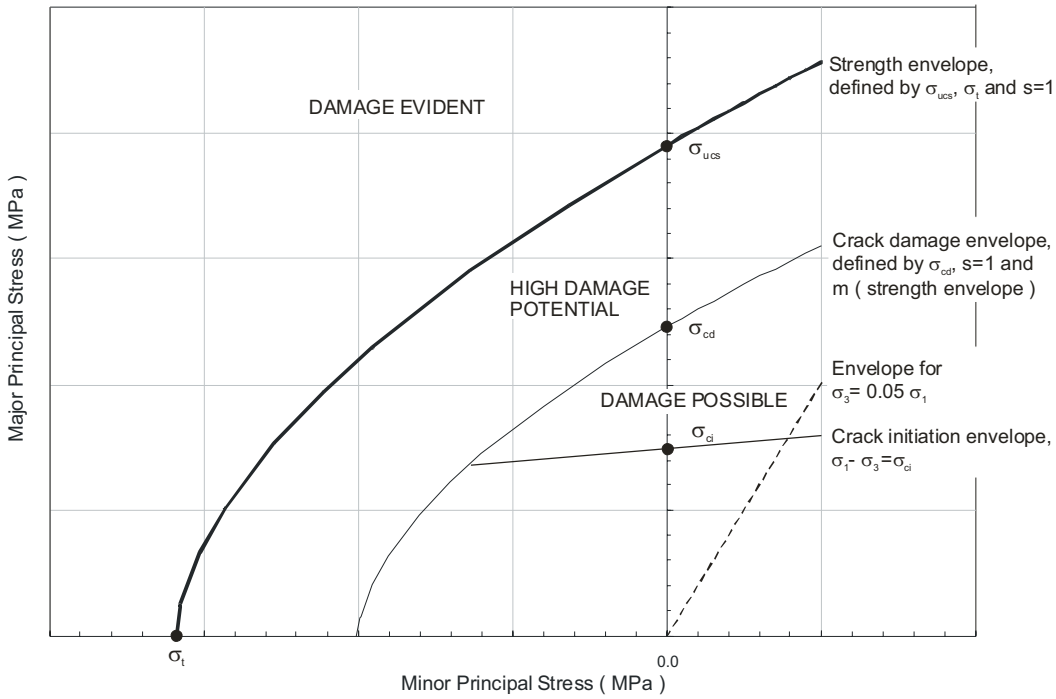

Figure 5-19. *Critical stress envelopes after Read et al. (1998).*

Metamorphic rocks are brittle and lose their bearing capacity rapidly with Class II type post-peak behaviour (Figure 5-20). Visually apparent fractures are formed immediately after the peak strength, associated with a 30% to 60% reduction in strength. With less than 5 MPa confinement, the metamorphic rock types has a minor residual strength after 0.3% axial strain. A confinement of 15 MPa stabilizes the post-failure behaviour somewhat, but the strength is still lost after a small amount of deformation. The changes in deformation and strength parameters above the crack damage stress and in the post-failure phase are defined by cyclic damage-controlled testing, and are presented as a function of damage. The damage is defined as the permanent volumetric inelastic strain accumulated in the sample with each loading cycle. During the first 0.1% of damage strain, the apparent Young's modulus decreases by approximately 10 GPa / 0.1% strain and, after that, approximately 3 GPa / 0.1% strain (Figure 5-27). The apparent Poisson's ratio increases approximately 0.1 / 0.1% strain and exceeds the theoretical maximum of 0.5 for an isotropic elastic rock at the point of formation of the visual fracture. In all the uniaxial cases, the crack damage stress equals the crack initiation stress up to 0.2% damage, and in the majority of the 3 MPa confined tests the corresponding damage level was 0.3% (Figure 5-28). At the point, when the crack damage stress is coincident with the crack initiation stress, the 95% confidence limits for axial stress are 20 MPa and 55 MPa. After this point, the post-failure behaviour is defined by the geometry of the visual fracture compared to the specimen geometry and the amount of confinement. The effect of a confinement pressure of less than 3 MPa is minor and the effect of damage on crack initiation and crack damage was obvious during the first 0.2% to 0.3% of damage.

The few tests on igneous rock (pegmatite) show that their general stress-strain behaviour is very similar to that of metamorphic rocks. Noticeable differences are slightly higher values for Young's modulus and Poisson's ration, a clearly lower tensile strength and the pealing-off type rupture of the test specimen.

Table 5-4. *Number of laboratory tests and borehole lengths for different rock types at Olkiluoto.*

Rock type		Number of laboratory tests						Percent of borehole data
		1A*	3A*	IT	DT	all		
Metamorphic rocks							95 %	78 %
Homogeneous gneiss							17 %	15 %
Mica gneisses	MGN	9	9	4	4	26	11 %	6 %
Mafic gneisses	MFGN	-	-	-	-	-	-	1 %
Quartzitic gneisses	QGN	-	-	-	-	-	-	1 %
Tonalitic-granodioritic -granitic gneisses	TGG	7	-	6	-	13	6 %	7 %
Migmatites							78 %	63 %
Stromatic gneisses	SGN	-	-	-	-	-	-	< 1%
Veined gneisses	VGN	70	45	41	14	170	73 %	45 %
Diatexitic gneisses	DGN	6	3	2	-	11	5 %	17 %
Igneous rocks							5 %	22 %
Pegmatic granite	PGR	4	2	6	-	12	5 %	22 %
Diabase	DB	-	-	-	-	-	-	< 1%
	Total	*96*	*59*	*59*	*18*	*232*		

* *includes damage controlled and low loading rate tests*

Table 5-5. *Apparent elastic deformation parameter values for Olkiluoto metamorphic rock types under different loading conditions.*

Parameter	Loading condition	Mean value	95% confidence for standard deviation	Number of samples
Young's modulus, E	direct tension	43 GPa	19 GPa	20
	uniaxial, 0.0075 MPa/s	57 GPa	14 GPa	15
	uniaxial, 0.75 MPa/s	63 GPa	12 GPa	63
	triaxial, σ_c = 0.5-15 MPa	63 GPa	10 GPa	40
Poisson's ratio, ν	direct tension	0.06 mm/mm	0.03 mm/mm	20
	uniaxial, 0.0075 MPa/s	0.28 mm/mm	0.05 mm/mm	15
	uniaxial, 0.75 MPa/s	0.25 mm/mm	0.06 mm/mm	63
	triaxial, σ_c = 0.5-15 MPa	0.20 mm/mm	0.05 mm/mm	40

Table 5-6. *Apparent strength parameter values for Olkiluoto metamorphic rock types under different loading conditions.*

Parameter	Loading condition	Average value	95% confidence limit for standard deviation	Number of samples
Tensile strength, σt	direct tension	7.9 MPa	2.2 MPa	19
	indirect, saturated	10.0 MPa	3.2 MPa	30
	indirect, dry	14.5 MPa	3.6 MPa	23
Crack initiation, σci	direct tension	2.5 MPa	1.4 MPa	4
	uniaxial, 0.0075 MPa/s	45 MPa	15 MPa	15
	uniaxial, 0.75 MPa/s	54 MPa	15 MPa	54
Crack damage, σcd	direct tension	5.8 MPa	3.2 MPa	4
	uniaxial, 0.0075 MPa/s	76 MPa	27 MPa	13
	uniaxial, 0.75 MPa/s	106 MPa	29 MPa	53
Peak strength, σP	uniaxial, 0.0075 MPa/s	96 MPa	34 MPa	13
	uniaxial, 0.75 MPa/s	115 MPa	28 MPa	72

Table 5-7. *Apparent elastic deformation parameters for Olkiluoto rock types.*

Parameter	Rock type	Mean value	Standard deviation	Number of samples
Young's modulus, E (GPa)	VGN	62	9	70
	DGN	65	7	6
	MGN	54	13	9
	TGG	64	5	7
	PGR	65	9	4
Poisson's ratio, ν (mm/mm)	VGN	0.25	0.04	70
	DGN	0.26	0.02	6
	MGN	0.29	0.04	9
	TGG	0.22	0.05	7
	PGR	0.29	0.05	4

Table 5-8. *Apparent strength parameters for Olkiluoto rock types.*

Parameter	Rock type	Mean value	Standard deviation	Number of samples
Peak strength, σ_P (MPa)	VGN	114	10	58
	DGN	116	11	6
	MGN	122	25	6
	TGG	109	5	7
	PGR	108	12	4
Crack damage stress, σ_{CD} (MPa)	VGN	104	22	48
	DGN	103	25	6
	MGN	104	42	6
	TGG	110	17	7
	PGR	108	8	4
Crack initiation stress, σ_{CI} (MPa)	VGN	52	21	49
	DGN	59	20	6
	MGN	58	47	6
	TGG	54	15	7
	PGR	55	12	4
Indirect tensile strength, $\sigma_{T,I}$ (MPa)	VGN	11.7	3.5	41
	DGN	10.0	2.3	2
	MGN	12.2	1.2	4
	TGG	14.4	2.7	6
	PGR	5.4	0.9	6
Direct tensile strength, $\sigma_{T,D}$ (MPa)	VGN	7.6	1.5	14
	DGN	-	-	0
	MGN	7.9	1.5	4
	TGG	-	-	0
	PGR	-	-	0

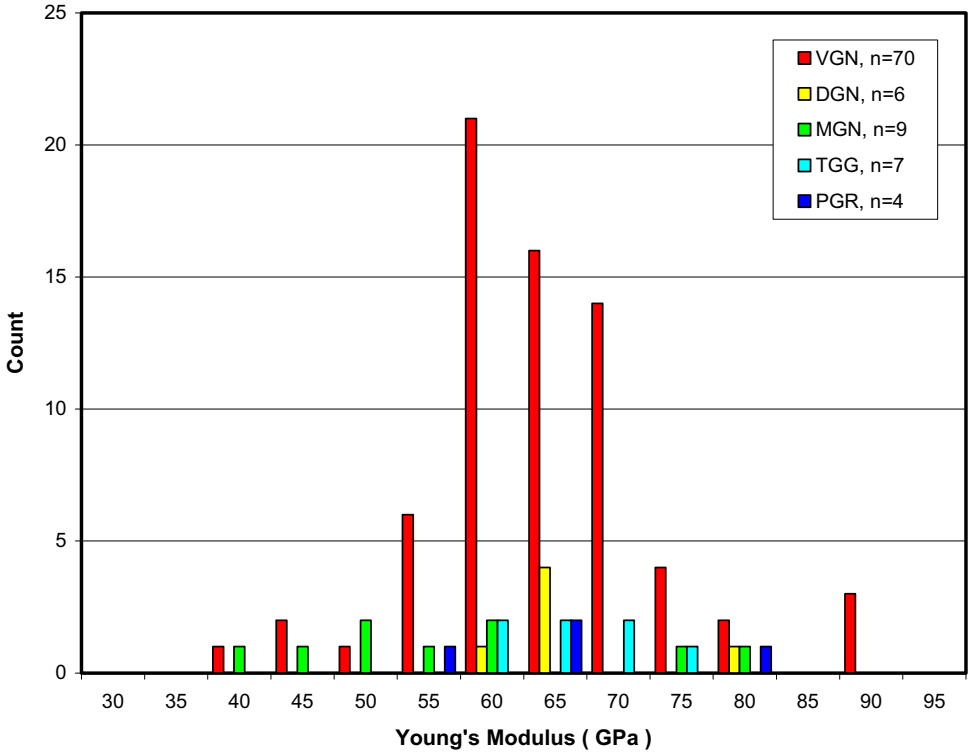

Figure 5-20. *Variation of apparent Young's modulus for Olkiluoto rock types.*

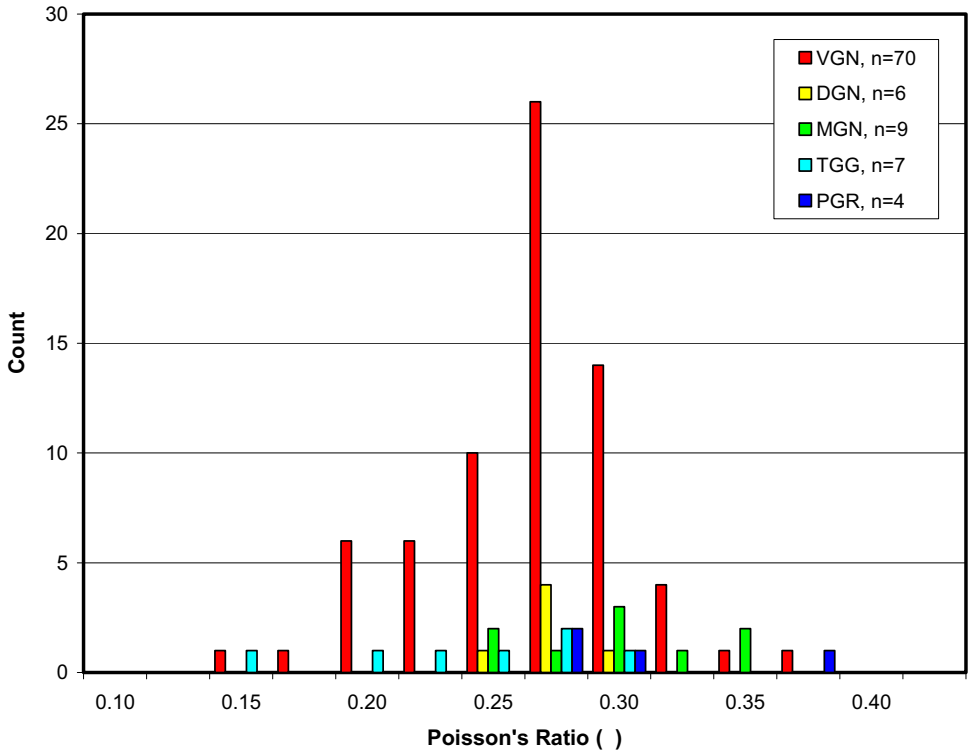

Figure 5-21. *Variation of apparent Poisson's ratio for Olkiluoto rock types.*

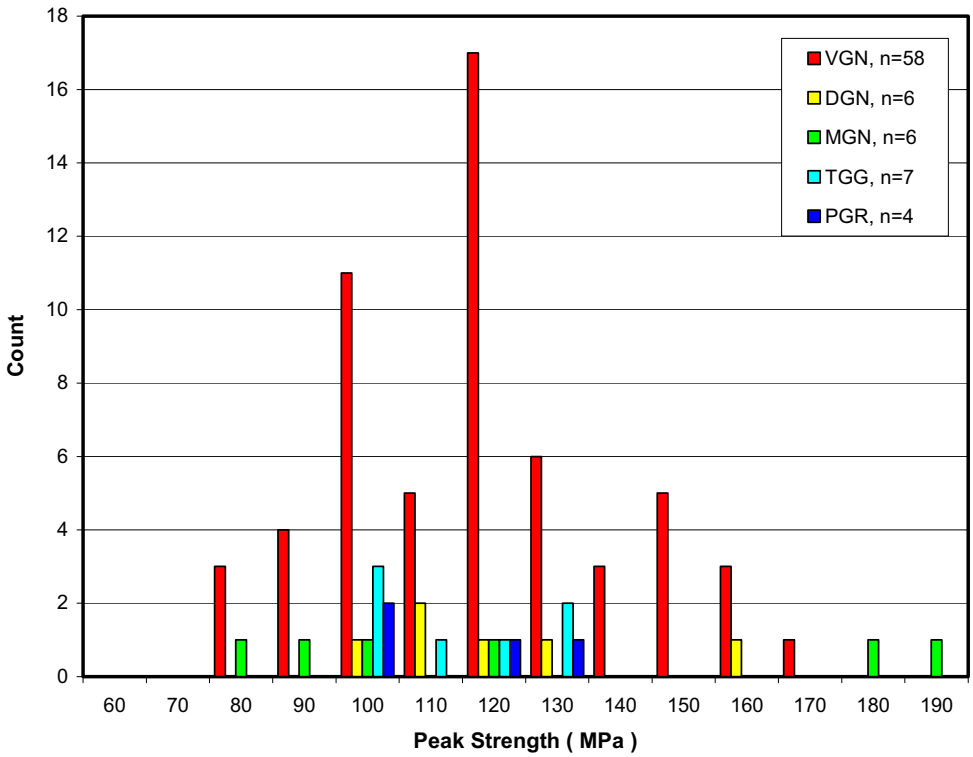

Figure 5-22. *Variation of peak strength for Olkiluoto rock types.*

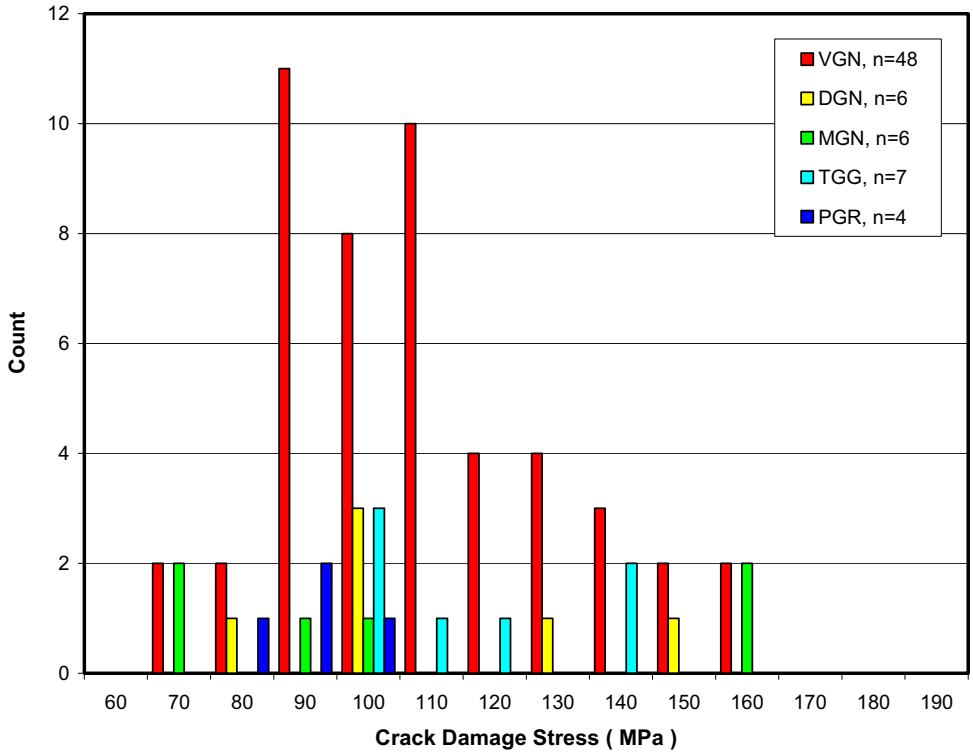

Figure 5-23. *Variation of crack damage stress for Olkiluoto rock types.*

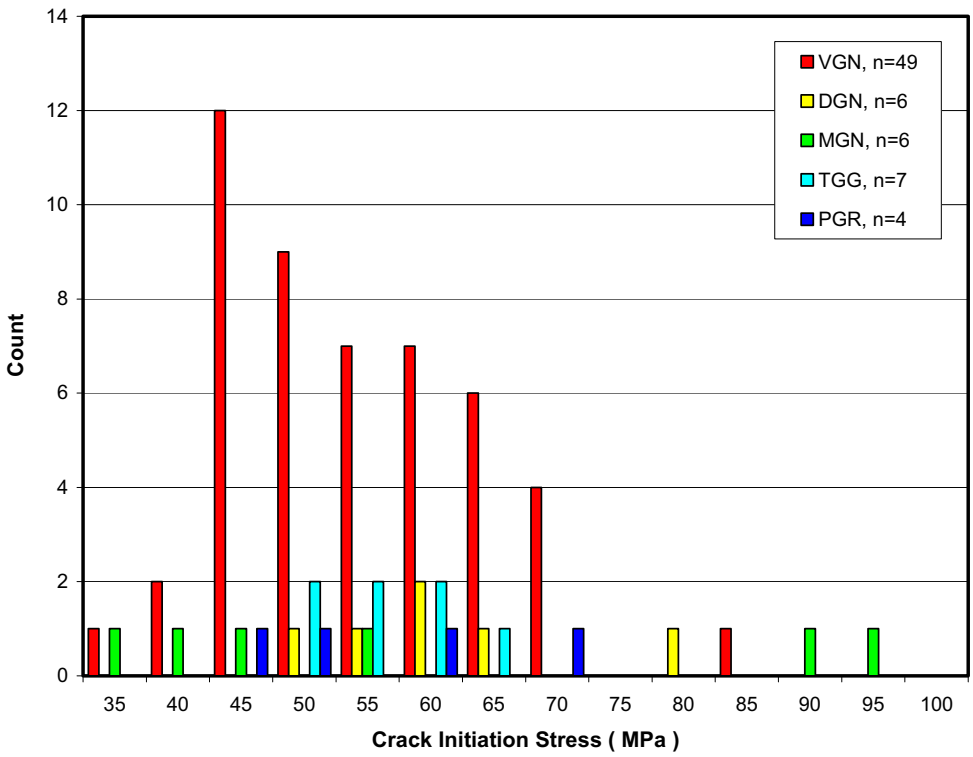

Figure 5-24. *Variation of crack initiation stress for Olkiluoto rock types.*

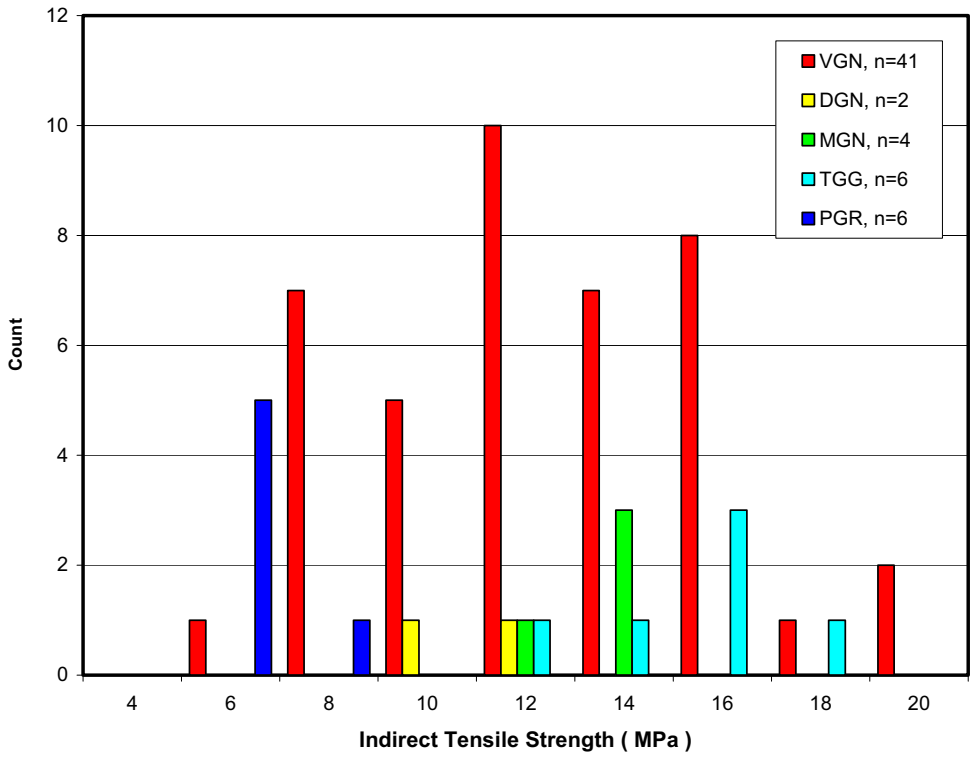

Figure 5-25. *Variation of indirect tensile strength for Olkiluoto rock types.*

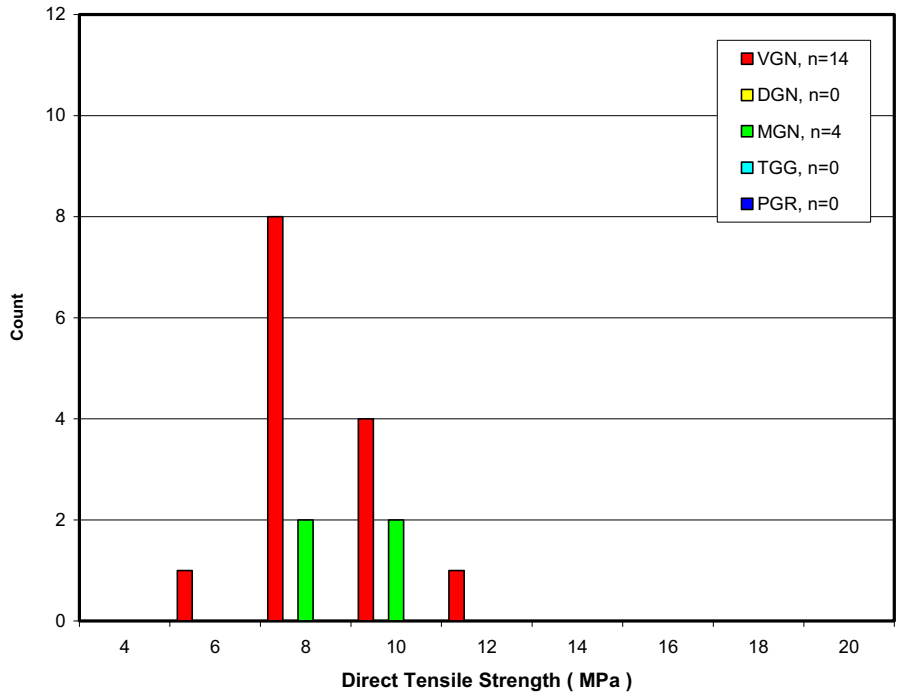

Figure 5-26. *Variation of direct tensile strength for Olkiluoto rock types.*

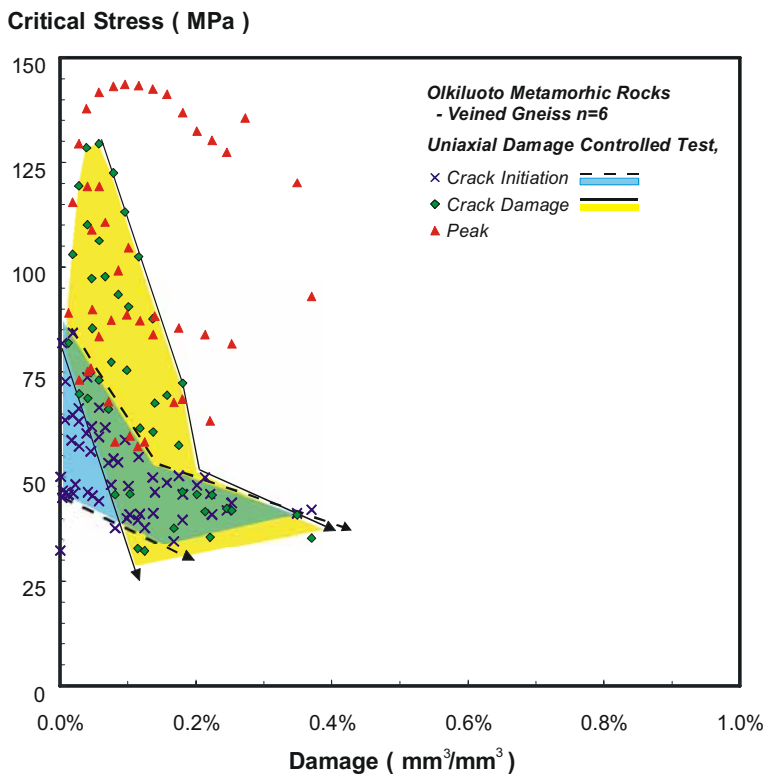

Figure 5-27. *Development of critical stress states in uniaxial damage controlled tests after the first detection of crack damage stress (Hakala & Heikkilä 1997b).*

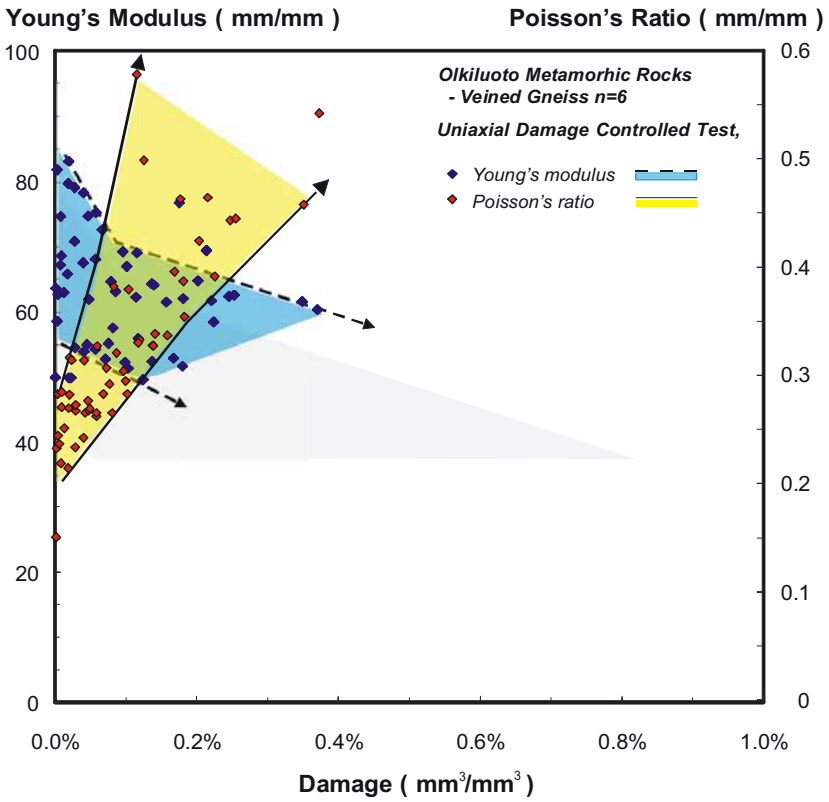

Figure 5-28. *Development of apparent deformation parameters in uniaxial damage controlled tests after the first detection of crack damage stress (modified from Hakala & Heikkilä 1997b).*

Comprehensive anisotropic testing has been carried out only for the major rock type - veined gneiss. Assuming transverse isotropy, the deformation anisotropy of veined gneiss is about 1.3 (E/E′) (Table 5-9 and Figure 5-29 and Figure 5-30), where E is the Young's modulus parallel to the foliation, and E′ perpendicular to the foliation. The tensile strength, crack damage stress and peak strength are dominated by the orientation of the foliation in a manner that would be expected from theoretical considerations, whereas the crack initiation stress is dominated only by the favourably-oriented weakest minerals (Figure 5-31 to Figure 5-34). Noteworthy is the large overlap of the standard deviation values

Table 5-9. *Elastic deformation parameters for Olkiluoto veined gneiss assuming transverse anisotropy.*

Young's modulus parallel to foliation	E	74	GPa
Young's modulus transverse foliation	E´	56	GPa
Poisson's ratio parallel to foliation	n	0.19	mm/mm
Poisson's ratio transverse foliation	n´	0.23	mm/mm
Shear modulus	G	23	GPa

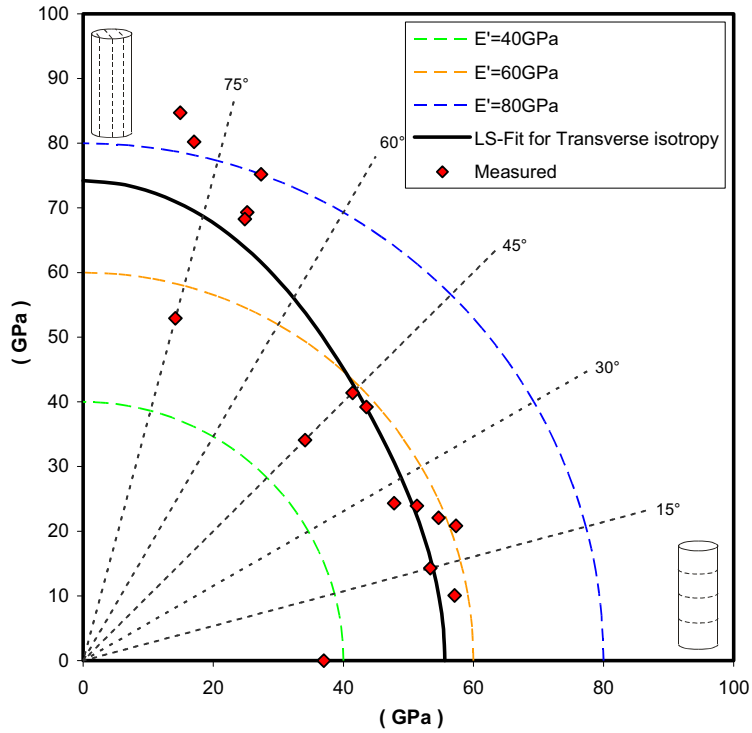

Figure 5-29. *Polar plot of apparent Young's modulus for Olkiluoto veined gneiss in different loading directions as a function of the schistosity/foliation (assumed as a plane for transverse anisotropy).*

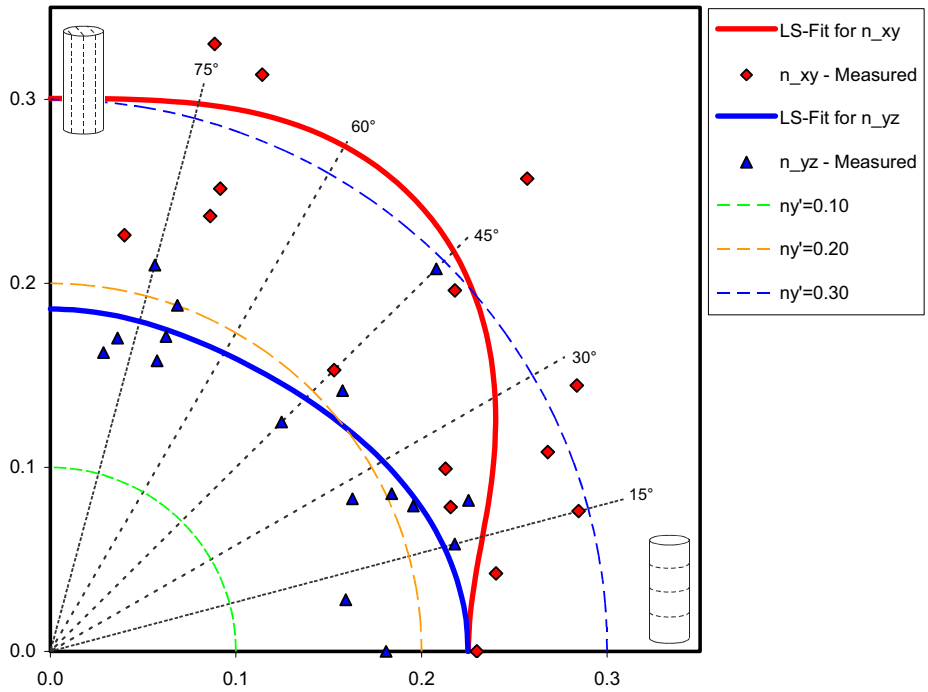

Figure 5-30. *Polar plot of apparent Poisson's rations for Olkiluoto veined gneiss in different loading directions as a function of the schistosity/foliation (assumed as a plane for transverse anisotropy).*

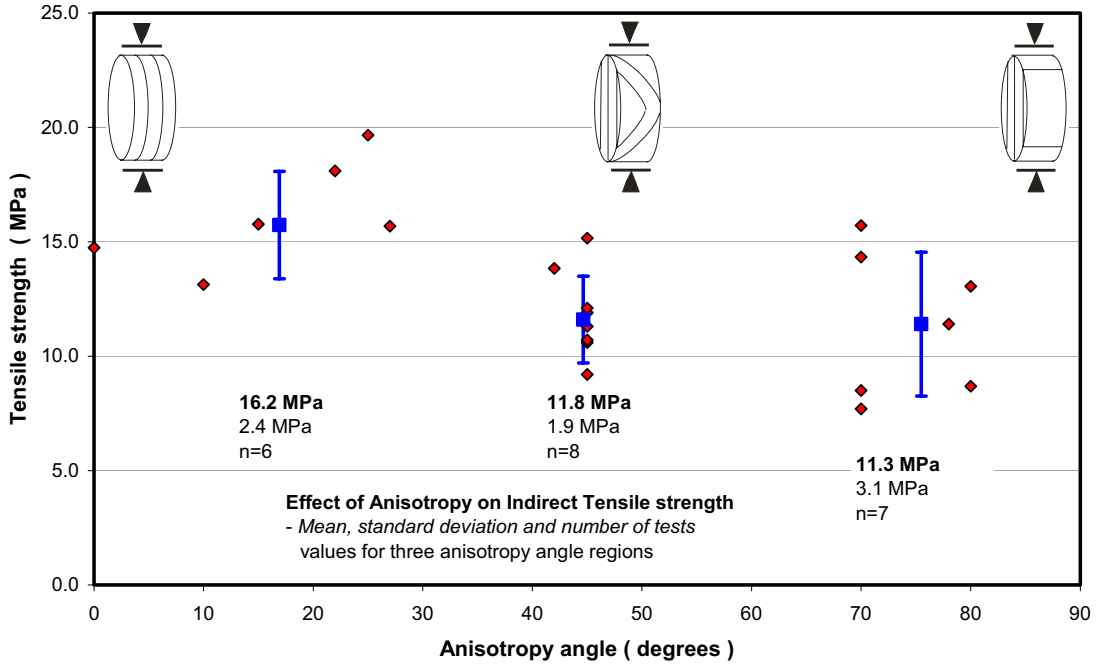

Figure 5-31. *Effect of anisotropy on the indirect tensile strength of dry Olkiluoto veined gneiss.*

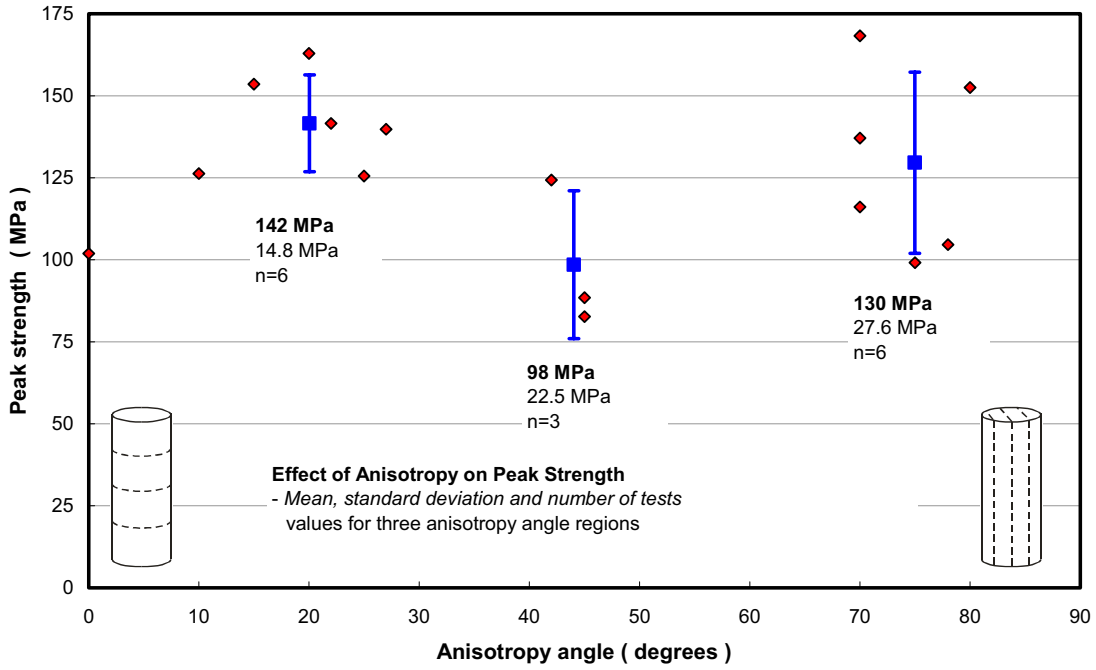

Figure 5-32. *Effect of anisotropy on the peak strength of dry Olkiluoto veined gneiss.*

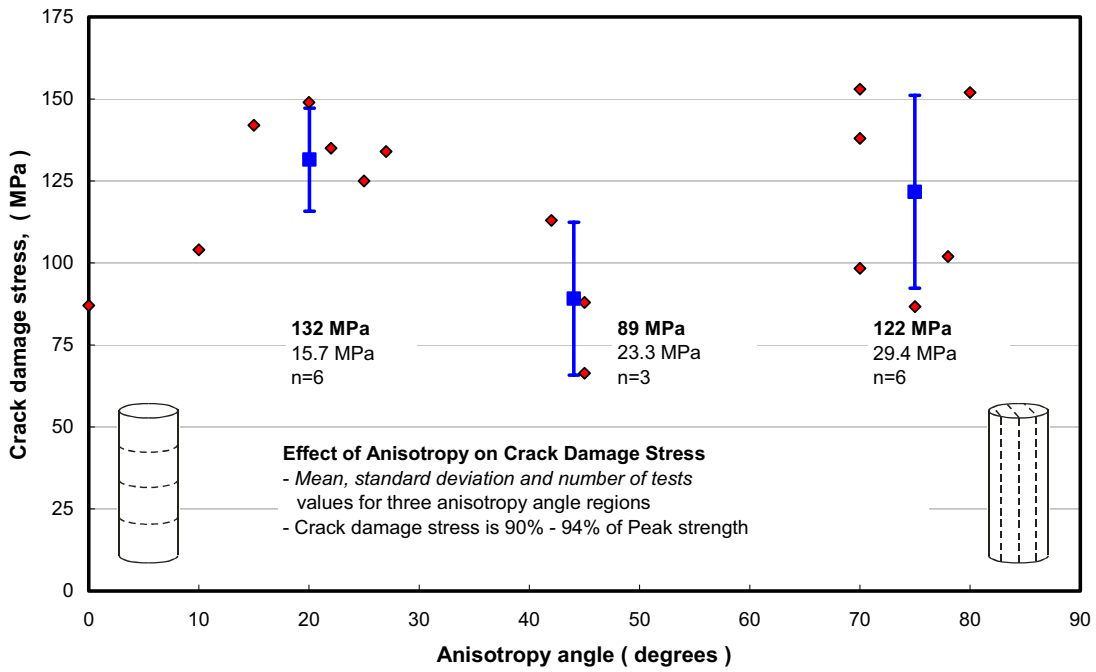

Figure 5-33. *Effect of anisotropy on the crack damage stress value of dry Olkiluoto veined gneiss.*

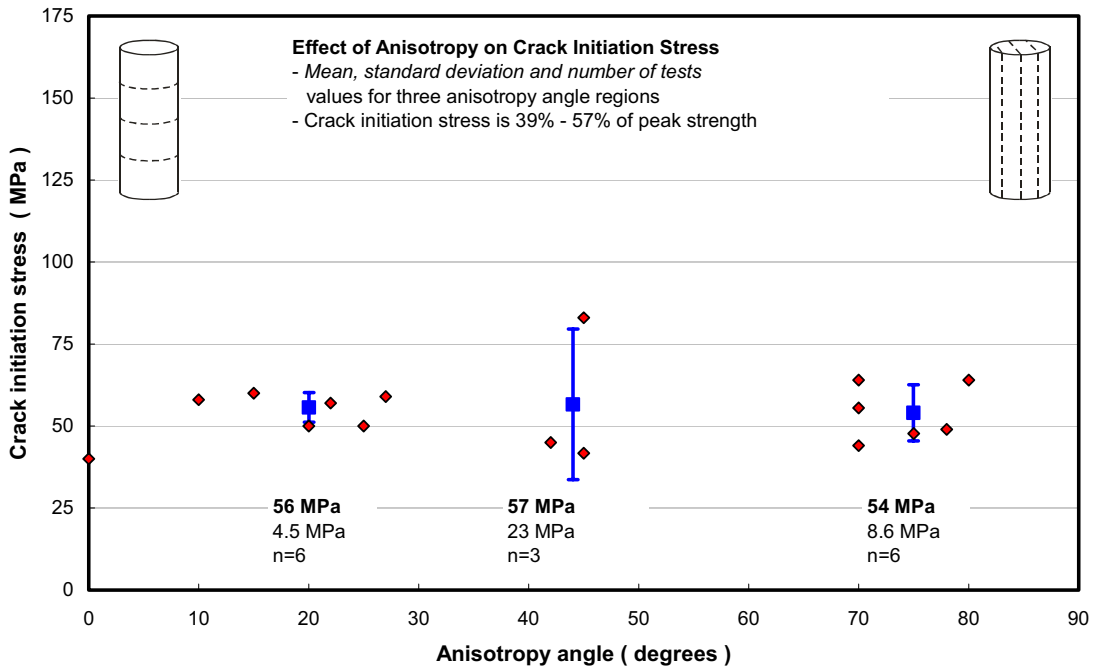

Figure 5-34. *Effect of anisotropy on crack initiation strength of dry Olkiluoto veined gneiss.*

A summary of uniaxial compressive strengths from the field tests of 38 deep boreholes (OL-KR1 - KR38) is presented in Table 5-10. The strength values given in the table are calculated using the point load index and a conversion factor, which is dependent on the rock type. Thus, the field values cannot be directly compared with the laboratory values, but give relative strength values for different rock types. The results are classified according to the rock type under seven rock type categories. The depth dependence was also studied and it was found that the strength values show no correlation with depth (Figure 5-35).

The strength values of the samples show noticeable variation, which is significant even when different rock types are considered separately (Figure 5-36). The high standard deviation (approximately 30 MPa) may be assumed to reflect the heterogeneous nature of the different rock types at Olkiluoto. It may also be due to the difficulty in defining the rock types for the samples, as their locations in the boreholes were not known accurately and there are frequent variations in rock types in the boreholes; with rock type boundaries often coinciding with the locations defined for the samples.

Since the mean strength values for different rock types vary only a little, in comparison with the large variation of strength values within each rock type, it may be concluded that the current lithological model has a low predictive capacity for the distribution of rock strengths at Olkiluoto. Based on the results presented here, the strength of rock appears to be only slightly dependent on the rock type, although this dependence was not examined statistically. For a more thorough analysis of the relationship between the strength properties and the lithology, the rock type of the samples should be defined more accurately, and the effects related to the rock's foliation, which is known to affect the rock strength properties (i.e. its direction with respect to the direction of loading) should also be studied.

Table 5-10. *Uniaxial compressive strength of the samples from boreholes OL-KR1-KR38 based on the point load index, median, average, standard deviation and number of samples in each category.*

	UCS [MPa] median	**UCS [MPa] mean**	**Standard deviation [MPa]**	**Number of samples**
Veined gneiss	*112*	*113*	*29,7*	*580*
Pegmatitic granite	*123*	*125*	*31,1*	*236*
Diatexitic gneiss	*116*	*117*	*30,4*	*192*
Tonalitic-granodioritic-granitic-gneiss	*128*	*129*	*27,9*	*118*
Mica gneiss	*135*	*139*	*35,2*	*72*
Mafic gneiss	*130*	*130*	*7,3*	*6*
Quartz gneiss	*147*	*151*	*32,7*	*4*
All	*118*	*119*	*31,1*	*1208*

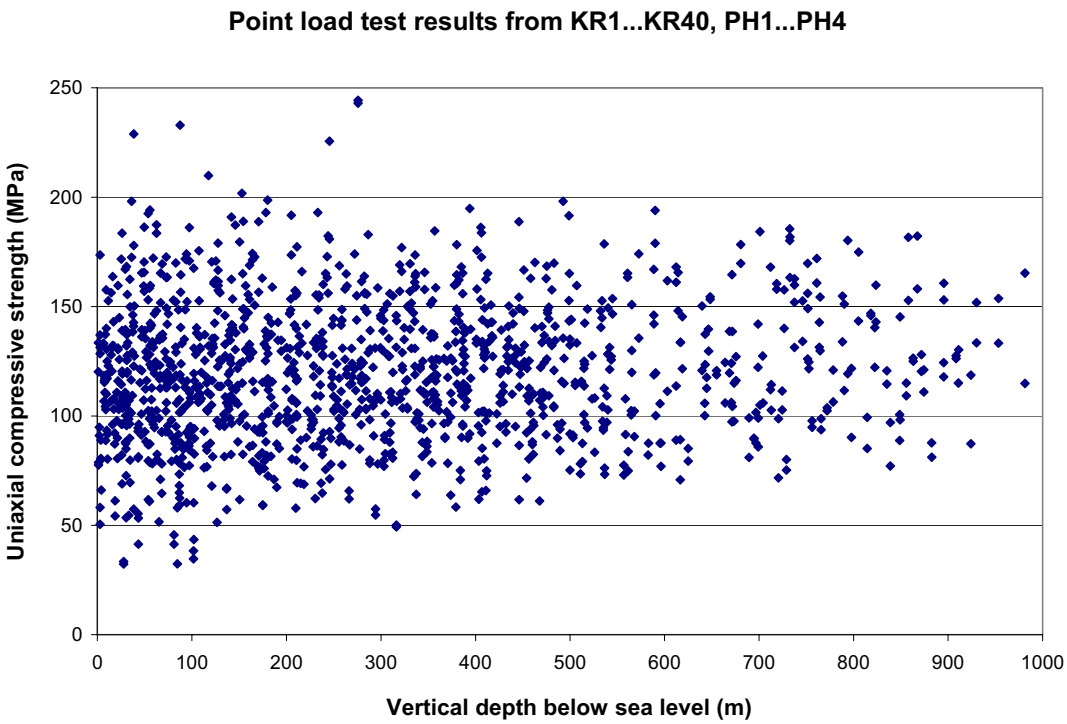

Figure 5-35. *Strength properties with vertical depth based on point load tests (boreholes OL-KR to KR40, OL-PH1, ONK-PH2 to PH4).*

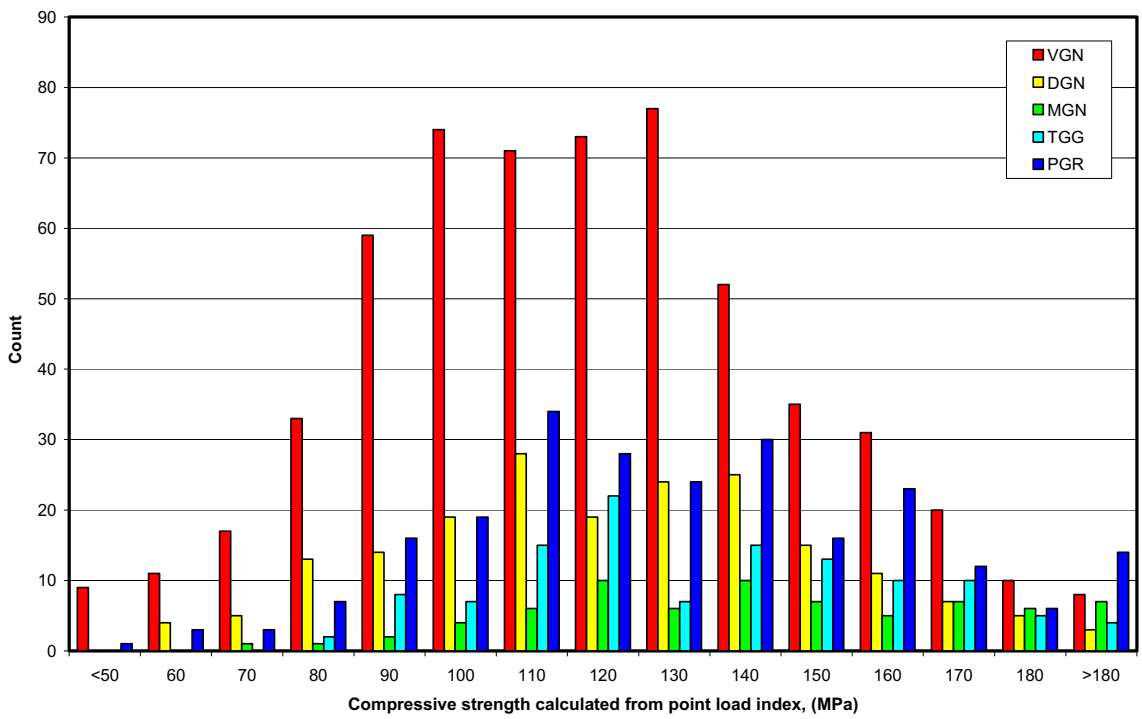

Figure 5-36. *Compressive strength of different rock types, values calculated from point load index test.*

5.4.3 Physical properties

In the laboratory, the dry density and porosity are defined and measured according to the ISRM Suggested Methods. These values were measured for Olkiluoto mica gneiss migmatite and granite/pegmatite using water immersion, storing at 100% humidity, and drying at 102°C, which is the method suggested by the ISRM (Hakala & Heikkilä 1997a). The defined porosity describes the amount of the accessible pore volume for groundwater penetration. The compressive P-wave velocity is defined, according to the ISRM suggested method, using a dried specimen. The transducer and receiver are pressed onto the specimen ends with a constant axial contact pressure of 65 kPa and the wave transmission on contact is improved with water (water is used only as a couplant on the contact surfaces). However, there can be difficulties with the transducer coupling.

The average dry density values and their deviations are presented in Table 5-11. The average porosity of Olkiluoto metamorphic rocks based on 120 specimens is 0.23% with a deviation of 0.088%. The corresponding values for pegmatitic granite based on 10 specimens are 0.37% and 0.069%.

Table 5-11. *Density values for Olkiluoto rock types.*

Parameter	Rock type	Mean value	Standard deviation	Number of samples
Density, g (kg/m^3)	VGN	2734	37	124
	DGN	2729	31	9
	MGN	2748	35	27
	TGG	2730	-	1
	PGR	2611	25	12

5.4.4 Thermal properties

The thermal properties of the rock are required as input data for determining the dimensions of the disposal vaults and for evaluating the thermal stresses induced by heat produced by the radioactive waste. The thermal properties of intact rock are determined mainly by their mineralogical composition. The average thermal conductivity of feldspars and micas is typically 2.0 - 2.5 W/mK; however, the conductivity of quartz is significantly higher at 7.7 W/mK. Most minerals are thermally anisotropic, and micas (biotite, muscovite) are particularly anisotropic, showing large variations in thermal conductivity depending on the direction of measurement. Thermal properties are also temperature-dependent and thermal conductivity and diffusivity decrease and heat capacity increases with increasing temperature.

The Olkiluoto gneisses are also thermally anisotropic and heterogeneous due to variations in their texture, mineral composition and the orientations of the migmatitic banding and the foliation. The typical range of thermal conductivity for the migmatitic gneisses determined in the laboratory is 2.3 – 3.2 W/mK (Figure 5-37, Table 5-12),

where the minimum values are interpreted to represent the values perpendicular to the foliation. The mean anisotropy factor based on the measurements is 1.25 ± 0.25 (Kukkonen et al. 2005).

A comparison of the results obtained in drillhole OL-KR2 indicates that in situ conductivity estimates are about 0.3 – 0.5 W/mK higher and in situ diffusivity estimates 0.1 – 0.2 10^{-6} m^2/s lower than laboratory data. The differences are not systematic, which is probably due to the heterogeneity of the rock (Kukkonen et al. 2005).

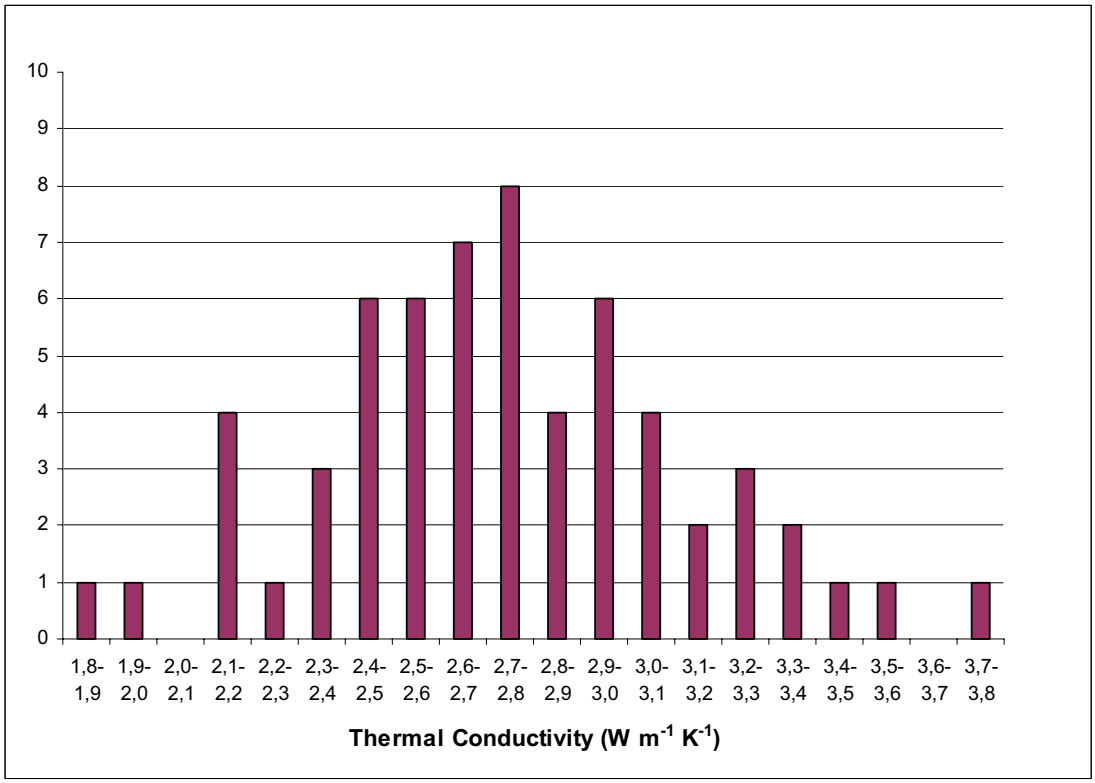

Figure 5-37. *Distribution of thermal conductivity of Olkiluoto migmatitic gneisses (laboratory tests).*

Table 5-12. *Thermal properties (conductivity and diffusivity) of the migmatitic gneiss at Olkiluoto determined in different drillholes (laboratory tests).*

Drill hole ID	Number N	Thermal Conductivity	Thermal Conductivity	Diffusivity	Diffusivity
		($W\ m^{-1}\ K^{-1}$)	($W\ m^{-1}\ K^{-1}$)	($10^{-6}\ m^2\ s^{-1}$)	($10^{-6}\ m^2\ s^{-1}$)
		Mean	Std Dev	Mean	Std Dev
OL-KR1	11	2,84	0,44	1,24	0,22
OL-KR2	26	2,76	0,27	1,35	0,17
OL-KR4	8	2,83	0,40	1,25	0,18
OL-KR9	8	2,78	0,47	1,20	0,22
OL-KR11	8	2,32	0,35	1,02	0,16
ALL	61	2,73	0,39	1,25	0,21

5.4.5 Drilling properties

The drilling parameters DRI (Drilling Rate Index) and CAI (Cerchar Abration Index) have also been determined for mica gneiss migmatite and grey (tonalite) gneiss at Olkiluoto (Äikäs et al. 2000) and estimated values of these parameters for the other rock types have been made on the basis of a literature review. The Vickers hardness of the rock types was calculated on the basis of the average mineral composition determined from thin section analysis and the results are shown in Table 5-13. With regard to the drilling properties, all the rock types at Olkiluoto are placed in the normal class of constructability, regardless of the drilling method (Äikäs et al. 2000).

Table 5-13. *Drilling parameters, strength and Vickers hardness for different rock types. The values presented are arithmetical means with standard deviations in parentheses (Äikäs et al. 2000) (see footnote).*

Rock type	DRI index (defined)	DRI index (literature)	CAI index	Peak strength (range MPa)	Vickers (average)	Vickers (range)
Mica gneiss migmatite[2]	45 (4.3)	50-70	4.3 (0.1)	80 – 140	713	382 - 948
Granite/ pegmatite	-	45 – 65 (granite)	-	115 – 150	807	720-895
Grey (tonalite) gneiss	55 (3.0)	45 – 65 *	3.7 (0.4)	80 – 110	672	535 - 822
Amphibolite/ metadiabase	-	40 - 60 (amphibolite) 30 – 45 (metadiabase)		100	559	410-708

** no values for grey (tonalite) gneiss were available, so the value for granite is applied here*

5.4.6 Mechanical properties of brittle deformation zones

As mentioned earlier in Section 5.2, the properties of the brittle deformation zones are the least developed of the rock mechanics properties. An initial approach to estimating the mechanical properties has been described in "Baseline conditions at Olkiluoto" Posiva (2003) and this approach is currently being further developed, as mentioned in Section 5.2 (Hudson et al. 2007). In that report, the brittle deformation zone features will be described in more detail with reference to their degree of localisation, from single discrete fractures, through shear networks to a pervasive foliation fabric. The scale of observation of the features can affect their apparent properties, so the effects of

[2] Note: The rock type names here use the old terminology. The data are not easily recalculated for the new terminology because there is no 1:1 correspondence.

the relative scales of the deformational features and the excavation size need to be ometrical considered.

5.4.7 Gemetrical and mechanical properties of fractures

5.4.7.5 Data available

The main data available for establishing parameters for the fractures and fracture sets are from the pilot hole and ONKALO tunnel mapping. The best data are the tunnel mapping data, because they include fracture length and waviness values and the fracture surfaces are not affected by drilling. Note that before 2006 the normal borehole logging system did not include rock mechanics parameters; to increase this knowledge, rock mechanics mapping of the ONKALO area drillholes was implemented during 2006, but the results of this mapping are not available for this report.

The parameters presented for the fractures are based only on the ONKALO tunnel mapping data, representing a depth range from zero to 120 m. The interpretation of the major fracture sets is normally carried out for each 5 m long tunnel section. From all the mapped fracture data, those fractures that are shorter than one metre and those which end in intact rock are removed. If the number of accepted fractures is too low for interpretation of the major fracture sets, then the neighbouring five metre sections are incorporated.

Major Fracture Sets

In the tunnel mapping essentially two major fracture sets exist (Figure 5-38). The dominant fracture set *Set 1a* is parallel with the foliation, dipping approximately 30º to the SE. The second fracture set *Set 2* is almost vertical, striking in a N-S orientation. The gently dipping dominant set *Set 1a* has a high variability, (Figure 5-38 and Figure 5-39). In the first 250 m, the horizontal set *Set 1b* is common but, at greater depth, there are many sections where all the sets, *Set 1b* to *Set 1f*, replace *Set 1a*. Set *Set 3* can be seen only at the surface.

If all 15,125 mapped fractures are studied together, the result is very similar (Figure 5-40). The highly variable *Set* 1 (*Sets 1a* to *1f*) and *Set 2* are almost the same, but *Set 3* cannot be seen, and instead another vertical set perpendicular to *Set 2* becomes more dominant. This second vertical set has been defined as a major fracture set only a few times (Figure 5-38). The considerable variation in fracture orientations is typical for the ONKALO area, the maximum concentrations being only 3% to 4%. All fracture sets are found in all rock types, but the occurrence of *Set 1a* is greater in the migmatites (VGN, DGN and SGN) and the amount of random fracturing is greater in the homogeneous gneisses (MGN,TGG, MFGN and QGN) (Figure 5-41). Note that the variability of Set 1 is also illustrated in Chapter 9, Figures 9-12, 9-13 & 9-14.

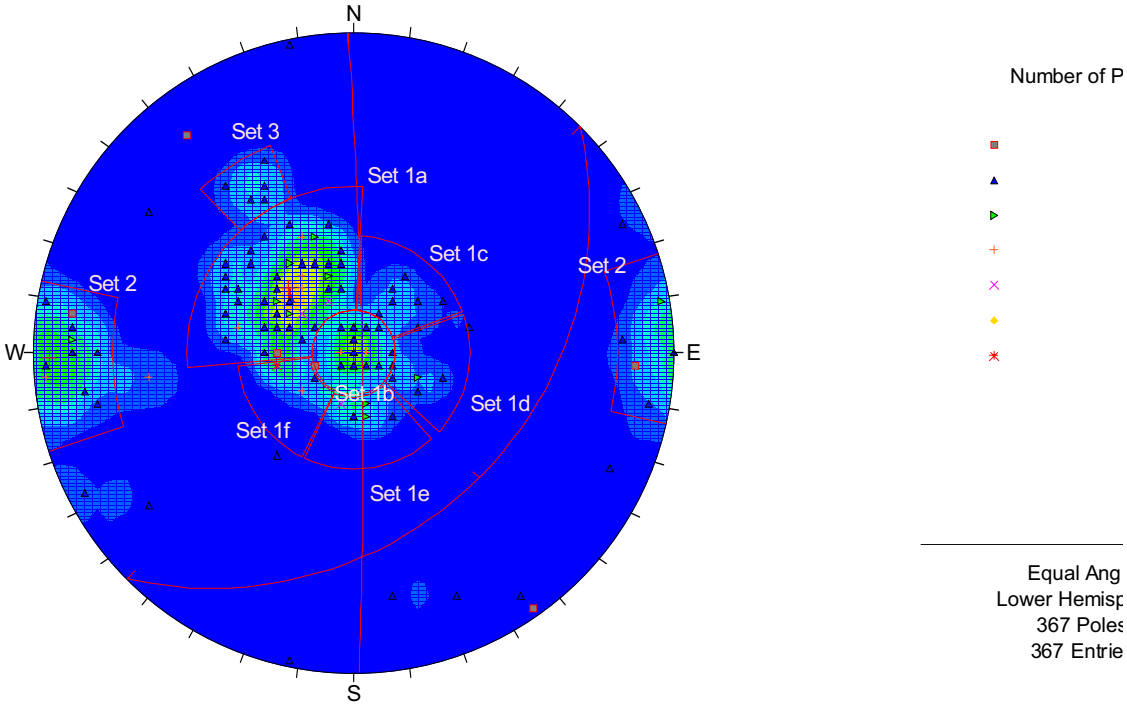

Figure 5-38. *Lower hemisphere plot of all ONKALO major joint sets from chainages 0 to 1190 m.*

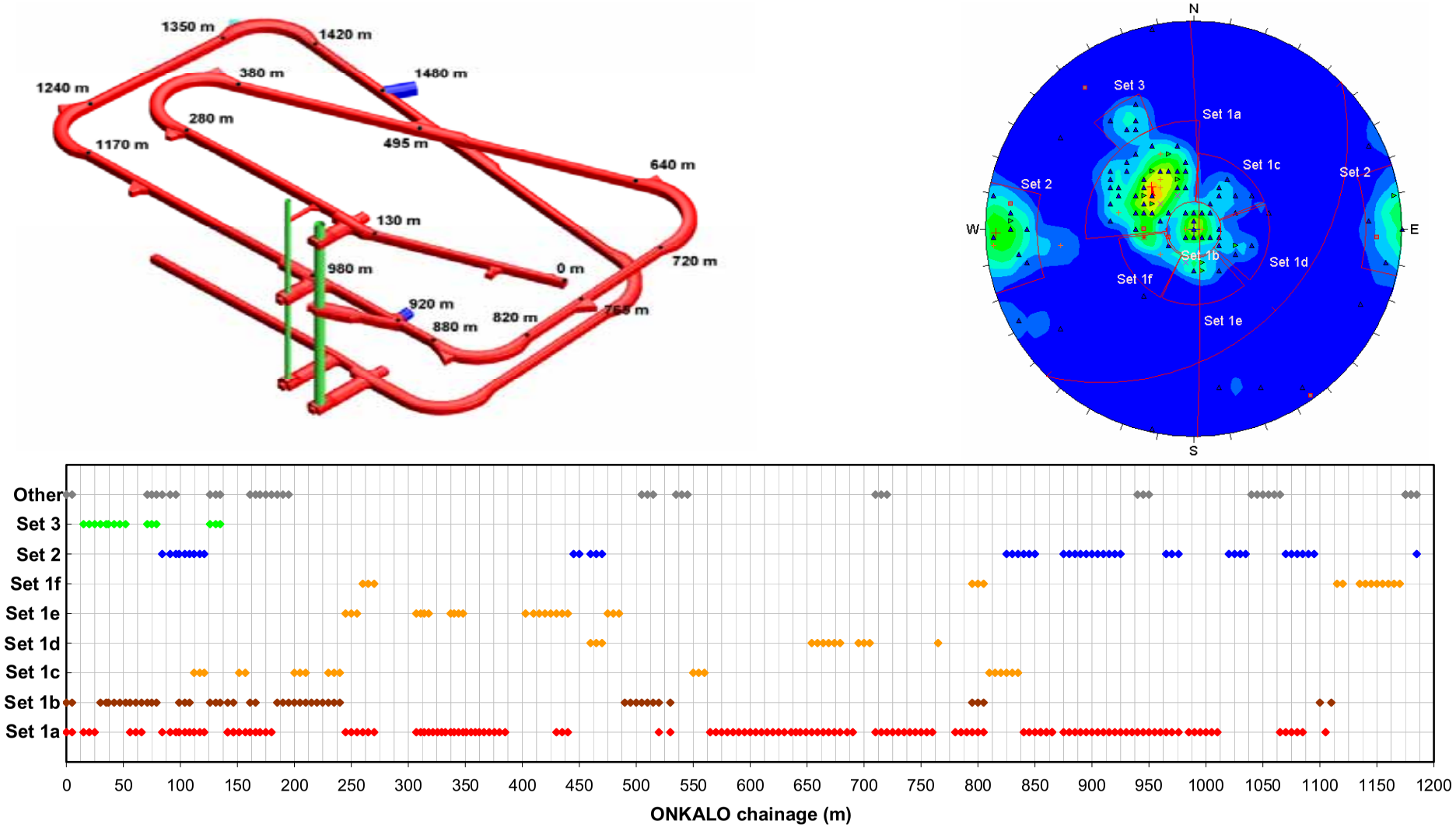

Figure 5-39. *Spatial variation of the major fracture sets encountered in the ONKALO tunnel mapping.*

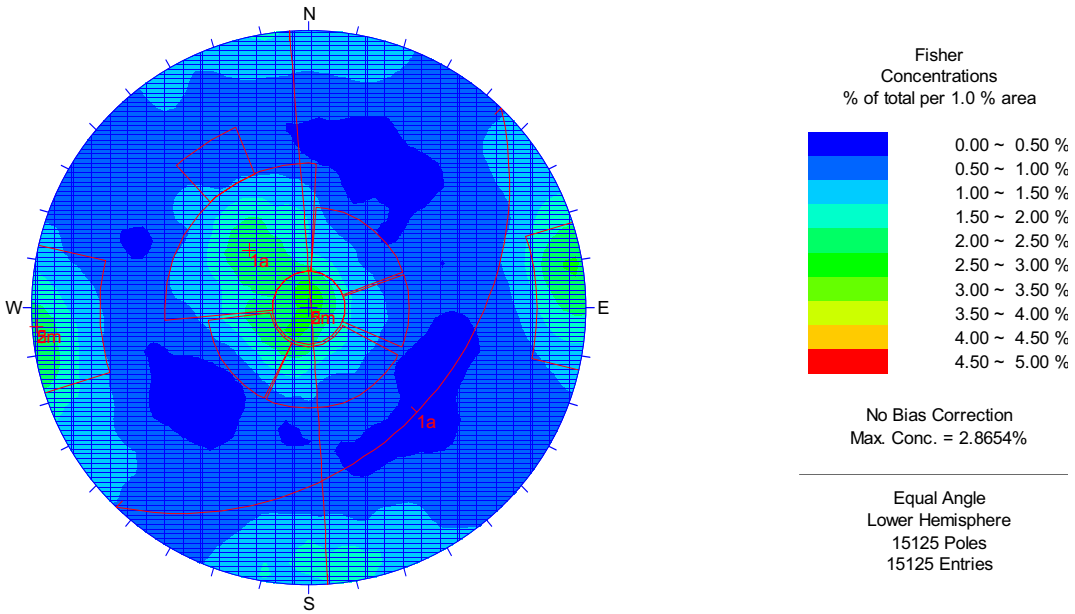

Figure 5-40. *Lower hemisphere plot of all ONKALO fractures from chainages 0 to 1190 m.*

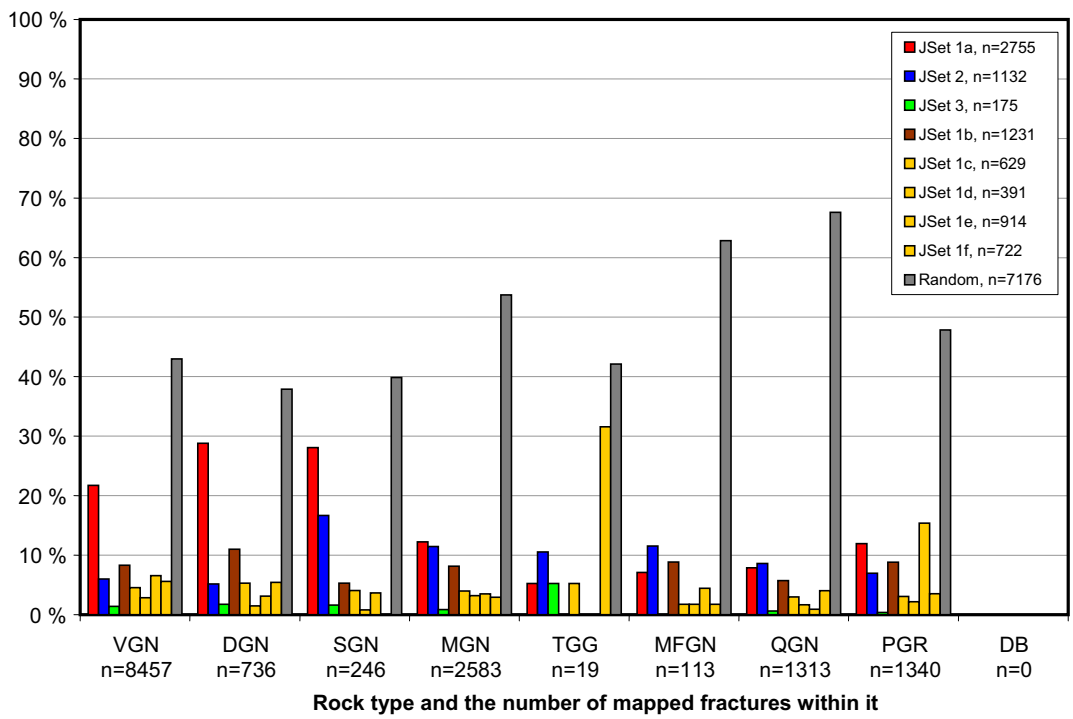

Figure 5-41. *Comparison of different fracture orientations within the different rock types.*

Number of Fracture Sets

The gently-dipping fracturing component is observed almost continuously, but there are long sections without vertical fracturing (Figure 5-39). The dominant number of fracture sets is one plus random (Figure 5-42). In terms of block fallout, the minimum number of faces that a block can have is four (a tetrahedral block); the tunnel periphery can form one face, so that a minimum of three fracture sets is then required for a rock block to be formed. This means that tunnel sections where occasional or systematic rock blocks can be formed, i.e. sections having two fracture sets plus a random component or three fracture sets, are most common in first 300 m. After that, such sections are less common and shorter.

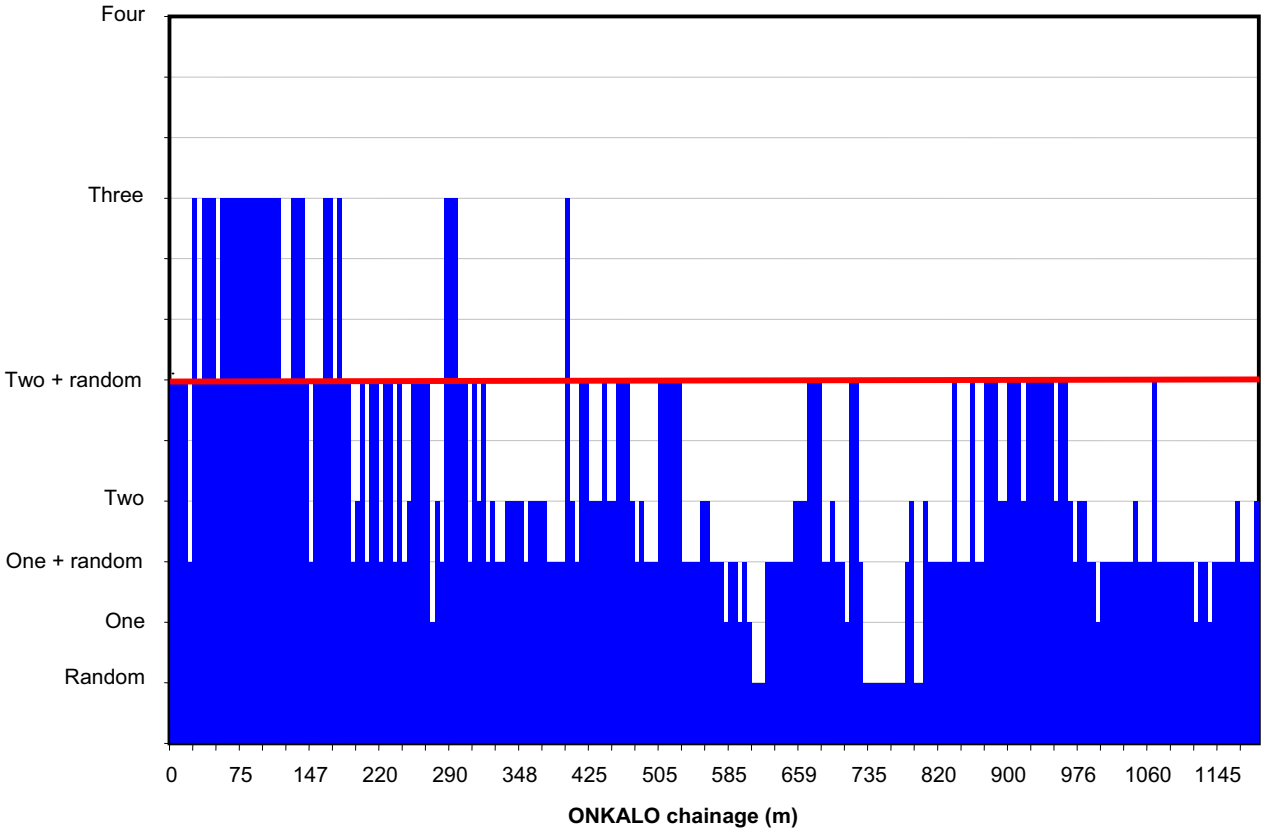

Figure 5-42. *Number of fracture sets defined from ONKALO tunnel mapping data. Block fall-out can only occur when three or more fracture sets are present, i.e. above the red line in the histogram.*

Fracture Intensity

Fracture intensity is described as the number/metre and more indirectly by the RQD value, which is defined as the sum of unfractured sections of rock over 10 cm long found in a one metre long drillhole or scanline. The ONKALO tunnel RQD value has

been estimated by one metre long scanlines for each 5 m long tunnel section. The mean RQD value for the ONKALO tunnel is 96: 50% of the values are between 90 and 100; and 95% of the values are between 70 and 100. The minimum value is 50 at chainage 285 m to 295 m, with another low value section, 55 < RDQ < 65, from chainage 260 m to 274 m.

Fracture Length and End-type

The fracture length data distributions are both truncated and censored: truncation occurs when fractures below a certain length are ignored; censoring occurs when fracture trace lengths above a certain length cannot be observed in their entirety, because of the limited dimensions of the excavation. For all fractures, both the length and end-type are mapped. The fracture can end in intact rock (R), at another fracture (J), or continue beyond the tunnel (C). About 70% of all fractures end in intact rock and about 60% of the fractures are shorter than 1.0 m (Figure 5-43). Note that the end-type has no correlation with the fracture set. Mean fracture lengths are from 0.5 m to 1.5 m, depending on the mode of the major fracture set, and 5% of the fractures are longer than the tunnel width of 5 m (Figure 5-44). The length of the gently-dipping fractures seems to be greater than the length of the vertical or random fractures, but this is partly caused by the orientation of the tunnel, which tends to bias the data.

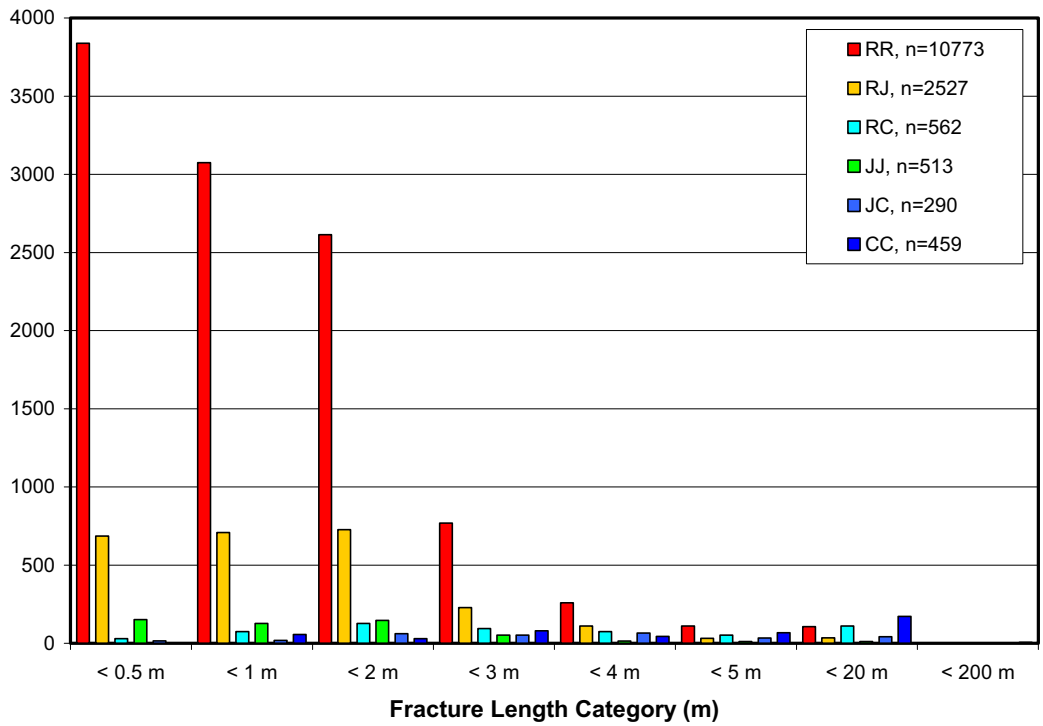

Figure 5-43. *Trace length and end-type for all mapped fractures in the ONKALO tunnel.*

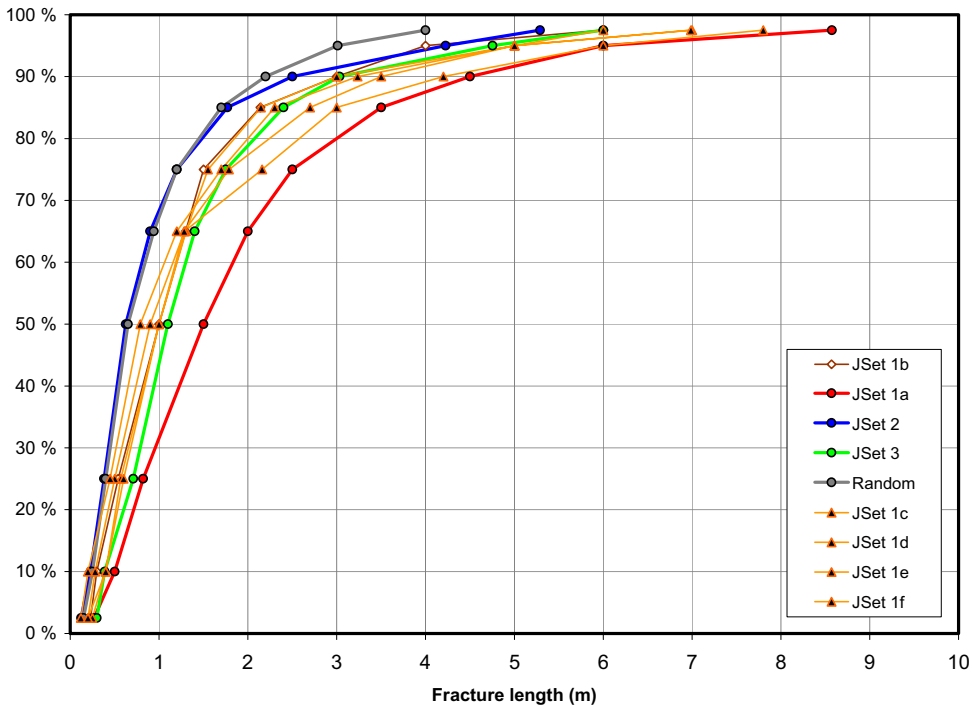

Figure 5-44. *Cumulative distribution of trace lengths for the different fracture sets for all mapped fractures in the ONKALO tunnel.*

Fracture Surface Parameters

The fracture roughness number, *Jr*, can have values between 0.5 and 4, the lowest values are for *planar slickensided* fractures and highest for *discontinuous* or *rough & undulating* fractures. The mean value of *Jr* is 2, with 50% of the values lying between 1.5 and 3 and 95% lying between 1 and 3. The *Jr* number seems to have a slight correlation with fracture length: the shortest fractures are more *planar* and the middle length fractures are more *undulating* and *rougher* than the average (Figure 5-45). The longest fractures dominate in the *slickensided planar* roughness category (*Jr*=0.5). The vertical N-S trending fracture set, Set 2, has more *smooth & planar* and fewer *rough & undulating* fractures than the other sets. The fracture end-type does not correlate clearly with roughness.

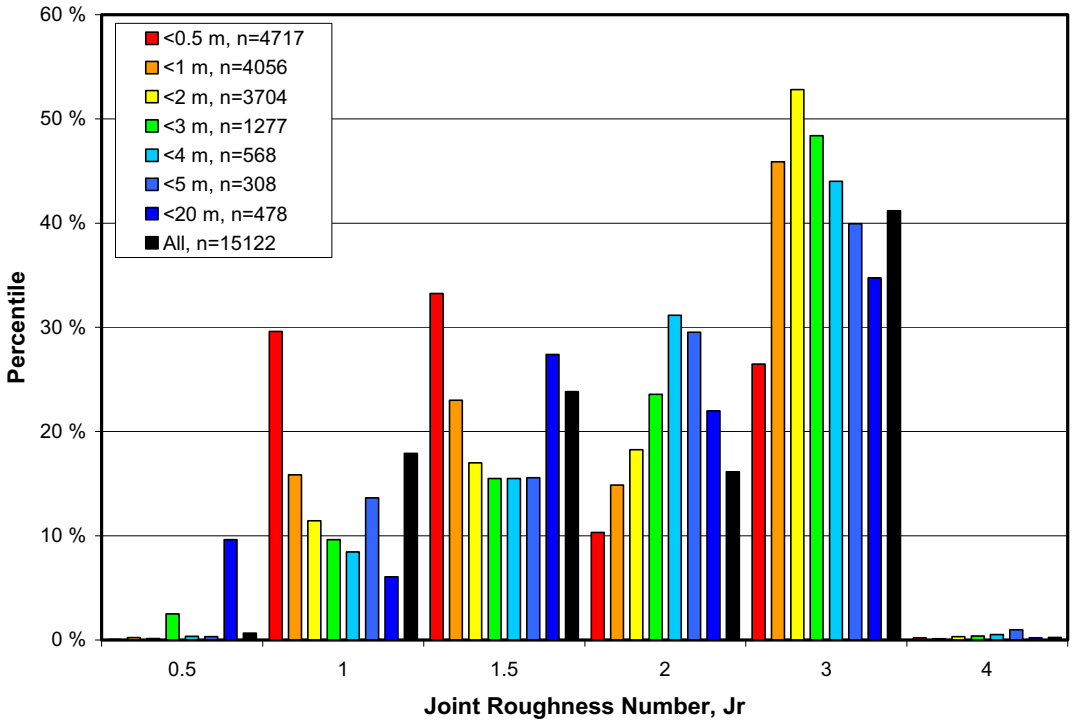

Figure 5-45. *Joint roughness number,* Jr, *and fracture length for all mapped fractures in the ONKALO tunnel.*

The fracture alteration number, *Ja,* can have values between 0.5 and 20. The lowest values are for *tightly healed & unaltered* fractures with *rock wall contact* and the highest for *thick mineral filled* fractures. The mean value of *Ja* is 2: 50% of the values lie between 1 and 4 and 95% are in the same range (Figure 5-46). The *Ja* number correlates with fracture length: the shortest fractures are more often unaltered or slightly altered (*Ja* is 1 or 2); whereas the medium length and long fractures (length > 1 m) more often have *softening or low friction clay mineral coatings* (*Ja* = 4) or *thin or thick mineral filling and can shear without rock wall contact (Ja ≥ 5)*. Furthermore, fractures for which either or both ends continue beyond the tunnel, often the long ones, are more altered (*Ja* ≥ 4). The vertical N-S trending fracture set, *Set 2,* has slightly more *unaltered* or *slightly altered* surfaces (*Ja* = 1 or 2).

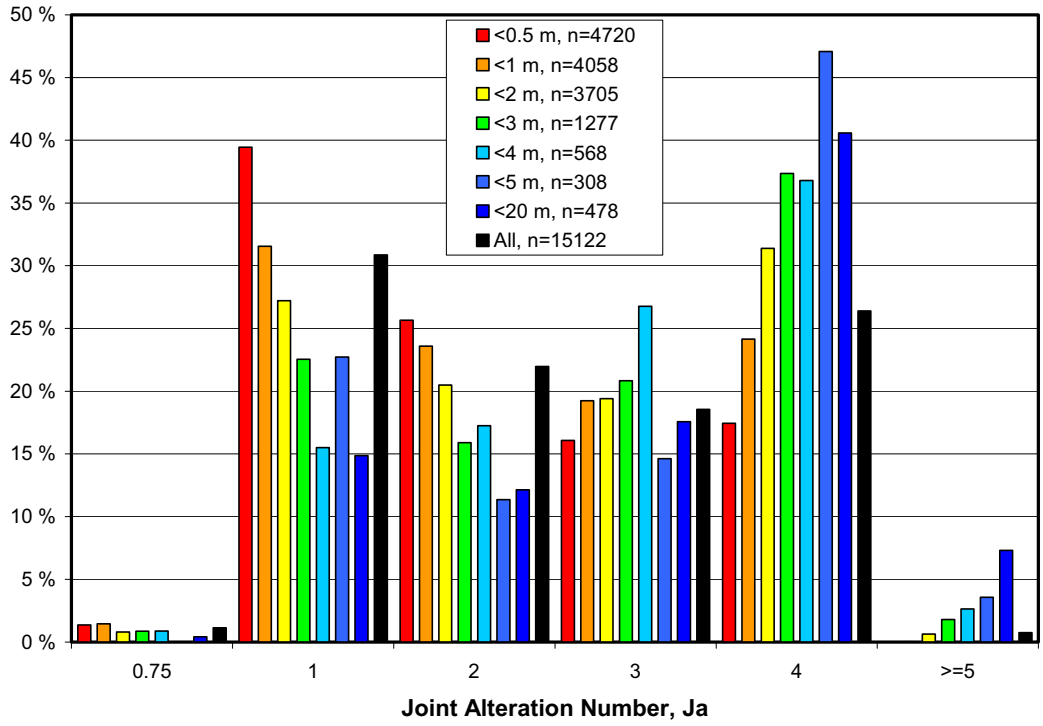

Figure 5-46. *Joint alteration number,* Ja*, and fracture length for all mapped fractures in the ONKALO tunnel.*

The friction angles of the fracture surfaces can be estimated from the *Jr* and *Ja* numbers, being *atan(Jr/Ja)*. The mean value for all fractures is 45°; 50% of the values lie between 27° and 56° and 95% lie between 14° and 72°. The portion of the longest fractures (length > 4m) is slightly greater for the low friction angle categories (Figure 5-47).

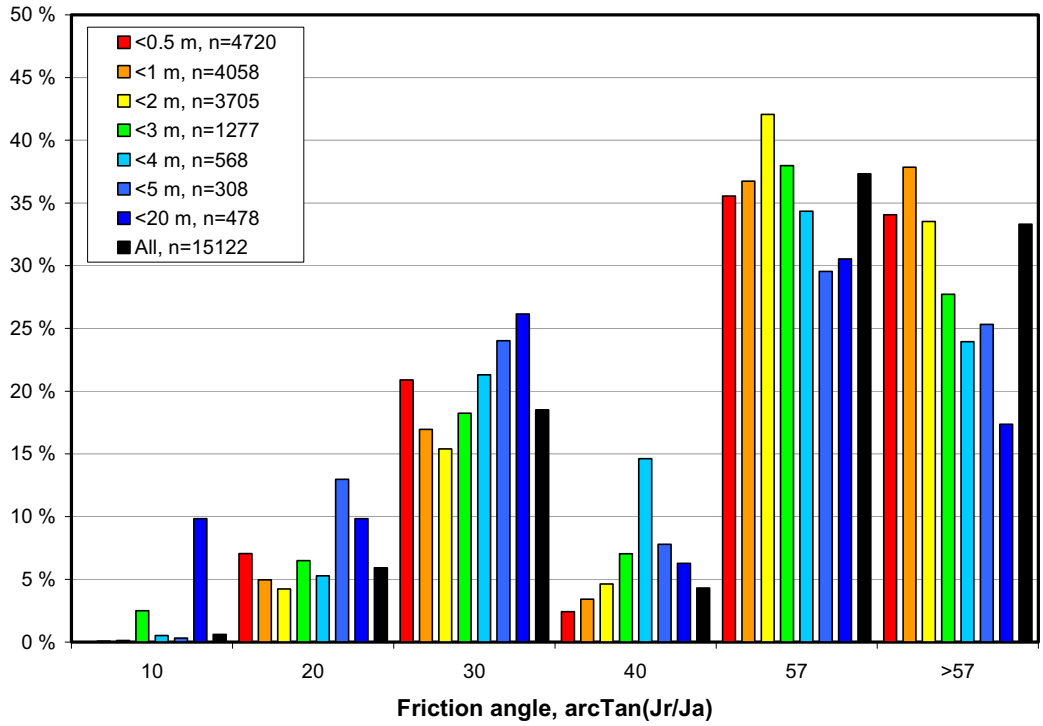

Figure 5-47. *Joint friction angle and fracture length for all mapped fractures in the ONKALO tunnel.*

Fracture undulation is defined via the amplitude from a 1 m long straight inspection line. The mean undulation value is 1 cm, 50% of the values lie between 0 cm and 3 cm and 95% between 0 cm and 10 cm. The shortest fractures are the most planar: 65% of these have no measured undulation (Figure 5-48), whereas the longest fractures have the greatest undulation. Undulation values also correlate with fracture end-type: fractures terminating in intact rock are the most planar and fractures having either or both ends continuing beyond the tunnel are the most undulating. The fracture undulation can be used to estimate the joint roughness coefficient, JRC, and the dilatation angle of the fractures.

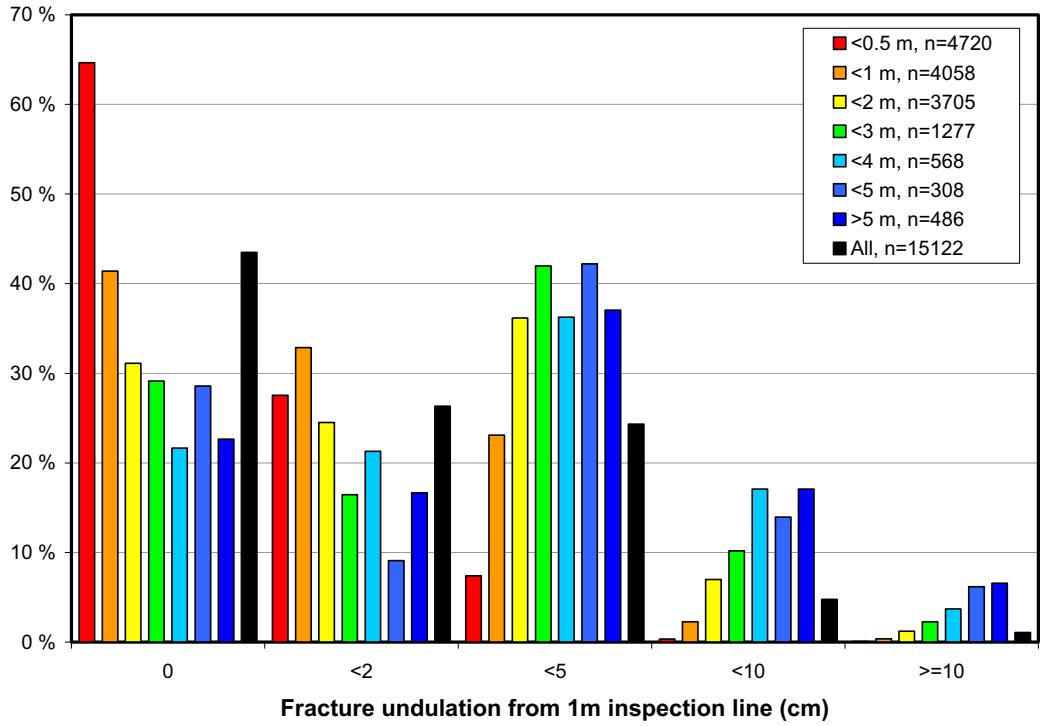

Figure 5-48. *Joint undulation and fracture length for all mapped fractures in the ONKALO tunnel.*

The measured joint aperture is non-zero for only 1.5% of the fractures: 1.25% have an aperture of <0.5 mm; 0.14% greater than1 mm; and only five fractures out of a total of 15,122 have an aperture between 5 and 10 mm.

At the time of writing, statistically reliable information on joint wall compressive strength did not exist, making it impossible to provide estimates of the normal stiffness and shear stiffness of the fractures. Based on preliminary results, however, these values are close to the intact rock strength for coated fracture surfaces and about 50% of the intact rock strength for filled fracture surfaces.

5.4.8 Mechanical properties of the rock mass

The mechanical properties of the rock mass have not been measured directly, but they can be estimated from the rock mass classification values using empirical correlation equations. This is discussed in the rock mechanics section of the Prediction-Outcome in Chapter 9 where three such empirical equations have been used to estimate the rock mass modulus from Q' values obtained from measurements on the pilot hole core and tunnel periphery.

5.4.9 Bedrock stability measurements

The microseismic (MS) network has operated since 2002 with only minor measuring breaks caused by lightning or construction work, which mainly affected only single

stations. The network has recorded both natural microseismic and excavation-induced events. Up to the end of 2005 there have been three events that might have been natural earthquakes, the remainder have been connected with the excavation (Saari 2006).

GPS measurements have shown minor, but expected movements between the stations, with movements generally being due to land lift in the Olkiluoto area. In OL-GPS9 the movements are interpreted to be the result of an open excavation under the GPS-station at the new power plant construction area, as the roof of such an excavation tends to rise because of the effect of horizontal stress (Ahola et al. 2006).

Two precise levelling campaigns have been conducted, the first in autumn 2003 and the second one in autumn 2005 (Lehmuskoski 2006) and no unexpected changes in measuring results have so far been detected.

5.5 Evaluation of uncertainties

This section evaluates the uncertainties in the various components of the Rock Mechanics modelling.

5.5.1 Evaluation of uncertainties relating to in situ stress

Stress is a tensor quantity with six independent components and is defined at a point in the rock mass. It is not possible to measure stresses directly: only normal stress components and normal strains can be measured; shear stresses and shear strains cannot be measured directly. Consequently, all stress measurement methods are indirect in nature (to various degrees), from which the in situ stress state can be inferred. The overcoring method relies, for example, on the measurement of strains, which can be related to stresses under certain assumptions of ideal behaviour; whereas, in hydraulic fracturing, water pressures are measured, which then can be related to the acting normal in situ stress component across a fracture. The Kaiser Effect method of estimating stresses relies on the assumption that previous maximum loading levels of the rock mass corresponds to the present in situ state of stress at a site.

It is inappropriate to discuss the *accuracy* of stress measurements (i.e. how close the measured values are to the true values), since the actual stress state in the field is not known beforehand. The *precision*, on the other hand (defined as a measure of the variation in measurement data), can be used to assess the scatter in individual values for a particular group of measurements. Amadei & Stephansson (1997) stated that the expected imprecision is at least 10-20%, even in rock masses that fulfil all the basic assumptions of the method. Leijon (1988) concluded that non-systematic measurement errors had a standard deviation of 2 MPa or less; whereas, repeated measurements showed a standard deviation of up to 4 MPa (depending on the rock type). Sjöberg & Klasson (2003) found that the typical imprecision for overcoring measurements using the *Borre* probe was at least 1-2 MPa in absolute numbers, with an additional relative imprecision of ± 10% (or more).

The scatter in the Olkiluoto data is fairly typical for the methods employed. It can be seen that the scatter in overcoring data is larger than for hydraulic fracturing, which can

be partly attributed to the fact that the representative volume of rock is larger for the latter technique.

The re-analysis of the overcoring data presented earlier in this report, enabled some uncertainties to be reduced. This involved, for example, the effects of anisotropy, which, to a large extent, were accounted for by stress calculations for the condition of transverse isotropy. It was also shown that the effects of anisotropy were not dramatic, when comparing the re-analysed data with the original stress data. Furthermore, the effects of core damage were partly addressed; however, due to lack of data, some uncertainty remains as to the possible effects of this.

Taken together, the following issues are judged to be the most important sources of uncertainties in the stress measurements carried out to date at Olkiluoto:

- ***Geology and brittle deformation zones.*** The variations in geology and in particular the presence of brittle deformation zones and their possible influence on the stress state have not been quantified at Olkiluoto. Whilst it is generally believed that stress redistributions occur near major structures, the existing data are too sparse to provide detailed evidence of such effects. The lack of data pertains both to in situ stress measurements near major structures and to the quantification of the mechanical behaviour of these zones and other structural features.

- ***Anisotropy.*** The rocks at Olkiluoto exhibit a pronounced anisotropy with respect to their mechanical properties. The effects of this anisotropy may also be present in the hydraulic fracturing measurements, which have not yet been analysed.

- ***Core damage.*** For overcoring measurements in vertical boreholes in a stress regime characterized by large horizontal stresses, the potential for core damage due to tensile failure in the axial direction is high. Analyses have shown that several measurements are probably affected by this to a various extent.

- ***Borehole orientation and hydraulic fracturing.*** The evaluation of hydraulic fracturing measurements requires that one of the principal stresses is parallel to the borehole; however, this was the case for only some of the boreholes. The majority of the hydraulic fracturing measurements were carried out in inclined boreholes, with the additional problem that the normal stress perpendicular to the hydraulic fracture was not the magnitude of the minimum horizontal stress, an effect that had to be compensated for. Unsuccessful hydraulic fracturing measurements were usually rejected because the hydrofractures did not initiate parallel to the borehole.

- ***Stress magnitudes from hydraulic fracturing.*** In hydraulic fracturing, the only stress component that is reliably determined is the minimum horizontal stress (or rather the stress normal to the initiated fracture), see for example Ito et al. (1999). The maximum horizontal stress is generally underestimated, whereas the vertical stress cannot be assessed at all.

- ***Geological history vs. the Kaiser Effect.*** Measurement of the Kaiser Effect provides an indication of the load that a rock sample has been subjected to previously. For an old shield region, such as that of Olkiluoto, with multiple periods of tectonic

activity, the mechanics of stress path and damage accumulation becomes very complex. Hence, it is far from clear that the load levels detected from the Kaiser Effect can be linked to the present, in situ state of stress in the rock mass. In addition, uncertainties regarding sampling (possible influence from core damage) and the time-dependent decay of the Kaiser Effect (from the time of sampling) prevail.

In conclusion, the dispersion in the stress data at Olkiluoto is typical for the methods used. The most significant uncertainties that affect the results are the presence of major fracture zones, the anisotropy of the rock, and possible core damage. Based on these findings, it is estimated that the absolute error in the stress magnitudes obtained could be as high as 5 MPa, whereas stress orientations could have an error of 30° or more in specific cases. However, for individual measurements the scatter can be larger than these values — up to 10 MPa in magnitude, 90° in trend and 30° in plunge, with the largest scatter in stress orientations being observed for the overcoring results.

5.5.2 Uncertainties in the intact rock properties

It should be noted that parameters in rock mechanics, such as the strength and deformation properties of rock, the inclination and orientation of fractures in a rock mass and the measured in situ stresses, do not have any single fixed value, but assume a wide range of values and are spatially variable in a crystalline rock mass. These variations are defined by a set of variables that describe the range of parameter values observed or expected and there is no way of predicting exactly what the value of one of these parameters will be at any given location. However, there is a high confidence in the intact rock property description.

The strength properties of the rocks are an example of a property which is spatially variable due to the heterogeneity of the rock mass. However, probability functions are able to indicate the relative likelihood that an essentially unknown variable will assume a particular value at a specified location. There are several ways of presenting this probability. If the distributions of properties are normal, the mean values and their standard deviations should be chosen to characterise the distribution. On the other hand, if the distributions of properties are skewed at different sites, if one test result departs significantly from other results, or if there are too few test values, it is sometimes better to choose median values and their quartiles, because these are independent of the nature of the distributions.

The majority, 73%, of laboratory tests have been conducted on veined gneiss giving reliable statistical information on stress-strain and strength behaviour (e.g. Table 5-10 and Figure 5-36. For mica gneiss, tonalitic-granodioritic-granitic gneiss, diatexitic gneiss and pegmatitic granite, few tests have been done, so the number is insufficient for any statistical approach. No laboratory test results on mafic gneisses, quartzitic gneisses, stromatic gneisses and diabase exist. Point load index tests conducted in the field indicate, however, that there are no large differences in properties between veined gneiss and the other rock types. The point load index test is an indirect tensile test, measuring unoriented and semi-controlled indirect tensile strength, and leading normally to higher deviations.

The clear anisotropy in the deformation and strength properties of the veined gneiss, which is related to the presence of the gneissic banding, has been studied only in recent tests. The deviation of the results is still considerable, but an additional problem is that, because of the small diameter of the deep boreholes, it has not been possible to obtain samples for testing at all orientations to the anisotropy. In particular, the most critical angles of 0 and 90 degrees are currently missing. The anisotropy of the other main rock types has not yet been studied, nor has the effect of the gneissic banding on other properties of the veined gneiss. Another problem is that the studied samples are not from the same location.

The effect of this anisotropy needs to be studied further, and samples will be most easily obtained from the ONKALO access tunnel. The orientation of the sampling borehole with respect to the gneissic banding can be selected, as required, and samples from effectively the same location with different orientations can then be obtained.

The effect of alteration (sulphidisation, illitisation and kaolinisation) on the rock properties should be better known and further studies are needed.

5.5.3 Uncertainties in physical properties

The majority of physical property tests are reliable and certain. However, during the testing, the system used to define the P-wave velocity was found to be unreliable due to uncertain transducer contacts and the determination of travel time was subjective. This led to a relatively high deviation of ±10%. The average P-wave velocity is 4446 m/s.

5.5.4 Uncertainties relating to thermal properties

The values in Table 5-12 are for intact rock as measured in the laboratory and there are questions as to how these values should be upscaled for use at the scale of the rock mass. The TERO probe has now been tested in situ to provide more information on such scale effects. The scatter in the results is also partly due to the anisotropy of the rock mass and this subject will require more consideration in the future.

5.5.5 Uncertainties related to fracture properties

There is an overall uncertainty due to a lack of data on the mechanical properties of fractures from direct measurements. This situation will be rectified, at least in part, when the existing boreholes are re-logged and the fracture information, also from ONKALO tunnel mapping is re-analyzed, taking into account the supporting geological information. Also, new samples of fractures at larger scales will become available from the ONKALO.

5.5.6 Uncertainties related to brittle deformation zone properties

In Section 5.4.7, it was noted that the properties of the brittle deformation zones are the least developed of the rock mechanics properties. The overall geometry of some of the zones has been well established by the Geology Group, but in other cases the geometry is uncertain. Moreover, the detailed geometry in terms of extent, undulation, variation in width, fracture content, etc. is unknown for all the deformation zones; and it is this latter

information that is required for an assessment of their rock mechanics properties (stiffness and strength) and their variability.

When a brittle deformation zone is intersected by a site investigation borehole, there is the advantage of core being available; however, such an intersection provides information at only one point on a large surface. In contrast, the ONKALO ramp can provide much better access to such zones and the ability to estimate both their detailed geometrical and their mechanical properties. The understanding and characterization of the brittle deformation zones will therefore progressively increase as they are studied throughout the length of the ONKALO. A report on the rock mechanics characterisation of these zones, concentrating on the information that can be gained from the geological descriptions, is scheduled for 2007 (Hudson et al., in preparation).

The main interaction of another discipline with rock mechanics is with geology – because much of the information on the lithology and geometry within the geological model is used in the rock mechanics analyses. The interaction of rock mechanics with hydrogeology involves understanding the effective stress (i.e. the normal components of the in situ stress tensor minus the hydraulic pressure) and the influence of the rock stress in closing/opening fractures, which affects the hydraulic conductivity. The interaction with hydrogeochemistry involves consideration of erosion/precipitation in fractures over time and the consequential effect on their mechanical properties. Further details of the interactions with the other disciplines are tabulated and discussed in Chapter 8.

5.5.7 Uncertainties related to rock mass properties

As was mentioned earlier, the rock mass properties are estimated via empirical formulae relating the rock mass classification values to the rock properties. There are several such empirical formulae, e.g. for estimating the rock mass modulus, and there is uncertainty concerning the most appropriate formula to use. However, the prediction-outcome studies help significantly in this regard, because some formulae provide much better agreement in terms of the prediction and outcome than others, and hence appear preferable.

This provides a relative method of choosing the most appropriate formulae. It will not be possible to provide absolute confirmation until there are supplementary data from seismic and extensometer measurements of tunnel displacements, which are scheduled when the ONKALO ramp reaches greater depths.

5.5.8 Evaluation of uncertainties to microseismic measurements

The identification of an individual event among the cluster of blasts from the tunnelling activities includes elements of uncertainty. The majority of the excavation-induced seismicity events tend to occur very close, in time and space, to the latest blast (Type A). These events often occur in swarms and their seismic signals do not represent a typical earthquake signal; they are associated with “fracture-dominated” rupture. Type B events are temporally and spatially distributed throughout the active excavation region. They represent “friction-dominated” slip in existing shear and fracture zones and have source properties similar to tectonic earthquakes. Type B events have many characteristics that make them easier to identify in comparison with type A events.

The accurate location of a seismic event is one of the key parameters for seismological interpretation; as if the location is incorrect, the subsequent seismological analysis is inaccurate. Continuous calibration of the seismic velocity model is, therefore, required during the course of the excavation of the ONKALO.

6 HYDROGEOLOGY

6.1 Objectives of hydrogeological modelling

A hydrogeological model is a conceptual and mathematical construct that serves to analyze, qualitatively and quantitatively, deep groundwater flow and transport at a site in a way that is useful for site characterization and performance evaluation. Specifically, the objectives of the hydrogeological modelling in this work are as follows:

Site understanding. Site understanding concerns the identification of dominating characteristics, e.g. the most important hydrogeological zones and essential boundary conditions and the overall dynamics of the site-specific groundwater flow system. At Olkiluoto the present-day conditions (or the conditions prevailing before the ONKALO excavation) are the consequence of the palaeohydrogeological evolution, driven mainly by climate change, and the associated changes in the shoreline position at Olkiluoto. An essential part of the site understanding is to establish that the modelling results are in reasonable agreement with hydrogeological observations and data. This is obtained through model calibration.

Cross-disciplinary coherent site modelling. The Olkiluoto Modelling Task Force (OMTF) has been established to ensure that there is sufficient integration between disciplines in producing Site Descriptive Models during the Site Investigation stage (for a detailed discussion on the descriptive modelling, see Andersson, 2003). Whilst the hydrogeological model clearly obtains crucial data and information from Geology (Chapter 4) and Hydrogeochemistry (Chapter 7), feedback needs to be supplied to these two disciplines and be taken into account in the next revision of the models.

Characterization of natural deep groundwater flow conditions. Hydrogeological flow modelling aims at detailed and specific characterization of the natural deep groundwater flow conditions through a set of calculated results, such as the pressure and salinity fields, flow rates and flow directions, and flow paths.

ONKALO impact evaluations and predictions. A compilation of the hydrogeological monitoring data to the end of 2005 has been compiled by Tammisto, Klockars & Ahokas (2006). While numerical flow simulations against these observations form an important basis for calibration, it is also of interest to carry out blind predictions for the possible future impact of the ONKALO – and thereafter repeat the outcome analysis on the basis of the actual monitoring results. Chapter 9 of this report will present the predictions for the impact of the ONKALO from the beginning of 2005 onwards. Whilst the outcome analysis in Chapter 9 will be based on the hydrogeological model developed in Posiva (2005), the predictions will be based on the calibrated flow model defined in this report.

Input to radionuclide transport assessments (to be covered in separate studies). Ultimately the hydrogeological modelling will also assess the distribution of flow and transport resistance in the near field; and these modelling results will directly serve as input to radionuclide transport analyses (as part of the Safety Case Portfolio). A

methodology to this end, to build upon the discrete fracture network modelling, is now being developed and to be employed in the update of the current model in 2008.

Future site evolution and performance of the repository (to be covered in separate studies). The Safety Case Portfolio, which will be appended to the application for a construction licence for the repository in 2012, details the future evolution of the site from the emplacement of the first waste canister in its deposition hole (Vieno & Ikonen 2005) Hydrogeologically, the future evolution is divided into a small number of stages. First, the stage of an open ONKALO and repository tunnels will have an impact on the site's hydrogeology for c. 100 years. This will be followed by a recovery of the pressure and salinity field after the closure of the repository. The "full recovery" may be delayed for a couple of thousand years (during the "thermal stage") because of the heat generation of the decaying nuclear waste while the site undergoes a gradual evolution due to land uplift.[3] The repository will be affected by the characteristics of the surrounding hydrogeochemical environment and its evolution. The update in 2008 of the groundwater flow model developed in this report will serve as a starting point for the hydrogeological evolution modelling to be reported in 2009.

Support for the tunnelling works (to be covered in separate studies). The hydrogeological flow modelling to be developed in this report will contribute to the assessment of grouting measures. This assessment would be an update of the report by Ahokas et al. (2006a), planned for 2007.

Technical planning of the repository (to be covered in separate studies). Hydrogeological conditions form the environment that is considered in the context of performance assessment. At the site scale, information about the most significant hydrogeological zones (i.e. those with a high transmissivity and greatest extent) delineates the rock blocks for potential spent fuel disposal. On a much smaller scale, a key issue is related to the saturation of the tunnel backfill and bentonite buffer. The time scales for full saturation will greatly depend on the magnitude of groundwater flux at the interfaces of the engineered barrier system. For the bentonite buffer, the impact of wetting from the surrounding rock mass determines the time scale for fully-developed swelling pressures (e.g. Börgesson & Hernelind 1999; Hökmark 2004; Börgesson, Fälth & Hernelind 2006).

6.1.1 Hydrogeological modelling in this report

This report updates the previous analysis of the hydrogeological characteristics of the deep bedrock at the site scale at Olkiluoto before the commencement of the ONKALO excavations, reported in Posiva (2005). Updating the hydrogeological modelling is motivated, by the following reasons: i) the development of a new geological model, as

---

[3] It is, however, somewhat misleading to talk about "full recovery" as, on the one hand, the system has been permanently altered from the natural one because of the removal of excavated rock and its replacement with waste canisters, bentonite buffer and tunnel backfill materials (also, some amount of grouting cement will be deposited in the bedrock). On the other hand, the system is experiencing a gradual but progressive change due to land uplift, meaning that it is difficult to determine the state against which such a "recovery" might be measured or gauged.

detailed in Chapter 4, ii) since the previous hydrogeological flow modelling, large amounts of new data have been collected from a number of new drillholes; in particular, a time-series of hydrogeological observations during the ONKALO excavations was recorded, iii) the updated flow modelling in this report will be based on the hydrogeological structural model that reconciles the geological model (Chapter 4) and the hydrogeological connections between drillholes. These connections have been identified by analysing hydrogeological responses to various field activities, and 4) the previous flow modelling found discrepancies between the results of numerical simulations and hydrogeological and hydrogeochemical observations. These discrepancies concern the presence of anomalously low water pressures in a few deep drillholes – KR2, KR4 and KR5 – and relatively strong salinities in the depth range 100 to 300 m in drillholes KR3 to KR5.

The analysis of deep hydrogeological conditions before the construction of the ONKALO commenced is based on numerically calculated fields of groundwater pressure and salinity, as primary parameters, and derived parameters of Darcy and flow velocities, and fluxes, flow rates, flowpaths and (advective) transport times in the flowpaths; as discussed in Chapter 8. Before presenting these results, the flow model's realism is ensured by calibrating it against observations of groundwater pressure and salinity in drillholes, and the hydrogeological impact of the ONKALO. The observed salinities are based on water samples and/or electric conductivity measurements with the Posiva Flow Log. The calibration stage strives for a reasonable and practical congruence between calculated results and measured parameters. This involves changing the properties of the flow model (e.g. transmissivities, porosities) in an iterative fashion until a passable conformity is attained. The calibration stage also covers the congruence of model results with hydrogeological observations related to the ONKALO's impact.

Chapter 9 of this report also compares the predictions made in the previous site model report for the first 100 m in the vertical with the actual observations, and subsequently analyses the reasons for any differences. As stated above, hydrogeological observations on the effect of the construction of the ONKALO are used in the calibration of the new hydrogeological flow model. Predictions regarding the impact of the unexcavated part of the ONKALO, based on the new hydrogeological flow model, are presented in Chapter 9.

Chapters 8 and 9 also cover sensitivity and uncertainty assessments in their respective subject areas. Typically, hydrogeological models are subject to various *parameter* uncertainties, whose impact on the simulation results needs to be addressed. In other words, the sensitivity of the model results to the uncertainties are quantified. A sensitivity analysis is, therefore, useful in indicating what system behaviour appears to be most sensitive to which parameters at what locations (Neuman et al. 2003). Whilst this also describes the *predictive* uncertainty, it also yields useful knowledge to guide future investigations which are targeted to reduce these uncertainties. In this study, the sensitivity and uncertainty analyses aim at quantifying the uncertainty in the calibrated flow model caused by uncertainty in the estimates of flow model parameters, thereby allowing identification of the key components for the groundwater flow in the Olkiluoto bedrock.

6.1.2 This chapter

This chapter first reviews the hydrogeological data and information about the Olkiluoto site, and then the hydrogeological flow model is described. This starts by defining the volume contained by the model, and setting the boundary conditions. After this, the hydrogeological structure of the model domain, the transmissivities of hydrogeological zones, the hydraulic conductivity of the sparsely fractured rock between them, and other model parameters are described. Much of the discussion is devoted to hydrogeological zones within the well characterized area (WCA), whereas for a properly set up model, structures outside this area must also be defined, as they offer the continuity of flow out of the WCA. The uncertainties associated with different modelling components and parameters are summarized, but their detailed evaluation takes place in Chapters 8 and 9.

Whilst the emphasis is on modelling the groundwater flow on the site, we also review a recent effort to model groundwater flow in a fracture network in connection with the KBS-3H project (Lanyon & Marschall 2006). This DFN modelling combines geological bedrock fracturing with the Posiva Flow Log and HTU-tool (constant head double-packer method) measurements for transmissivity.

The chapter concludes with reviewing the lessons learned about the use of the detailed site-specific data; in addition, a number of ideas to be implemented in the future and issues to be tackled have been identified and are to be summarized in this report.

6.2 Hydrogeological data and information

This section reviews the in situ hydrogeological observations and measurements carried out at Olkiluoto until the end of 2005. This body of site data is part of the data set baseline, "data freeze," supporting the hydrogeological modelling efforts described in the current report.

The first deep drillhole was drilled at Olkiluoto in 1989 and the observation of heads in drillholes KR1-KR5 was started in June 1991. Since 1991, freshwater head observations have been recorded in each of the drilled drillholes. Head observations in packed-off drillholes, are reported in Ahokas & Herva (1993), Hänninen (1996), Lehtimäki (2001), Voipio et al. (2003) and Ahokas et al. (2005). Hydraulic data also consist of transmissivities measured systematically in all drillholes (KR1-KR39) by the Posiva Flow Log (PFL) method (Öhberg & Rouhiainen 2000). In addition, long-term pumping test results (Ylinen & Väätäinen 1992, Niva 1996, Jääskeläinen 1998, Vaittinen & Ahokas 2005) have been an essential input for the compilation of the hydraulically *most transmissive* zones of the central investigation area. A summary of long-term hydrogeological monitoring at the Olkiluoto site, including references to numerous pertinent reports, is given by Voipio et al. (2003).

The hydrogeological monitoring data gathered since the previous Site Description (Posiva 2005) has been reported by Tammisto, Klockars & Ahokas (2006), who add one more year to the monitoring data reported earlier by Ahokas, Klockars & Lahdenperä (2005) and Voipio et al. (2004). The body of data collected in 2005 is further expanded

with observations from drillholes KR29 to KR39 (of which drillholes KR35 to KR39 were utilized from the latter part of 2005 onwards).

Vaittinen, Nummela & Ahokas (2007) carried out an analysis of the hydrogeological responses to field activities since 1991. The full exploitation of the results of this study is deferred to the next revision of the Site Descriptive Modelling.

Hydrogeological information is integrated with the brittle deformation zone model by Paulamäki et al. (2006). Also, the results of geophysical "Mise-à-la-masse" studies (Ahokas et al. 2006a) are used in the modelling of *hydrogeological zones*. The groundwater flow modelling in this work is based on water table data, knowledge of the land uplift rate and groundwater salinities.

6.2.1 Measured transmissivities of rock fractures

In this section we introduce the measured transmissivities which form the basis of determining the effective properties, transmissivities, of the hydrogeological zones, as well as the effective hydraulic conductivity of the *sparsely fractured rock mass* between the deterministic hydrogeological zones.[4] This data analysis has been carried out by Ahokas et al. (2006b) and will be summarized in Section 6.3.4.

The measurements of the hydrogeological properties associated with groundwater flow in the Olkiluoto rock characterize flow in bedrock fractures. Whilst the flow is to be channelled within such fractures, due to their inherent heterogeneity, the determination of the transmissivity is based on a conceptualization of an ideal radial flow field between the drillhole and a perimeter at the so-called influence radius. In other words, there is an implicit assumption that the fracture is homogeneous.[5] An error of some magnitude may ensue from this, as well as from the uncertainty associated with the influence radius. In the calculation of T values, a constant value of radius of influence (r_0=14 m) in Thiem's equation (de Marsily 1986) has been used. For r_0=1 m the factor is 0.55 and for r_0=1000 the factor is 1.72.

The transmissivities are customarily measured with two types of instrument, the Hydraulic Testing Unit (HTU) and the Posiva Flow Log (PFL) (Hämäläinen 2005, Öhberg & Rouhiainen 2000), and are aimed at measuring the transmissivities of individual fractures intersecting the drillholes between the packers of the measuring device. A comparison study of the transmissivities obtained with the two types of instruments is detailed by Ahokas (2001), who reports that the HTU instrument yields clearly greater transmissivities than the PFL in fractured parts of the bedrock. Ahokas (2001) attributes this difference to the overpressure the HTU applies between the

---

[4] The reader is reminded that the nomenclature is not fully established. Formerly, the hydrogeological zones were often called "fracture zones", or "hydrogeological structures" whereas the rock outside them has also been termed "intact rock", "average rock", or "averagely fractured rock".

[5] More precisely, the inference of the transmissivity is based on the assumption of a radial *pressure drawdown* field rather than radial *flow rate* field around the drillhole intersecting the fracture. Evidently, the pressure field exhibits a lot weaker channelling than the flow rate.

packers in the measuring process, which means there is a possibility of short-circuiting back to the drillhole. The PFL, on the other hand, does not apply any overpressure (with respect to the pressure in the rest of the drillhole) between the rubber disks isolating the measured section from the rest of the drillhole. As Ahokas (2001) points out, the risk of short-circuiting is greatest in intensively fractured parts of the bedrock (i.e. hydrogeological zones) and, consequently, the two instruments agree well with each other elsewhere in the bedrock where such a short-circuiting is less likely.

It can be seen from Figure 6-1 that the spatial distribution of transmissivities greater than 10^{-8} m^2/s shows one of the most salient characteristics of the measured transmissivities: they exhibit a very strong concentration close to the surface. The total 'inventory' of fractures observed in drillhole KR14 is 856. Of these a transmissivity has been measured with the Posiva Flow Log for 77 fractures. In other words, less than one tenth of all the geological fractures are 'hydraulically active' or 'water-bearing', taking into account the measurement limit. The uppermost 50 m of the drillhole includes about one third of the total geological fracturing for this drillhole, which has a depth of greater than 500 m.

The concentration in measured transmissivities toward the surface is actually weakened somewhat by the fact that a number of the deep drillholes at Olkiluoto have a surface casing of 40 to 50 m, indicating that this topmost section has been left unmeasured.[6] The customary assumption attributes such a distinct trend in the transmissivity to the lithostatic stress, which increases linearly at shallow depths, thus reducing the apertures of fractures – in particular those having sub-horizontal orientations. This is not, however, the only explanation, as the density (frequency) of fractures clearly decreases at a depth of several tens of metres. In Figure 6-2 the high transmissivities at shallow depths are enclosed within a blue loop. Below this group the frequency of high transmissivities abruptly decreases, but at greater depth another spatial grouping of high transmissivities is met. In Section 6.3.3 this group of elevated transmissivities below a sounder rock layer is associated with an important hydrogeological zone system (HZ20; the domain of high transmissivities above it encloses the HZ19 hydrogeological zone system). A more careful examination reveals that at yet greater depth, another group of enhanced transmissivities is encountered (indicated with a dotted line in Figure 6-2) but is clearly of less significance.

[6] Basically, all deep drillholes have a surface casing, but some of them have a short "B" drill hole in their immediate neighbourhood which may have only shallow surface casing. In the illustrations of the transmissivities, the B drillhole measurements are conjoined with the "main" drillhole.

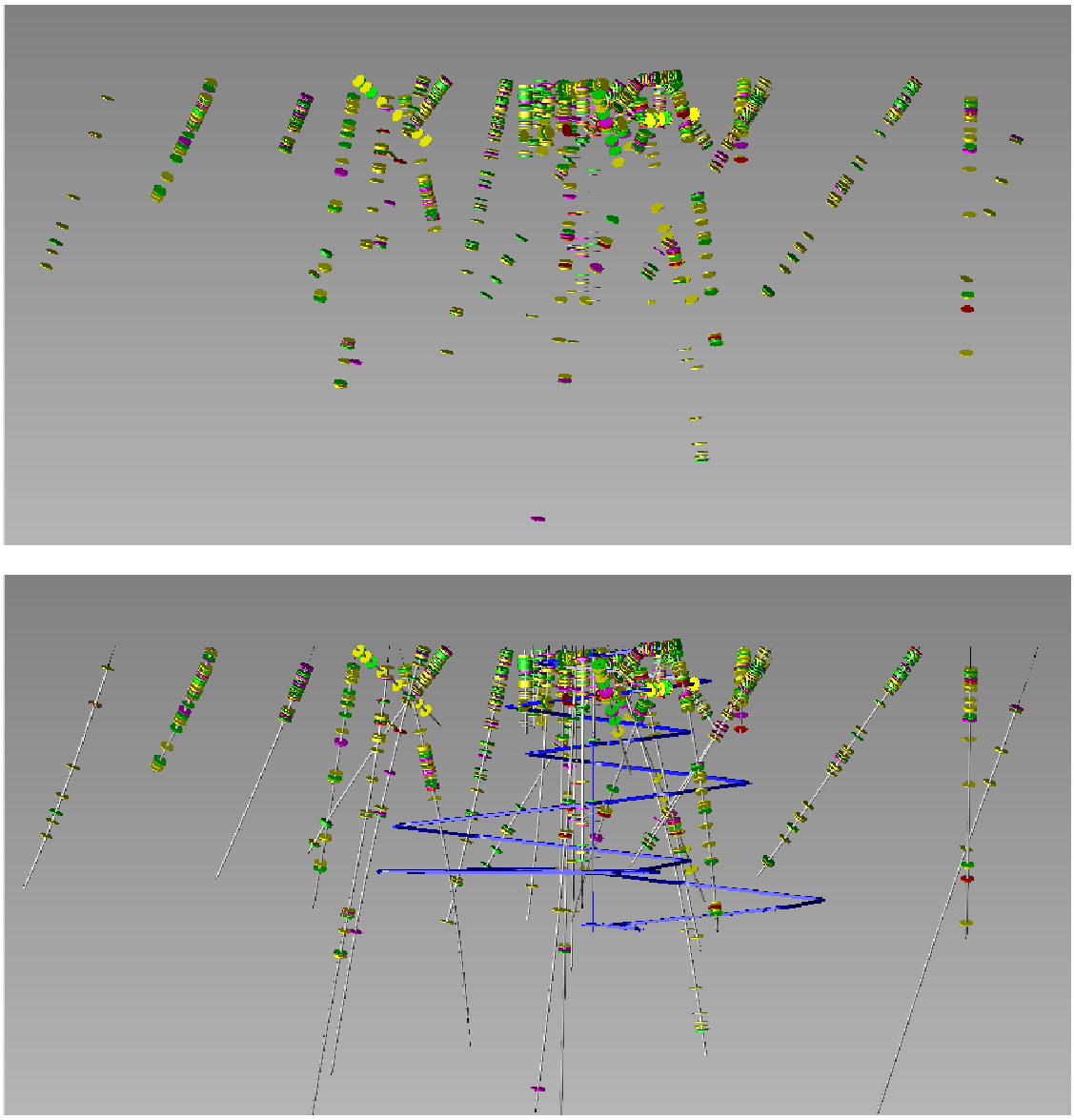

Figure 6-1. *Measured transmissivities greater than* $T=10^{-8}$ m^2/s*, displayed with drillholes and the ONKALO spiral in the lower figure. The colour indicates the magnitude of the transmissivity; to be defined in Figures 6-2 to 6-7.*

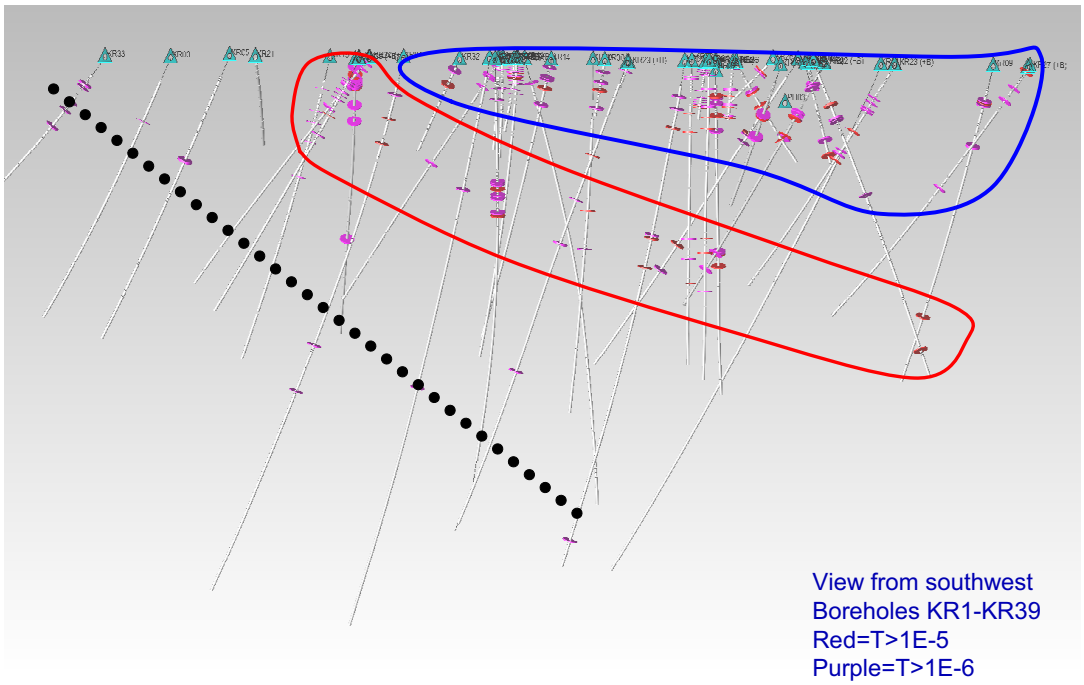

Figure 6-2. *Measured transmissivities greater than $T = 10^{-6}$ m^2/s indicated with purple disks. Three distinct areas of spatial grouping of high transmissivities are indicated. The blue line encircles the uppermost zone that coincides with the volume that encloses the HZ19 hydrogeological zone system. Below it is another area that is associated with the HZ20 hydrogeological zone system. The dotted line indicates the group that is associated with the HZ21 hydrogeological zones. See the text for details.*

The transmissivity measurements at Olkiluoto in several tens of drillholes are summarized in decreasing order (see Figures 6-3 to 6-7). As already noted, the measured values show a clear concentration toward the ground surface. This is consistent with the observations of fracturing in general: for example one third of all the fractures in drillhole KR14 are located within the first 50 m from the surface. In Figure 6-3 very high transmissivities, greater than $10^{-5}m^2/s$, are concentrated around the ONKALO. This is an observational bias, as the density of the drillholes is largest there. Furthermore high transmissivities tend to exist close to the ground surface – very few highly transmissive fractures are found at great depths. This may be understood as the influence of lithostatic stress that tends to close fractures with predominantly horizontal orientations. This phenomenon, a decrease in the hydraulic conductivity with depth, was also noticed when studying early datasets from Finnish investigation sites (Niemi 1994). Many of the drillholes in the vicinity of the ONKALO are rather shallow and have shorter surface casings than deeper drillholes of a few hundred metres in length (which typically have a surface casing of c. 40 m). This further strengthens the concentration of high transmissivities in the vicinity of the ONKALO – although there is no geological reason for such an *actual* concentration of high transmissivities.

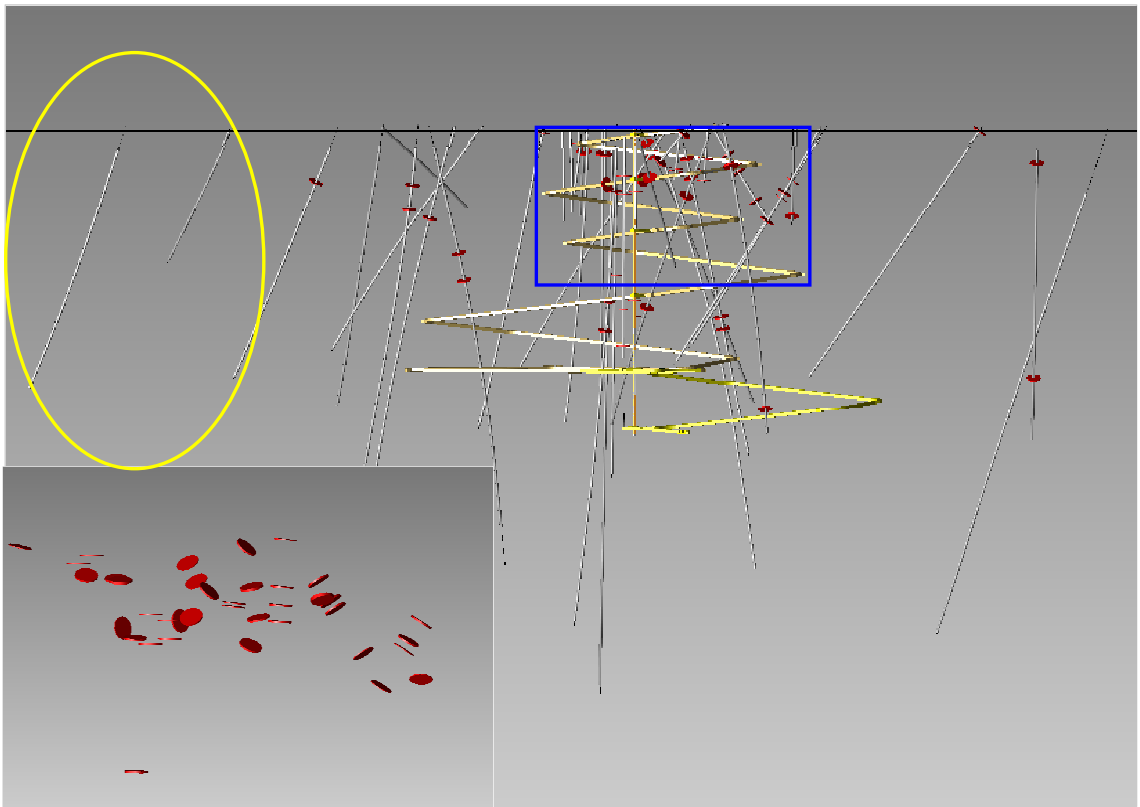

Figure 6-3. *Measured transmissivities greater than $T=10^{-5}$ m^2/s marked with red disks. The total number of such values in the figure is 57. Drillholes are also shown and the ONKALO is visualized with a spiral. The view is from due south. A close-up of the measurements within the blue rectangle is shown in an insert. Drillholes KR3 (left) and KR33 (right) lie within the yellow oval. See the text for discussion.*

From a statistical point of view the usual tenet "prescribes" that the transmissivity of rock fractures obeys a lognormal distribution. Accordingly, the higher end of the range of observed transmissivities should represent only a small portion of the total data. Whilst the formal validity of the lognormal distribution in the dataset has not been explored, it appears to be roughly in line in the sense that the number of transmissivities greater than 10^{-5} m^2/s is about 4% of the all measured values (values that are higher than the lower limit of the Posiva Flow Log, i.e. 10^{-10} m^2/s; see Ahokas et al. 2006b for a detailed discussion, and Hellä et al. 2006 who also find support for a lognormal distribution). The number of measured transmissivities in the range from $10^{-6}m^2/s$ to 10^{-5} m^2/s (Figure 6-4) is already much greater than the number of transmissivities measured above this interval (Table 6-1). Clearly a decrease in the number of transmissivities toward the higher end would also be consistent with other typical distributions (e.g. a power-law distribution). On the other hand the lognormal distribution also stipulates that toward the lower end of the distribution the number of measured transmissivities should also reduce. This is seen in the whole dataset, as reported by Ahokas et al. (2006b); and summarized here in Table 6-1. Where it can be seen that roughly equal population of the transmissivities exist in intervals 10^{-8} m^2/s to 10^{-7} m^2/s and 10^{-9} m^2/s and 10^{-8} m^2/s. However, there is no conclusive evidence of a lognormal distribution, as the lower end of the transmissivity distribution (10^{-10} m^2/s) is very close to the detection limit of the Posiva Flow Log.

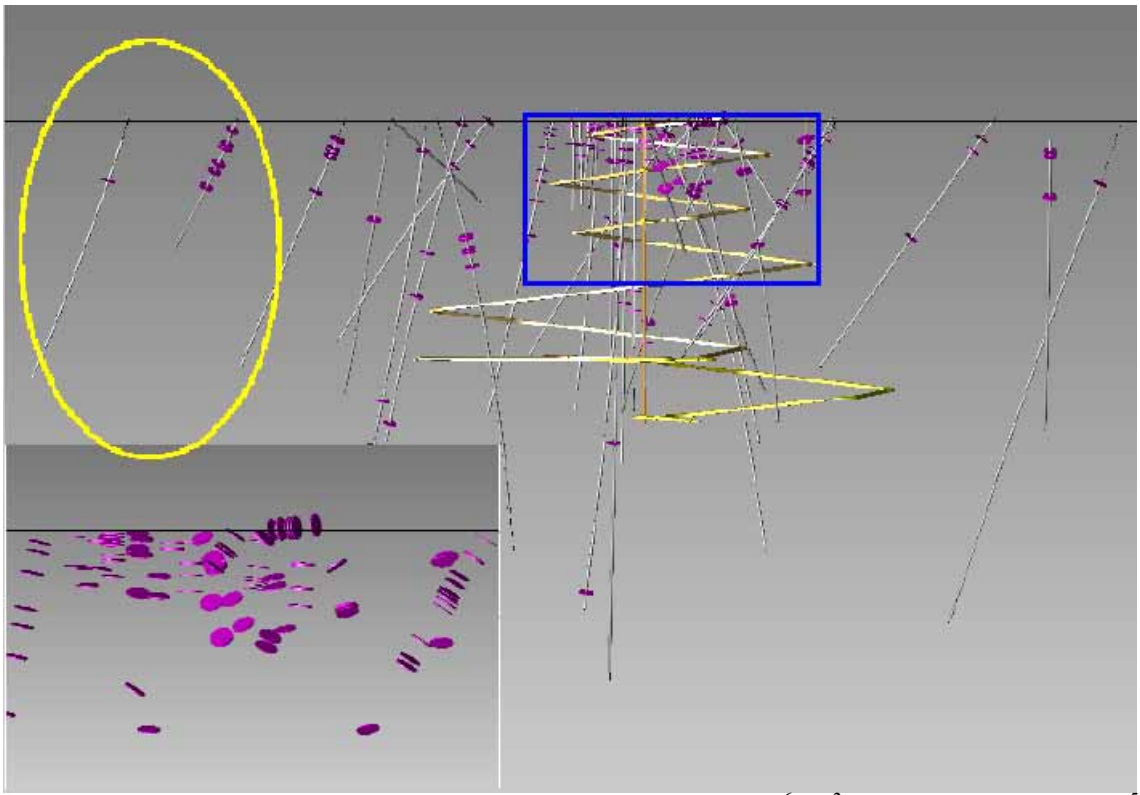

Figure 6-4. *Measured transmissivities greater than 10^{-6} m^2/s but less than 10^{-5} m^2/s shown by violet disks (Ahokas et al. 2006b). The total number of these values in the figure is 146. Drillhole trace shown and the ONKALO is visualized with a spiral. The view is from due south. A close-up of the measurements within the blue rectangle is shown in the insert. Drillholes KR3 (left) and KR33 (right) lie within the yellow oval. See the text for discussion.*

Although there is an increased frequency of measured transmissivities toward the surface, Figures 6-3 to 6-7 seem also to give the impression that this is less obvious for lower transmissivities. In other words, transmissivities in the range 10^{-9} m^2/s to 10^{-8} m^2/s are more evenly distributed vertically than, say, transmissivities in the range 10^{-6} m^2/s to $10^{-5}m^2/s$. Another and more striking characteristic of the transmissive bedrock fracturing is its heterogeneous distribution. This is clearly illustrated, for example, by the transmissive fracturing in drillholes KR3 and KR33 (these are marked with a yellow oval in Figures 6-3 to 6-7), as drillhole KR3 clearly intersects fewer transmissive fractures than KR33. A similar observation of the unevenness in the number of measured transmissivities in different drillholes was also made by Lanyon & Marschall (2006). Such a pattern is an indication of the spatial correlation(s) in the transmissive fracture statistics on the scale of the domain probed by the drillholes. There has been no attempt to provide a qualitative description of this effect.[7]

[7] Niemi (1994) carried out a variogram analysis of 30 m hydraulic conductivity data from five investigation sites explored at that time, including Olkiluoto, finding support for a spatial correlation on the 100 m scale. While the resolution of 30 m packer interval is too coarse to facilitate determining the transmissivity of individual fractures, her study did not address the spatial structure between drillholes.

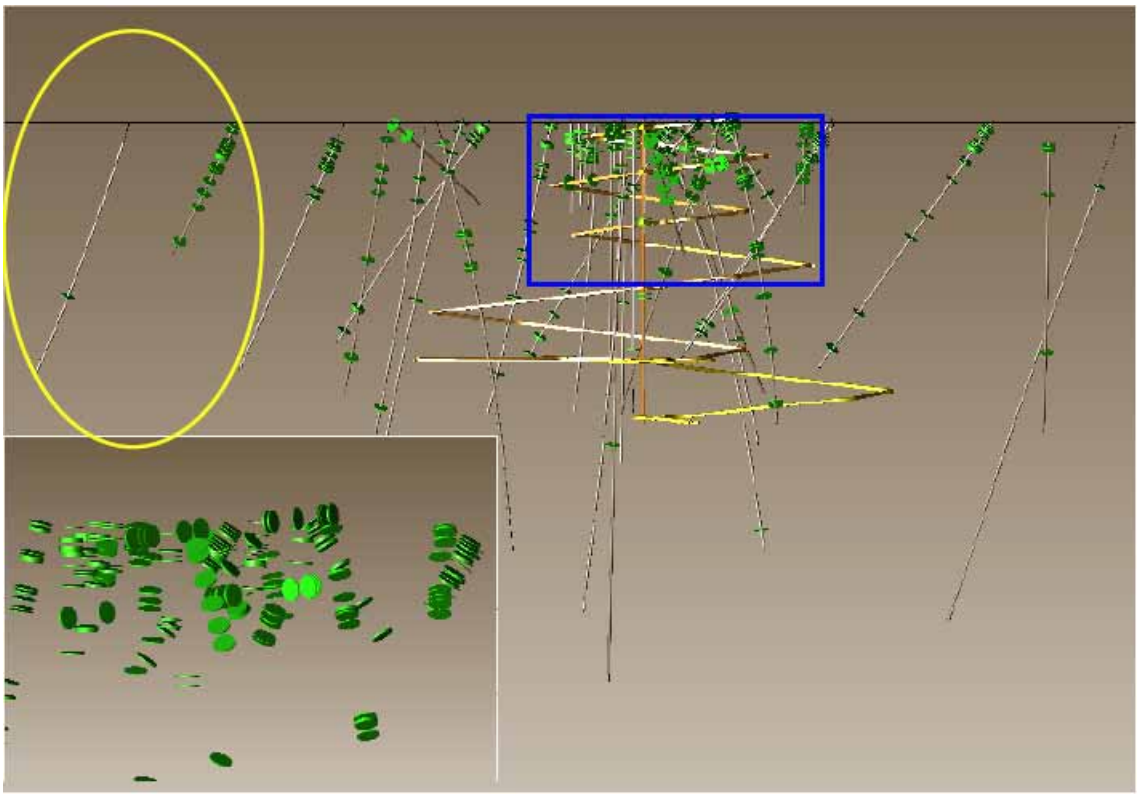

Figure 6-5. *Measured transmissivities greater than 10^{-7} m^2/s but less than 10^{-6} m^2/s indicated by green disks (Ahokas et al. 2006b). The total number of these values in the figure is 288. Drillhole traces are shown and the ONKALO is visualized with a spiral. The view is from due south. A close-up of the measurements within the blue rectangle is shown in the insert. Drillholes KR3 (left) and KR33 (right) lie inside the yellow oval. See the text for discussion.*

In the construction of the flow model, the dataset introduced in this section will be used for estimating the *effective* transmissivities of the hydrogeological zones as well as the hydraulic conductivity of the intervening "sparsely fractured" rock mass.

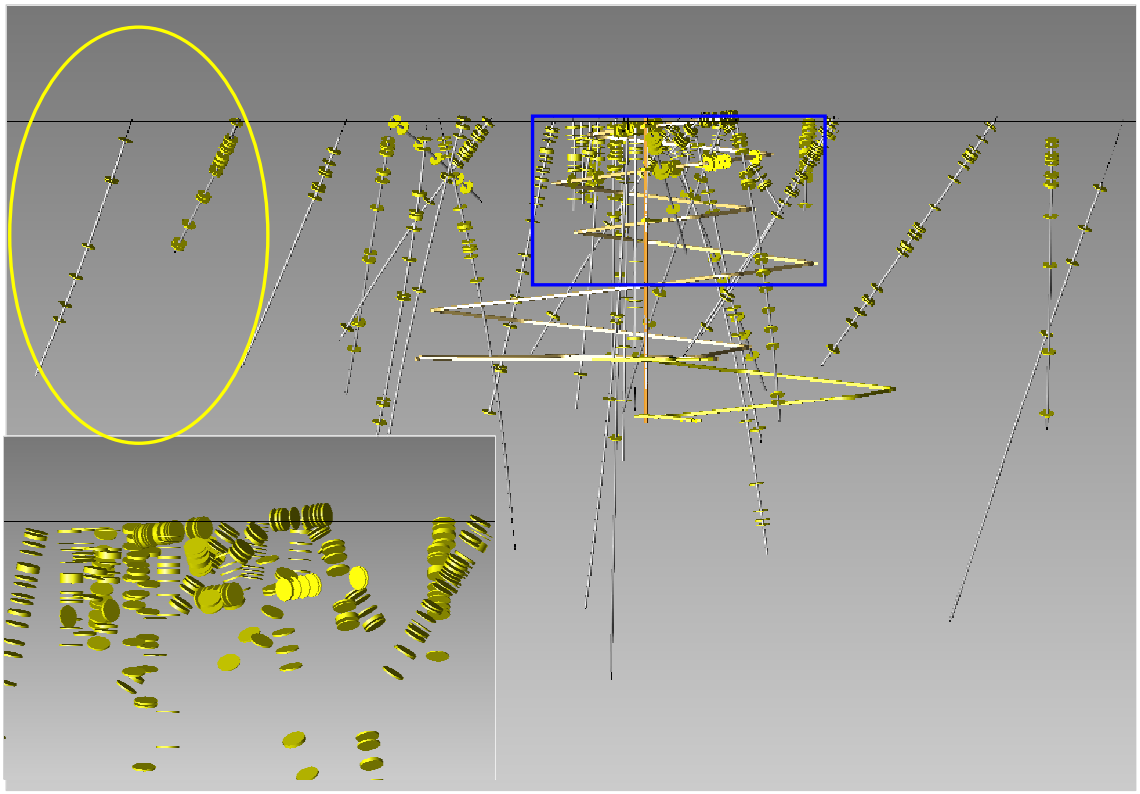

Figure 6-6. *Measured transmissivities greater than 10^{-8} m^2/s but less than 10^{-7} m^2/s indicated by golden disks (Ahokas et al. 2006b). The total number of these values in the figure is 463. Drillhole traces are shown and the ONKALO is visualized with a spiral. The view is from due south. A close-up for the measurements within the blue rectangle is shown in the insert. Drillholes KR3 (left) and KR33 (right) lie inside the yellow oval. See the text for discussion.*

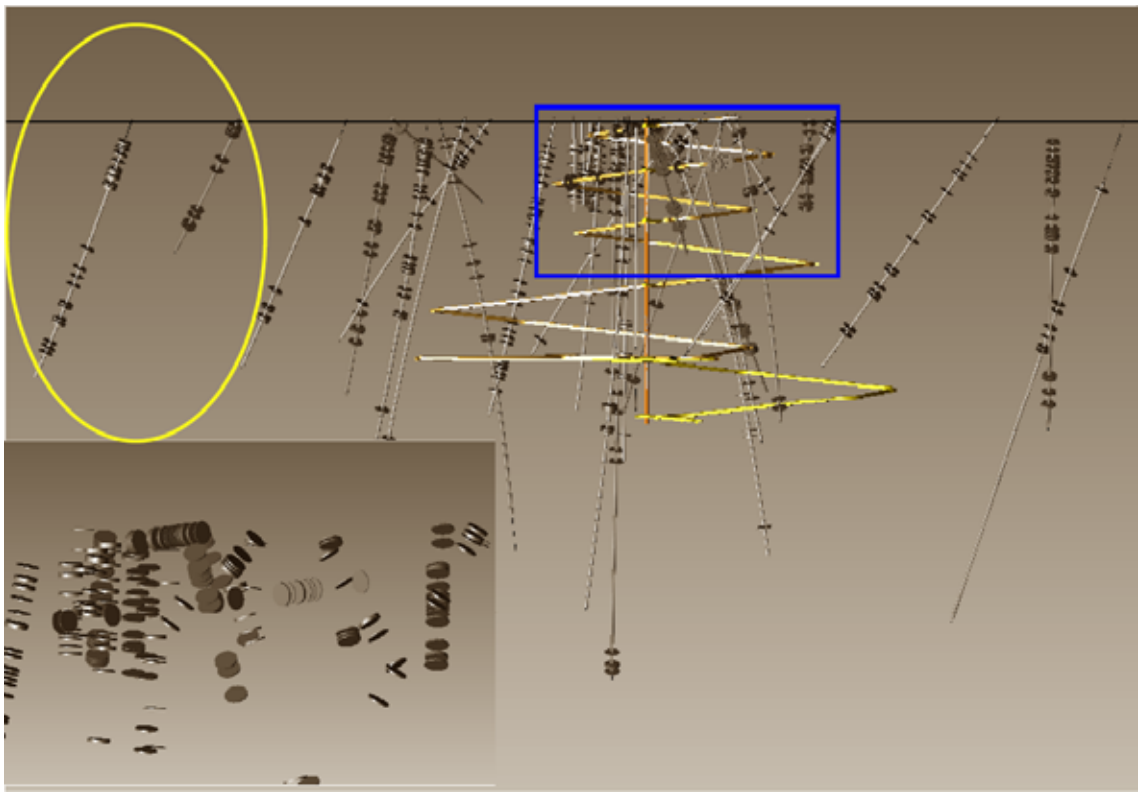

Figure 6-7. *Measured transmissivities greater than 10^{-9} m^2/s but less than 10^{-8} m^2/s indicated by grey disks (Ahokas et al. 2006b). The total number of these values in the figure is 409. The view is from due south. Drillhole traces are shown and the ONKALO is visualized with a spiral. A close-up of the measurements within the blue rectangle is shown in the insert. Drillholes KR3 (left) and KR33 (right) lie inside the yellow oval. See the text for discussion.*

Table 6-1. *Number of measured transmissivities per order of magnitude intervals. The total number of transmissive fractures (i.e. with transmissivities above 10^{-10} m^2/s) is comparable to the number of faults, 1700 (see Chapter 4), but is clearly a small portion of all fractures, which number c. 40000 in total.*

Transmissivity interval	**Number of fractures (relative portion of the whole dataset)**
over 10^{-5} m^2/s	57 (4%)
10^{-6} m^2/s to 10^{-5} m^2/s	146 (10%)
10^{-7} m^2/s to 10^{-6} m^2/s	288 (19%)
10^{-8} m^2/s to 10^{-7} m^2/s	463 (31%)
10^{-9} m^2/s to 10^{-8} m^2/s	409 (28%)
10^{-10} m^2/s to 10^{-9} m^2/s	114 (8%)
Total	1477

6.2.2 Water table and land uplift

The level of the water table in the overburden has been monitored in groundwater observation tubes (PVP holes), and shallow drillholes (PA, PP, PR, L drillholes) in the bedrock. In 2005, the water table was monitored in 57 holes (Tammisto, Klockars & Ahokas 2006), which is equal to the number of the observation points reported for the earlier period 2003–2004 (Ahokas, Klockars & Lahdenperä 2005).

The water table used for the numerical groundwater flow modelling in this study is based on the mean of the measurements over several years before construction of the ONKALO commenced. For locations not covered by actual measurements, a simple correlation between the island's topography and water table is assumed (Posiva 2003), yielding the piezometric surface shown in Figure 6-8. The highest point at Olkiluoto is 18 m above sea level, whilst the corresponding elevation of the water table is only 10 m. For the groundwater flow model this mean water table is taken to correspond to the top boundary condition for the groundwater pressure before the ONKALO excavations (see Section 6.3.2).

The recent data (Tammisto, Klockars & Ahokas 2006; Ahokas, Klockars & Lahdenperä 2005) have not been formally updated for the purpose of the current groundwater flow modelling, but the impact of these data is not seen as significant, as no anomalies or apparent trends which could possibly be associated with the construction of the ONKALO impact has been reported. The fact that the construction of the ONKALO appears to have had no impact on the level of the groundwater table (at least up to the end of 2005) can be taken as a true observation that itself affects the calibration of the flow model.

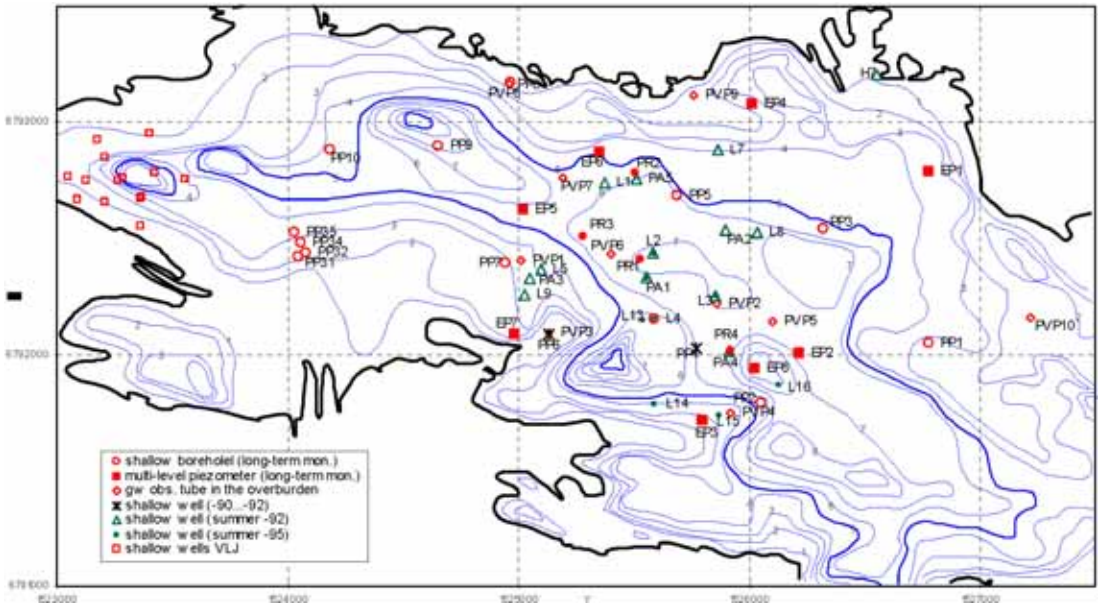

Figure 6-8. *The water table before the commencement of the ONKALO excavations (Posiva 2003). By the end of 2005 monitoring data do not show any discernible impact of the excavation of the ONKALO (Ahokas, Klockars & Lahdenperä 2005; Tammisto, Klockars & Ahokas 2006).*

The water table in Figure 6-8 represents a snapshot of the conditions that prevailed just before the commencement of the ONKALO excavations. The change in the level of the water table over previous decades has been limited, as the current land uplift rate at Olkiluoto, of 6 mm per year, has been quite constant since Olkiluoto's reappearance as an island c. 2800 years ago (Figure 6-4). The net effect of land uplift and global sea level rise was to gradually enlarge the area of the island and increase the elevation of the groundwater table. Land uplift is to continue for many millennia into the future, resulting in recession of the shoreline and rendering Olkiluoto an inland site (Mäkiaho 2005). Year-to-year changes are dominated by annual precipitation, but are effectively suppressed when considering multi-year averages.

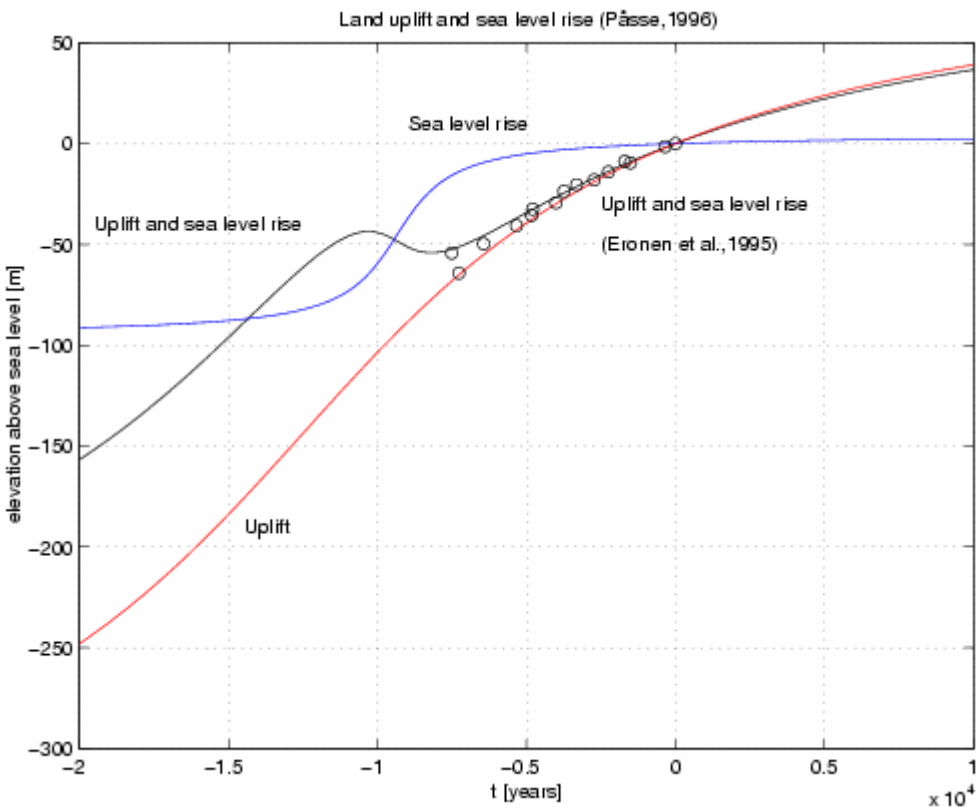

Figure 6-9. *The net effect of land uplift (red curve) and seawater rise (blue curve) together with a few actual elevations of the land surface as determined by Eronen et al. (1995). The figure also displays Påsse's (1996) extrapolations into the past and the future. The change in the position of the shoreline, which is a result of the net effect of land uplift and sea level rise, together with the topographic relief, governs the evolution of the water table after the reappearance of Olkiluoto as an island.*[8]

---

[8] This is a simplifying statement. One critical parameter is the precipitation. Even if the present day annual average rainfall (c. 600 mm) is implicitly assumed, the details of the water table depend on – in addition to the shoreline position and topography – numerous intricate processes and near-surface characteristics. However, in this work we adopt the simple approach to deal with the past evolution of water table, as is discussed in Section 6.3.2.

6.2.3 Groundwater pressure/freshwater head

Groundwater pressure – expressed as freshwater head – has been measured in several packed-off sections of piezometers and drillholes (Tammisto, Klockars & Ahokas 2006; Ahokas, Klockars & Lahdenperä 2005; Voipio et al. 2004). Many of the drillholes have either been equipped with packers or kept open for PFL observations at some point in the past. The presence of open drillholes produces artificial hydrogeological connections in the bedrock – thus also affecting groundwater pressures in packed-off drillholes – but no effort to quantify their impact has been carried out. However, it has been assumed that the impact is rather weak, as the pressure levels in the packed-off sections show good repeatability to date. In some cases, a link between the pressure observation and seasonal conditions, or sea level, is evident; sporadic and scattered responses are associated with various field activities, and weaker fluctuations are due to, for example, tidal effects (Voipio et al. 2004).

A compilation and analysis of the hydrogeological responses to field activities was carried out in 2006 by Vaittinen, Nummela & Ahokas (2007). The interpretation of hydraulic connections in their work is based on the analysis of observed changes in measured hydraulic heads due to certain investigation activities. These activities may increase the freshwater head, e.g. drilling a drillhole, or more typically decrease the head, e.g. due to cleaning pumping, difference flow logging with pumping, and groundwater sampling. Several pumping tests and overpressure tests have also been carried out to study flow connections.

The groundwater pressures corresponding to natural conditions (i.e. the time before the commencement of the ONKALO excavations) constitutes a critical part of the calibration objectives. The calibration data for groundwater pressure is detailed in Section 6.3.3 and, up to the end of 2005, no noticeable and consistent impact of the ONKALO on the measured groundwater pressures had been recorded. Sporadically, there have been short surges in water inflow into the pilot holes in the ONKALO when they have intersected transmissive fractures, with associated pressure responses before grouting has taken place, following which the undisturbed pressure levels have again been re-established.

The lack of response to the ONKALO excavations, together with the observations of the ONKALO inflow rates, establishes the hydrogeological characteristics of the site, which need to be reproduced in numerical groundwater flow simulations.

6.2.4 Groundwater and sea water salinity

The distribution of the groundwater salinity at Olkiluoto is based on quality-assessed water samples from drillholes and electric conductivity measurements associated with Posiva Flow Log measurements (Palmén et al. 2004).[9] The highest analyzed salinities

---

[9] Throughout this text "salinity" is used to mean Total Dissolved Solids (TDS) concentration. Usually this differs from the concentration of chloride only. For the groundwater flow modelling in this work the only essential coupling is the dependence of the groundwater density on its TDS concentration (see Section 6.3.1).

to date are TDS = 84 g/L (Pitkänen, Partamies & Luukkonen 2004; see also Chapter 7). These inferred groundwater salinities are used in determining the initial state of the salinity distribution 8000 a ago and are also used in the calibration stage of the flow modelling.

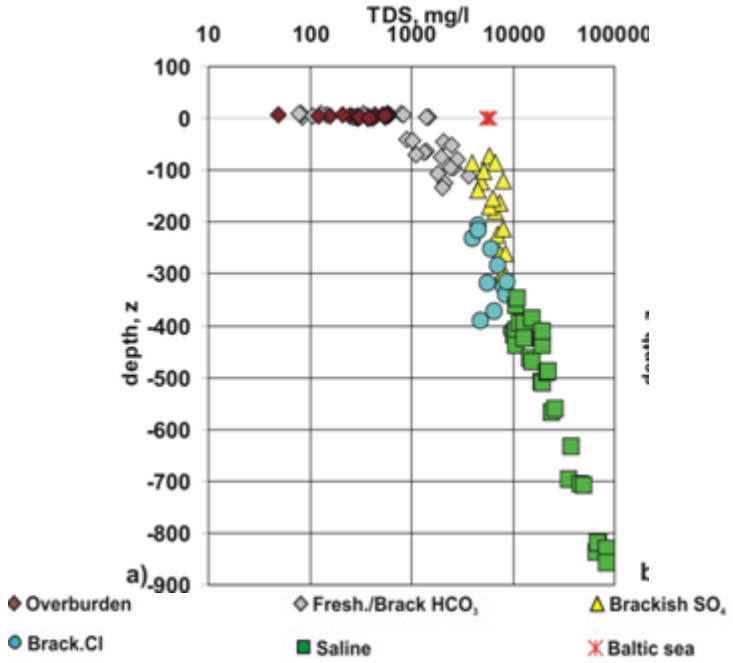

Figure 6-10. *The observed TDS concentration as a function of depth. The highest observed salinities are c. 83 g/L. See Section 7.3.1.1 for a detailed discussion.*

In the numerical flow modelling, the groundwater salinity distribution is used to estimate the initial state of the salinity at the peak salinity of the Littorina Sea.

The salinity of the water above Olkiluoto has evolved since the melting of the last ice sheet. The subsequent freshwater Ancylus Lake was followed eventually by the Littorina Sea, which was more saline that the current Baltic Sea. This increased salinity has been inferred indirectly from fossils of Littorina molluscs, which can only live in water with a relatively high salinity, and the inferred peak salinity of the Littorina Sea has been estimated to be about 12 g/L (Westman et al. 1999). This value is used in the numerical flow simulation as the value of the salinity of the top of the model. With time, it decreases to a half, which is the TDS concentration of the current Baltic Sea.

6.2.5 The Posiva Flow Log flow rates

The Posiva Flow Log (PFL) measures groundwater exchange rates between the open drillhole and the bedrock (more specially, bedrock fractures) surrounding it (Öhberg & Rouhiainen 2000). The actual monitoring measurements for this parameter with the PFL started in 2005 (Tammisto, Klockars & Ahokas 2006; Pöllänen & Rouhiainen 2006). It is noted that the PFL measurements are not directly related to *natural* flows,

as the presence of the open drillhole themselves results in the very parameter to be measured. In the situation in which an open drillhole is only intersected by one fracture no water exchange would ensue and thereby the PFL would not detect any flow, even if great groundwater flows took place within the fracture itself – except if the drillhole is being pumped. A special device is being developed in order to measure flow along fractures and it is planned to bring this device into use in 2006 (Section 6.2.6.)

The magnitude of the flow along the open drillhole also depends on the hydrogeological zones which the drillhole connects. As the conductance of the drillhole is known approximately, by assuming laminar flow in a pipe of radius 3.8 cm, thereby giving a conductance of c. 8 m^3/s, the open drillholes could be explicitly incorporated as well-defined features in the flow modelling. However, the flow in an open drillhole depends on the local properties of the hydrogeological zones which it intersects. The effective transmissivities of such zones have been defined on the site scale, but the local flow conditions will not necessarily correspond to the volumetric flow in the overall hydrogeological zone. In other words, the site scale flow model is likely to be inadequate in resolution and in purpose to calculate the flow in any specific open drillhole. A more suitable solution might be the use of an integrated parameter based on the individual flow rates in the open drillholes: for example a simple sum of the many (all) observed flow rates under reasonably steady-state external conditions. The problem that will need careful attention is related to various sporadic, short-term field activities which may greatly affect individual drillholes and thus violate the requirement of such steady-state conditions.

6.2.6 Posiva Cross Flow measurements

A new instrument, the Posiva Cross Flow meter, is being finalized and it is brought into use in late 2006.

6.2.7 Inflow of groundwater in the ONKALO

The total inflow into the ONKALO has been measured by two methods. Until September 2005 the total inflow rate was observed by measuring the amount of water which had flowed to the bottom of the tunnel during weekends. From July 2005 onwards the total inflow has been calculated as the difference between the recorded volume of water used for drilling and other activities in the ONKALO and the volume of water pumped out of the ONKALO - although this method has considerable uncertainties (Tammisto, Klockars & Ahokas 2006). Both sets of flow rates are shown

in Figure 6-11. Only one value of inflow into the ONKALO tunnel was measured in 2004 and a rate of 0.9 L/min on 27 December 2004 was obtained.

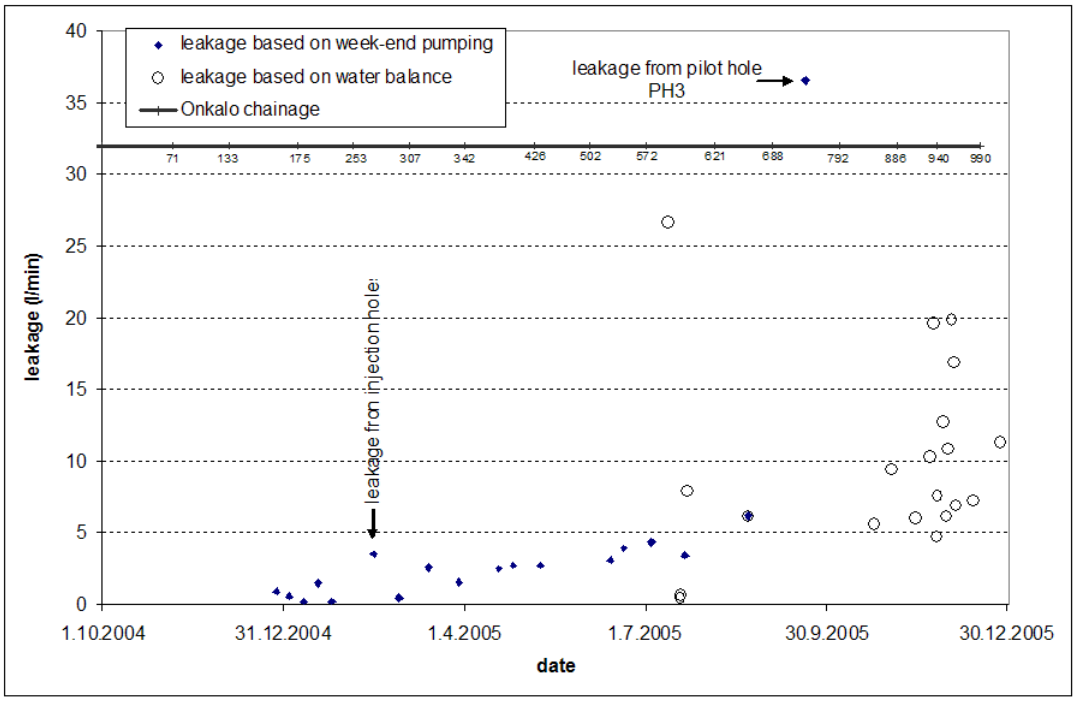

Figure 6-11. *The total observed leakage (inflow rate) of groundwater into the ONKALO in 2004 and 2005. Negative (i.e. incorrect) values are not shown (Tammisto, Klockars & Ahokas 2006).*

6.3 Groundwater flow model on the site scale

6.3.1 Model components and parameters

Groundwater flow modelling builds on a complex assemblage of components and parameters that are processed to conform to the objectives, the general data and knowledge and the numerical modelling method (Figure 6-12). The term "components" refers to the conceptual building blocks of the model:

- The boundary conditions and initial state for the parameters to be solved for as primary (unknown) variables. These parameters are groundwater pressure and groundwater salinity.

- The structural model of hydrogeological zones. In particular, the connectivity of the network of hydrogeological zones has a considerable influence on the characteristics of the deep groundwater flow at the site.

- The hydrogeological properties specifying the hydraulic conductivities and flow porosities of the hydrogeological zones and the averagely fractured rock mass between them.

The definition of the model parameters involves their description as physical parameters with respect to the mathematical model for flow and transport. The hydrogeological flow modelling in this work is based on a mathematical model for flow in a porous medium. The underpinnings of the mathematical model are Darcy's law and the law of conservation of mass, which are reduced to the equation of flow (see, e.g. Bear 1972 for a thorough discussion) describing the pressure as the unknown parameter.

A model striving for a realistic description of a natural system – that is a model consisting of a number of hydrogeological units, encompassing a complex initial state and (time-dependent) boundary conditions – is quite involved in practice. The solution for the primary parameters is found by numerical means. The computer code used in the numerical simulations of the site scale groundwater flow model is FEFTRA™, VTT's in-house groundwater flow modelling system, which is based on the finite element method (FEM). The code has been developed to handle the (usual and technically exceedingly intricate) problems associated with flow and mass transport in FEM models (e.g. Laitinen 1995).

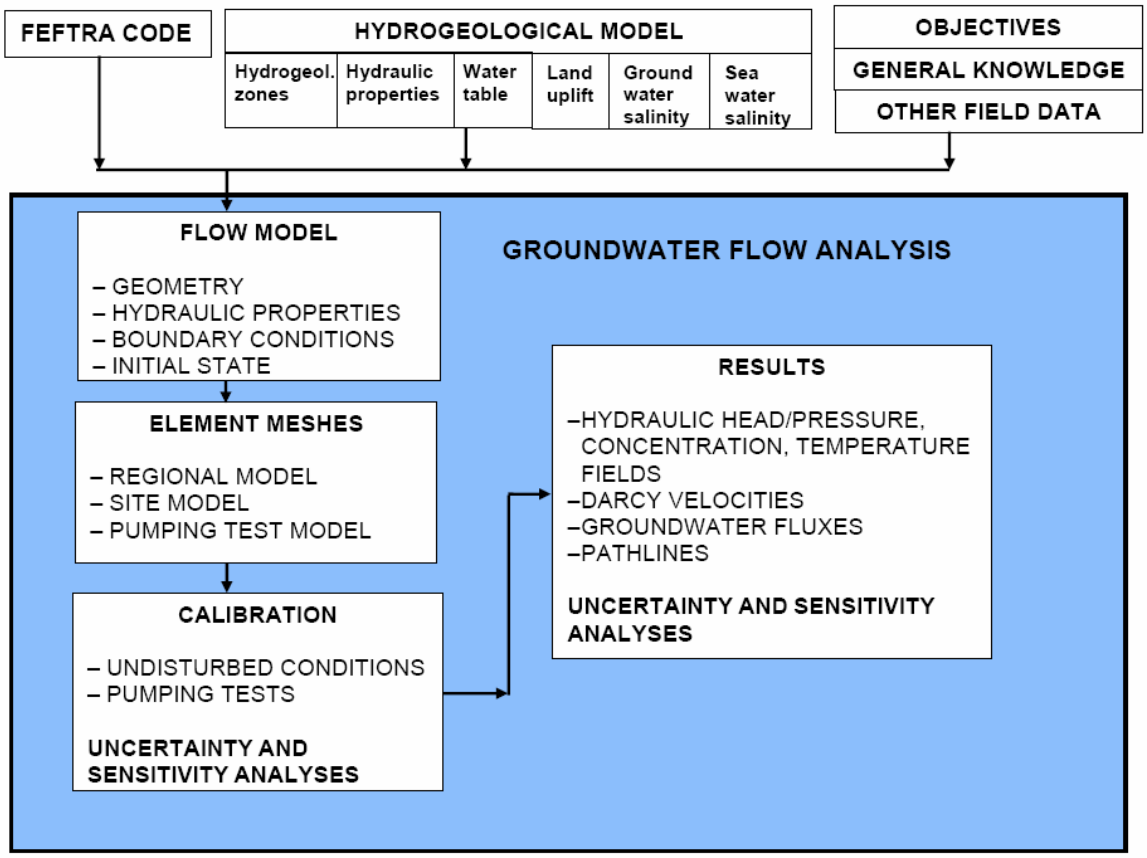

Figure 6-12. *Components and modelling stages of practical groundwater flow analysis for the site and ONKALO areas.*

Groundwater pressure [SI unit Pa] is the primary quantity for which the corresponding boundary conditions have to be specified. The practical approach in this work to determining the boundary conditions will be described in Section 6.3.2. Darcy's law describes a relationship between the pressure field, more specifically, the pressure gradient and the strength of the flow, or the Darcy velocity (also termed the "specific discharge"). The two fields are related to each other through a coefficient, that, in three dimensions, is called the hydraulic conductivity.

Hydraulic conductivity, K [m/s], which is a spatially highly variable parameter in crystalline bedrock. The hydraulic conductivity is a lumped parameter, whose value depends on the properties of the groundwater via its density ρ [kg/m^3] and viscosity μ [Pa·s] so that:

$$K = \kappa \frac{\rho g}{\mu}$$

where κ is the intrinsic permeability [m^2], which is the property of the medium only.

The high spatial variability of the hydraulic conductivity means that determining its distribution with confidence has proved to be a most challenging problem in hydrogeology. In this work, simplifications and approximations will be applied. For features with a distinct two-dimensional character, such as deformation zones with a high conductivity, the corresponding parameter is called the transmissivity.

Transmissivity, T [m^2/s], which, for a *porous* zone exhibiting two-dimensional flow characteristics, may be formally calculated by multiplying the hydraulic conductivity by the thickness of the hydrogeological zone. (The effective transmissivities in this work are shown in Table 6-2 in Section 6.3.4 on page 211.)

Groundwater salinity, c, [kg/m^3] expressed also in unit g/L, affects the density of water. In this work, the dependency is described with a simple polynomial of the first order, although somewhat more complex forms have also been proposed. Because saline water is transported by the flow of groundwater, the salinity undergoes temporal changes. For the hydrogeological modelling on the site scale, salinity must also be specified for each position. Clearly this can only be done through the use of simplifying assumptions, which nevertheless, are based as much as possible on actual site-specific data.

At Olkiluoto the groundwater salinity reaches 84 g/L. The salts in groundwater are transported by the flow of groundwater and the flow equation must, therefore, be accompanied by an equation that models the transport of salinity in groundwater. In this work, the transport of salts is modelled with the advection–dispersion equation (ADE). Large differences in the salinity – or more precisely, differences in the density of groundwater - affect the flow which, in turn, affects the groundwater salinity, as the dissolved substances are being transported by the flow. This means that the flow equation and the ADE, form a coupled set of equations, which must be solved with an iterative numerical scheme.

Flow porosity, n_f, [–] expresses the proportion of water-filled volume per unit volume. Only a part of the porosity is connected to groundwater flow paths, whilst the remainder (actually, the major part) of the water can be considered as being stagnant. This unconnected porosity is not considered from the point of view of groundwater flow so that only the flow porosity is important. Values of flow porosity 0.001 to 0.0001 are often used.[10] The final values in the flow model are obtained through matching calculated results with the observed groundwater salinity. In reality, the flow and matrix porosities vary. The flow porosity is also related to other properties of rock, such as hydraulic conductivity. Various simplified and uncertain relations exist between flow porosity and conductivity (e.g. Taivassalo and Saarenheimo 1991). In order to obtain more realistic values, the approach introduced by Löfman (1999) is applied in the calibration. The approach assumes the parallel fracture idealization and the flow porosity n_f is related to the fracture spacing a_f [m] and fracture aperture b_f [m] through $n_f = b_f /(b_f + a_f)$.[11] The fracture aperture may be obtained through the cubic law from the fracture spacing and hydraulic conductivity, assuming that the spacing increases to double with each 500 metres (see Löfman 1999 for details). The surface (z=0) values of the fracture spacing are based roughly on reported fracture densities (7 and 20 fractures per metre for the sparsely fractured rock and the hydrogeological zones, respectively).

Matrix (or diffusion) porosity, n_m [–] represent the part of interconnected cavities that do not contribute to the flow porosity. In the case of saline groundwater this porosity has a capacity to affect the flow indirectly though diffusional transport processes, which will change the salinity of water in the pores of pressure gradient-driven flow. Often it is assumed that the matrix porosity is some ten times as large as the flow porosity.

Dispersivity (expressed as longitudinal a_L and transverse a_T dispersion lengths [m]) describes the spreading of a concentration front during groundwater flow.

6.3.2 Boundary conditions and initial state

The solution with a numerical scheme of the finite element mesh for unknown fields of primary variables, pressure and TDS concentration, stipulates that the respective fields must be specified or conditioned on the model boundaries at all times and everywhere within the model domain at the initial state.

In the horizontal plane the perimeter of the volume of the hydrogeological flow model is set to be located so that the impact of the uncertainty associated with the boundary conditions on its lateral boundaries is unimportant. This should also cover the

---

[10] There are, however, hydrogeological zones (e.g. HZ19C as is to be discussed later) that essentially are single fractures with a variable aperture. In such cases no flow porosity can be determined. Instead, assuming the so called cubic law, one may define the hydraulic aperture which – under the assumption of laminar flow and a parabolic velocity profile across the fractures aperture – subsequently relates the flow rates in the hydrogeological zone to a flow velocity.

[11] Fracture spacing and fracture aperture are model parameters related to strength of diffusive mass transfer rather than actual (hydrogeologic) rock fracturing at the site.

circumstances that clearly are different from the present-day conditions or the conditions before the commencement of the ONKALO excavations. For example, in the far future, due to land uplift and eventually due to the development of colder climatic conditions, the external conditions affecting the groundwater circulation at the site will change. In the flow model these transient changes in the external conditions are taken into account with time-dependent boundary conditions (see, Posiva 2006 for an expanded discussion) on the surface; however the impact of these kinds of external conditions on the lateral boundaries of the flow model is difficult to parameterize. Making the model large enough horizontally also serves to deal with uncertainties in future boundary conditions under circumstances which will be very different from those currently operating.

The horizontal area of the model volume is a polygon of c. 28 km^2, so that the island itself (with an area of 10 km^2) is well contained by the model area (Figure 6-13). In the vertical direction, the model extends two kilometres below the ground surface.[12]

Technically the top surface of the model is set to z = 0 m (the present sea level). On the top surface the pressure boundary condition is calculated from the elevation of the water table as discussed below.

[12] More precisely, the flow model extends from z = 0 m to z = –2000 m.

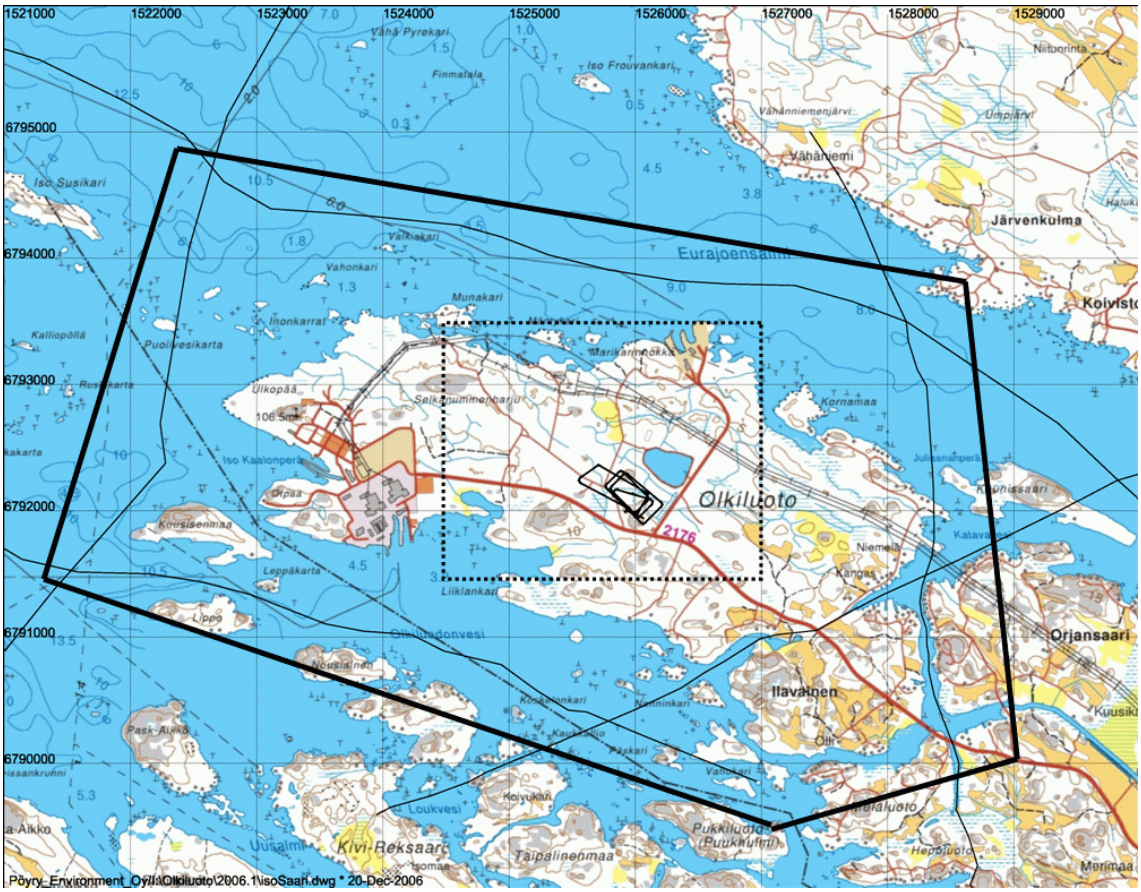

***Figure 6-13**. Outlines of the model volume (polygon with solid line)) and Well Characterised Area (WCA, rectangle with dashed line).*

Initial state of groundwater TDS concentration

The initial state is defined as the peak value of TDS during the Littorina Sea stage, 8000 years ago. As described in Chapter 7, the salinity of the Littorina Sea at this time is 12 g/L (see also Westman et al. 1999). The subsurface TDS concentration at this initial state is based on the approximate profile of the present day concentrations (Figure 6-14).

Uncertainty and sensitivity

The initial state salinity is based on current observations of deep groundwater salinities and indirect knowledge of the salinity in the early Littorina Sea stage. On the one hand, the concentration at shallow depths cannot be sensitive to the initial state if some typical average freshwater infiltration takes place (say, 2% of the annual precipitation). On the other hand, the relatively high concentrations in the 100 to 300 m depth range in a few drillholes (KR3–KR5) must be related to the initial state, and this determines the minimum salinity in the upper part of the bedrock in the initial state. The peak TDS concentration of the Littorina Sea in the model, 12 g/L, exceeds this minimum with a considerable margin. According to Westman et al. (1999) the maximum salinity of the

Littorina Sea was between 10 to 15‰, whilst the salinity may have reached 20‰.[13] This will be introduced as part of the sensitivity analysis of the initial state; although it seems unlikely these high TDS concentrations were attained or prevailed in the Olkiluoto region for prolonged periods of time.

In a similar sense, the TDS concentrations at depth in the initial state can only be at least as high as the highest TDS concentrations seen today at depth. There is no process that would lead to an increase in the initial state concentrations within the model. We do not, therefore, consider a situation with an enhanced TDS concentration at depth, as it would immediately lead to discrepancies with the observations, unless these elevated concentrations were assigned to the rock below the deepest drillholes. In such a case, however, the impact would be small within the volume of rock probed by the current drillholes.

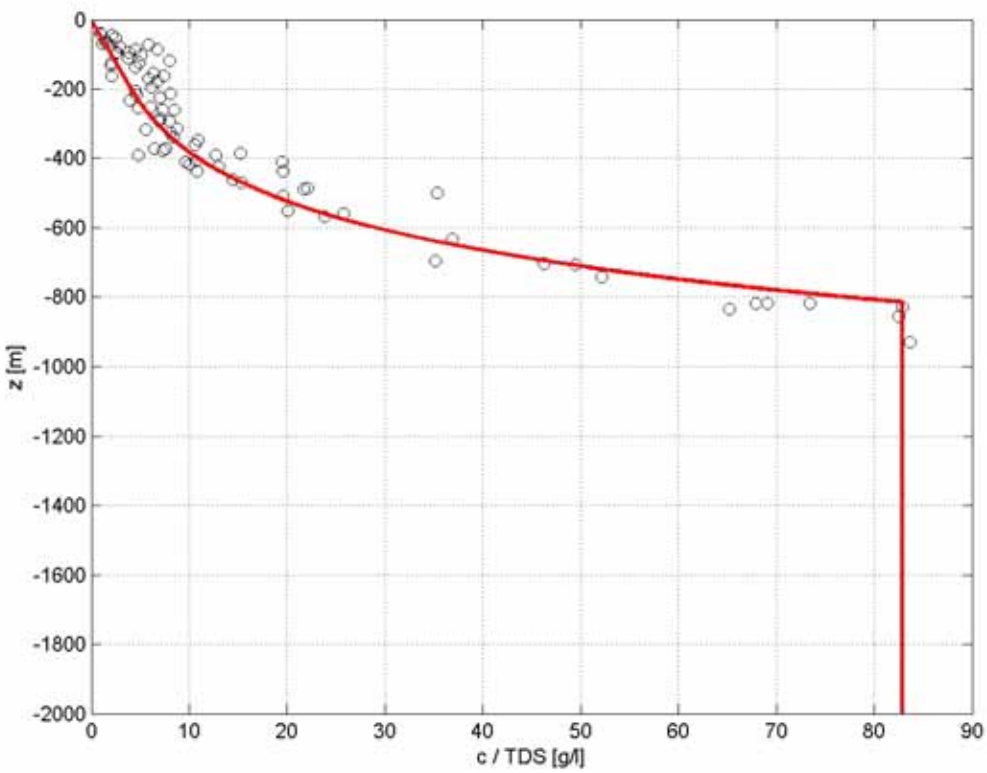

Figure 6-14. *The salinity (TDS) concentration in the bedrock at the initial state at 8 ka BP indicated by the approximate fit to the present day concentrations.*

[13] The literature uses different units for the concentration, but there is a near one-to-one correspondence between the concentration expressed in per mille (‰) and grams per litre (g/L). Also, the literature often, somewhat loosely, speaks about salinity concentration, but the meaning usually is the TDS concentration.

Groundwater TDS concentration – boundary conditions

The TDS concentration on the lateral and bottom boundaries is set according to the initial state (Figure 6-14). On the top of the model for the areas representing the sea the estimated past Baltic Sea water salinity (TDS) is used. This estimation is shown in Figure 6-15. For the landmass of the (growing) island, zero salinity is used.

Uncertainty and sensitivity

The uncertainty and sensitivity case associated with the (time-dependent) concentration boundary condition is derived from that of the initial state. The initial state uncertainty case for the Littorina Sea salinity is taken to prevail for a few thousands of years after the initial time.

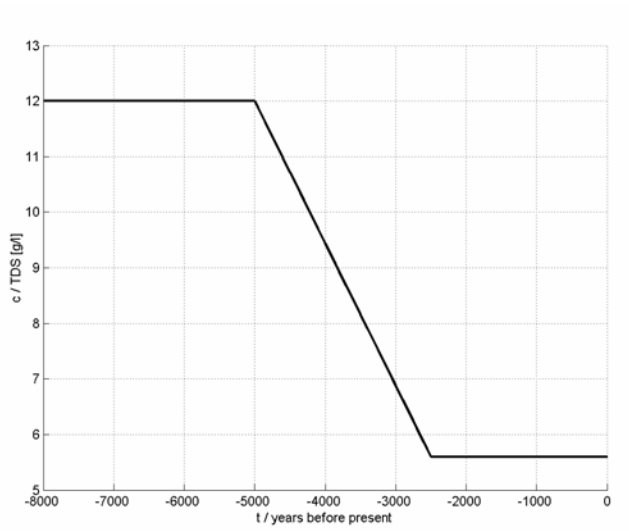

Figure 6-15. *The time-dependent boundary condition for the TDS concentration. For a discussion on the past Baltic Sea salinity see Chapter 7 and Westman et al. (1999).*

Groundwater pressure – Initial state

The initial state of the groundwater pressure is calculated from the initial groundwater salinity field, shown in Figure 6-14. In other words, the initial pressure field is hydrostatic.

Groundwater pressure – boundary conditions

The lateral boundaries of the model are chosen to be approximately 200–300 m outside major regional water divides that are relatively distant from the well characterized area. On the lateral boundaries a no-flow boundary condition may thus be used which, from the point of view of the numerical calculations, is the simplest possible boundary condition. However, the hydrostatic boundary condition will be used in Chapter 8. In order to investigate the effect of uncertainty regarding these boundary conditions, the no-flow boundary condition was also assumed, which however resulted in no significant

change in the calculated results within the well characterized area. On the bottom, a no-flow boundary condition is applied.

On the top of the model, the present-day water table and land uplift scenario by Påsse (1996) introduced in Section 6.2.2 are used to determine the pressure boundary condition. After the rise above the sea surface, the elevation of the water table for each point on the surface increases linearly to its present-day value. Consequently, zero pressure is applied on the whole top surface as long as the island is below sea level.

Uncertainty and sensitivity

The most important uncertainty of the boundary conditions is associated with the *water table,* because of its close location to the area of central interest, however, there is usually no information available about the water table in a specific highly transmissive hydrogeological zone. It is likely that in such a case the actual water table elevation is lower than that based on a correlation between the topography and water table (see Section 6.3.2) as otherwise unrealistically high groundwater flux rates are induced. While the boundary conditions on the lateral and bottom boundaries of the model are only assumed, the significance of any such uncertainty is considered to be low in comparison, as these boundaries are far from the area of central interest. This assumption can be checked by changing these respective boundary conditions to prescribed pressures and then examining the consequences.

6.3.3 Structural model for hydrogeological zones

In this section, the structure of the hydrogeological model is introduced. This structure is described in terms of different hydrogeological zones of the model. In the site and ONKALO areas (see Figure 4-2) the main geological input to the hydrogeological bedrock model describes a number of brittle deformation zones (BFZ, see Chapter 4.3.4; Paulamäki et al. 2006). The hydrogeological properties of each such BFZ have been determined with drillhole measurements of transmissivity. The extensive dataset gathered clearly indicates that not all the brittle deformation zones are hydrogeologically significant. Furthermore, in some cases clearly elevated transmissivities cannot be associated with any structure in the brittle deformation model in version 0 of the geological model (Ahokas et al. 2007). The hydrogeological flow model may, thereby, introduce structures that – while not possessing a geological character by the criteria of Paulamäki et al. (2006) – are clearly showing up in the hydrogeological data (Ahokas et al 2007). In particular, a single individual fracture may not have merited being modelled as a zone, whilst it may be significant in terms of groundwater flow. For example, such a fracture intersects drillhole KR14 at a depth of 50 m (see Figure 6-16).

A key input in constructing the hydrogeological structural model is the brittle deformation zone model described in Chapter 4. For the hydrogeological structural model we adopt a similar convention in naming the zones as that introduced in Chapter 4, except that instead of calling them brittle deformation zones, it was agreed the zones in the hydrogeological model are called Hydrogeological Zones, denoted with

prefix "HZ". It was also decided that hydrogeological zones with at least one measured transmissivity greater than $T = 10^{-7} m^2/s$ should be explicitly incorporated in the hydrogeological model.

The strategy in developing the updated flow model included a priority to describe the hydrogeological zones within the planned repository host rock block, i.e. depth level 420 m (Ahokas et al. 2007). This was pursued while adopting the brittle deformation model of the geological model as a starting point. The brittle deformation zone model was reconciled with the measurements of transmissivity and hydrogeological responses to various field activities (pumping tests, water sampling, etc.). The hydrogeological responses to various field activities strongly suggested the existence of three gently-dipping, hydrogeologically dominant zone systems: HZ19, HZ20, and HZ21. These had already been described in the previous flow model (RH19, RH20 and RH21 according Vaittinen et al. 2003) and, due to their indisputable hydrogeological significance, it was decided that they should also be kept in this model. As explained by Ahokas et al. (2007), some of the hydraulic responses can be measured over distances up to 1 km. For example the responses that are interpreted as being transmitted by the HZ19 system are also detectable in places where the geological model does not describe any brittle deformation zone (Figure 6-16).

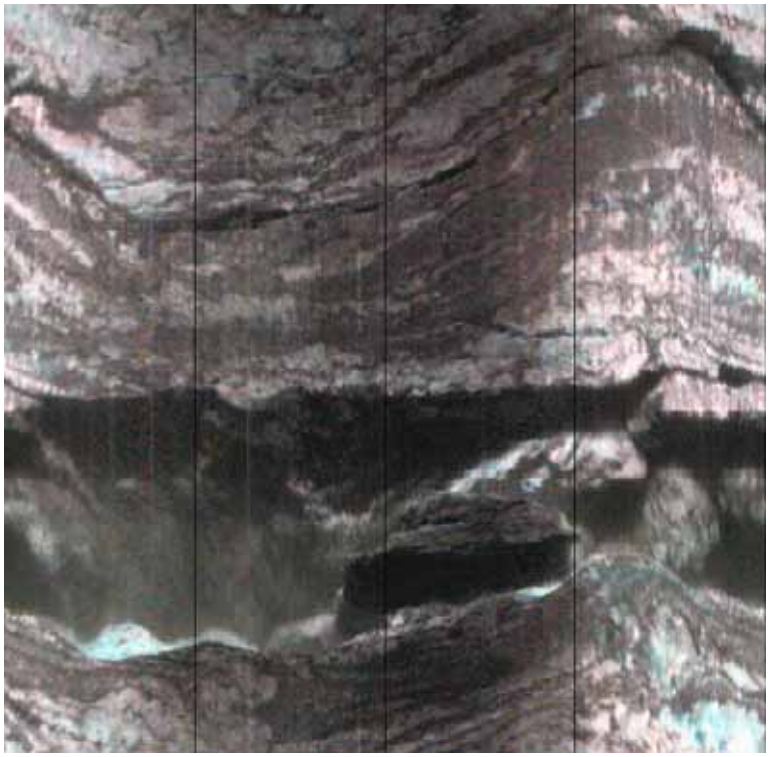

Figure 6-16. *A circa 7 cm opening in drillhole KR14 at a depth of 50 m. The length of the figure is c. 20 cm. In the hydrogeological model this intersection is associated with fracture zone HZ19C. The measured transmissivity at the intersection is* $10^{-5} m^2/s$ *(Ahokas et al. 2007) and strong responses were detected on this spot in a pumping test in 2002 (Pöllänen & Rouhiainen 2004). There is no correspondence with this in the geological model.*

Next, the key hydrogeological characteristics of the zones identified in the well-characterized area are summarized. In other words, their spatial locations, as well as their transmissivities, will be introduced. The reader is referred to (Ahokas et al. 2007) for a detailed account of all the hydrogeological zones. The hydrogeological zones in the well-characterized area are:

- HZ19A
- HZ19B
- HZ19C
- HZ20A
- HZ20AE
- HZ20B_ALT
- HZ21
- HZ21B
- HZ001
- HZ002
- HZ003
- HZ004
- HZ008
- BFZ099

HZ19A and HZ19C

Hydrogeological zone HZ19A is subhorizontal (with a dip of 12° and dip direction of 140°) and is intersected by many drillholes. Zone HZ19A is strongly supported by deformation zones BFZ011 and BFZ051. These brittle deformation zones have slickensides and geological indications of water flow.

Hydrogeological Zone HZ19C is oriented parallel to HZ19A, but is located on average approximately 35 m below the latter. Also the eastern part of zone BFZ034 fits well with zone HZ19C (Figure 6-17). This deformation zone is fractured and also has slickensides.

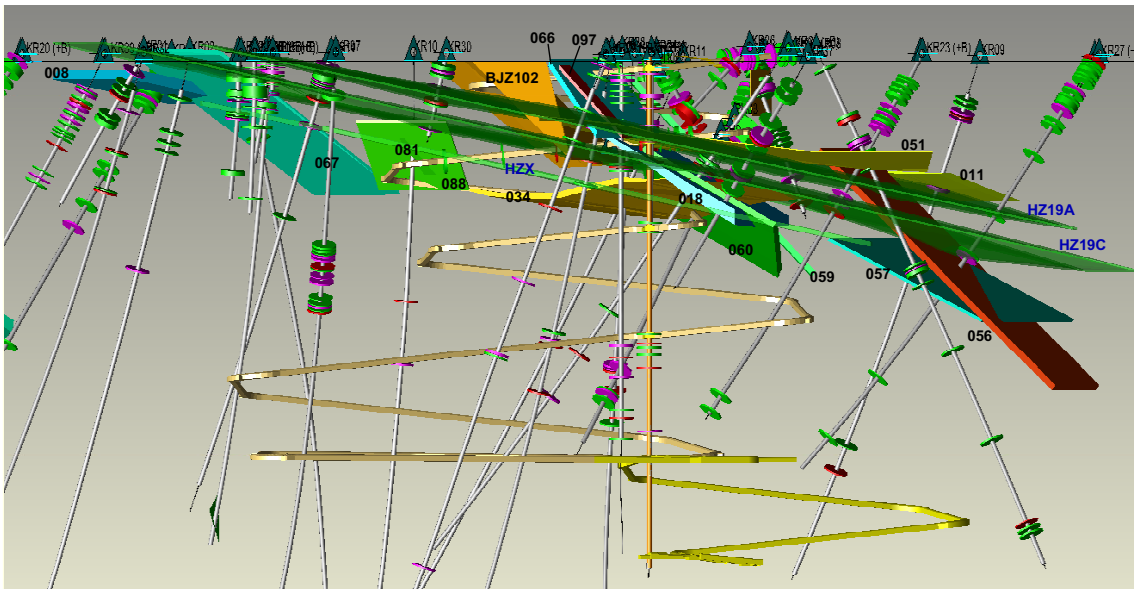

Figure 6-17. *Zones HZ19A and HZ19C together with deformation zones in close proximity. A possible zone HZX is also shown.*

A large number of drillholes intersect hydrogeological zone HZ19A and a number of high transmissivities have been observed at these intersections (Figure 6-18) although, because of a couple of lower values (down to 10^{-10} m^2/s), the geometric mean (1.6×10^{-6} m^2/s) is clearly smaller that the maximum value of 5×10^{-5} m^2/s. The point values cover a depth range without a distinctive trend. On the other hand, due to the gentle dip of the structure the deepest point value is at the depth of only c. 200 m.

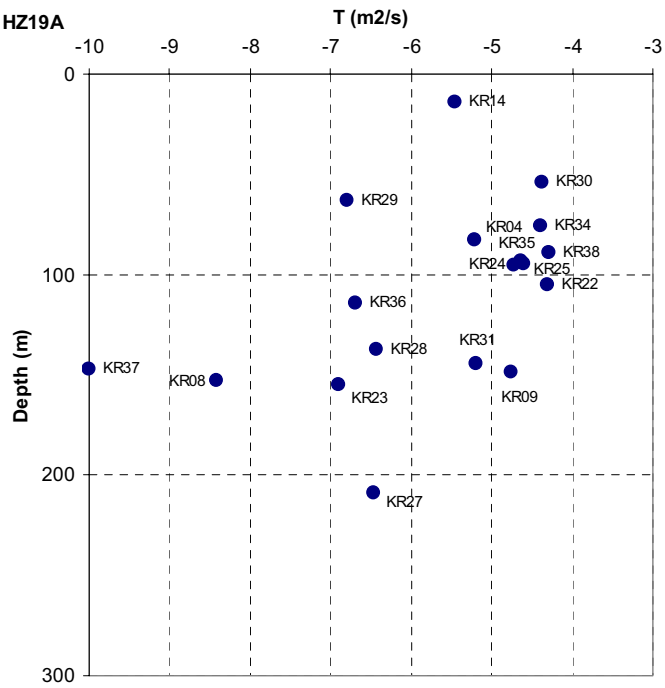

Figure 6-18. *Measured transmissivities of hydrogeological zone HZ19A (Ahokas et al. 2007).*

As hydrogeological zone HZ19C is located at a couple of tens of meters below HZ19A – this zone is intersected by the same drillholes but at greater depth. It is remarkable that very high point values are met much deeper in this zone than its parallel companion, but the two low values in drillhole KR08 and KR09 reduce the geometric mean, T_G, of this zone to approximately the same level (Table 6-2 on Page 211). A photograph at the zone's intersection in drillhole KR14 was shown earlier in Figure 6-16, displaying the actual character of this hydrogeological zone as a single fracture.

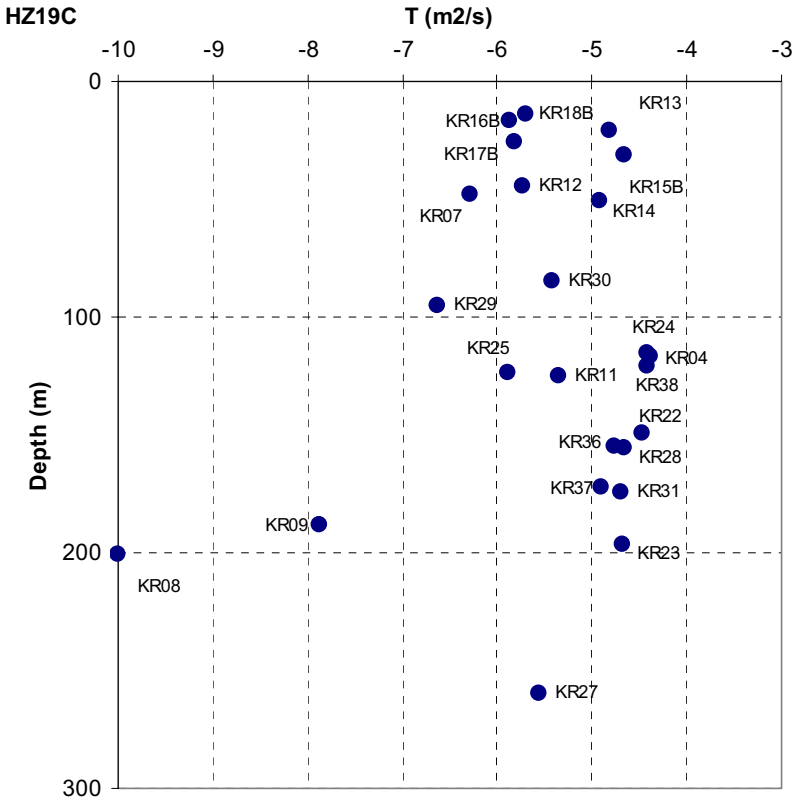

Figure 6-19. *Measured transmissivities of hydrogeological zone HZ19C (Ahokas et al. 2007).*

HZ19B

Hydrogeological zone HZ19B (with a dip of 23° and dip direction of 180°) possesses a steeper dip than the previous two zones so that it intersects zones HZ19A and HZ19C (Figure 6-20). Also this zone is intersected by many drillholes (Ahokas et al. 2007).

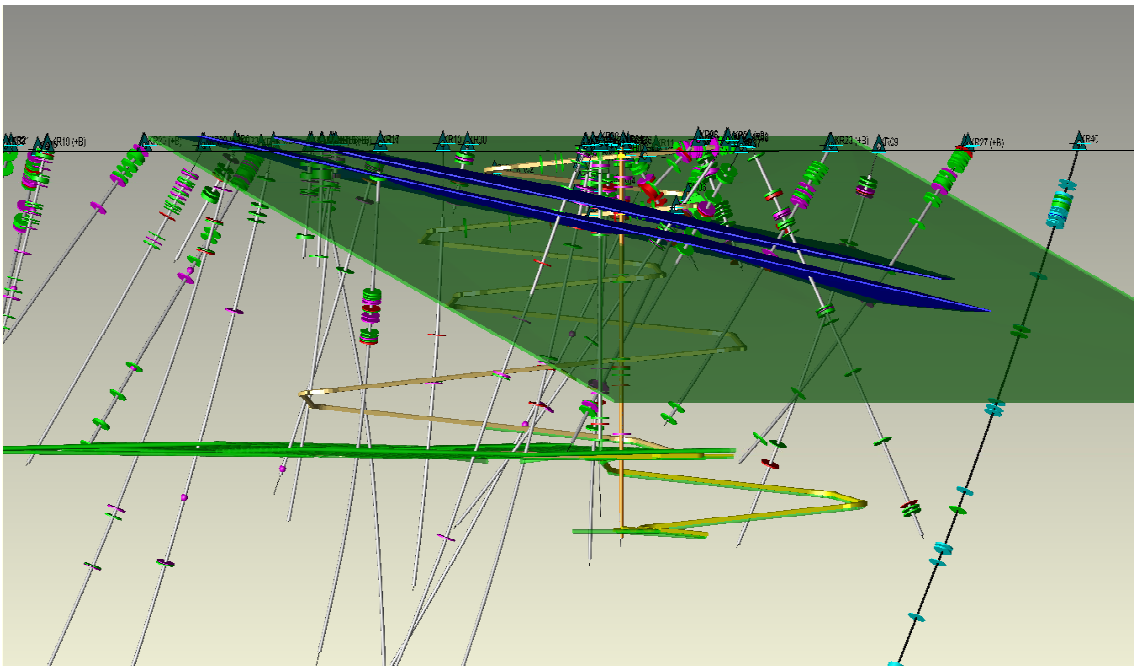

Figure 6-20. Hydrogeological *zones HZ19A (upper blue), HZ19B (green) and HZ19C (lower blue) (Ahokas et al. 2007).*

In many respects the measured point values associated with this hydrogeological zone resemble those for zone HZ19A and HZ19C. As a result – whilst the number of data points is somewhat smaller than those two hydrogeological zones – the geometric mean is similar and the standard deviation of the point values a little larger.

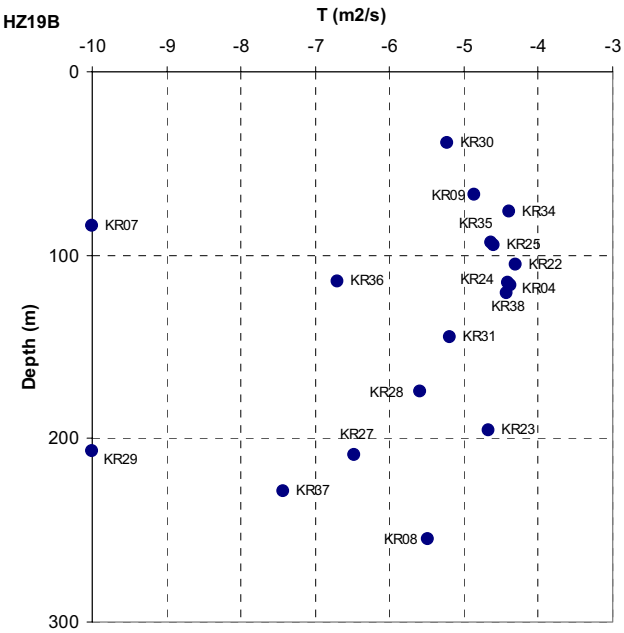

Figure 6-21. *Measured transmissivities of hydrogeological zone HZ19B (Ahokas et al. 2007).*

HZ20A and HZ20B_ALT

The two hydrogeological zones (with a dip of c. 16° and dip direction of 130°) run almost in parallel without a direct connection to the surface. Their gentle dip makes them resemble the pair of hydrogeological zones HZ19A and HZ19C. Similarly the lower of the two, HZ20B_ALT, is located 40 to 50 m below HZ20A (Figure 6-22). According to Ahokas et al. (2006b) the pair is intersected by many drillholes.

Brittle deformation zones BFZ021 and BFZ080 clearly support the orientation of HZ20 zones. Brittle deformation zone BFZ098 is also intersected by the same drillholes in the northwest and indicates the possible extension of the HZ20 zones towards the northeast (Figure 6-23). Brittle deformation zones BFZ019 and BFZ073 also intersect almost the same drillhole sections as the hydrogeological HZ20 system.

The intersection associated with brittle deformation zone BFZ021 at section OL_KR29_BJI_25147_25184 is slightly altered and weathered with 9 fractures having clay mineral infills (Paulamäki et al. 2006). The fractures mainly assume the direction of the foliation, which dips gently to the SE. The intersection associated with brittle deformation zone BFZ080 at section OL_KR25_BJI_36931_37320 contains thick (max. 5 cm) calcite bearing, water-conducting fractures (20 fractures). A consistent medium transmissivity (10^{-6} m^2/s) has been measured in this intersection (Figure 6-24). The fractures at the intersection are randomly orientated, usually with almost horizontal dips.

Intersection OL_KR25_BJI_36931_37320, associated with brittle deformation zone BFZ080, contains thick (max. 5 cm) calcite bearing, water-conducting fractures (20

fractures) and the Wellcad-picture shows a large fracture/cavity (Paulamäki et al. 2006). A consistently high transmissivity (5×10^{-5} m^2/s) has been measured at this intersection.

Brittle deformation zone BFZ019 is characterized by slickensides with slight pyrite coatings at intersection OL_KR10_BFI_27147_27159, and shows water conducting fractures and slickensides at intersection OL_KR25_BFI_34700_35225 (Paulamäki et al. 2006). A notable transmissivity (5×10^{-6} m^2/s) is measured in the former intersection and a high transmissivity (2×10^{-5} m^2/s) in the latter (Figure 6-24).

Intersection OL_KR7_BFI_22701_22880 associated with brittle deformation zone BFZ073 exhibits a porous character with cavities that are visible and with grain-filled fractures. In places on fracture surfaces, pyrite and clay minerals can be detected. Strong geophysical anomalies are also associated with this section (Paulamäki et al. 2006). A high transmissivity ($10^{-5}m^2/s$) is measured in the intersection.

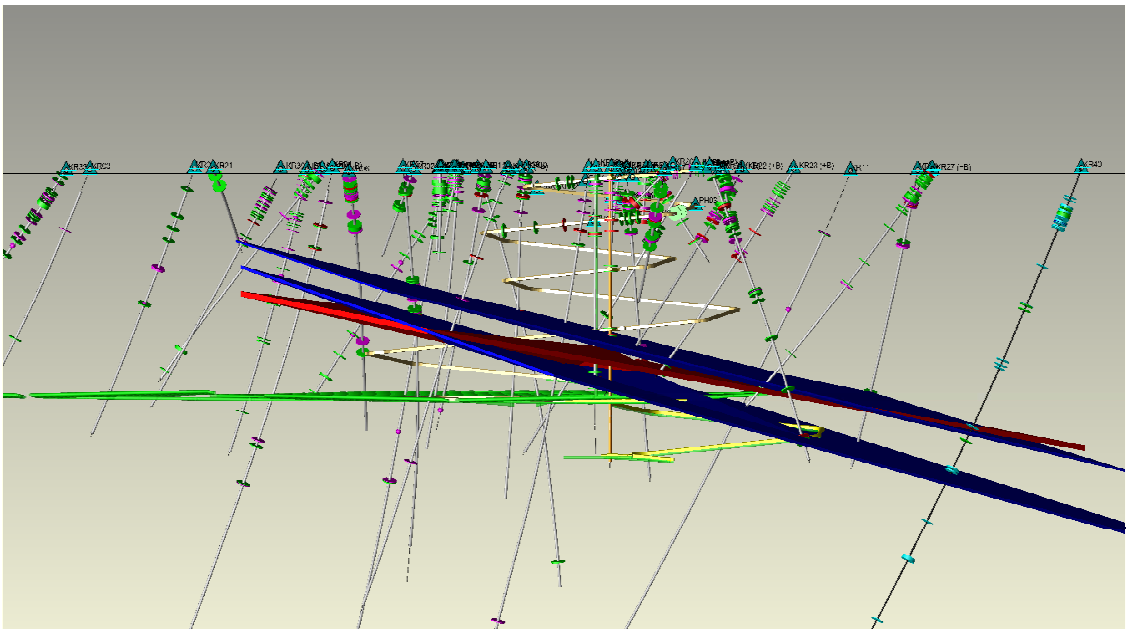

Figure 6-22. *Zones HZ20A (upper blue), HZ20B (red) and HZ20B_ALT (lower blue). View from the south-west. Fracture zone HZ20B is shown as it is the uncertainty case to replace HZ20B_ALT.*

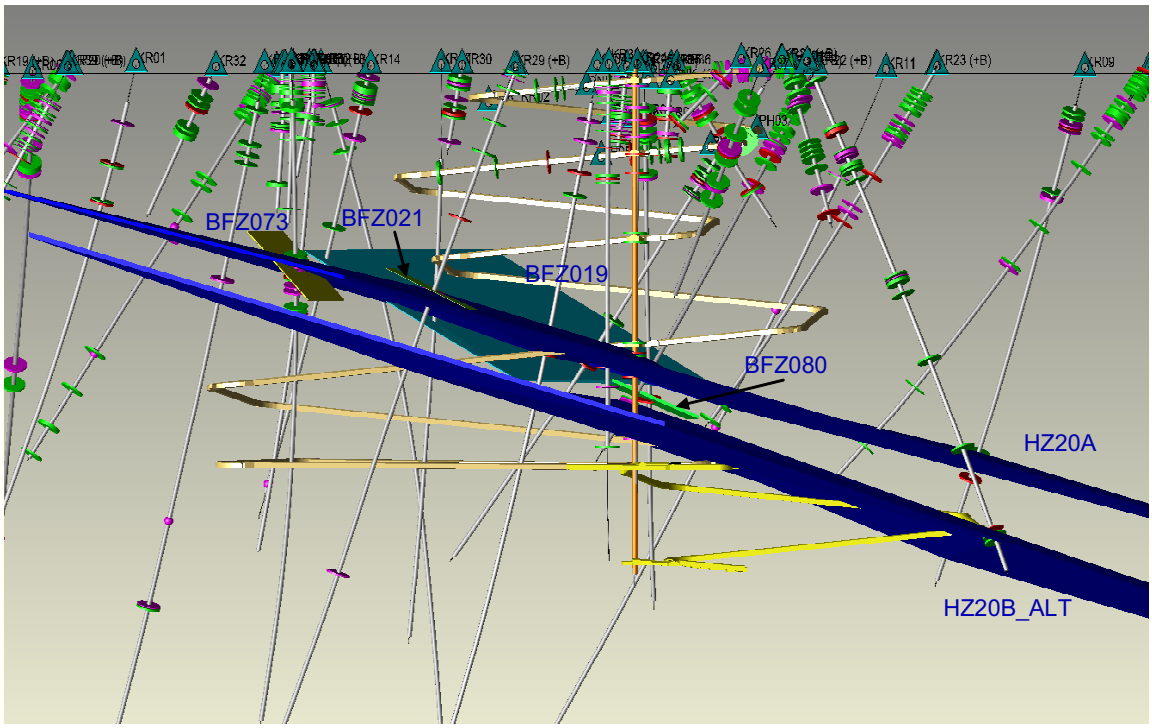

Figure 6-23. *Zones HZ20A and HZ20B_ALT together with deformation zones with approximately the same location and direction.*

The measured transmissivities for hydrogeological zones HZ20A (Figure 6-24) and HZ20B_ALT (Figure 6-24) yield high effective transmissivities (8×10^{-6} m^2/s and 3×10^{-6} m^2/s , respectively).

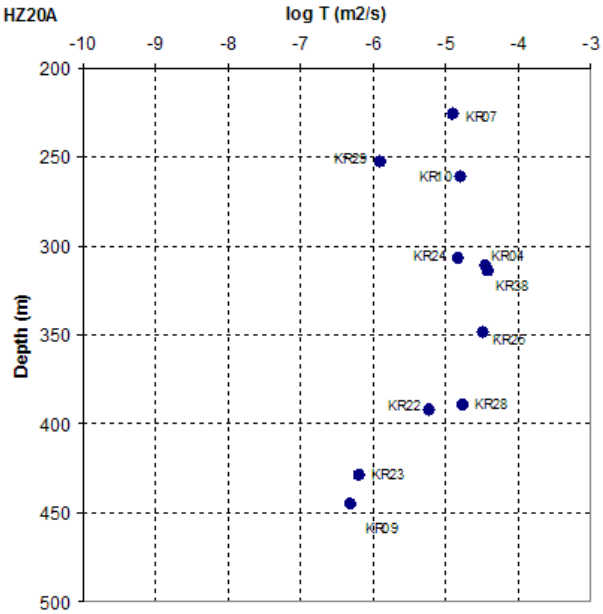

Figure 6-24. *Measured transmissivities of hydrogeological zone HZ20A (Ahokas et al. 2007).*

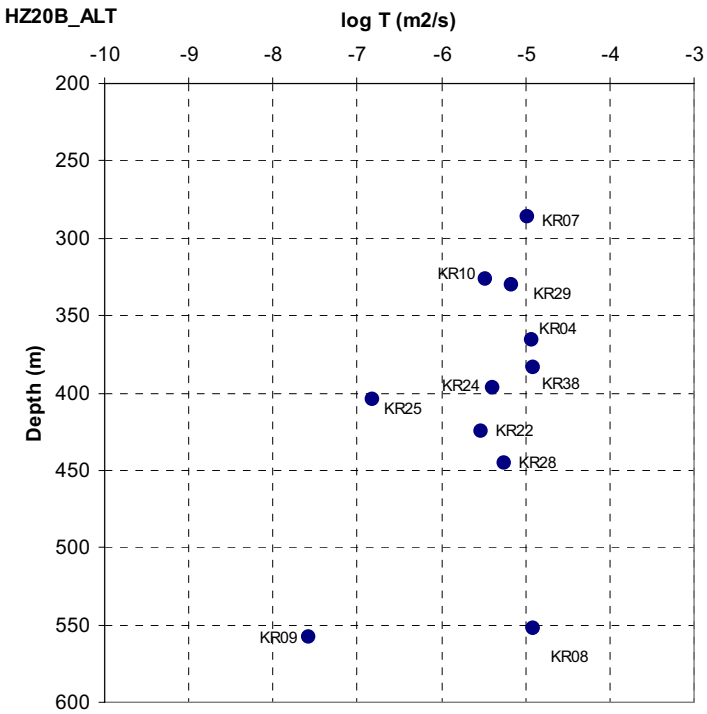

Figure 6-25. *Measured transmissivities of hydrogeological zone HZ20B_ALT (Ahokas et al. 2007).*

HZ21

Hydrogeological zone HZ21 (with a dip of 19° and dip direction of 165°) derives its name from a similar structure RH21 in the previous hydrogeological flow model (see, Posiva 2005; Ahokas et al. 2007). Hydrogeological zone HZ21 is directly supported

by brittle deformation zone BFZ002. The geological data from this brittle deformation zone describes the presence of slickensides and indications of water flow (Paulamäki et al. 2006), which are consistent with the measured elevated transmissivities. A few other deformation zones – BFZ001, BFZ049, BFZ062, BFZ064, and BFZ093 – are also located in close proximity to hydrogeological zone HZ21 (Figure 6-26). At intersection OL_KR29_BFI_74570_74730, brittle deformation zone BFZ093 is associated with slickensides and geological indications of water flow (Paulamäki et al. 2006). This is consistent with the Posiva Flow Log that indicates a transmissive fracture at a drillhole depth of 747 m.

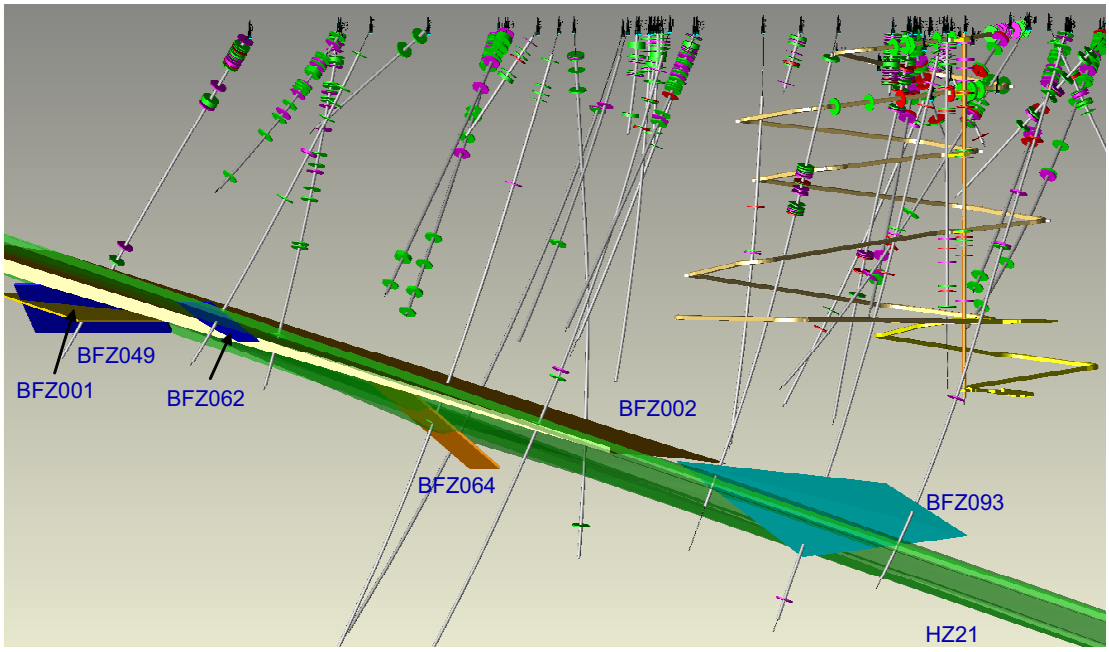

Figure 6-26. *Zone HZ21 and deformation zones in close proximity. Note in particular, BFZ002 (Ahokas et al. 2007).*

The measured transmissivities associated with hydrogeological zone HZ21 show a great variability (Figure 6-27), the effective value being approximately T_G = 1.6×10^{-8} m^2/s which is rather low.

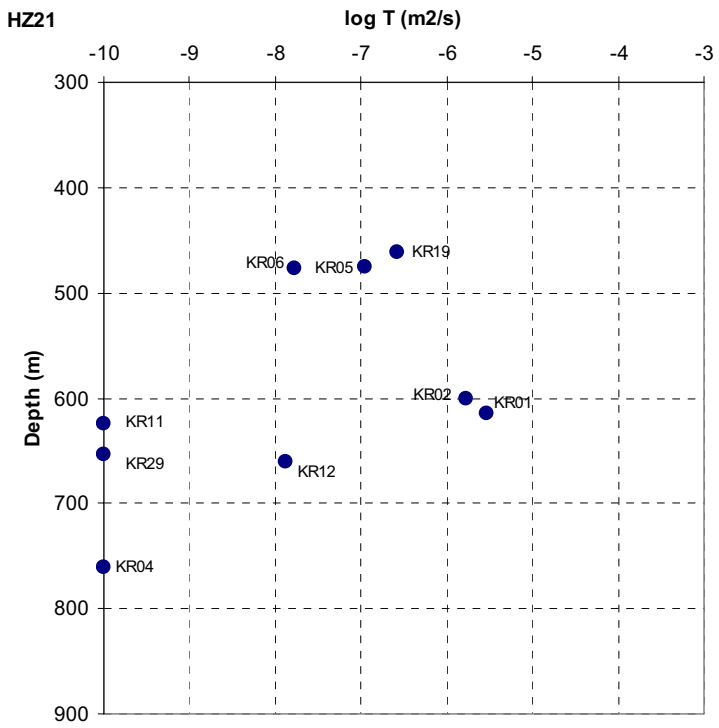

Figure 6-27. *Measured transmissivities of hydrogeological zone HZ21. (Ahokas et al. 2007).*

HZ21B

Hydrogeological zone HZ21B (with a dip of 30° and dip direction of 159°) derives its name from a similar zone in the previous flow model (Posiva 2005; Ahokas et al. 2007). A brittle deformation zone BFZ064 is located in the vicinity of the plane of the hydrogeological zone (Figure 6-28). The intersection with drillhole KR2 of this brittle deformation zone at OL_KR2_BFI_60080_60477 contains slickensides and shows geological indications of water flow, which is consistent with the elevated transmissivity measured at this intersection.

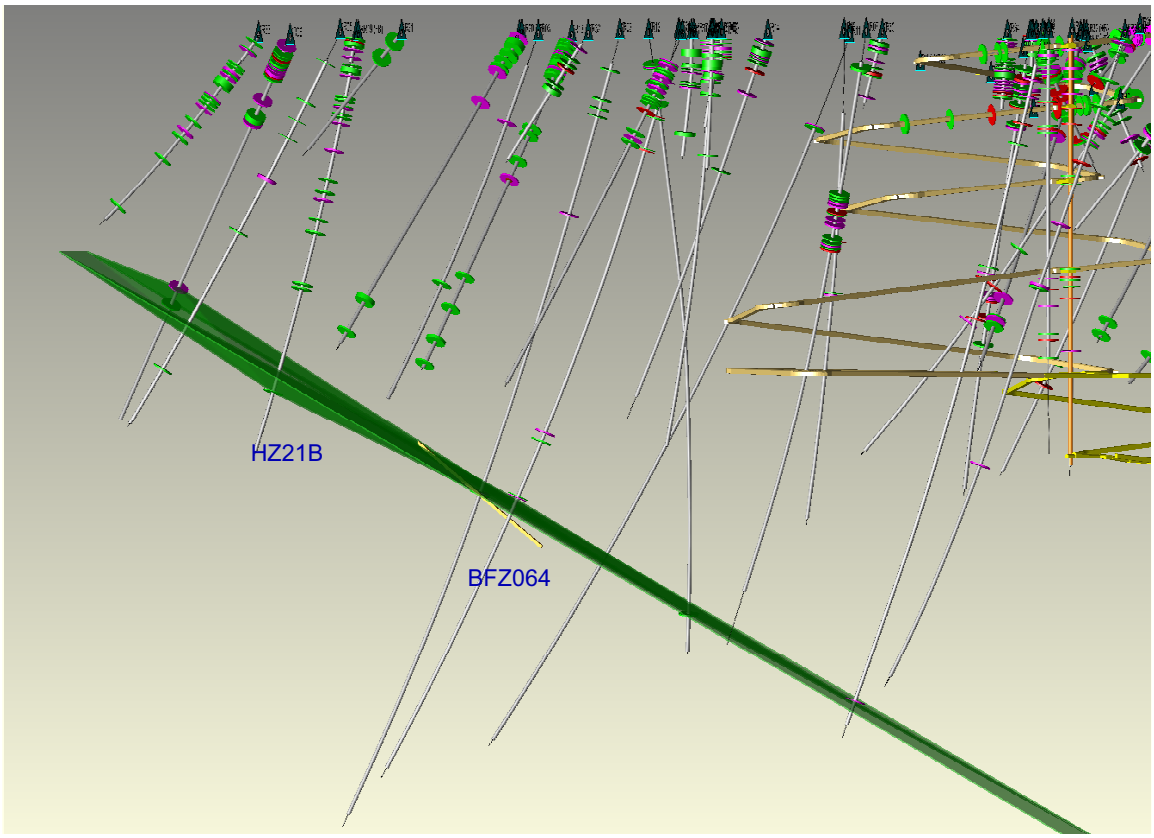

Figure 6-28. *Hydrogeological zone HZ21B and brittle deformation zone BFZ064. ONKALO tunnels and drillholes are also shown (Ahokas et al. 2007).*

The measured transmissivities for this hydrogeological zone show quite moderate variability (Figure 6-29). On the other hand, one measured transmissivity at a depth of greater than 850 m is surprisingly high, at 10^{-5} m^2/s. The effective transmissivity of this hydrogeological zone is $T_G = 8\times10^{-7}$ m^2/s.

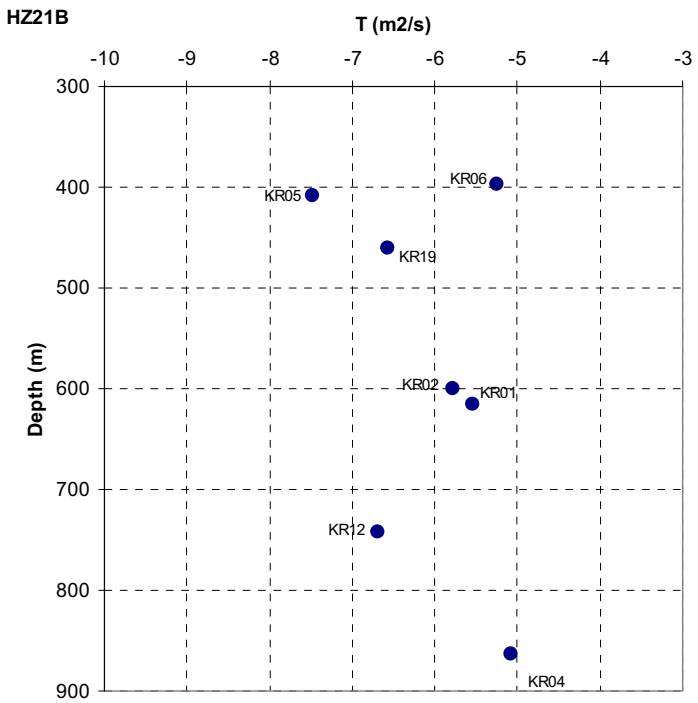

Figure 6-29. *Measured transmissivities of hydrogeological zone HZ21B (Ahokas et al. 2007).*

BFZ099

Brittle deformation zone BFZ099 (with a dip of 35° and dip direction of 167°) is located in the vicinity of hydrogeological zones HZ21 and HZ21B (Figure 6-30). The deformation zone runs almost parallel to hydrogeological zone HZ21B but more than 100 m above it. The brittle deformation zone has been intersected by a large number of drillholes. Most of the intersections contain slickensides and/or show indications of water flow. The measured transmissivities associated with this deformation zone show a clear tendency for higher values in the upper part (Figure 6-31). Thus in the model two effective values have been assigned to this deformation zone. For the upper part, that is above 500 m depth, $T_G = 5\times10^{-7}$ m^2/s; and for the lower part $T_G = 8\times10^{-9}$ m^2/s.

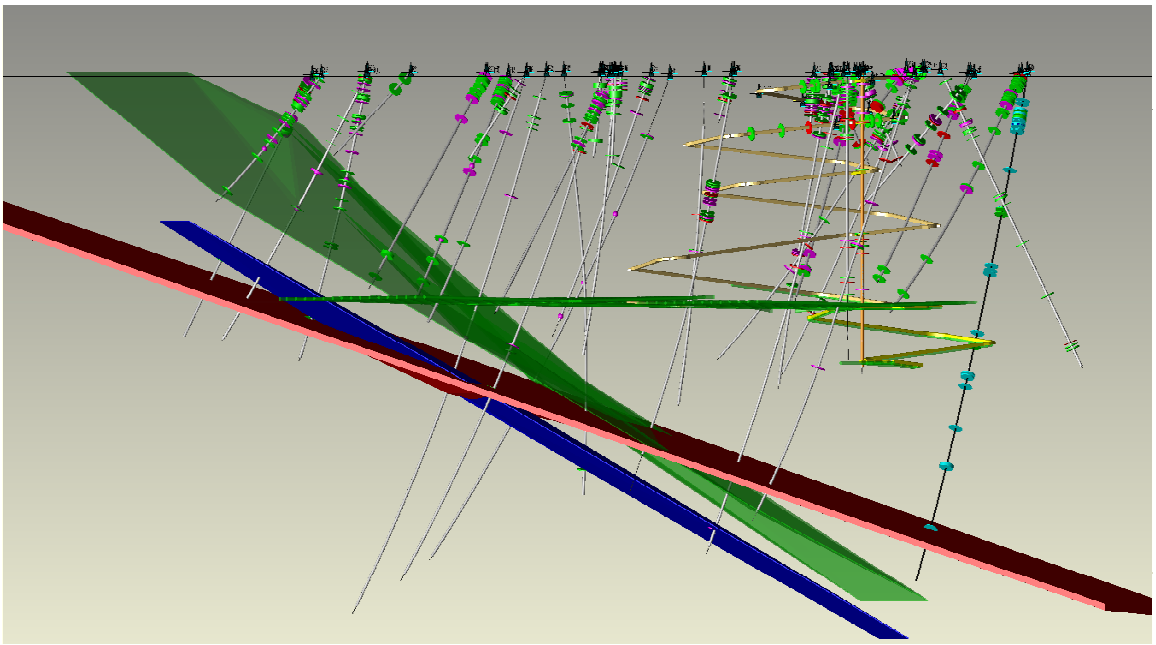

Figure 6-30. *Zones HZ21 (red), HZ21B (blue) and BFZ099 (green). ONKALO tunnels and drillholes together with measured transmissivities (Ahokas et al. 2007). View from the southwest.*

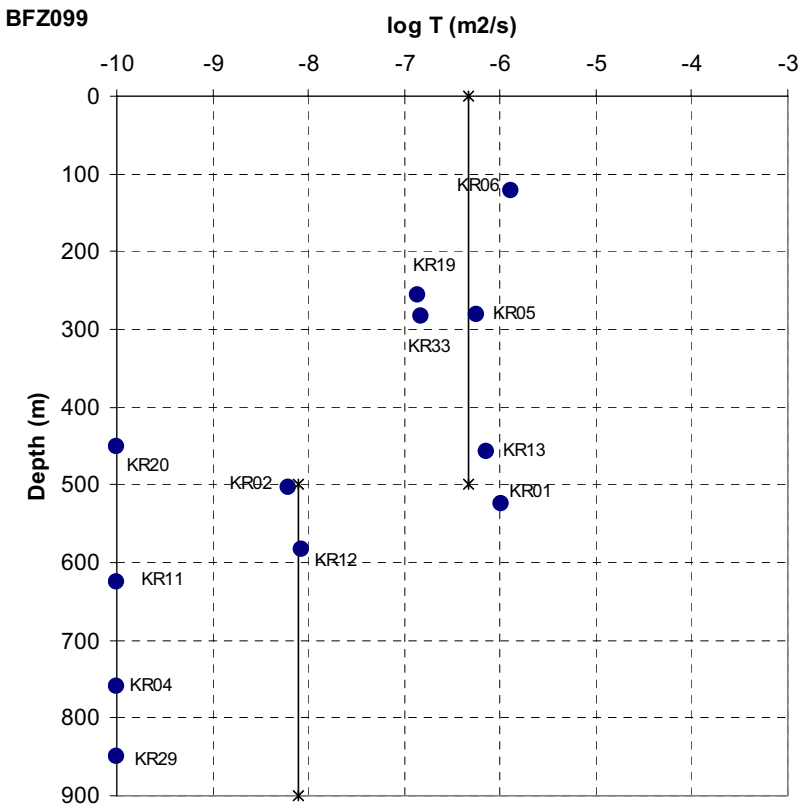

Figure 6-31. *The measured transmissivities associated with brittle deformation zone BFZ099. The two vertical lines indicate the geometric means in the upper and lower part of the deformation zone. (Ahokas et al. 2007)*

HZ001

Hydrogeological zone HZ001 (with a dip of 32° and dip direction of 169°) nearly coincides with brittle deformation zone BFZ005 (Figure 6-32). In the vicinity of this brittle deformation zone anomalously low groundwater pressures have been detected which are co-located with elevated transmissivities. HZ001 has, therefore, been introduced and chosen to stand for the brittle deformation zone in the hydrogeological structural model. The extent, location and the direction of zone HZ001 is strongly supported by deformation zone BFZ005. Some other deformation zones are also in close proximity and have similar orientation, as can be seen in Figure 6-32. Brittle deformation zones BFZ082, BFZ083, and BFZ087 at their intersections with drillhole KR19 contain slickensides and/or show geological indications of water flow. Slickensides and/or geological indications of water flow have also been observed at intersections of drillhole KR15 and brittle deformation zone BFZ052; drillhole KR12 and brittle deformation zone BFZ070; drillholes KR14 and KR15, and brittle deformation zones BFZ075 and BFZ090.

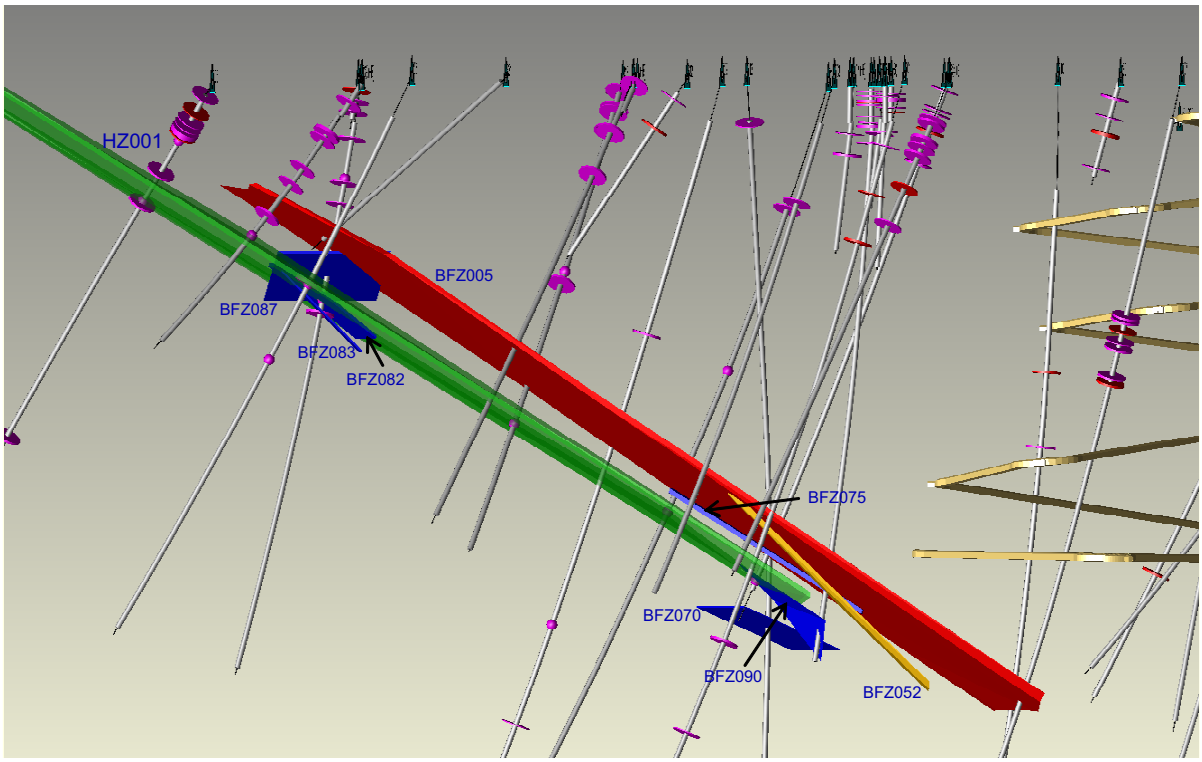

Figure 6-32. *Hydrogeological zone HZ001. View from the west-southwest. Low heads are shown in purple. Transmissivities are shown as discs (T >10^{-5}m^2/s red, 10^{-5}>T>10^{-6}m^2/s purple, 10^{-6}>T>10^{-7}m^2/s).*

According to the interpretation by Ahokas et al. 2007, hydrogeological zone HZ001 shows a rather consistent division of the measured transmissivity values into two depth intervals. The deeper interval is from c. 250 m down to 500 mbsl, whereas the upper covers the depth interval down to 250 m from the surface. On the other hand, we can

see that even the shallowest measured value is from much deeper than 100 m and one could speculate there might be even higher transmissivities closer to the surface, which remain unknown, because the gentle dip of the zone results in its near surface portion being outside the WCA. The effective transmissivity of the interval above z = –250 m is $T_G = 4\times10^{-6}$ m^2/s, whilst the value of two orders of magnitude lower is calculated for the deeper interval.

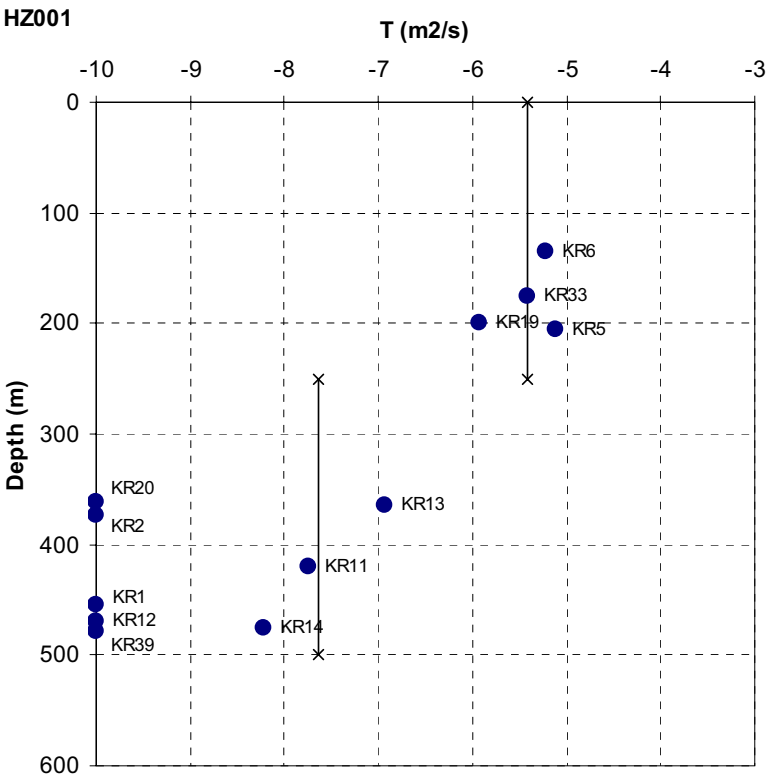

Figure 6-33. *Measured transmissivities of hydrogeological zone HZ001 according to interpreted intersections with the drillholes (Ahokas et al. 2007). The vertical lines indicate the two depth zones for each of which an effective value is determined.*

HZ002

The orientation of zone HZ002 (with a dip of 5° and dip direction of 118°)– shown in Figure 6-34 and 6-35 – is strongly supported by deformation BFZ047 and BFZ095 as can be seen in Figure 6-34. Some other deformation zones also exist nearby, as shown in Figure 6-36.The orientation of other deformation zones is mainly steeper than for brittle deformation zones BFZ047 and BFZ095. The figure indicates that the area is, being relatively close to the surface, densely populated with brittle deformation zones which usually involve slickensides or show indications of water flow. Hydrogeological zone HZ002, whilst modelled within the volume of these brittle deformation zones, has

also been introduced to account for the responses to pumping tests (see Ahokas 2006b for details) between drillholes KR1 and KR2; and KR1, KR20, KR14 and KR18.

The transmissivities associated with this hydrogeological zone vary mostly between 10^{-5} and 10^{-7} m^2/s (Figure 6-37) and show relatively small variability (the standard deviation is only 0.6 (log scale)).

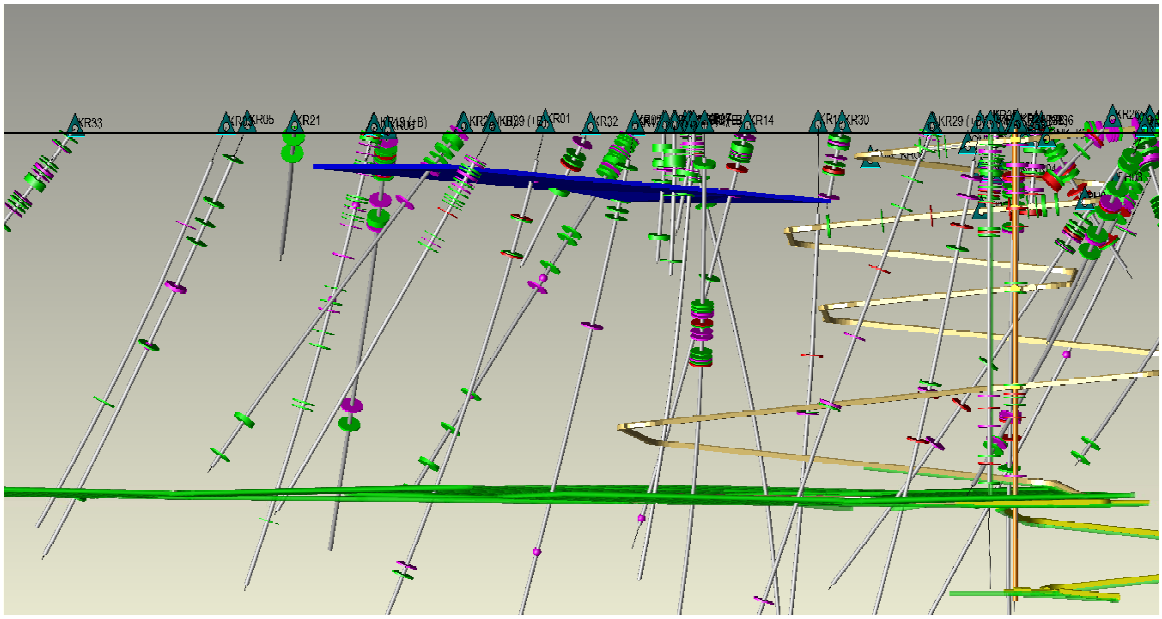

Figure 6-34. *Hydrogeological zone HZ002 (Ahokas et al. 2007)[0]. View from the south-west. Transmissivities are shown as discs (T >10^{-5} m^2/s red, 10^{-5}>T>10^{-6} m^2/s purple, 10^{-6}>T>10^{-7} m^2/s green).*

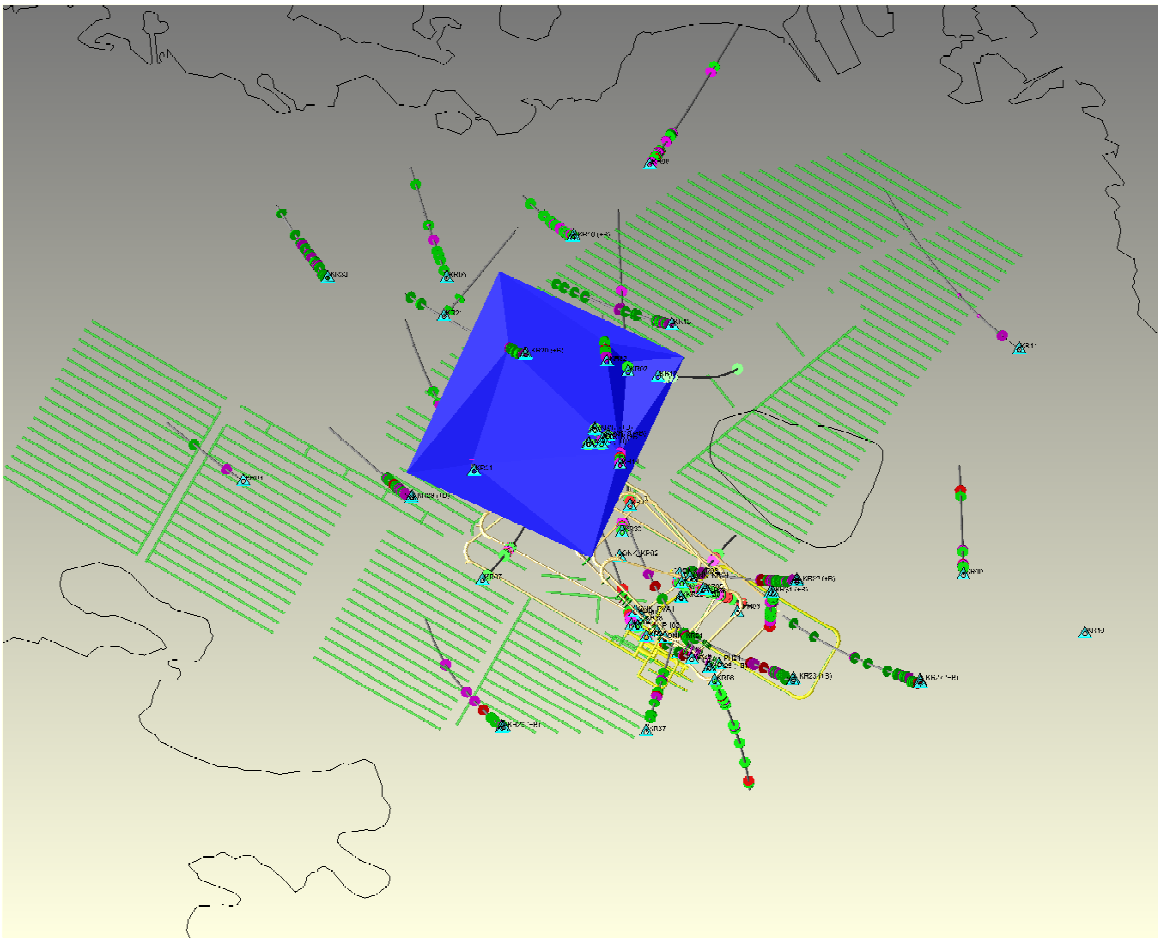

Figure 6-35. *Hydrogeological zone HZ002 (Ahokas et al. 2007). Drillholes and planned repository tunnels together with the shoreline are shown. View from above.*

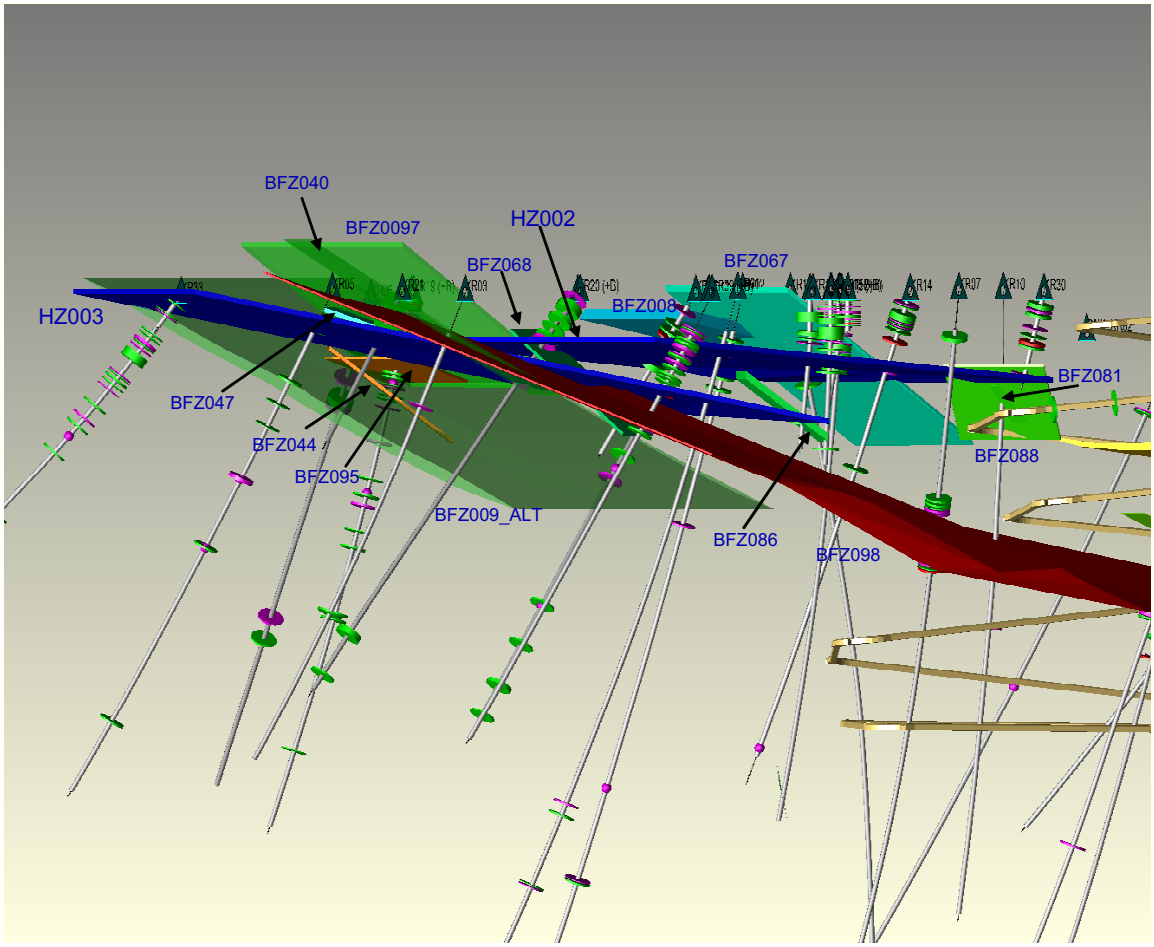

Figure 6-36. *Hydrogeological zones HZ002 and HZ003 together with deformation zones BFZ047 and BFZ09 and a few other brittle deformation zones at shallow depths (Ahokas et al. 2007).*

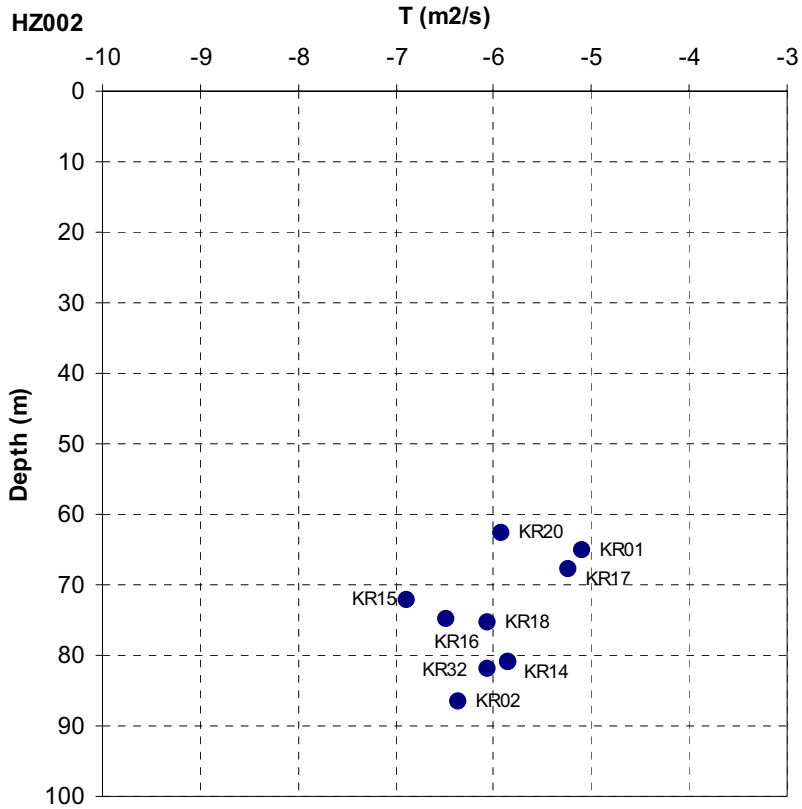

Figure 6-37. *Measured transmissivities of hydrogeological zone HZ002 (Ahokas et al. 2007).*

HZ003

As shown in Figure 6-36, hydrogeological zone HZ003 (with a dip of 11° and dip direction of 137°) is located in the vicinity of HZ002 and a number of brittle deformation zones at shallow depths (Figures 6-38 and 6-39). In a similar manner to hydrogeological zone HZ002, HZ003 has also been introduced to account for the hydrogeological responses between drillholes KR1, KR5 and KR20, and KR39 and KR20 detected during hydraulic testing.

The measured transmissivities associated with this hydrogeological zone vary between 10^{-8} and 10^{-5} m^2/s (Figure 6-41) yielding an effective transmissivity of $T_G = 6\times10^{-7}$ m^2/s while the standard deviation is 1.3 (log scale) (Ahokas et al. 2007).

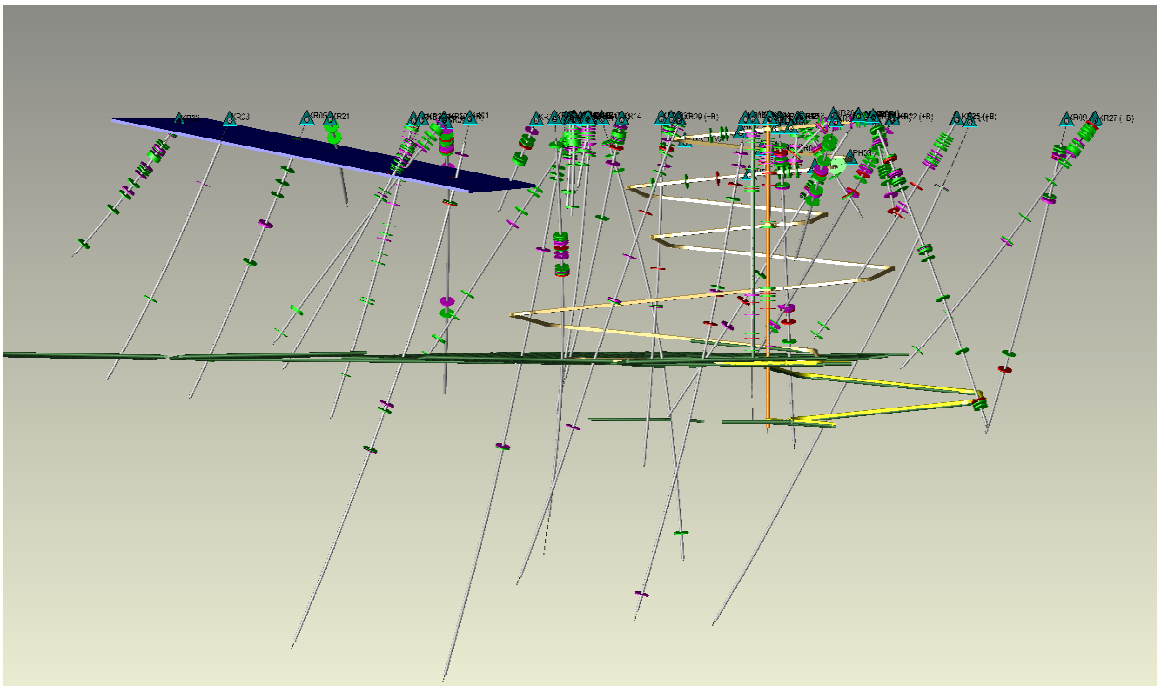

Figure 6-38. *Hydrogeological zone HZ003 (Ahokas et al. 2007). View from the southwest. Transmissivities are shown as discs (T >10^{-5} m^2/s red, 10^{-5}>T>10^{-6} m^2/s purple, 10^{-6}>T>10^{-7} m^2/s green).*

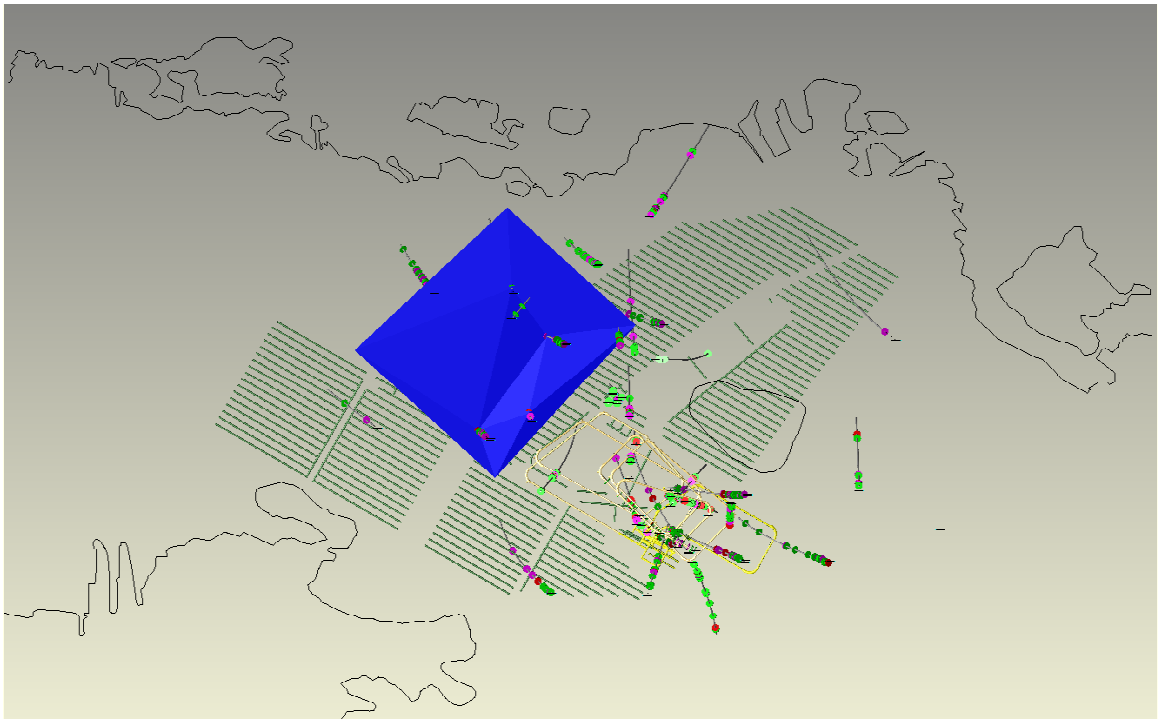

Figure 6-39. *Hydrogeological zone HZ003 (Ahokas et al. 2007). Drillholes and planned repository tunnels together with the shoreline are shown. View from above.*

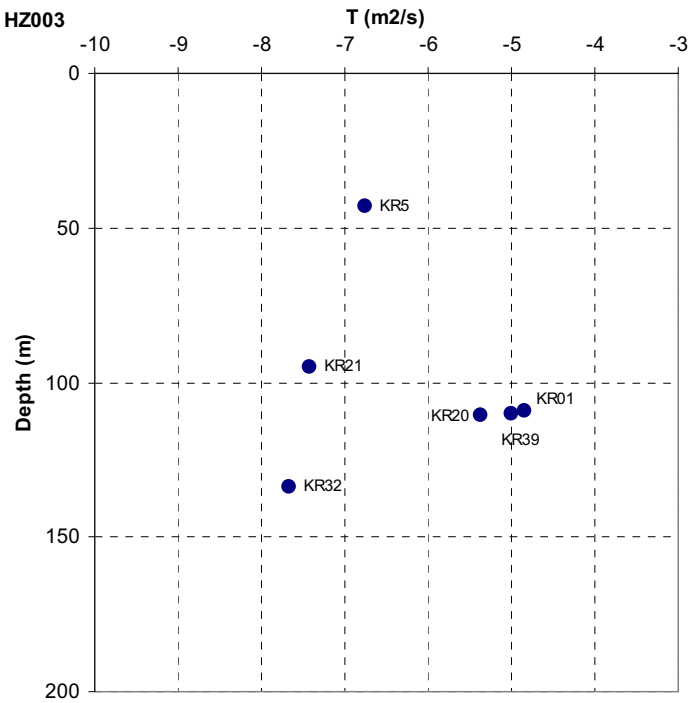

Figure 6-40. *Measured transmissivities of hydrogeological zone HZ003 (Ahokas et al. 2007).*

HZ004

A vertical hydrogeological zone HZ004 has been included in the model to account for the indications of more vertically-oriented hydrogeological connections in the east of the ONKALO, close to drillholes KR23 and KR29. The geological model describes steeply-dipping brittle deformation zone BFZ053 with slickensides in the vicinity of the drillholes. The geological model also describes some other brittle deformation zones in the vicinity: of these brittle deformation zones subhorizontal BFZ012 and steeply dipping BFZ013, with indications of a capacity for water flow, reach the surface. A lineament in the lineament model of Kuivamäki (2005) coincides with hydrogeological zone HZ004 - the previous hydrogeological model described a vertical zone (R7) coinciding with this lineament. The hydrogeological zone is modelled as a large and vertical structure.

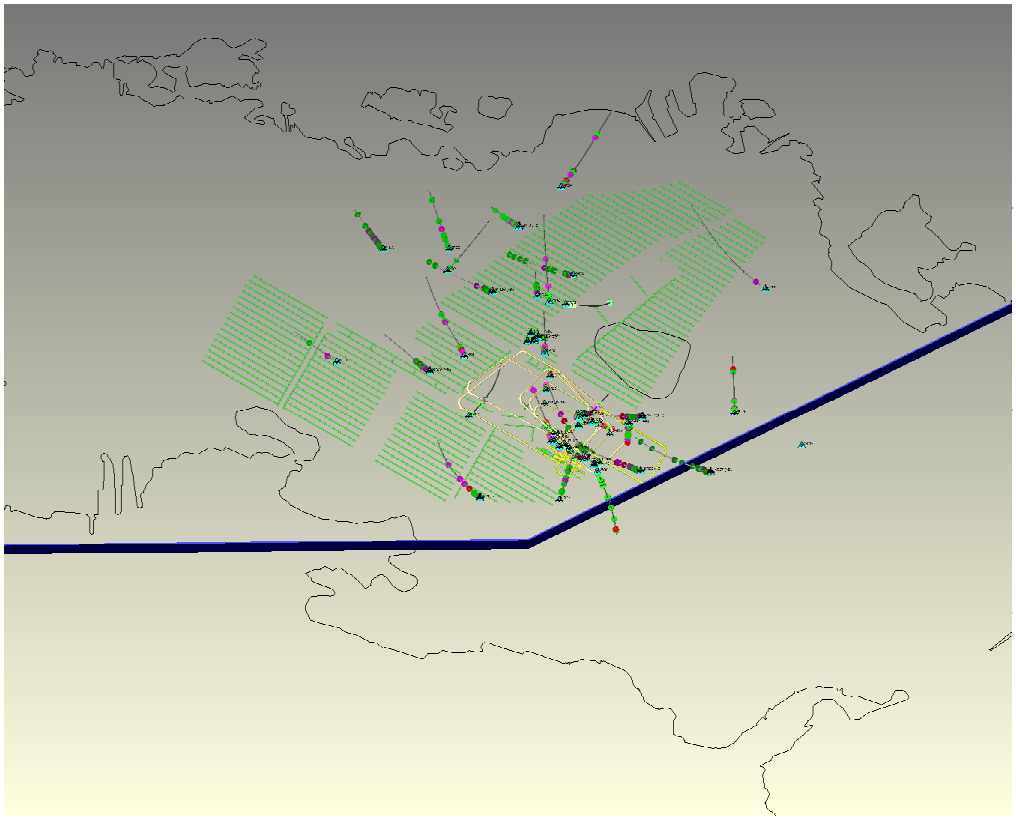

Figure 6-41. *Hydrogeological zone HZ004 together with drillholes and planned repository tunnels (Ahokas et al. 2007). View from above.*

There are two measured transmissivities for hydrogeological zone HZ004. In drillhole KR8 at a depth of 280 m the measured value is 5×10^{-8} m^2/s, whereas in drillhole KR27 a ten times greater transmissivity has been measured at a depth of 130 to 190 m. Because of the low number of measurements, the effective transmissivity c. $T_G = 2\times10^{-7}$ m^2/s is very uncertain.

HZ008

Zone HZ008 (with a dip of 30° and dip direction of 117°) is based on investigations in the VLJ repository (Ahokas & Äikäs 1991) and the extension of the zone is as reported for structure RH8 in bedrock model 2003/1 (Vaittinen et al. 2003). The transmissivity of zone HZ008 is 10^{-5} m^2/s. The location of the zone is shown in Figure 6-42.

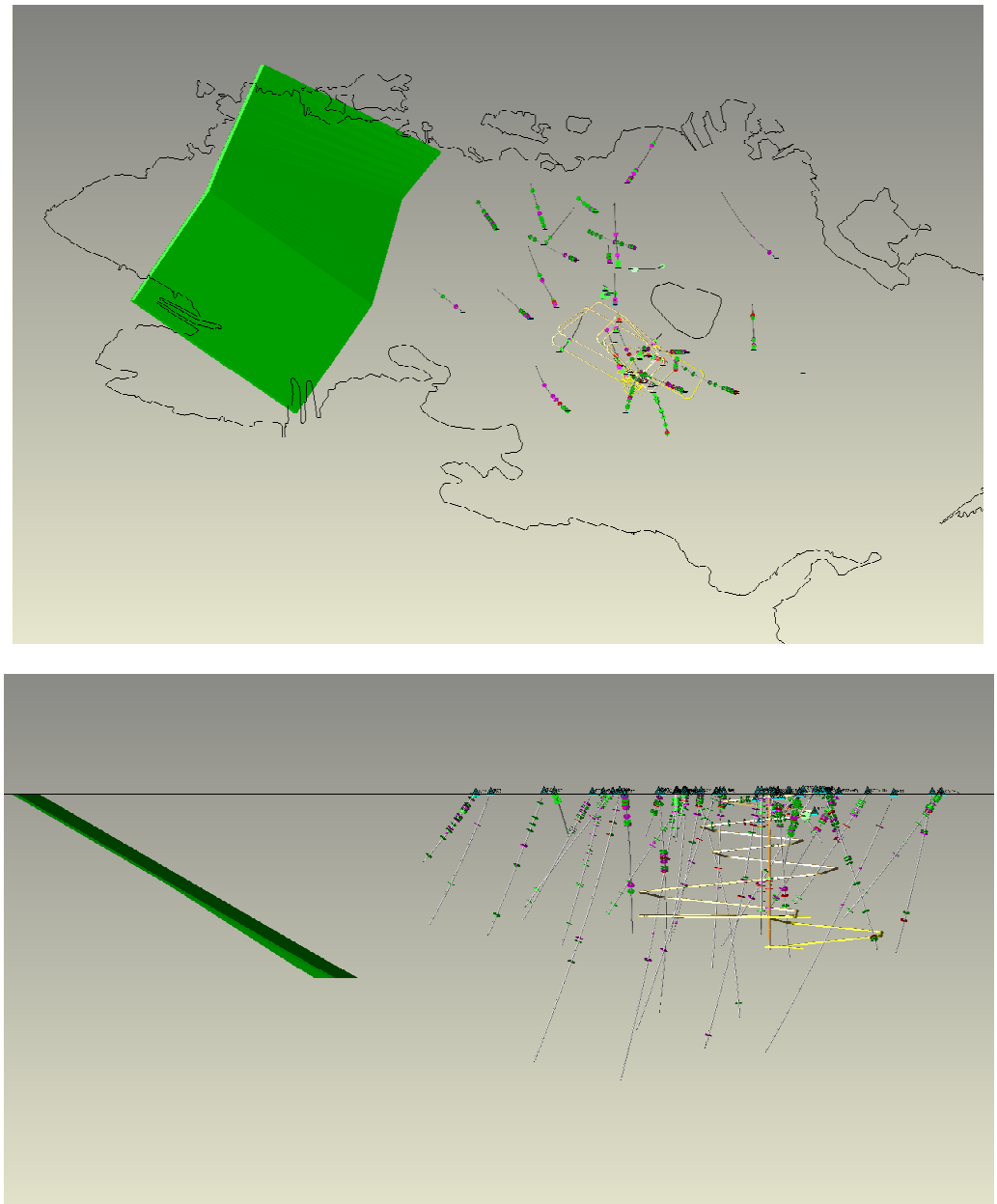

Figure 6-42. *Hydrogeological zone HZ008. Top: view from above; bottom: view from south-west (Ahokas et al. 2007).*

In addition to the geological zones introduced above, the model also includes a few lineaments in order to offer a natural continuation of the hydrogeological connections from within the well characterized area to the more regional hydrogeological zones. The lineaments identified in Kuivamäki (2005) were re-assessed and those judged most realistic were singled out and included explicitly in the complete description of the hydrogeological zones in the flow model (Figure 6-43).

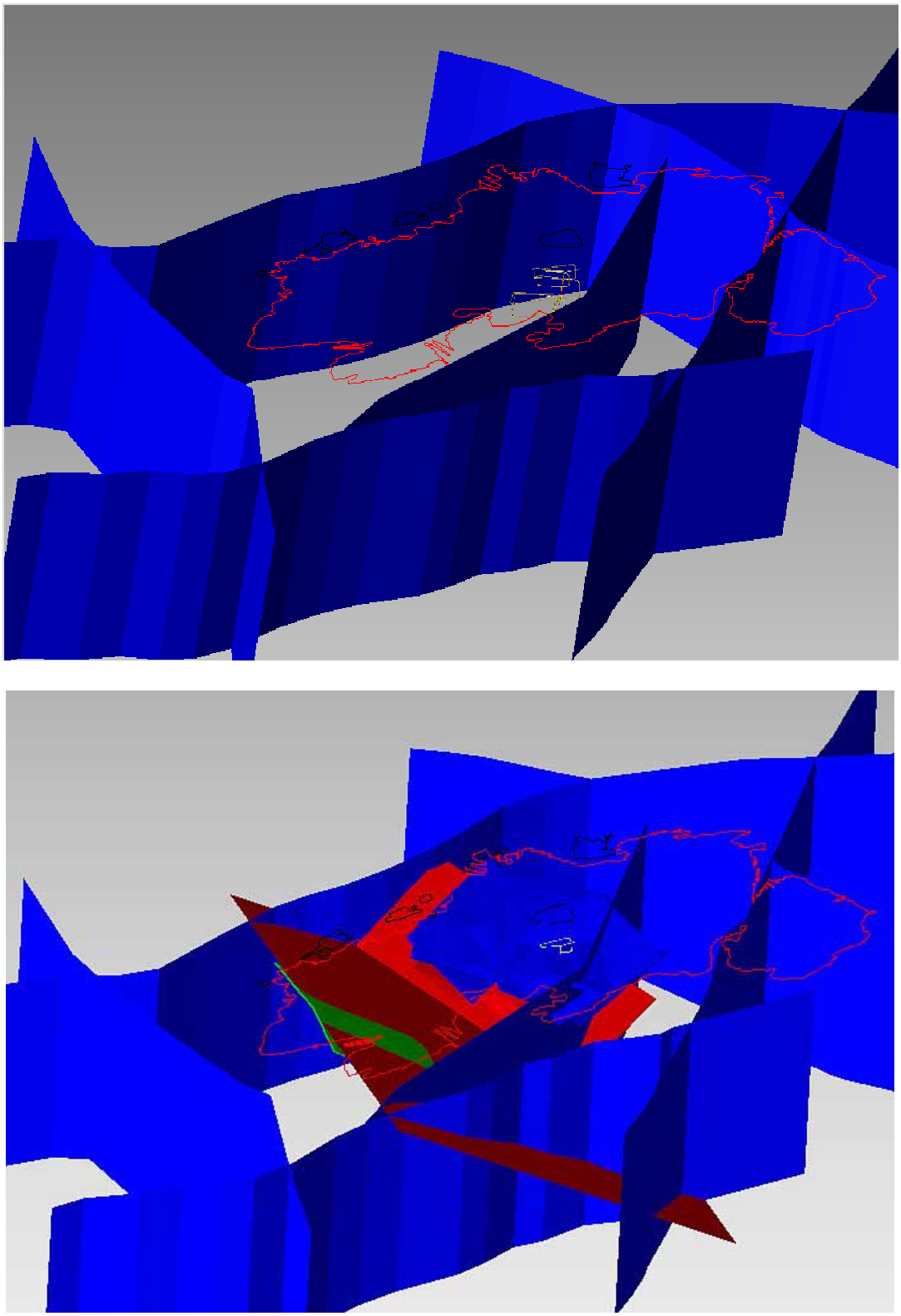

Figure 6-43. *The lineaments in the hydrogeological flow model (top) and all hydrogeological zones (bottom) in the hydrogeological flow model (Ahokas et al. 2007). In addition to the hydrogeological zones (i.e. the planar features in the figure) the figure displays the shoreline of the island (red line) and the (visible) part of the ONKALO.*

Sensitivity and uncertainty cases of the hydrogeological structure model

The structural model is based on mapping and observations in the drillholes. Consequently, whereas hydrogeological connections between the drillholes are straightforward to establish, based on the response data from various field activities, the connections outside the volume probed by the drillholes are subject to great uncertainties. On the other hand, it is clear that bedrock fracturing extends beyond this well investigated rock volume. In other words it is likely that a bias will arise due to the limited coverage of drillhole investigations. It also is possible that this bias will affect the flow modelling results in the well-characterized area.

Unfortunately there is no definitive approach to solving this problem – the lack of specific information is a fundamental uncertainty. In order to quantify the possible impact of this uncertainty, two "alternative" structural models are devised. In the first approach (applied in this study) several of the hydrogeological zones were extended in a lateral direction so that they intersected the lineaments enclosing the island. Whilst extending the hydrogeological zones (Figure 6-44), care is taken not obviously to violate any of the drillhole data, however, an examination of this approach against what was explained in Section 4.5 – *that the fault zones may actually be discontinuous* – suggests that this type of extension may be unjustified. Therefore, another representation for the structural model is introduced.

The second alternative (not applied in this study) would be to generate stochastic bedrock fracturing *outside* the well characterized area. For example, Hellä et al. (2004) determined sets of statistical parameters to describe various structural populations as follows:

- Intensity (area per unit volume [m^2/m^3]) P_{32}
    - 0.0345 for the depth less than 100 m,
    - 0.0051 deeper than 100 m
- Orientation; dip direction/dip
    - 360°/0° for the depth less than 100 m (i.e. horizontal)
    - 160°/20° deeper than 100 m
- Size, lognormal distribution with
    - mean of 250 m,
    - standard deviation (ln) 0.7.

Out of the many distributions in (Hellä et al. 2004) another one could also be possible.[14] For the transmissivity distribution, the statistics developed by Hellä et al. (2006) could be used.

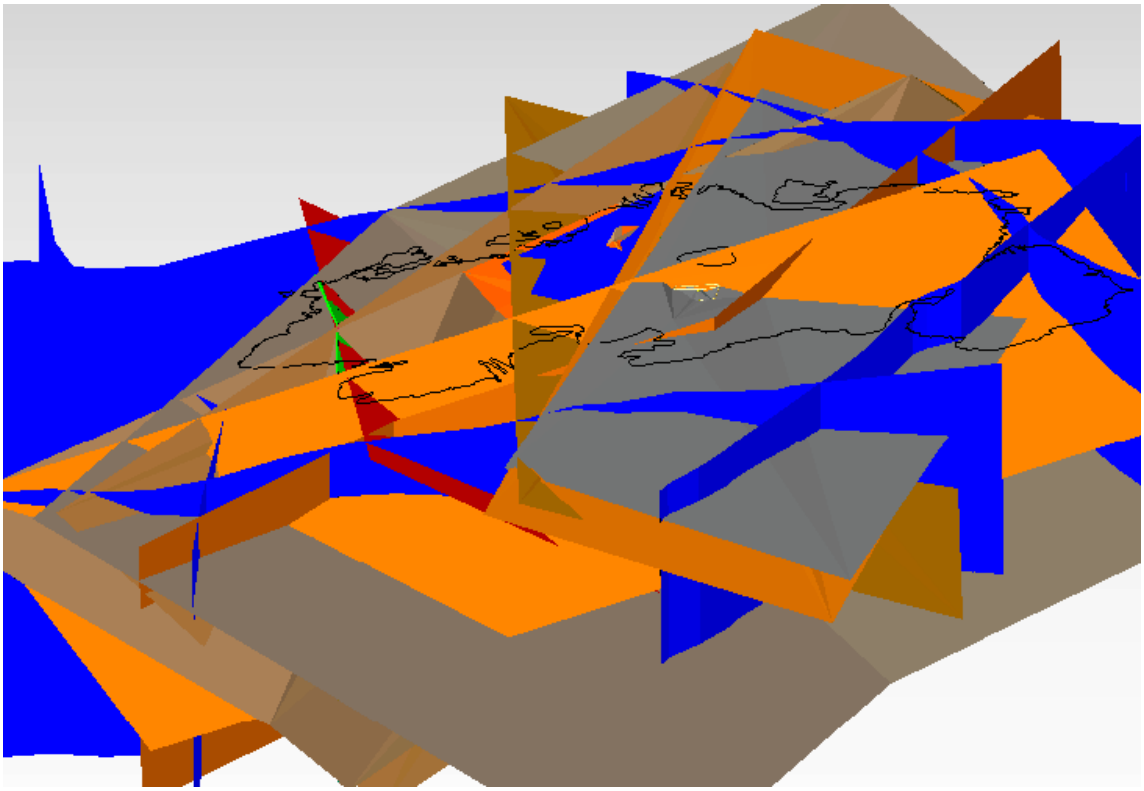

Figure 6-44. *An alternative structural model devised for regional connectivity (Ahokas et al. 2007). The Olkiluoto shoreline is presented with a black line. See the text for details.*

In addition to the alternative structural model depicted in Figure 6-44, Ahokas et al. (2006b) proposes a few alternative interpretations which bear an element of uncertainty. Whilst these are not covered in Chapter 8, the alternative cases Ahokas et al. (2006b) introduces are the following:

- HZ20B replacing HZ20B_ALT
- Possible zone HXZ.

---

[14] Hellä et al. (2004) *assumed* that hydrogeological zones were *smaller* than fracture or crushed zones. We do not consider that this assumption is well-founded, as many of the deterministic hydrogeological zones are clearly larger than most of the geological brittle deformation zones. For this reason, we adopt the size Hellä et al (2004) determined for fracture and crushed zones, instead of the parameters they developed from hydraulic zones.

- Hydraulic connections between HZ002, HZ003, and HZ19 system.

- The drillholes are in most cases oriented in almost the same direction (in order to intersect the plane of foliation at a high angle). Consequently, Paulamäki et al. (2006) note the lack of possible N-S and NW-SE-striking fault zones, which may exist between the parallel drillholes. In order to explore the significance of such an uncertainty from the hydrogeological perspective, Ahokas et al. (2007) describes a corresponding steeply-dipping hydrogeological zone that resides within the well characterized area, without being intersected by the drillholes.

6.3.4 Hydrogeological properties - porous medium description

In this Section we determine the hydrogeological properties of the hydrogeological zones and the rock mass between them. Specifically, the hydrogeological properties include:

- Transmissivities of hydrogeological zones. They are modelled as two-dimensional features, as described earlier, making the transmissivity the proper parameter to govern the volumetric flow rate in these hydrogeological units. It is possible to calibrate the transmissivity of a few fracture zones against the extensive dataset collected in the course of the site investigations at Olkiluoto (for a summary see Vaittinen 2006).

- Hydraulic conductivity of the rock mass between the fracture zones. This governs the volumetric flow rate in the hydrogeological unit in question. As the hydraulic conductivity is relatively low, and thus yields overall flow rates that are considerably lower than those for the hydrogeological zones, the calibration of the hydraulic conductivity of the sparsely fractured rock mass is not well supported by field data, as is the case for the hydrogeological zones.

- Flow and matrix porosity. The porosities govern the time scales of evolution. In the context of this work, the porosities may show up in the salinity concentration observed today (or rather before the ONKALO excavations), possibly making it amenable to calibration efforts. Some values may be found in the literature. In this work we adopt values used in earlier studies and apply a reasonable window of uncertainty for quantifying the related sensitivity.

- Longitudinal and transverse dispersivity in the bedrock. The dispersivities affect the spreading of concentration fronts in the flow field in a porous medium. It is important to realize that the dispersivity is in many respects quite different from the parameters mentioned above. Instead of being a material property, it rather is a model fitting parameter which is characteristic of the particular scale of the studied transport problem (see e.g. de Marsily, pp. 230–243).

Transmissivities of the hydrogeological zones

The determination of the transmissivity of the hydrogeological zones builds on the concept of the structure of the hydrogeological model, as discussed in Section 6.2.1.

Section 6.3.3 introduced the measured point-value transmissivities of each hydrogeological zone identified within the well-characterized area.[15] Because the practical flow modelling strives for a properly simplified approach to specify the hydrogeological properties of the hydrogeological zones, we strive for a single representative or *effective* value. According to effective medium theory, the effective transmissivity T_{eff} in a uniform flow field is obtained as the geometric average T_G of the point values, T_i, that is

$$T_{eff} = T_G = \left(\prod_{i=1}^{n} T_i \right)^{1/n} = \exp\left[\frac{1}{n} \sum_{i=1}^{n} \ln(T_i) \right], \qquad (6\text{-}1)$$

where n is the number of point values associated with the hydrogeological zone in question (see, e.g. Renard & de Marsily 1997, Vidstrand, 1999; and a recent review by Sanchez-Vila, Guadagnini & Carrera 2006).

For these cases, the effective transmissivities were calculated for both intervals. The effective values calculated using Equation (6-1) by Ahokas et al. (2007) provide effective transmissivities for the hydrogeological zones in the study area, and are presented in Table 6-2, where the supporting basic statistical parameters are also listed. For zones HZ001 and BFZ99, the data pointed to a separation of the point values into two depth intervals.

Unfortunately there are no direct data or information about the hydrogeological significance of the lineaments. For this work, we chose to assign them a transmissivity of $T = 10^{-5}$ m^2/s.

The transmissivity of some hydrogeological zones may be further adjusted through calibration against observed hydrogeological responses from various field activities. These activities include pumping tests (Vaittinen 2006 and references therein) and the observations associated with the ONKALO excavations. The calibration of the flow model will be discussed in Chapter 8.

---

[15] It can be argued, though, that "support" scale of the drillholes' finite diameter means that the measured transmissivities may not be true point-values, especially if the actual heterogeneity takes place over even shorter scales. Examining this question, formally requiring a down-scaling approach, has not been tried, as nothing seems to indicate it would yield notably improved estimates of the effective properties.

Table 6-2. *Basic statistics of measured transmissivities of zones and proposed depth-dependent values to be used in hydrogeological flow modelling (Ahokas et al. 2007). The flow porosities in the right-hand column were calculated from the T_G values.*

wZone name	Number of data points	std of log(*T*)	Max log(*T*)	*log* T_G (m^2/s)	*Flow porosity*
HZ001, depth interval 0–250m				**–5.4**	1.3×10^{-2}
deeper than 250m				**–7.6**	2.3×10^{-3}
HZ001	**12**	2.1	**–5.1**	–7.9	1.8×10^{-3}
HZ002	**9**	0.6	**–5.1**	–6.0	7.9×10^{-3}
HZ003	**6**	1.3	**–4.9**	–6.2	6.8×10^{-3}
HZ004	**2**	0.7 *)	**–6.3 *)**	–6.8 *)	4.3×10^{-3}
HZ008	**1**	-	**–5.0**	–5.0 **)	1.7×10^{-2}
HZ19A	**18**	1.6	**–4.3**	–5.8	9.2×10^{-3}
HZ19B	**18**	1.8	**–4.3**	–5.7	9.9×10^{-3}
HZ19C	**24**	1.3	**–4.4**	–5.5	1.2×10^{-2}
HZ20A	**11**	0.7	**–4.4**	–5.1	1.6×10^{-2}
HZ20AE	**7**	1.2	**–4.9**	–6.0	7.9×10^{-3}
HZ20B	**11**	0.4	**–4.8**	–5.2	1.5×10^{-2}
HZ20B_ALT	**11**	0.9	**-4.9**	–5.5	1.2×10^{-2}
HZ21	**9**	1.8	**–5.5**	–7.8	2.0×10^{-3}
HZ21B	**8**	0.9	**–5.1**	–6.1	7.3×10^{-3}
BFZ099, depth interval 0 to 500m				–6.3	6.3×10^{-3}
BFZ099, deeper than 500m				–8.1	1.6×10^{-3}
BFZ099	**12**	1.8	**–5.9**	–7.8	2.0×10^{-3}
Lineaments	none	N/A	**N/A**	–5	1.7×10^{-2}

*) **Very** uncertain
**) One value measured in YD18 (VLJ-repository area) (Ahokas & Äikäs 1991)

Uncertainty and sensitivity cases

The uncertainty associated with each effective value is clearly lower for those hydrogeological zones for which the number of point values is relatively high. This group of hydrogeological zones comprises hydrogeological zone systems HZ19, HZ20, HZ21, the upper part of BFZ099 and HZ002. Conversely, for hydrogeological zone HZ004, with only two measured transmissivities, the uncertainty of the effective transmissivity is high. The uncertainty is greatest for the lineaments, but, on the other

hand, as they are located far from the well-characterized area, the significance of this uncertainty is considered to be small.

In Chapter 8 the sensitivity of the calculated results to the transmissivity of hydrogeological zones will be explored by employing the maximum values presented in Table 6-2.

Hydraulic conductivity of the rock mass between hydrogeological zones

Although a large part of the observed transmissivities – and all of the values greater than 10^{-5} m^2/s – were associated with the hydrogeological zones, a significant number of them were interpreted to represent the hydrogeological characteristics of the sparsely fractured rock mass between the zones. From the modelling point of view the essential difference between the sparsely fractured rock and the hydrogeological zones is the dimensionality: the former will be modelled as a three dimensional porous medium. Therefore, although the point values, which provide the basis for determining the hydraulic conductivity, are similar to those associated with the hydrogeological zones (because of the difference in the dimensionality), the effective property (hydraulic conductivity, rather than transmissivity) is determined somewhat differently (Ahokas et al. 2007).

The effective hydraulic conductivity of the bedrock (K_{eff}) is calculated as

$$K_{eff} = T_G / D_T$$

based on geometric means of measured high transmissivities (T) and their frequency (actually the distances between high T values (D_T) outside modelled zones). Transmissivities higher than 10^{-8} m^2/s are taken into account and values in close proximity are assumed to belong to one hydraulic feature (narrow zone), if supported by geological or hydrogeological data. Measured transmissivities are presented in Figure 6-45 as cumulative plots and divided into five depth intervals, i.e. 0–50, 50–100, 100–200, 200–400, 400–900 m below sea level. The corresponding distances (log) between transmissive features are presented in Figure 6-46.

Calculated values of K_{eff} in different depth intervals are presented in Table 6-3 and in Figure 6-47, where corresponding values or curves that were used or proposed for earlier models (Löfman 1999; Posiva 2005) are also shown. Alternative values of K_{eff} were calculated using medians of cumulative plots of Figures 6-45 and 6-46 and they are shown in Figure 6-44 as open diamonds.

The reasons for the differences between the values from 2004 and 2006 are:

- K_{eff} for 2006 for depth interval 0–50 m is smaller, due to the better understanding of deterministic zones at shallow depths. In other words, many high T values are now considered as belonging to zones HZ19A and C – earlier they were associated with the rock mass outside the zones.

- Higher values of K_{eff} for 2006 at greater depths may be due to the differences in the way in which narrow deterministic zones were defined, i.e. many drillhole sections

in close proximity were assumed to form one feature in the data analysis for 2004 – in the current model the average separation of distinct zones can now be smaller, which increases the potential number of such zones and increases the K_{eff}.

Table 6-3. *Calculated values of K_{eff} [m/s] of the measured hydraulic conductivities not associated with any hydrogeological structure, modelled explicitly in the Olkiluoto area flow model. See (Ahokas et al. 2006) for details. The values in column "2004" are those determined from measurements for the flow modelling in (Posiva 2005) before the calibration and column K_{fm} presents the corresponding values after the calibration. Column "2006" in turn, presents the values used as the initial hydraulic conductivity for sparsely fractured rock in this rock. The last column presents the values determined in the calibration of the flow model.*

Depth interval (m)	K_{eff}, 2004	K_{fm}, 2004, (Posiva 2005)	K_{eff}, 2006	K_{fm}, calibrated values in this report	
				Inside WCA	*Outside WCA*
0–50	1.6×10^{-7}	10^{-9}, horiz. 10^{-7}, vertical	6×10^{-8}	6×10^{-8}, hor. 1×10^{-9}, vert.	3×10^{-7}, hor. 5×10^{-9}, vert.
50–100	9×10^{-9}	1×10^{-10}	2×10^{-8}	1×10^{-9}	5×10^{-9}
100–200	3×10^{-9}	3×10^{-11}	7×10^{-9}	7×10^{-10}	3.5×10^{-9}
200–400	1.3×10^{-9}	1×10^{-11}	4×10^{-9}	4×10^{-10}	2×10^{-9}
400 and deeper	3×10^{-10}	3×10^{-12}	9×10^{-10}	9×10^{-11}	4.5×10^{-10}

It is interesting to compare the values in Table 6-3 with those determined from upscaling of the discrete fracture network modelling for the depth range 300 to 800 m at Olkiluoto by Lanyon & Marschall (2006). They found values of the hydraulic conductivity for a few cases and three principal components ranging from 2×10^{-11} m/s to 6×10^{-10} m/s. These values are well in accord with the calibrated values in this report, which does not, however, consider the potential anisotropy of the hydraulic conductivity of the deep bedrock.

The effect of the lack of any explicitly modelled zones outside the well-characterised area can be taken into account by increasing the value of K_{eff}. The same factor of 5, as was used for the 2004 flow model, has been used for the hydraulic conductivity of the averaged rock mass between the hydrogeological zones outside the well characterized area (Ahokas et al. 2007).

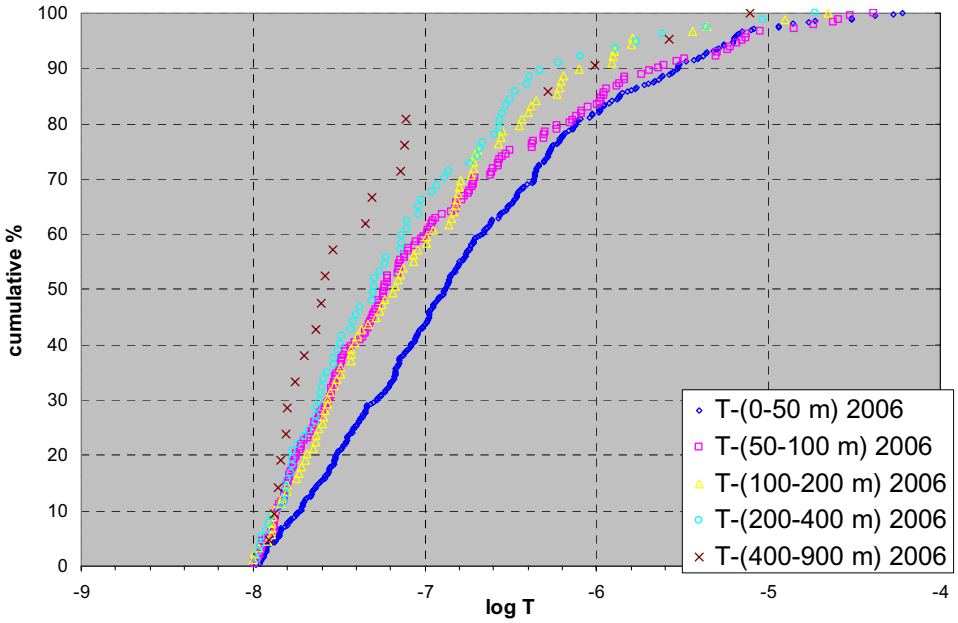

Figure 6-45. *Cumulative plots of transmissivities measured in the bedrock (outside modelled zones) and divided into five depth intervals (Ahokas et al. 2007).*

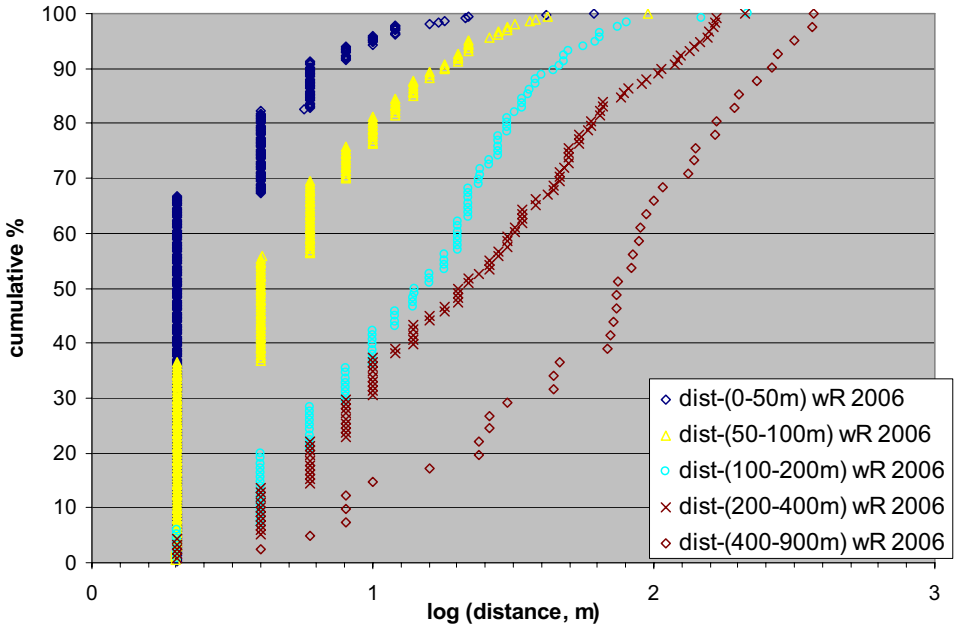

Figure 6-46. *Distances (log) between transmissive features in the bedrock outside Modelled zones as cumulative plots and divided into five depth intervals (Ahokas et al. 2007).*

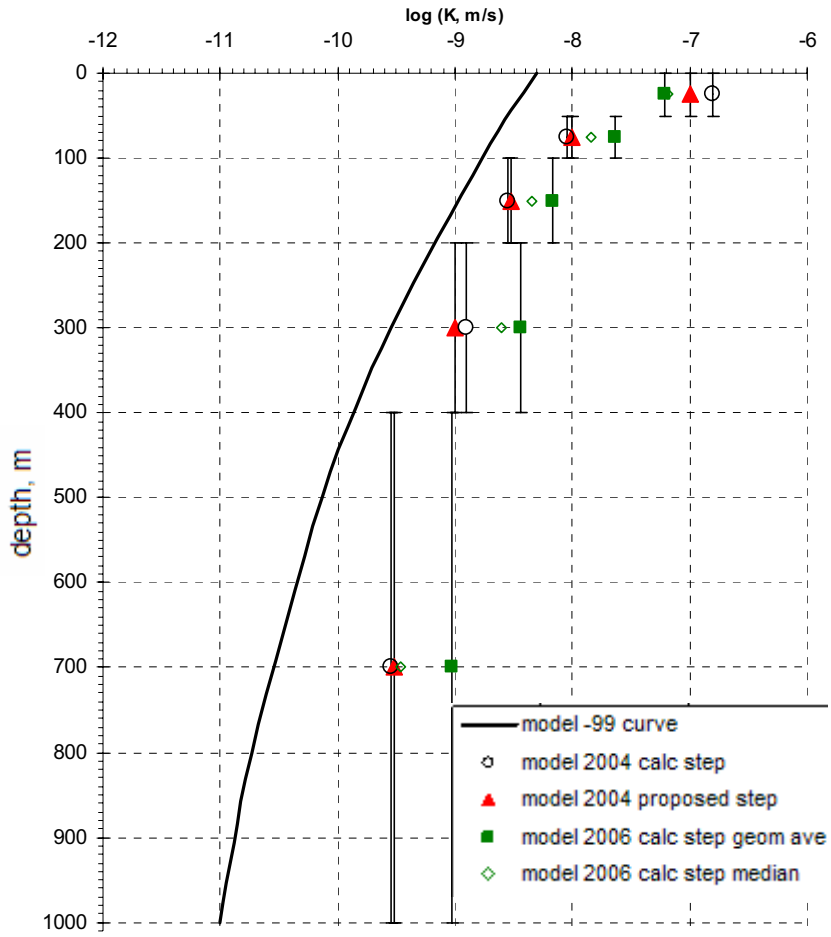

Figure 6-47. *Graphical presentation of calculated values of K_{eff} for different depth classes (Ahokas et al. 2007). Old values (curve or step) proposed for use in earlier models (Löfman 1999, Löfman 2005) are also shown.*

Uncertainty and sensitivity cases

The sensitivity of the calculated results to the uncertainty of the hydraulic conductivity of the rock mass between the hydrogeological zones is assessed using two cases:

- Initial hydraulic conductivity values (see Table 6-3) used unless otherwise mentioned
- Hydraulic conductivity values as in Site Description 2004 (see Table 6-3).

Flow and Matrix Porosities, and uncertainty cases

There is no detailed site-specific knowledge of the flow and matrix porosities, although a study by Autio et al (1998) found a total porosity of 1.4×10^{-3} for undisturbed rock.

For the purposes of this work, two alternative approaches is applied for the flow and matrix porosities. Firstly, a customary approach is adopted depicting the flow porosity to be constant and a small portion, one tenth, of the total porosity, and using the values from the Site Description 2004 (Posiva 2005) as a basis; see Table 6-4. Secondly, as was already described earlier in Section 6.3.1, the flow porosity is conceptualized as coupled to transmissivity and/or hydraulic conductivity. As the transmissivities and hydraulic conductivity are based on hydraulic test data, they are used to determine respective the flow porosities whereas, for the matrix porosity, a customary assumption is adopted to set it to ten times that of the flow porosity. The primary effect of the flow porosity is setting the time scale of evolution – a porosity of one tenth of the base case value would make the rate of evolution ten times faster. Also the matrix porosity affects the time evolution of the TDS concentration field, as it offers "extra" storage that seeks an equilibrium with the TDS concentration in the flowing porosity at a rate of mass transfer determined by diffusion (the associated timescale of the evolution is, therefore, long).

Table 6-4. *The values for the porosity (n_f and n_{tot}) together with three sensitivity cases (the constant porosity approach).*

	Base case	higher porosity	lower porosity	Coupled porosity and conductivity
Hydrogeological zones (flow/total)	1×10^{-3}/ 1×10^{-2}	5×10^{-3} / 5×10^{-2}	2×10^{-4} / 2×10^{-3}	Table 6-2
Sparsely fractured rock mass	2×10^{-4} / 2×10^{-3}	1×10^{-3}/ 1×10^{-2}	4×10^{-5} / 4×10^{-4}	Figure 6-48

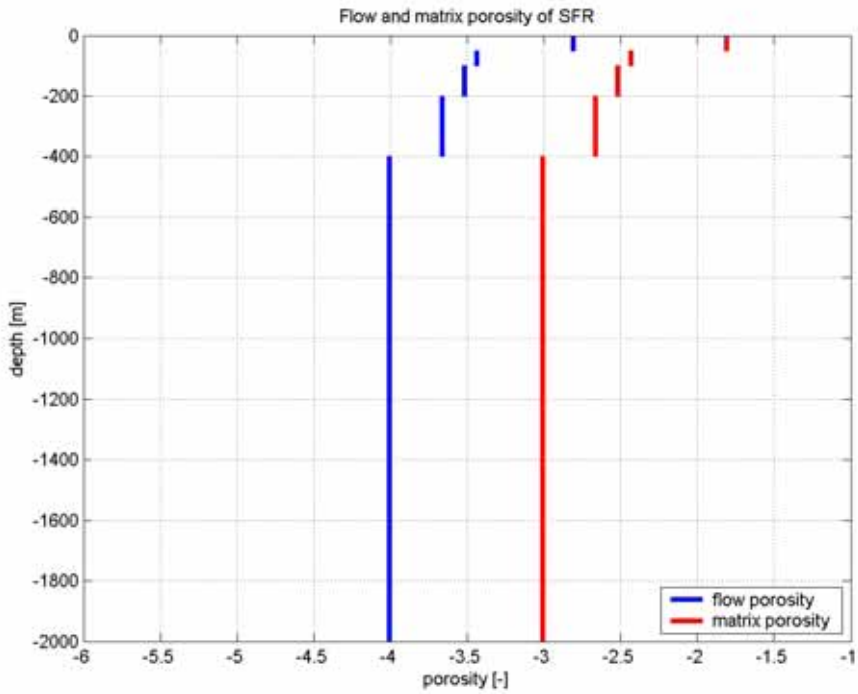

Figure 6-48. *Alternative values for the flow and matrix porosity of the sparsely fractured rock (SFR) inside the Well Characterised Area (WCA). The values are calculated from the cubic relation between the fracture aperture, the fracture spacing and the hydraulic conductivity (see Löfman 1999 for details).*

Dispersivities

Whilst the dispersivity clearly is a relevant parameter in the ADE, no site-specific information exists about the longitudinal or transverse dispersion lengths[16]. On the other hand, assigning proper values to the dispersivity has proved to be a difficult question – a conclusive solution is lacking, even today, in the case of fractured rock.

The literature encompasses a very large body of studies on dispersivity, the clear majority of which deal with truly porous media, with only a small portion being dedicated to transport in fractured hard rocks.

Gelhar & Axness (1983) made use of stochastic theory to derive a simple equation to estimate the longitudinal dispersivity ε_L:

$$\varepsilon_L = \sigma^2_{\ln K} \lambda / \gamma^2 \qquad (‡)$$

[16] This discussion is pertinent to macrodispersivity, i.e. the dispersivity on the scale of (velocity or conductivity) averaging or homogenization in the model. A similar perception of homogenization is also taken in the context of field studies at large scales (see, e.g. Gelhar, Welty & Rehfeldt 1992).

where $\sigma^2_{\ln K}$ is the variance of ln K, K is the hydraulic conductivity, λ is the correlation scale (more specifically, distance to the exp(–1) correlation), and γ is the flow factor (of which the numeric value in an isotropic case is $\gamma=1+\sigma^2_{\ln K}/6$)[17]. In order to make use of the formula (‡) one needs to know the values of the variance and the correlation scale, which are very hard to obtain from site data.

A generally adopted tenet is that a value computed with equation (‡) actually represents an asymptotic value towards which the dispersivity is supposed to converge. However, a thorough review by Gelhar, Welty & Rehfeldt (1992) demonstrated that this kind of asymptotic behaviour was not captured by field tests (carried out up until 1992) but, instead, the longitudinal dispersivity seems to be 10% of the size of the flow field (or transport distance) explored.

Furthermore, one of the objectives of the hydrogeological flow modelling is to explore the upward movement of a sharp saline–freshwater front (e.g. Vieno et al. 2003; Posiva 2005; Ahokas et al. 2007). In other words, the aim is to study the phenomenon of upconing by numerical means. In this context, the modelling of immiscible fluids is of interest, that is, where dispersivity is zero — thus leading one to incorporate as small a dispersivity as possible in the numerical simulations (although, for the sake of numerical stability, a larger than zero dispersivity must be used). Indeed, it is evident that the dispersion in this context should clearly be treated somewhat differently, as it is expected that the gravitation pull exerted on denser fluid located below a freshwater domain tends to decrease the dispersion in an upward direction. As Egorov, Demidov & Schotting (2005) put it: *"However, when high-concentration-gradients are present, gravity forces acting at the small-scale, stabilize the front between brine and water"*. This has been confirmed with experiments (e.g. Jiao & Hötzl 2004; Watson et al. 2002 and references therein). In line with studies by Egorov, Demidov & Schotting (2005), Jiao & Hötzl (2004), and Watson et al. (2002) we adopt a similar approach to that of the previous studies (Vieno et al. 2003; Posiva 2005; Ahokas et al. 2007) that attempt to maintain the concentration gradients as sharp as is numerically manageable and apply a reasonable window of uncertainty for quantifying the sensitivity of the calculated results on the dispersivities (Table 6-5). The uncertainty cases also include a case of weaker dispersion than the base case. Numerically this is more demanding, rendering it impractical for use in all numerical simulations in connection with this study.

---

[17] This is the equation derived for the longitudinal dispersivity by Gelhar & Axness (1983). While they also derived results for the transverse dispersivity, it is customary to set it as a fraction (e.g. one fourth, one tenth) of the value for the longitudinal dispersivity.

Table 6-5. *The values of the dispersion lengths together with two sensitivity cases. The longitudinal and transverse dispersion lengths are denoted with a_L and a_T, respectively. See the text for an associated discussion and reasoning.*

	Initial values	Weaker dispersion	Stronger dispersion
a_L [m]	50	25	100
a_T [m]	13	6	25

6.4 DFN modelling

As no discrete fracture network flow modelling is carried out for this report, a study that was carried out in connection with the so called KBS-3H project in 2006 is reviewed. The next revision of the Site Descriptive Model (scheduled for 2008) will include a thorough DFN analysis on the groundwater flow in the repository host rock block. In developing the next Site Descriptive Model, separate DFN flow modelling studies are also planned to make better use of the site data – in particular the use of flow and transmissivity measurements – and modelling methodology to investigate issues related to, for example, the hydraulic connectivity of fracture networks and the heterogeneity of fracture planes. Furthermore, the integration of the hydrogeological DFN modelling and the rock mechanical site description at Olkiluoto will be explored. A further discussion on the future plans related to the hydrogeological DFN modelling at Olkiluoto is given in Section 6.4.4.

DFN flow modelling makes use of the geological DFN parameters that describe the statistics of the orientation and size distributions of fracture sets, together with the intensity (e.g. P_{32}) for each such set. At Olkiluoto such information has recently been produced by Tuominen et al. (2005) for a shallow block in the vicinity, and by Poteri (2001) and Hellä et al. (2006) for deep bedrock. Based on the latter study, Lanyon & Marschall (2006) carried out DFN analyses for the safety case of a KBS-3H repository at Olkiluoto. In this report the main findings from this study are reviewed. Earlier analyses of the deep groundwater flow in DFN networks have been carried out by Poteri & Laitinen (1999).

6.4.1 Background

DFN modelling is applied as part of the studies of the long-term evolution of the KBS-3H repository, applying site-specific information of the Olkiluoto site (Lanyon & Marschall 2006). The main issues addressed by the DFN modelling are the probability of high inflow points, which may cause buffer erosion, time transients of the inflows after construction of emplacement tunnels and interference between emplacement tunnels and operations tunnels.

The purpose of the study is to examine the impact of conceptual model uncertainties, alternative repository design options and different closure scenarios on the evolution of the repository system. The study has been divided in two subtasks: an initial phase of geometrical calculations, followed by a phase of hydrodynamic calculations.

6.4.2 DFN models

The DFN model is based on the representation of the hydrogeological features at different scales. The features considered are Major Fracture Zones (MFZ), Local Fracture Zones (LZF) and associated water conducting fractures (LFZ-WCF) and Water Conducting Fractures in the background rock (BR-WCF).

The description of the DFN model is based on the existing structural model and a parameterisation of the fracturing. MFZs are based on the bedrock model of the Olkiluoto site (version 2003/1, Vaittinen et al., 2003). The geometries of the LFZs and WCFs are based on the previous DFN models, mainly on the DFN applied by La Pointe and Hermansson (2002).

Hydrogeological properties of the WCFs are estimated based on the available flow logging data, which is available for most of the drillholes at Olkiluoto. Stochastic DFN flow modelling requires the specification of distributions for the spatial density distribution (P_{32}), orientation, size and fracture transmissivity. These data applied in the DFN modelling were determined in a study by Hellä et al. (2005).

The DFN model aims to provide a representation of the fracturing at a rather detailed scale. MFZs are not the primary target of the model and they have been included in the model only for consistency and to understand their influence on the effective properties. All MFZs included in the model are deterministic and all have transmissivity of 10^{-5} m^2/s. Internal consistency of the model is maintained by removing all drillhole sections connected to the Major Fracture Zones (MFZs) from the flow logging data before the transmissivity distribution of the WCFs was assessed.

As a summary, the construction of the KBS-3H DFN model employed the same DFN parameterization as the previous models and no new interpretations of fracture observations were made. However, this is the first DFN model of the Olkiluoto site that collects the existing fracture data at different scales into a single hydrogeological model.

The KBS-3H DFN study includes a reference case and three alternative variants: transmissivity distribution extended towards less transmissive fractures, a fracture length – transmissivity correlation and a channel variant.

6.4.3 Results

Geometric simulations

All geometric calculations were performed on a 2400×1600×100 m^3 block at 400 m depth. The generation region for the fracture network was much larger to avoid edge-effects. The number of WCFs in a model range from about 20 000 for the reference case to 110 000 for the extended reference case, with a cutoff at 10^{-11} m^2/s. In the channel model there are approximately 30 000 WCFs, but each WCF is represented by up to 100 sub-fractures resulting in over 1 500 000 sub-fractures

The geometric simulations indicated very consistent layout across all the model variants and realizations. Fracture intersection statistics for different DFN alternative models

showed very similar results for all model variants. All models were equally well calibrated to the drillhole intersection statistics, implying also that the tunnel intersection statistics are similar.

There were some indications from the flow logging data that flowing fractures are more clustered than the random, uniform density applied in the DFN model. It was also identified that the DFN model may help to identify the drillhole sections that are outside the range expected for the averagely fractured rock.

Inflow estimates were calculated using results of the geometric simulations and the Thiem equation for steady state radial flow. Each intersecting WCF was modelled with a constant head drop of 400 m at 50 m radius from the tunnel. Hydraulic apertures have been calculated from the fracture transmissivity, by assuming a water density of 1000 kg/m^3 and a viscosity of 10^{-3} Pa·s. Grouting of the intersecting fractures is easily taken into account by adjusting the fracture transmissivities.

Highly transmissive intersecting WCFs are sealed ($T>2.65\times10^{-8}$ m^2/s) and typically a 300 m drift is divided into 2 compartments by a single seal. Total inflows to the compartments (prior to grouting) within a drift are on average about 1.5 l/min.

Flow simulations

Flow simulations have been performed for the estimation of the effective permeability and for the simulations of the excavation and closing of the single KBS-3H drift.

Effective K

The effective permeability was calculated for 10 realisations on a $2400\times1600\times500$ m^3 block. Results indicate that the minimum principal permeability is subvertical and that the maximum permeability is in the plane of the major structural trend. Away from MFZs, the minimum hydraulic conductivity is around 10^{-11} m/s and the maximum hydraulic conductivity around 10^{-9} m/s.

Tunnel excavation and closing

The simulation model applied in this study is based on the extended reference case. The modelling domain is a cylinder of 400 m long and 50 m radius around the drift. A constant head boundary condition is applied at the outer boundary of the modelling domain. It is assumed that excavation of the 300 m tunnel takes 30 days and that the tunnel is open for 25 days during the emplacement and sealing of the supercontainers.

The inflows reach steady-state levels quite quickly after the end of excavation. Lower transmissivity fractures are likely to be of lower diffusivity, resulting in longer transients, whilst pressure changes within the matrix are likely to be very slow indeed. However, given that the bulk of the inflow will be associated with more permeable fractures, the models suggest that there is no need to simulate the detailed excavation procedure and an initial steady-state inflow condition can be used for the simulation of drift closure.

Pressure also recovers relatively quickly after closure. The dominant factor is the length of time required to fill up the gap volume prior to the start of pressure recovery. Transients associated with pressure recovery are relatively swift and controlled by the storage associated with the drift elements.

6.4.4 Hydrogeological DFN modelling plans for the future

DFN models have several applications related to site characterisation and safety evaluation to model and assess the effects of variability of the bedrock properties and to make predictions of the bedrock properties. Of special interest for the safety case are flow properties in the repository host rock in order to understand the hydrogeochemical evolution of the near field and the performance of the engineering barriers (see e.g. Lanyon & Marschall 2006). Moreover, the potential coupling between hydrogeology and rock mechanics (e.g. Koyama 2005) may allow us to estimate the possible changes in the hydrogeological properties under various and transient load conditions related to the next glacial period. An important application of the DFN-based flow modelling is the derivation of the transport routes and resistances used in the radionuclide transport calculations. DFN models can also be used to estimate the number of canisters expected to be damaged by possible future earthquakes (see e.g. La Pointe & Hermansson 2002) and in layout planning.

The DFN studies carried out so far have been based on a very limited number of data compared to what is now available. Currently, there is a notably increased number of data, both fracture data and transmissivity measurements, from new drillholes, exposures and especially from the ONKALO. Revised mapping of the fracture data provides a more uniform fracture data set for the analysis and there have major revisions over the past few years in the geological modelling, which provides the framework for the description of the fracturing. Therefore, a number of analyses and interpretations, including a comparison of data from pilot holes with tunnel mapping and experiments in the tunnel, the integration of hydraulic data with fracture data and a study of the various correlations between hydraulic fracturing and other rock and fracture properties, are envisaged to define the best possible input data for a revised DFN model. The work aims at the compilation of a DFN model to be applied in radionuclide transport modelling, as outlined in Posiva (2006). As the analytical tasks described above have just started, this report discusses the DFN modelling only to a limited extent and mainly by referring to the study by Lanyon & Marschall (2006) and other previous work. Future versions of the Site Report will include an updated DFN description and DFN-based flow modelling.

6.5 Consistency with other disciplines

Geology

A key input is provided from the geological model, version 0 (introduced in Chapter 4). More specifically, the Brittle Deformation Model version 0 forms an underlying skeleton for the hydrogeologically connected network at the site scale. This geological model was reconciled with hydrogeological data, in particular pumping tests and responses to various field investigations, and information that facilitated the description

of a network of hydrogeological zones present between the drillholes. In addition, outside the well characterized area, lineaments were sorted for confidence.

Only some of the brittle deformation zones are explicitly modelled on the site scale. An important reason for this is that Ahokas et al. (2007) adopted a transmissivity criterion (T=10^{-7} m^2/s) for individual measurements associated with each brittle deformation zone, so that the hydrogeological model could only describe a hydrogeological zone if one measured transmissivity agreed with the criterion. Otherwise this transmissivity was included in the measurements that were used to determine the hydraulic conductivity of the rock mass between the hydrogeological zones. Moreover, even those brittle deformation zones that evidently were co-located with a corresponding zone in the hydrogeological model, are usually much smaller that their hydrogeological counterparts. This is probably due, at least in part, to the fact that there has been no systematic effort to identify any correlation between drillholes.

Furthermore, as was exemplified with Figure 6-16, some bedrock features (or rather such intersections as in Figure 6-16) of hydrogeological importance have not been considered in the bedrock model version 0. It remains a task for the OMTF to assess the representation of such features in the geological model updates in the future. The extensive body of hydrogeological response data associated with various field activities conveys true information about hydraulic connections over large distances in the bedrock. Considering this information as another source of geophysical data encourages the development of a fully consistent description among the different disciplines.

In the future more sophisticated geological assessments may improve the realism of the hydrogeological model even further. The geological model is likely to pursue the identification of correlations or connections between drillholes, and this may also help in supporting analyses of the hydrogeological responses between the drillholes, for example, producing a more unequivocal hydrogeological description, thereby decreasing the related uncertainty.

Furthermore, the possible formation of splays, that took place during shearing in the brittle deformation phase into the rock surrounding a deformation zone, may be considered. This would mean that, for example, hydrogeological responses may also be detected at some distance from the plane of the parent deformation zone. The knowledge of the direction of shearing may also be used in judging the need for describing an anisotropic transmissivity for a hydrogeological zone.

Hydrogeochemistry

The hydrogeochemical analyses of groundwater samples provide values of the TDS concentrations at the site. The values show a vertical profile with a trend of higher salinities with increasing depth. The current-day observations of the TDS concentrations in deep drillholes are used as a calibration target for the corresponding model results and hydrogeochemical interpretations describe the end members of groundwater bodies. As these end members may be linked to sources of water associated with different characteristic time periods during the evolution of the site (e.g. glacial melting, Littorina sea, meteoric recharge), a dynamic, time-dependent system can be described and be reconciled with the groundwater flow simulations. As will be detailed in Chapter 8, a

reasonable consistency can be achieved between the hydrogeological model and hydrogeochemical interpretations.

Rock mechanics

A large body of literature has been published exploring hydromechanical coupling under various conditions (Yeo, de Freitas & Zimmerman 1998; Stephansson, Hudson & Jing (eds.) 2004; Min et al. 2004; Matsuki et al. 2006; Koyama et al. 2006). Published reports have shown, for example, the connection between fracture characteristics (aperture, orientation) and the susceptibility of the fractured rock's hydraulic properties to respond to *changes* in the stress state. Whilst there are rather few actual stress state measurements from Olkiluoto, in the future it might be possible to use a correlation to relate the change in the stress state to the change in the hydrogeological properties of fracture networks.